

Written Testimony of Dr. Noah S. Diffenbaugh
Hearing on “The Science Behind Impacts of the Climate Crisis”
March 12, 2021

Congress of the United States
House of Representatives
Committee on Science, Space, and Technology

Thank you Chairwoman Johnson, Ranking Member Lucas, and the members of the Committee for the invitation to testify.

My name is Noah S. Diffenbaugh. I am the Kara J Foundation Professor in the School of Earth, Energy and Environmental Sciences at Stanford University, and the Kimmelman Family Senior Fellow at Stanford’s Woods Institute for the Environment. I am testifying before the committee in my personal capacity, not on behalf of Stanford University.

I study Earth’s climate, including how changes in regional and local conditions – such as extreme weather events – affect people and ecosystems. I received my Ph.D. degree from the University of California–Santa Cruz in 2003. I am an elected Fellow of the American Geophysical Union (AGU), the largest scientific society of Earth and space sciences in the world. For more than a decade, I have served as an Editor of peer-review journals published by the AGU, including a four-year term as Editor-in-Chief of *Geophysical Research Letters*, one of the leading peer-review journals publishing climate science research. I have been a lead author for a number of scientific assessments, including the IPCC Fifth Assessment Report and the California Climate-Safe Infrastructure Working Group.

The subject of this hearing of the Committee on Science, Space, and Technology is “The Science Behind Impacts of the Climate Crisis”. I will focus my remarks on the topics noted in your invitation letter, including recent improvements in our understanding of how climate change is contributing to increased risk from extreme events such as wildfire, drought, and severe storms; the disproportionate impacts on vulnerable communities; the importance of quantifying climate impacts and risk for achieving Paris Agreement targets; and the implications for mitigation and adaptation solutions.

The brief summary is that:

- (i) Extreme events are increasing in frequency and severity, including those that are unprecedented in our historical experience;
- (ii) We are not adapted to these changes, meaning that global warming is already impacting people and ecosystems in the United States and around the world, including through financial costs, loss of life and destruction of habitat, with disproportionate impacts on poor and marginalized communities;
- (iii) The greater the global warming that occurs in the future, the more these risks will intensify, including non-linear intensification of many impacts;

(iv) As a result, achieving the Paris Agreement global warming goals will reduce the impacts that we experience, including reducing the financial costs of further climate change;

(v) However, even if the Paris Agreement global warming goals are achieved, there will still be more climate change than has already occurred, and hence adaptation will be necessary to avoid further impacts; and

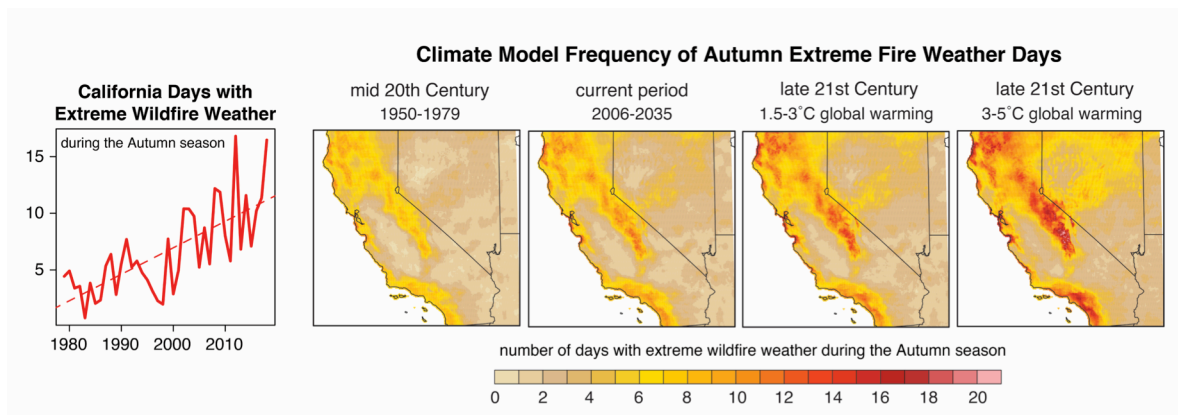
(vi) Research is needed to successfully develop and deploy the mitigation and adaptation solutions that are necessary to curb the intensification of climate extremes and the associated impacts on people and ecosystems.

We now have ample evidence that global warming has increased the risk of many kinds of climate and weather extremes (e.g., [NAS, 2016]), including extreme heat, heavy rainfall, storm-surge flooding, severe drought, and extreme wildfire conditions. And by increasing the frequency of extremes in multiple locations, climate change is increasing the odds that multiple extremes happen simultaneously, which is increasing the odds that our infrastructure and disaster management systems are stretched past their limit.

The last year has brought these accelerating risks into stark relief. While it has felt like an unrelenting string of bad luck, this is the world that global warming has created: a world in which more extreme conditions happen simultaneously, both on top of each other in a given location, and at the same time in different parts of the country and the world. And when an additional, unrelated disruption occurs – like a global respiratory pandemic – it is now much more likely to coincide with extreme climate conditions, ratcheting up the stress on our disaster response systems.

This is exactly what happened in California this summer: a dry winter was followed by a very warm spring that caused rapid snowmelt, which was followed by a record summer heat wave, leading to record- or near-record fuel loads. The heat wave was unusually humid, which led to a very unusual lightning siege, which caused hundreds of wildfires. Having so many fires burning in such flammable conditions simultaneously stretched the firefighting resources beyond their limit, resulting in more than 1 million acres burned in less than two weeks, and more than 4 million acres burned for the season, including five of the six largest wildfires in California’s recorded history.

There are now multiple lines of evidence that global warming has increased wildfire

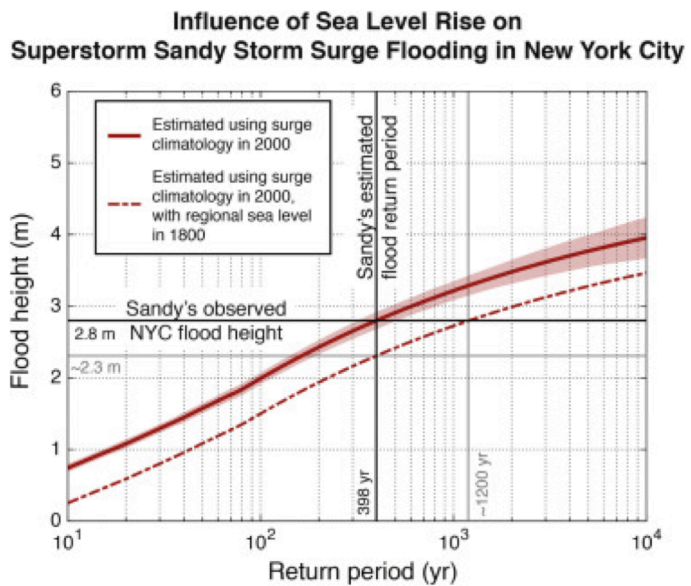


Adapted from Goss et al. (2020)

risk in California and the American West. Previous work has shown that the annual area burned has increased approximately 10-fold in the West over the past 4 decades [Duffy et al., 2019], and that rising temperatures have increased fuel loads, contributing around half of the increase in area burned [Abatzoglou and Williams, 2016]. This effect has also been prominent in California [Williams et al., 2019]. In addition, this summer my colleagues and I published a paper showing that the frequency of extreme wildfire weather has more than doubled in California during the autumn season [Goss et al., 2020]. Critically, we find that global warming is increasing the risk that periods of extreme wildfire weather overlap across far-flung regions of the state.

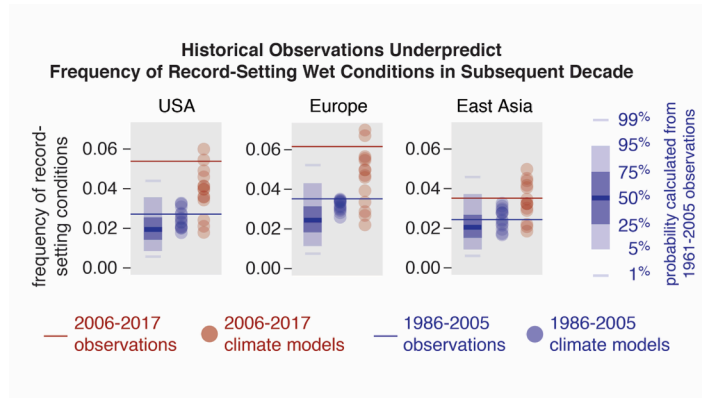
Given limited resources, many of our disaster response systems are designed to pre-stage resources in areas that are likely to experience disasters, meaning that those systems become stressed – sometimes beyond the breaking point – when multiple events occur simultaneously. And because the increasing co-occurrence of extreme events is a global phenomenon, it is creating novel challenges for our globalized economy, including our globalized risk management systems. This was made starkly clear in late 2019, when autumn wildfires in California overlapped with spring fires in Australia, stressing the limited aircraft and other resources that normally move between the hemispheres during the seasonal transition. In addition, that same combination of warm and dry conditions that increases wildfire risk has other impacts, including on our food system. Several studies, including from my research group, have shown that “bread basket” regions that are responsible for the majority of the world’s grain production are now much more likely to experience adverse growing conditions in the same year, compared with just a few decades ago [Sarhadi et al., 2018].

Recent hurricane seasons have put similar stresses on our disaster preparation and response systems. In 2017, Hurricane Harvey’s record rainfall produced one of the most expensive disasters in U.S. history. In addition, with multiple hurricanes striking the U.S. and Caribbean, there were too many landfalls for ships to transport supplies to all affected areas fast enough. The 2020 Atlantic hurricane season was even more active, with more named storms than any previous year in recorded history, and some areas – including Louisiana and Guatemala – experiencing multiple landfalls in rapid succession.



Swain et al. (2020) [adapted from Lin et al., 2016]

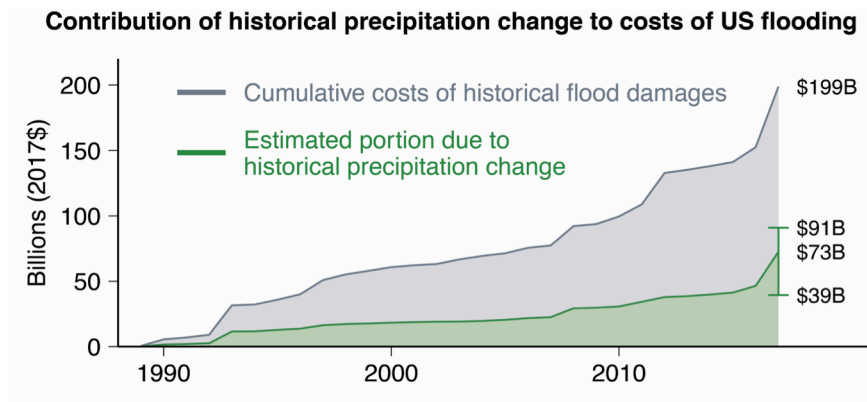
While there is still uncertainty about exactly how global warming influences the number of hurricanes, we know that the warming of the ocean increases the energy available for storms (e.g., [Emanuel, 2005; Trenberth et al., 2018]). We also know that the warming of the atmosphere has increased the likelihood that hurricanes produce extreme precipitation, like occurred during Hurricane Harvey (e.g. [Emanuel, 2017; Trenberth et al., 2018]) and Hurricane Florence in 2018 [Reed et al., 2020]. And we know that the sea level rise that has already occurred has increased the risk of extreme storm surge flooding, like what occurred in New York City during Superstorm Sandy in 2012 [Lin et al., 2016], and this season along the Gulf Coast when storms rapidly intensified before making landfall.



Adapted from Diffenbaugh (2020)

Disasters are ultimately a function of the difference between the magnitude of the hazard and the level of preparation [IPCC, 2012]. We have now crossed the threshold where the climate envelope for which so many of our systems have been designed, built and operated is exceeded with increasing frequency [Diffenbaugh, 2020] – from our disaster management systems, to our electrical grids, to our water and transportation infrastructure. Crossing that threshold means that we’re now living in a world where our status quo risk management systems are inadequate. And as a consequence, in the absence of adaptation, we can expect more big disasters to happen in more places more often, with poor and marginalized communities experiencing the greatest vulnerability.

Recent research shows that this is already costing us financially. In January, my research group published a paper documenting that historical changes in precipitation – particularly intensification of the extreme wet events – account for approximately one third of the cumulative flood damages in the U.S. over the past three decades [Davenport et al., 2021]. Using similar research methods to analyze the impact of temperature variations on aggregate economic activity, colleagues have estimated that historical warming has cost the U.S. economy approximately 5 trillion dollars within the past two

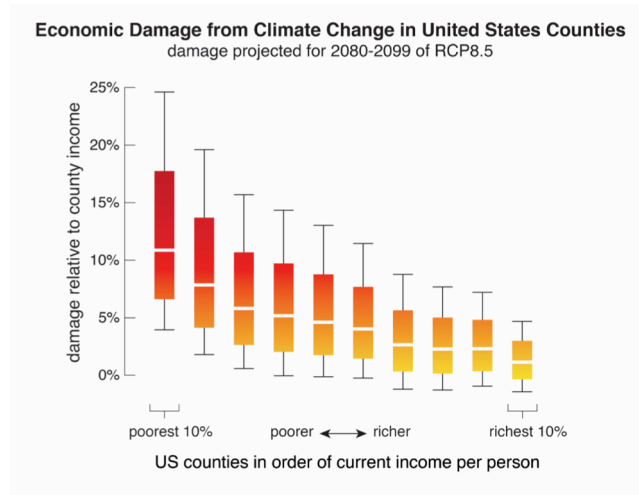


Adapted from Davenport et al. (2021)

decades [Burke and Tanutama, 2019]. These economic impacts are likely to accelerate in the U.S. at higher levels of global warming, with the poorest counties being harmed

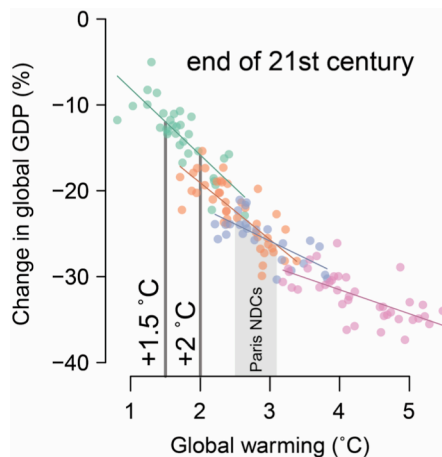
around twice as much as the richest counties, exacerbating existing economic inequality [Hsiang et al., 2017; Duffy et al., 2019].

These impacts on economic inequality are not confined to the United States. For example, my collaborator and I have documented that country-level economic inequality is approximately 25% greater today than in a counterfactual world in which historical global warming had not occurred [Diffenbaugh and Burke, 2019]. The strongest contributor has been the accumulated effects of diminished GDP growth in countries that are already warm, including our neighbors in Central and South America.



Duffy et al. (2019) [adapted from Hsiang et al., 2017]

Fortunately, there are options. Over the long-term, achieving the Paris Agreement goal of holding global warming below 2°C will substantially curb the intensification of these impacts. For example, we have evidence that the frequency of extreme conditions such as extreme heat, extreme precipitation, extreme storm surge flooding and extreme wildfire weather will increase less at 1.5 or 2°C than at 3 or 4°C (e.g., [IPCC, 2014; Diffenbaugh et al., 2018; Sarhadi et al., 2018; Allen et al., 2019; Goss et al., 2020; Davenport et al., 2021]). Likewise, in addition to substantially reducing the level of global economic damages [Burke et al., 2018], the Paris Agreement goals are also very likely to reduce the magnitude of economic damage in the poorest countries [Burke et al., 2018], and in the poorest U.S. counties (e.g., as in [Burke and Tanutama, 2019; Duffy et al., 2019]).



Adapted from Burke et al. (2018)

Therefore, in terms of reducing the risks of high-impact climate change, there is substantial benefit to achieving the Paris Agreement goals. Further, in addition to curbing the severity of climate change, many of the mechanisms that we have for reducing emissions can also increase resilience to climate stresses by providing critical energy resources to communities whose development and well-being have been hampered by energy poverty and/or pollution, and by increasing the resilience of the energy system overall. We also have opportunities to increase resilience by investing in marginalized communities,

which we know are both more vulnerable and more exposed to climate extremes. And carefully considering how and where we build – and how we preserve and manage ecosystems – as we provide for growing needs for fair and equitable housing and livelihoods is important for managing a range of climate risks, including wildfires in the West, hurricanes in the Southeast, and floods in the Midwest. And, in addition to all of these “win-win” opportunities, avoiding frequent, widespread, devastating disasters will require re-designing our infrastructure and disaster risk management around the growing likelihood that multiple unprecedented events occur simultaneously – locally, regionally and around the world.

How can we do this? In your invitation letter, you asked me to “Please include any research gaps or recommendations of additional investments in climate science that the Committee should address.” Given the unprecedented climate events that we are already facing, and the high confidence that further warming will lead to further intensification of those unprecedented conditions, the reality is that successfully managing the risks of climate change – including both the unequal impacts across society and the costs born by all Americans – will require acceleration of both mitigation and adaptation actions. We have sufficient understanding to begin that acceleration.

In addition, in order to achieve the level of mitigation that is necessary to stabilize the climate system and the level of adaptation that is necessary to respond to the further climate change that will occur, additional research is needed. In particular, a cohesive research agenda that integrates mitigation and adaptation in support of a climate-resilient nation would include the following six themes:

(i) improved observational and modeling capacity for predicting extreme events across weekly, seasonal and decadal timescales;

(ii) R&D for both the technologies and large-scale deployment necessary to transition to a secure, reliable, equitable net-zero-emissions energy system;

(iii) improved understanding of the climate impacts of “overshooting” the Paris Agreement goals, as well as the options for – and risks of – negative emissions technologies;

(iv) R&D for development, implementation and deployment of adaptation approaches across a variety of geographic, climatic and socioeconomic contexts;

(v) information, methodologies and decision support for updating the design guidelines and operational practices for our local, state and national infrastructure to be resilient in the current and future climate; and

(vi) improved understanding of how to generate synergies between mitigation, adaptation and other policy priorities such as economic growth, job creation, environmental conservation, and economic, racial and environmental justice.

In addition, the pandemic has revealed many limitations in our real-time observing systems, including critical Earth system elements such as real-time measurements of greenhouse gas emissions and the vertical structure of air pollutants in the atmosphere, as well as real-time measurements of human elements that are critical for the Earth system, such as real-time measurements of economic activity and its consequences [*Diffenbaugh et al.*, 2020].

As recent events have made painfully clear, climate change is already impacting us. Decades of objective, thorough, systematic research show that we can expect those impacts to intensify as long as global warming continues. Addressing this challenge will require both mitigation and adaptation, including the research necessary to make each of those possible.

I applaud the Committee for working on these critical issues, and thank you for the opportunity to provide this testimony. I look forward to discussing any questions that you may have.

REFERENCES

- Abatzoglou, J. T., and A. P. Williams (2016), Impact of anthropogenic climate change on wildfire across western US forests, *Proc. Natl. Acad. Sci.*, *113*(42), 11770–11775.
- Allen, M., P. Antwi-Agyei, F. Aragon-Durand, M. Babiker, P. Bertoldi, M. Bind, S. Brown, M. Buckeridge, I. Camilloni, and A. Cartwright (2019), Technical Summary: Global warming of 1.5° C. An IPCC Special Report on the impacts of global warming of 1.5° C above pre-industrial levels and related global greenhouse gas emission pathways, in the context of strengthening the global response to the thre,
- Burke, M., and V. Tanutama (2019), *Climatic constraints on aggregate economic output*, National Bureau of Economic Research.
- Burke, M., W. M. Davis, and N. S. Diffenbaugh (2018), Large potential reduction in economic damages under UN mitigation targets, *Nature*, *557*(7706), 549–553, doi:10.1038/s41586-018-0071-9.
- Davenport, F. V., M. Burke, and N. S. Diffenbaugh (2021), Contribution of historical precipitation change to US flood damages, *Proc. Natl. Acad. Sci. U. S. A.*, *118*(4), doi:10.1073/pnas.2017524118.
- Diffenbaugh, N. S. (2020), Verification of extreme event attribution: Using out-of-sample observations to assess changes in probabilities of unprecedented events, *Sci. Adv.*, *6*(12), eaay2368, doi:10.1126/sciadv.aay2368.
- Diffenbaugh, N. S., and M. Burke (2019), Global warming has increased global economic inequality, *Proc. Natl. Acad. Sci. U. S. A.*, *116*(20), doi:10.1073/pnas.1816020116.
- Diffenbaugh, N. S., D. Singh, and J. S. Mankin (2018), Unprecedented climate events: Historical changes, aspirational targets, and national commitments, *Sci. Adv.*, *4*(2), doi:10.1126/sciadv.aao3354.
- Diffenbaugh, N. S. et al. (2020), The COVID-19 lockdowns: a window into the Earth System, *Nat. Rev. Earth Environ.*, *1*, 470–481, doi:10.1038/s43017-020-0079-1.
- Duffy, P. B. et al. (2019), Strengthened scientific support for the Endangerment Finding for atmospheric greenhouse gases, *Science (80-.)*, *363*(6427), doi:10.1126/science.aat5982.
- Emanuel, K. (2005), Increasing destructiveness of tropical cyclones over the past 30 years, *Nature*, *436*(7051), 686–688.
- Emanuel, K. (2017), Assessing the present and future probability of Hurricane Harvey’s rainfall, *Proc. Natl. Acad. Sci.*, 201716222.
- Goss, M., D. L. Swain, J. T. Abatzoglou, A. Sarhadi, C. A. Kolden, A. P. Williams, and N. S. Diffenbaugh (2020), Climate change is increasing the likelihood of extreme autumn wildfire conditions across California, *Environ. Res. Lett.*, *15*(9), 94016, doi:10.1088/1748-9326/ab83a7.

- Hsiang, S., R. Kopp, A. Jina, J. Rising, M. Delgado, S. Mohan, D. J. Rasmussen, R. Muir-Wood, P. Wilson, and M. Oppenheimer (2017), Estimating economic damage from climate change in the United States, *Science* (80-.), 356(6345), 1362–1369.
- IPCC (2012), *Managing the risks of extreme events and disasters to advance climate change adaptation*, edited by C. B. Field, V. Barros, T. F. Stocker, D. Qin, D. J. Dokken, K. L. Ebi, M. D. Mastrandrea, K. J. Mach, G. K. Plattner, and S. K. Allen, Cambridge University Press, Cambridge, UK, and New York, NY, USA.
- IPCC (2014), Summary for Policymakers, in *Climate Change 2014: Impacts, Adaptation, and Vulnerability. Contribution of Working Group II to the Fifth Assessment Report of the Intergovernmental Panel on Climate Change*, edited by C. B. Field et al., pp. 1–32, Cambridge University Press, Cambridge, United Kingdom, and New York, NY, USA.
- Lin, N., R. E. Kopp, B. P. Horton, and J. P. Donnelly (2016), Hurricane Sandy’s flood frequency increasing from year 1800 to 2100, *Proc. Natl. Acad. Sci.* , 113(43), 12071–12075, doi:10.1073/pnas.1604386113.
- NAS (2016), *Attribution of Extreme Weather Events in the Context of Climate Change*, The National Academies Press, Washington, D.C.
- Reed, K. A., A. M. Stansfield, M. F. Wehner, and C. M. Zarzycki (2020), Forecasted attribution of the human influence on Hurricane Florence, *Sci. Adv.*, 6(1), eaaw9253, doi:10.1126/sciadv.aaw9253.
- Sarhadi, A., M. C. Ausín, M. P. Wiper, D. Touma, and N. S. Diffenbaugh (2018), Multidimensional risk in a nonstationary climate: Joint probability of increasingly severe warm and dry conditions, *Sci. Adv.*, 4(11), eaau3487.
- Trenberth, K. E., L. Cheng, P. Jacobs, Y. Zhang, and J. Fasullo (2018), Hurricane Harvey links to ocean heat content and climate change adaptation, *Earth’s Futur.*, 6(5), 730–744.
- Williams, A. P., J. T. Abatzoglou, A. Gershunov, J. Guzman-Morales, D. A. Bishop, J. K. Balch, and D. P. Lettenmaier (2019), Observed impacts of anthropogenic climate change on wildfire in California, *Earth’s Futur.*, 7(8), 892–910.

Primer

Attributing Extreme Events to Climate Change: A New Frontier in a Warming World

Daniel L. Swain,^{1,2,3,*} Deepti Singh,⁴ Danielle Touma,⁵ and Noah S. Diffenbaugh⁶

¹Institute of the Environment and Sustainability, University of California, Los Angeles, Los Angeles, CA, USA

²Capacity Center for Climate and Weather Extremes, National Center for Atmospheric Research, Boulder, CO, USA

³The Nature Conservancy of California, San Francisco, CA, USA

⁴School of the Environment, Washington State University, Vancouver, WA, USA

⁵Bren School of Environmental Science and Management, University of California, Santa Barbara, Santa Barbara, CA, USA

⁶Department of Earth System Science and Woods Institute for the Environment, Stanford University, Stanford, CA, USA

*Correspondence: dlswain@ucla.edu

<https://doi.org/10.1016/j.oneear.2020.05.011>

The emerging field of extreme-event attribution (EEA) seeks to answer the question: “Has climate change influenced the frequency, likelihood, and/or severity of individual extreme events?” Methodological advances over the past 15 years have transformed what was once an unanswerable hypothetical into a tractable scientific question—and for certain types of extreme events, the influence of anthropogenic climate change has emerged beyond a reasonable doubt. Several challenges remain, particularly those stemming from structural limitations in process-based climate models and the temporal and geographic limitations of historical observations. However, the growing use of large climate-model ensembles that capture natural climate variability, fine-scale simulations that better represent underlying physical processes, and the lengthening observational record could obviate some of these concerns in the near future. EEA efforts have important implications for risk perception, public policy, infrastructure design, legal liability, and climate adaptation in a warming world.

Looking beyond the Mean Climate

There is now an extremely high level of scientific confidence that human activities are the only plausible explanation for the observed $\sim 1.2^{\circ}\text{C}$ rise in global mean temperature, and a human fingerprint has likewise been found in numerous other changes in climate. However, although the mean climate is a useful metric of overall climate change, it remains a statistical construct: no place actually experiences its local mean. Moreover, the aspects of climate change that have the greatest effects on society and ecosystems—such as heatwaves, downpours, hurricanes, droughts, and wildfires—are inherently far from the mean. Therefore, to understand, mitigate, and adapt to climate changes that could harm the health and well-being of humans and ecosystems, it is imperative to understand how (and why) these climate-related extremes are changing in a warming world.

This branch of climate science, often referred to as extreme-event attribution (EEA), has evolved rapidly in recent years. This evolution has faced a number of challenges. In particular, structural limitations in process-based climate models, as well as temporal and geographic limitations of historical observations, lead to substantial challenges in quantification and validation. However, recent methodological advances, coupled with longer observational records and improved climate models, have opened the door to systematically addressing the question of whether climate change has influenced the likelihood and/or severity of individual extreme events.

Viewing Climate Change through an Extreme-Weather Lens

The news media and public often ask: “Did climate change cause this specific extreme weather event?” In a very literal

sense, the answer to such a rigidly posed question will always be “no.” All events in the dynamically coupled Earth system are ultimately the product of numerous complex, interrelated processes acting across a wide range of spatiotemporal scales. There will thus rarely (if ever) be a traceable singular cause for any specific event, and variability will always play an important role. Indeed, as recently as a decade ago, a common response from scientists was that “no single weather event can be attributed to climate change.”

Weather and climate, of course, are not the same. Weather describes variations on very short day-to-day timescales, whereas climate integrates over much longer time horizons. A key step forward in the development of EEA has been the acknowledgment that weather and climate exist on a continuum. Because climate describes the aggregate statistical properties of weather—in other words, the plausible envelope of weather conditions at a particular point in time—it encompasses not only “typical” conditions but also rare, high-magnitude weather extremes. From this perspective, understanding multi-decadal climate change can reasonably be framed as an exercise in quantifying shifts in the overall probability distribution of day-to-day weather conditions.

As a result, climate scientists have increasingly recognized that the strict question of binary causality is ill posed. Because climate is inherently a probabilistic descriptor of largely stochastic underlying weather processes, it stands to reason that scientific investigations into the influence of climate change upon extreme weather events should also be framed in probabilistic terms. Additionally, a considerable body of evidence suggests that human-caused changes in the low-probability, high-consequence “tails” of the weather distribution could be considerably different from what might be inferred from extrapolating shifts in



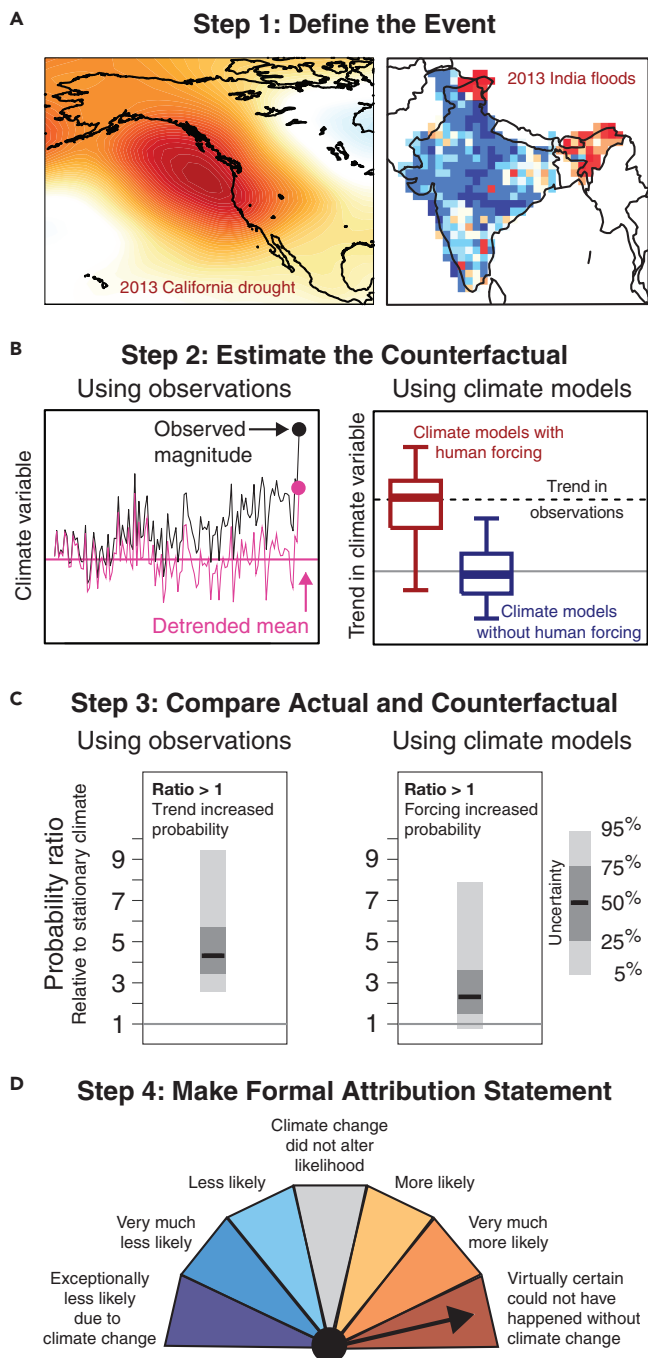


Figure 1. Four Key Steps of EEA

Illustration of the typical EEA workflow using examples from the existing literature.

(A) Define the extreme climate event, here illustrated by the magnitude of anomalous high pressure during a drought event (adapted from Swain et al., 2014, left) and of extreme precipitation during a flood event (adapted from Singh et al., 2014, right).

(B) Calculate the counterfactual climate by using real-world observations and/or climate models (adapted from Diffenbaugh et al., 2017).

(C) Compare actual and counterfactual climates, again by using real-world observations and/or climate models (adapted from Diffenbaugh et al., 2020).

(D) Make a formal attribution statement regarding whether anthropogenic climate change contributed to the likelihood and/or severity of the extreme event (adapted from Lewis et al., 2019).

the mean. Therefore, a growing number of studies have instead begun to ask a more nuanced question: “Has climate change influenced the frequency, likelihood, and/or severity of the extreme event?” This seemingly subtle shift in perspective transforms an essentially unanswerable question about absolute causality into one that is both scientifically tractable and practically actionable—and that can be directly addressed with existing observational and numerical modeling tools.

Diverse Attribution Approaches but Shared Epistemology

As the field of EEA has rapidly expanded over the past decade, different research groups have pioneered a range of novel approaches. Virtually all approaches share a common epistemology: using some combination of real-world observations, numerical climate-model simulations, and rigorous statistical techniques to separate the effects of actual human influence on the climate system from a counterfactual “climate without human influence.” It is critical to understand both this general scientific framing and the specific methodological variations because results can be strongly dependent on the assumptions and analysis techniques employed. In the sections that follow, we first outline the basic methodological steps that are shared across most EEA studies (Figure 1) and then more deeply explore the range of approaches and assumptions that have historically been employed in different contexts.

Key Steps in EEA

1. Define the event. What spatiotemporal scale and physical variable(s) best characterize the event? Given an extreme heatwave, for instance, appropriate metrics might include daily maximum temperatures for a specific city, weekly average temperatures for a region, combined heat and humidity metrics, or underlying event drivers such as the strength of the atmospheric underlying high-pressure system.
2. Estimate the “counterfactual” climate. Quantifying the influence of global warming requires quantification of the magnitude and/or likelihood of the event in a counterfactual climate without human influence. One approach is to quantify changes in the probability of the event in climate-model simulations without anthropogenic climate forcing. Alternative approaches include removing the long-term trend from the historical climate time series, using statistical relationships between the climate variable and global temperature, and using observational data from a time period with little anthropogenic influence.
3. Compare actual and counterfactual climate. Are there statistically distinguishable differences in the probability and/or severity of the event between the actual and counterfactual climates? A number of different metrics have been used, including the fractional difference in event magnitude, the ratio of event probability (often called the “risk ratio”), and the portion of the total risk contributed by anthropogenic activities (i.e., the “fraction of attributable risk”). In addition, uncertainty quantification is a critical priority for both model- and observation-focused approaches. Key sources of uncertainty include the statistical quantification of the probability of the event,

Influence of Sea Level Rise on Superstorm Sandy Storm Surge Flooding in New York City

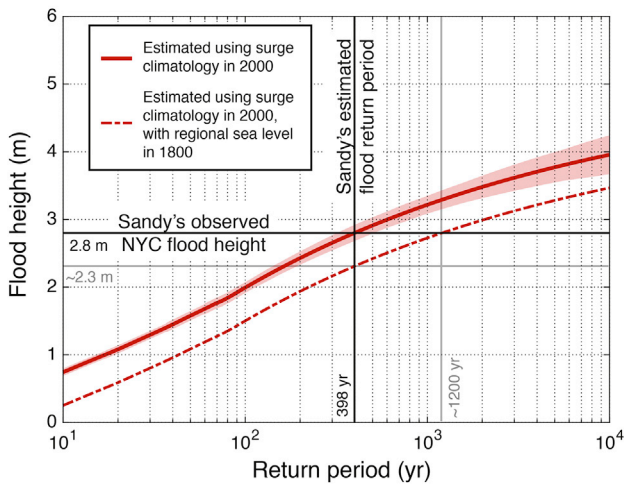


Figure 2. Example of a Conditional and Ingredient-Based EEA Assessment

Results from a conditional and ingredient-based EEA assessment of the influence of one particular aspect of climate change (sea-level rise) upon the observed level of coastal inundation during a specific historical storm event in New York City (Superstorm Sandy during October 2012). The upward and leftward shift of the red curve shows that sea-level rise increased the severity (depth) of the inundation by $\sim 20\%$ but increased the likelihood of the observed level of inundation (i.e., decreased the return period) by $\sim 300\%$. Adapted from Lin et al., 2016.

the ability of climate models to accurately simulate the observed variability of the climate variable, the magnitude of the “forced response” simulated by different climate models, and the “irreducible uncertainty” in the forced response contributed by internal climate variability.

4. Make a formal attribution statement. Most EEA approaches use a very high bar for attribution: the typical null hypothesis is that human-caused climate change did *not* influence the magnitude or probability of the event, and rejecting that null requires a “beyond a reasonable doubt” standard. If there is sufficient evidence of a statistically distinguishable difference in the actual versus counterfactual climate, the null hypothesis can be rejected, and an affirmative attribution statement can be made at a specific confidence level. Given the multiple sources of uncertainty, attribution statements often include multiple components (i.e., “there is a 95% likelihood that global warming increased the probability of the event by at least a factor of 2.86”). New frameworks have been suggested to simplify the final attribution statement (Figure 1D).

Absolute, Conditional, and “Ingredient-Based” Approaches

Initial decisions regarding how to define the event can influence the entire EEA process described in Figure 1. In addition to the decisions regarding appropriate physical metrics and spatio-temporal scales, there is also a deeper philosophical choice regarding which aspects of the event are most important and how far down the chain of complex physical causality the attribu-

tion methodology can be reasonably extended. These decisions can ultimately shape the final EEA conclusion.

Consider an attribution study focused on the coastal inundation produced by a large hurricane making landfall at some specific location. One possible approach would be to consider the full sample of all hurricanes that affected the region and ask whether there has been a change in the likelihood of flooding exceeding the observed threshold. This might be referred to as an “absolute” approach because it considers overall changes in event likelihood without accounting for the specific initial conditions (i.e., the study is not preconditioned on the fact that a large hurricane occurred at that specific location and at that specific time) or the contribution of any particular contributing factor (e.g., sea level, precipitation intensity, and storm strength). As a result, absolute approaches can complicate efforts to understand which specific aspect of climate change has contributed to changes in the probability or severity of the extreme event. For example, without methods to isolate specific conditions, it would be difficult to differentiate between contributions from sea-level rise (which increase background water levels), increasing atmospheric water-vapor content (which contributes to the precipitation intensity of a given storm), and warming ocean temperatures and decreasing vertical wind shear (both of which act to intensify hurricanes).

Another approach, often referred to as the conditional or “storyline” approach, takes certain aspects of the event conditions as given (such as the large-scale atmospheric conditions at the time of the event) and asks whether climate change has had a detectable effect upon modulating the outcome of the event. Often, such attribution studies involve perturbing a subset of relevant physical variables characterizing the state of the real-world atmosphere and/or ocean by an increment commensurate with the effect of climate change. In the hurricane example, a conditional approach might involve using the real-world atmospheric conditions from 5 days before the storm made landfall as initial conditions in a model simulation but prescribing sea surface temperatures with the anthropogenic ocean warming trend removed. A key strength is that the conditional approach can help isolate the influence of specific physical aspects of climate change. A significant weakness is that this approach cannot diagnose changes in the overall probability of the event or the probability of individual constituent physical conditions.

An alternative to the absolute and conditional frameworks is the “ingredient-based” approach (Figure 2). Here, investigators first ascertain the most essential physical conditions known to contribute to the severity of a given event and then assess changes in the probability of these conditions. This approach aims to combine some of the key strengths of the absolute and conditional approaches because it (1) enhances understanding of how anthropogenic climate change is influencing the underlying physical drivers of extreme events, including the probability that they co-occur; (2) makes no assumptions regarding the specific set of initial conditions that produced the event; and (3) potentially enables attribution of event types that are poorly simulated in climate models and/or sparsely sampled in observational datasets.

Magnitude versus Frequency Definitions

Fundamentally, two aspects of extreme events are typically assessed in attribution studies: the probability and the severity

Examples of Collective Attribution

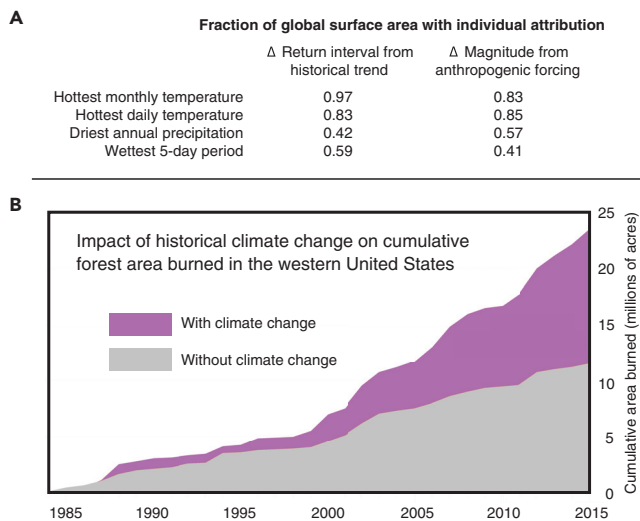


Figure 3. Example of Collective EEA Assessments

(A) Collective EEA for multiple physical event types (hot, dry, and wet events on different timescales) on a global scale with a large climate-model ensemble (adapted from Diffenbaugh et al., 2017).

(B) Collective EEA for a specific event type (wildfire risk, as measured by area burned) directly illustrates the contribution of climate change relative to a counterfactual climate without human influence (adapted from Gonzales et al., 2018).

(Figure 2). The probability of an event is often defined as a rate of exceedance of a fixed threshold defined with a historical baseline—for instance, exceeding the 99.99th quantile of daily precipitation during the years 1920–1980. Conversely, the severity of an event is often defined as a magnitude associated with a given probability, such as “design floods” that are based on the magnitude of the 100-year recurrence interval.

The probability and severity definitions can be two sides of the same analytical coin (Figure 2). However, the differences between these definitions are sometimes highly consequential for both broader communication and practical decision making. For example, regional sea-level rise over the past two centuries increased the severity of Superstorm Sandy’s flooding in New York City by 22% (from ~2.3 to ~2.8 m for an event of Sandy’s observed probability). According to the same analysis (Lin et al., 2016), that same sea-level rise tripled the probability of the observed flooding (from ~1,200- to ~400-year return period for an event of Sandy’s observed severity). In colloquial terms, a ~20% increase might sound modest, whereas a tripling sounds very large indeed—perhaps leading to a wide divergence in public perception regarding a study’s outcome.

Yet, both of these are equally valid—and statistically consistent—metrics for quantifying the role of climate change, and both are potentially useful in different contexts. The probability-based metric, for example, could be highly relevant in a civil engineering context. Given that water infrastructure ranging from drainage culverts to large dams is typically designed to accommodate events defined by fixed historical thresholds (e.g., the amount of precipitation associated with a 100-year recurrence interval), increases in the probability of exceeding the original design threshold imply increased risk that the exist-

ing design capacity could be exceeded. The magnitude-based metric, on the other hand, is of heightened relevance in a legal and public policy context—instances in which it could be important to know the fraction of known losses contributed by climate change.

Individual versus Collective Event Attribution

Another key point of distinction is the difference between individual event attribution and what can be described as “collective event attribution.” Individual event attribution seeks to answer the question: “Has global warming influenced the likelihood or severity of a specific observed historical event?” Conversely, collective event attribution seeks to answer the question: “Has global warming influenced the overall likelihood or severity of extreme events of a certain type?” (Figure 3). Individual event attribution might focus, for example, on whether the vegetation flammability in the vicinity of Paradise, California, in November 2018 (the time and location of California’s deadliest and most destructive wildfire in modern history) was made more likely or more severe by global warming. Collective event attribution, on the other hand, might focus on whether climate change has increased the overall likelihood of high vegetation flammability in the western United States (and, hence, that the record-setting vegetation flammability was “consistent with” changes that would be expected from climate change).

Recently, research groups have begun to offer “rapid response” climate attribution targeted toward real-time weather events and sometimes make a formal attribution statement before the event even takes place. Emerging methods that apply an anthropogenic signal to numerical weather forecasts enable evaluations that are highly specific to the conditions of a given individual event. In addition, rapid statements can also be predicated on precomputed metrics via collective event-attribution methodologies that use large samples of observations and climate-model simulations to evaluate a particular type of extreme.

Similar collective attribution methodologies have also been used to quantify the fraction of a region or the globe over which anthropogenic forcing has already influenced the probability of record-setting events (Figure 3) and to verify event-attribution methodologies by using out-of-sample prediction-verification frameworks.

Scientific Stumbling Blocks

Although the science of EEA has advanced dramatically since the benchmark attribution study of the 2003 European heatwave (Stott et al., 2004), several substantial challenges remain. The most prominent relate to uncertainties surrounding the creation and analysis of the counterfactual climate. Researchers have used both statistical and climate-modeling approaches to quantify the counterfactual, although there is no consensus on which of these methods is the most suitable representation of event probability or severity in the absence of human influence.

The challenge of the counterfactual is exacerbated by the fact that, in many cases, it remains difficult to estimate the event probability in the current climate. For sufficiently severe events, the existing observational record might simply be too temporally and/or geographically limited to enable robust probability quantification. One option is to use parametric curve fitting or other statistical techniques from extreme value theory to approximate the

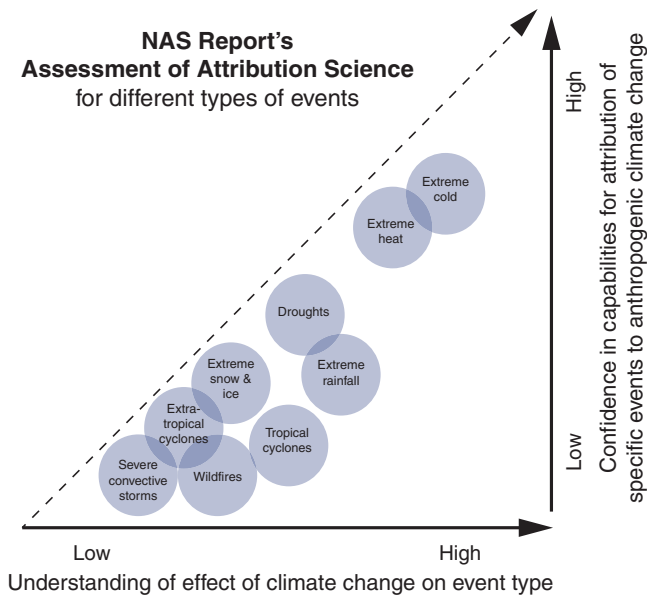


Figure 4. Confidence in EEA by Physical Event Type

Qualitative depiction of the relative levels of confidence in the ability to perform robust EEA as a function of physical event type. Such confidence varies considerably across different atmospheric and Earth system phenomena as a result of differences in understanding regarding how climate change can affect underlying drivers, as well as differences in how these processes are represented in observations and/or climate-model simulations. In general, confidence is highest for events most directly relating to temperature (such as extreme heat) and lowest for events occurring on small spatial scales (such as severe convective storms). Adapted from NASEM, 2016.

recurrence interval of the event. However, multiple studies have demonstrated that such statistical approaches are extremely sensitive to the assumed functional form of the underlying distribution and yield estimates of present-day probability that vary by orders of magnitude. Large climate-model ensembles, which offer much larger sample sizes, can help avoid the need to make such assumptions about the underlying distribution. Yet this alternative is still subject to the major caveat that present-generation climate models cannot always reliably capture the underlying physical processes responsible for certain types of events.

This caveat points to the larger question of whether climate models are fit for purpose in the context of EEA. A major challenge is the trade-off between the fine model resolution that is necessary for resolving the physical phenomena that produce certain types of extreme weather and the large ensembles and long integrations that are needed for fully characterizing internal climate-system variability and distinguish the signal of climate change. For instance, climate models are able to represent $\sim 10^3$ -km-scale high-pressure systems responsible for extreme heatwaves, but most are still too coarse to capture the full intensity and behavior of $\sim 10^2$ -km-scale tropical cyclones and face even greater challenges in simulating localized extreme precipitation events, which can occur on spatial scales that are smaller than a single global climate model grid cell. These climate-model limitations are a key reason why the level of confidence associated with EEA statements varies considerably by the type of extreme event (e.g., very high confidence for heatwaves versus only moderate confidence for tropical cyclones; Figure 4).

Together, these limitations raise the distinct possibility that studies finding no influence of climate change are simply reflecting the limitations of either the observational record or climate-modeling capabilities. A key philosophical consideration thus emerges: does an “absence of evidence” regarding the role of climate change mean that there is truly “evidence of absence”? Clarifying why it can be difficult to distinguish between these two possible interpretations of a negative attribution result is an important aspect of communicating the results of such studies to decision makers and the public.

The Way Forward

Recent developments in climate modeling and interdisciplinary Earth system science highlight the potential for rapid near-term advancement of EEA. Perhaps the most important development has been the growth of the EEA field, which has expanded the number of researchers developing, testing, and applying attribution methods to a wide variety of extreme events disrupting human and natural systems around the world. Efforts to systematically compare—and independently verify—different methods have begun to emerge. Further codification of these efforts and open access to underlying tools and data will help accelerate EEA capacity. In addition, efforts to develop clear and consistent shared language around communicating the specific characteristics or ingredients of the event being attributed, along with associated scientific uncertainties, will help the public and decision makers better understand the role of anthropogenic climate change.

Growth in supercomputing resources has enabled continued improvement in climate-model resolution, ensemble size, and integration length, allowing for increased physical realism in simulating processes that are critical in the evolution of extreme events. Indeed, targeted studies are now routinely conducted at sufficiently fine resolution that strong vertical motions—such as occur during many extreme precipitation events, severe thunderstorms, and tropical cyclones—can be explicitly represented. Although such “non-hydrostatic” simulations are still generally limited in their spatial and temporal scope, early indications are that this approach offers substantial promise for improving model representation of complex weather and climate phenomena. Similarly, the generation of multiple, single-model large ensembles (which use identical boundary forcings and model physics but perturbed initial conditions) is also a promising development for EEA because it allows for the intercomparison and refinement of predictive skill across individual model variations. It also enables more accurate quantification of the probability of an event within the context of historical climate variability, potentially offering a partial solution to the inadequacies of the existing observational record. Similarly, large “single-forcing” ensembles that isolate the influence of various anthropogenic greenhouse gases, aerosols, and land uses will help distinguish between the respective roles of potentially competing anthropogenic influences.

Given the rising public profile of climate change, the relevance of EEA for real-world applications in the legal, public-policy, and climate-adaptation arenas will only continue to increase. For example, as oil companies and other entities face potential civil liability for global warming, a key question in assigning culpability and subsequent penalties becomes whether climate change has

demonstrably increased the likelihood and/or severity of extreme events that have caused loss and damage. Likewise, observed increases in destructive extreme events have increasingly factored into public investment decisions, including infrastructure funding requirements and state and federal disaster declarations. Civil engineering and design considerations are increasingly incorporating new information about the changing characteristics of extremes in order to maintain adequate safety margins and long-term resilience in a rapidly changing world.

Ultimately, it is clear that EEA is more than just a scientific exercise to improve communication of climate risks: it requires rigorous scientific methods to directly and quantitatively address an increasingly wide range of urgent, societally relevant questions that have long-term implications for human well-being. EEA can also help individuals and decision makers make sense of contemporary disasters, helping to contextualize real-world events relative to historical points of reference and aiding in disaster preparedness and climate-adaptation activities. Indeed, as EEA plays an increasingly prominent role in shaping public perception of climate risks, it could ultimately influence collective action to avoid levels of climate change that pose unacceptable risks to human and natural systems.

ACKNOWLEDGMENTS

D.L.S. was supported by a joint collaboration between the Institute of the Environment and Sustainability at the University of California, Los Angeles, the Center for Climate and Weather Extremes at the National Center for Atmospheric Research, and the Nature Conservancy of California. N.S.D. acknowledges support from Stanford University. D.S. acknowledges support from Washington State University. D.T. acknowledges support from University of California, Santa Barbara.

RECOMMENDED READING

Angéllil, O., Stone, D., and Wehner, M. (2017). An independent assessment of anthropogenic attribution statements for recent extreme temperature and rainfall events. *J. Clim.* *30*, 5–16.

Deser, C., Lehner, F., Rodgers, K.B., Ault, T., Delworth, T.L., DiNezio, P.N., Fiore, A., Frankignoul, C., Fyfe, J.C., Horton, D.E., et al. (2020). Insights from Earth system model initial-condition large ensembles and future prospects. *Nat. Clim. Change* *10*, 277–286.

Diffenbaugh, N.S., Singh, D., Mankin, J.S., Horton, D.E., Swain, D.L., Touma, D., Charland, A., Liu, Y., Haugen, M., Tsiang, M., et al. (2017). Quantifying the influence of global warming on unprecedented extreme climate events. *Proc. Natl. Acad. Sci. U S A* *114*, 4881.

Diffenbaugh, N.S. (2020). Verification of extreme event attribution: using out-of-sample observations to assess changes in probabilities of unprecedented events. *Sci. Adv.* *6*, eaay2368.

Ekuruzel, B., Boneham, J., Dalton, M.W., Heede, R., Mera, R.J., Allen, M.R., and Frumhoff, P.C. (2017). The rise in global atmospheric CO₂, surface temperature, and sea level from emissions traced to major carbon producers. *Clim. Change* *144*, 579–590.

Gonzalez, P., Garfin, G.M., Breshears, D.D., Brooks, K.M., Brown, H.E., Elias, E.H., Gunasekara, A., Huntly, N., Maldonado, J.K., Mantua, N.J., et al. (2018). Southwest. In *Impacts, Risks, and Adaptation in the United States: Fourth National Climate Assessment, Volume II*, D.R. Reidmiller, C.W. Avery, D.R. Easterling, K.E. Kunkel, K.L.M. Lewis, T.K. Maycock, and B.C. Stewart, eds. (US Global Change Research Program), pp. 1101–1184.

Harrington, L.J., and Otto, F.E.L. (2019). Attributable damage liability in a non-linear climate. *Clim. Change* *153*, 15–20.

Haustein, K., Otto, F.E.L., Venema, V., Jacobs, P., Cowtan, K., Hausfather, Z., Way, R.G., White, B., Subramanian, A., and Schurer, A.P. (2019). A limited role for unforced internal variability in twentieth-century warming. *J. Clim.* *32*, 4893–4917.

Lewis, S.C., King, A.D., Perkins-Kirkpatrick, S.E., and Wehner, M.F. (2019). Toward calibrated language for effectively communicating the results of extreme event attribution studies. *Earth's Future* *7*, 1020–1026.

Lin, N., Kopp, R.E., Horton, B.P., and Donnelly, J.P. (2016). Hurricane Sandy's flood frequency increasing from year 1800 to 2100. *Proc. Natl. Acad. Sci. U S A* *113*, 12071–12075.

McKinnon, K.A., Poppick, A., Dunn-Sigouin, E., and Deser, C. (2017). An “observational large ensemble” to compare observed and modeled temperature trend uncertainty due to internal variability. *J. Clim.* *30*, 7585–7598.

National Academies of Sciences, Engineering, and Medicine (2016). *Attribution of Extreme Weather Events in the Context of Climate Change* (The National Academies Press). <https://doi.org/10.17226/21852>.

Otto, F.E., Massey, N., van Oldenborgh, G.J., Jones, R.G., and Allen, M.R. (2012). Reconciling two approaches to attribution of the 2010 Russian heat wave. *Geophys. Res. Lett.* *39*, <https://doi.org/10.1029/2011GL050422>.

Otto, F.E., Philip, S., Kew, S., Li, S., King, A., and Cullen, H. (2018). Attributing high-impact extreme events across timescales—a case study of four different types of events. *Clim. Change* *149*, 399–412.

Pfrommer, T., Goeschl, T., Proelss, A., Carrier, M., Lenhard, J., Martin, H., Niemeier, U., and Schmidt, H. (2019). Establishing causation in climate litigation: admissibility and reliability. *Clim. Change* *152*, 67–84.

Shepherd, T.G., Boyd, E., Calel, R.A., Chapman, S.C., Dessai, S., Dima-West, I.M., Fowler, H.J., James, R., Maraun, D., Martius, O., et al. (2018). Storylines: an alternative approach to representing uncertainty in physical aspects of climate change. *Clim. Change* *151*, 555–571.

Singh, D., Horton, D.E., Tsiang, M., Haugen, M., Ashfaq, M., Mei, R., Rastogi, D., Johnson, N.C., Charland, A., Rajaratnam, B., et al. (2014). Severe precipitation in Northern India in June 2013: causes, historical context, and changes in probability. *Bull. Am. Meteorol. Soc.* *95*, S58–S61.

Stott, P.A., Stone, D.A., and Allen, M.R. (2004). Human contribution to the European heatwave of 2003. *Nature* *432*, 610–614.

Stott, P.A., Christidis, N., Otto, F.E.L., Sun, Y., Vanderlinden, J.-P., van Oldenborgh, G.J., Vautard, R., von Storch, H., Walton, P., Yiou, P., et al. (2016). Attribution of extreme weather and climate-related events. *WIREs Clim. Change* *7*, 23–41.

Swain, D.L., Tsiang, M., Haugen, M., Singh, D., Charland, A., Rajaratnam, B., and Diffenbaugh, N.S. (2014). The extraordinary California drought of 2013/2014: character, context, and the role of climate change. *Bull. Am. Meteorol. Soc.* *95*, S3–S7.

CLIMATOLOGY

Unprecedented climate events: Historical changes, aspirational targets, and national commitments

Noah S. Diffenbaugh,^{1,2*} Deepti Singh,^{3,4} Justin S. Mankin^{3,5,6}

The United Nations Paris Agreement creates a specific need to compare consequences of cumulative emissions for pledged national commitments and aspirational targets of 1.5° to 2°C global warming. We find that humans have already increased the probability of historically unprecedented hot, warm, wet, and dry extremes, including over 50 to 90% of North America, Europe, and East Asia. Emissions consistent with national commitments are likely to cause substantial and widespread additional increases, including more than fivefold for warmest night over ~50% of Europe and >25% of East Asia and more than threefold for wettest days over >35% of North America, Europe, and East Asia. In contrast, meeting aspirational targets to keep global warming below 2°C reduces the area experiencing more than threefold increases to <10% of most regions studied. However, large areas—including >90% of North America, Europe, East Asia, and much of the tropics—still exhibit sizable increases in the probability of record-setting hot, wet, and/or dry events.

INTRODUCTION

Recognition of the proportional relationship between cumulative carbon emissions and global temperature change represents one of the most important insights of climate science during the past decade (1–3). This proportional relationship, which is seen in both the historical record and climate model simulations (3), has catalyzed a transition to international policy structures that are built around cumulative emissions (4, 5), culminating in the United Nations (UN) Paris Agreement (6). Given the structure of the Paris Agreement, there is a specific need to compare the levels of cumulative emissions identified in the nationally determined contributions (NDCs; which represent the actual country commitments) and the more aspirational targets of “aggregate emission pathways in order to hold the increase in global average temperature to well below 2°C above pre-industrial levels and to limit the temperature increase to 1.5°C above pre-industrial levels” (6).

Differences in the mean climate between the UN cumulative emissions targets and the UN cumulative emissions commitments could be large enough to affect natural and human systems (7). However, for a number of reasons, it is likely that the highest-impact differences between the UN targets and commitments will be driven by differences in the response of extreme events. First, when observing the historical record, it is clear that the most acute climate vulnerabilities are associated with extremes (8–10). These vulnerabilities are seen across human and natural systems, including both wealthy and poor communities, and both terrestrial and marine ecosystems (10). Second, assessments of the potential impacts of future climate change identify changes in the frequency and/or intensity of extremes as a primary driver of future risks (10–13). This is particularly true for smaller increases in climate forcing, where small changes in the mean can create high-impact changes in extremes (14–18). Comparing potential impacts between the UN targets and commitments therefore requires rigorous, observationally based quantification of changes in the likelihood of extremes (19–21).

Changes in various quantiles of extremes have been thoroughly explored (3, 10, 13). However, accurately quantifying the probability that

future events exceed the most extreme value found in the historical record poses unique challenges (22). For example, the magnitudes of many recent record-setting events have been particularly extreme relative to the length of available historical observations. The limited observational sample, combined with the nonstationarity of the historical time series, creates numerous challenges for quantifying the true underlying variability and hence the true probability of the record event (23). Likewise, if the UN’s aspirational targets are to be achieved, then emissions will need to be dramatically reduced over the near-term decades (24). Those near-term decadal time scales exhibit substantial ambiguity between the signal of climate forcing and the noise of climate variability, particularly on the regional and local scales at which extreme events occur (22, 25–27).

Despite these methodological challenges, the distinct risks posed by unprecedented events create a pressing need to quantify their probabilities at cumulative emissions levels consistent with the UN targets and commitments. We therefore extend the methods of Diffenbaugh *et al.* (22), who developed multiple metrics for testing the influence of global warming on the severity and probability of historically unprecedented events. However, whereas Diffenbaugh *et al.* focused exclusively on the historical period using a single climate model, we extend their methods to quantify the probability of record-setting hot, cold, wet, and dry extremes at all available observational grid points, using multiple climate models, for both historical climate forcing and future forcing windows. These future forcing windows are selected to be consistent with global warming of ~1° to 2°C and ~2° to 3°C, allowing us to quantify the differing risks of unprecedented climate extremes associated with the UN aspirational targets versus the UN NDC commitments (28).

Although numerous studies and assessments have examined the response of extreme events to changes in climate forcing (19, 29–31), our analyses expand on these previous efforts in a number of ways. First, we compare the influence of human forcing on the probability of unprecedented extremes for multiple metrics, both during the historical period and for future periods consistent with the UN cumulative emissions budgets. This comparison enables quantification of the level of adaptation—in terms of increased climate risk—that will be required if different targets are achieved and of the value—in terms of avoided climate risk—associated with different levels of emissions mitigation.

Second, previous analyses of changes in extreme events have been largely confined to changes in simulated quantile thresholds, which

Copyright © 2018
The Authors, some
rights reserved;
exclusive licensee
American Association
for the Advancement
of Science. No claim to
original U.S. Government
Works. Distributed
under a Creative
Commons Attribution
NonCommercial
License 4.0 (CC BY-NC).

Downloaded from <http://advances.sciencemag.org/> on February 14, 2018

¹Department of Earth System Science, Stanford University, Stanford, CA 94305, USA.

²Woods Institute for the Environment, Stanford University, Stanford, CA 94305, USA.

³Lamont-Doherty Earth Observatory of Columbia University, Palisades, NY 10964, USA.

⁴School of the Environment, Washington State University, Vancouver, WA 98686, USA.

⁵NASA Goddard Institute for Space Studies, New York, NY 10025, USA.

⁶Department of Geography, Dartmouth College, Hanover, NH 03755, USA.

*Corresponding author. Email: diffenbaugh@stanford.edu

often do not represent the record-setting event (19, 29–31). Our analyses provide a new quantification of uncertainty in the probability of unprecedented events that is grounded in the observed historical statistics of multiple extreme climate metrics. Because the UN emissions budgets span overlapping uncertainty in global temperature change (28), this observationally based treatment of uncertainty is particularly critical for quantifying differences in unprecedented event probabilities between the UN targets and commitments.

RESULTS

The CLIMDEX project has archived a suite of globally gridded observed and simulated extreme event indices (29, 32). We analyze eight of the CLIMDEX indices, which together provide two metrics

each for hot, cold, wet, and dry extremes [Fig. 1 and fig. S1; see Materials and Methods for descriptions of the observations and Coupled Model Intercomparison Project (CMIP5) simulations].

Across the eight extreme indices, the probability of the warmest night exhibits the most widespread response to increasing forcing, with almost half of the global-scale return interval ratios exceeding 5 for cumulative emissions consistent with 2° to 3°C of global warming (Fig. 1B). [In this case, a ratio of 5 means that cumulative emissions of ~3500 gigatons (GT) of CO₂ increase the probability of exceeding the historical maximum warmest night by a factor of 5 relative to the world without human influence.] The hottest day, mildest cold night, and mildest freeze length also exhibit substantial sensitivity, with approximately a quarter of the global-scale return interval ratios exceeding 5 for cumulative emissions consistent with 2° to 3°C (Fig. 1, A, C, and D).

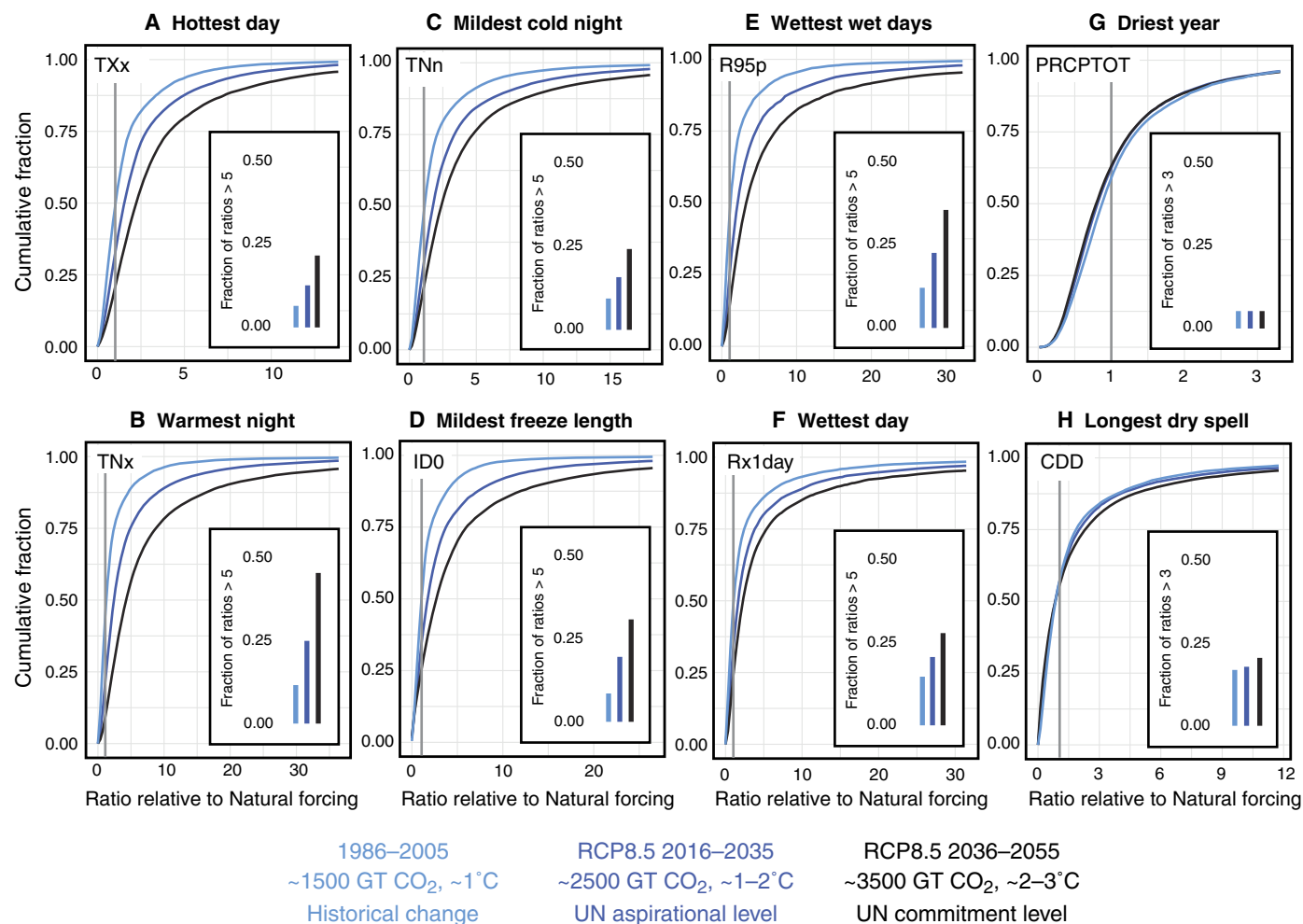


Fig. 1. The global change in probability of exceeding the historically unprecedented event at three levels of forcing. Global-scale cumulative distribution functions (CDFs) are calculated from all bootstrapped return interval ratios at all observationally available grid points for each level of anthropogenic forcing (see Materials and Methods). The horizontal axis is the change in probability calculated as the return interval ratio between the natural and anthropogenic forcing. For example, a ratio of 5 means that, in the anthropogenic forcing, the probability of exceeding the most extreme historically observed value is five times the probability in the world without human influence. The vertical axis is the cumulative fraction of all ratios calculated at all available grid points that are less than or equal to a given ratio. Insets show 1 minus the value on the vertical axis, which gives the fraction of ratios that are greater than a given ratio. For example, if a given CDF curve intersects 5 on the horizontal axis and 0.75 on the vertical axis, then 75% of all calculated return interval ratios are less than or equal to 5, and the inset will show that 25% of all calculated ratios are greater than 5. The dark gray vertical line in each panel shows where the return interval ratio between the natural and anthropogenic forcing is equal to 1, meaning that the probability of exceeding the most extreme historically observed value is equivalent in the natural and anthropogenic forcing. The three levels of anthropogenic forcing are the 1986–2005 period of the Historical simulations (~1500 GT CO₂ emitted and ~1°C of global warming above the pre-industrial), the 2016–2035 period of the RCP8.5 simulations (~2500 GT CO₂ and ~1° to 2°C), and the 2036–2055 period of the RCP8.5 simulations (~3500 GT CO₂ and ~2° to 3°C).

Wet events show more widespread sensitivity than dry events, with more than a quarter of the global-scale return interval ratios exceeding 5 for both extreme wet metrics (wettest day and wettest wet days) for cumulative emissions consistent with 2° to 3°C (Fig. 1, E and F). In contrast, although both the driest year and the longest dry spell already exhibit increases in probability in the current climate, they exhibit little additional increase in global extent for cumulative emissions consistent with either 1° to 2°C or 2° to 3°C (Fig. 1, G and H).

The historical forcing has already increased the probability of both the hottest day and the warmest night over most of the observational area (Fig. 2, A and D, and fig. S2). For the hottest day, the historical forcing has increased the probability relative to natural forcings (that is, ratios >1) for more than half of the available data points in East Asia (56.3%), more than two-thirds in North America (70.9%), and more than three-quarters in Europe (76.7%), Australia (82.4%), and southern South America (85%). The historical increases are even more widespread for the warmest night, with ≥90% of the available data points in North

America, Europe, Australia, and southern South America exhibiting ratios of >1, and almost 10% in East Asia exhibiting ratios of >3. Exceeding 2°C of global warming increases the probability of the hottest day substantially. For example, whereas less than 10% of the available data points in Europe exhibit hottest day ratios of >3 (relative to Historical) for cumulative emissions consistent with 1° to 2°C of global warming, more than half (51.7%) exhibit ratios of >3 for cumulative emissions consistent with 2° to 3°C. Similarly, in East Asia, the median hot day ratio remains below 3 (relative to Historical) for all available data points for cumulative emissions consistent with 1° to 2°C of global warming, but more than a quarter of those data points (28.6%) exhibit ratios of >3 for cumulative emissions consistent with 2° to 3°C.

The probability that the coldest events of the year become more mild also increases substantially as cumulative emissions increase (Fig. 3). Most of high-latitude Eurasia and North America have already experienced increased probability that the coldest night of the year exceeds the mildest value on record (Fig. 3A). These increases in probability intensify

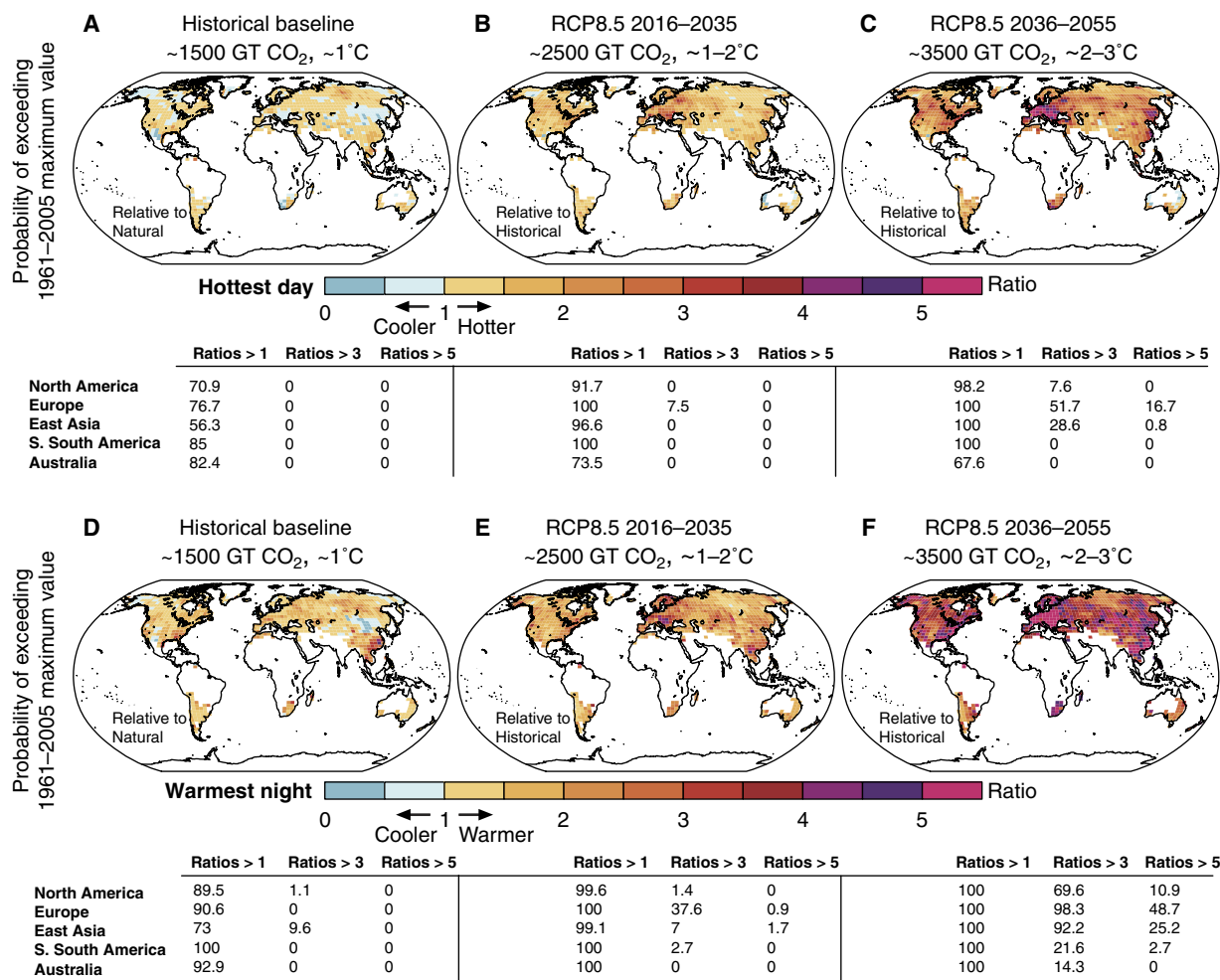


Fig. 2. The change in probability of exceeding the historically unprecedented hot event at three levels of forcing. Maps show the median value of the bootstrapped return interval ratios between the lower and higher forcing. (Full distributions for all grid points are shown in Fig. 1). For ratios reported as “relative to Natural,” the lower forcing is that for a world without human influence; for ratios reported as “relative to Historical,” the lower forcing is the combined human and natural forcing that occurred during the historical period (see Materials and Methods). (A to C) Median return interval ratio for the hottest maximum daily temperature of the year (maximum TXx value; “hottest day”). (D to F) Median return interval ratio for the warmest minimum daily temperature of the year (maximum TNx value; “warmest night”). As described in Materials and Methods, the analysis is limited to the areas with observed values in the CLIMDEX data set (missing areas shown in white; fig. S1). See fig. S2 for regional boundaries used in the regional summary calculations.

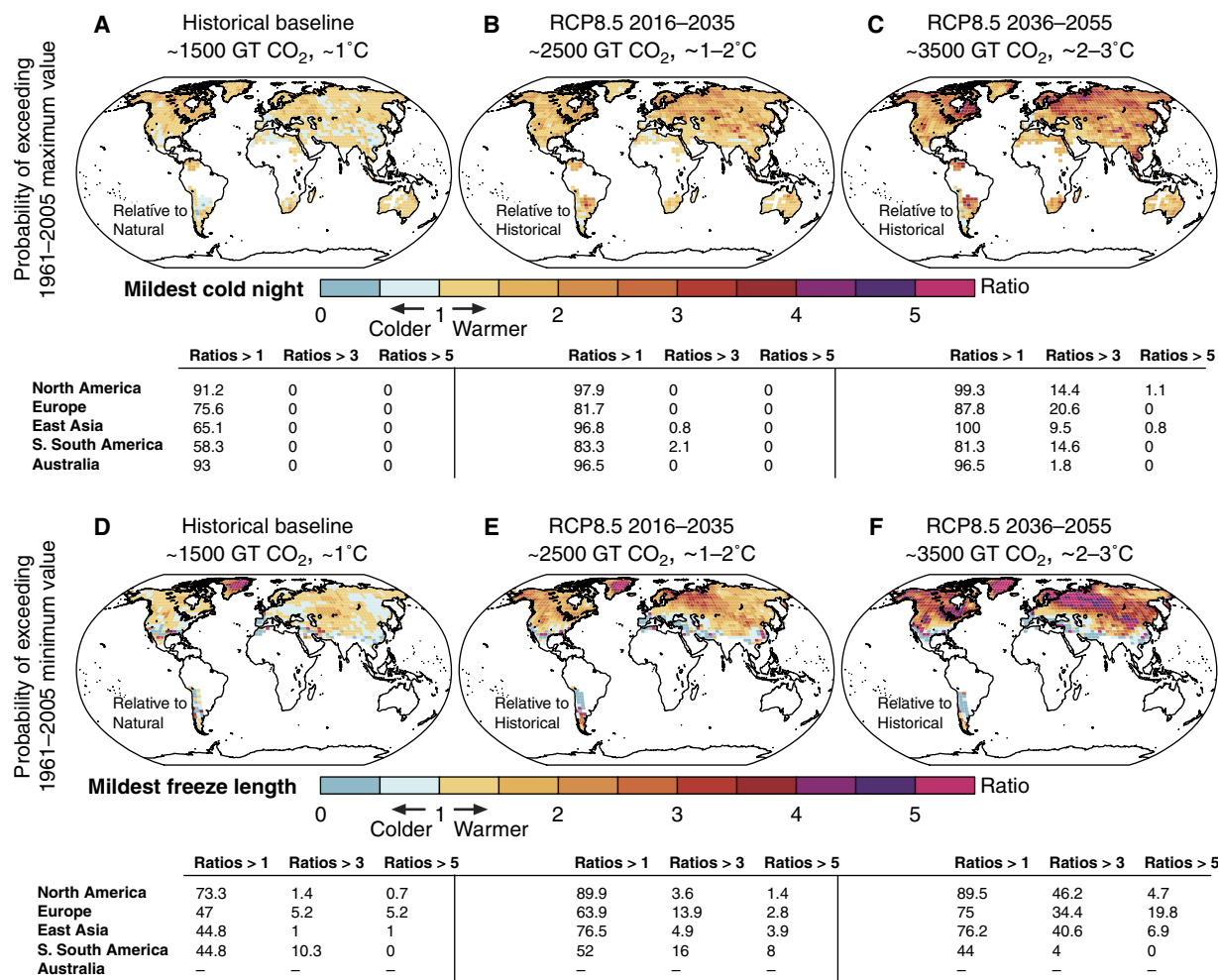


Fig. 3. The change in probability of exceeding the historically unprecedented mild cold event at three levels of forcing. As in Fig. 2, but for coldest minimum daily temperature of the year (maximum TNn value; “mildest cold night”) and number of days with maximum temperature below 0°C (minimum IDO value; “mildest freeze length”).

at higher levels of forcing, with return interval ratios of >2 (relative to Historical) for cumulative emissions consistent with 1° to 2°C of global warming (Fig. 3B), and ratios of >3 for cumulative emissions consistent with 2° to 3°C (Fig. 3C). Areas of high-latitude Eurasia and North America also exhibit particularly strong increases in the probability of the mildest freeze length, including return interval ratios of >4 (relative to Historical) over large areas of Eurasia for cumulative emissions consistent with 2° to 3°C (Fig. 3F).

As with temperature extremes, large fractions of the observed area already exhibit increased probability of record-level wet events, including ≥70% of the available data points in North America, Europe, East Asia, southern South America, and Australia for both extreme wet metrics (Fig. 4, A and D). The fraction of available points that exhibit increases in probability of record-level wet events expands for cumulative emissions consistent with 1° to 2°C of global warming (Fig. 4, B and E). However, the intensification of wet event probability is substantially greater for cumulative emissions consistent with 2° to 3°C, with 15 to 60% of the available data points in North America, Europe, East Asia, and southern South America exhibiting ratios of >3 (relative to Historical) for both metrics (Fig. 4, C and F). We note that the increases in probability are generally more substantial and widespread for the

fraction of total precipitation falling in wet days (“wettest wet days”) than for the magnitude of the wettest single day of the year (“wettest day”). This difference suggests that the risk of increasing extreme wet events is greater than what is indicated by the wettest single event and can occur across a broader range of the precipitation distribution—and therefore potentially result in more sustained wet conditions.

Compared with hot, cold, and wet events, increases in extreme dry probabilities are less widespread (Figs. 1 and 5). This discrepancy is caused primarily by the fact that substantial areas experience decreasing probability of both the driest year and the longest dry spell (Fig. 5). These areas of decreasing dry probabilities are concentrated in the high latitudes, where precipitation increases are most robust (33). However, the fact that continued increases in cumulative emissions do not cause substantial increases in extreme dry probabilities at the global scale (Fig. 1) does not mean that the probability of dry events is not responsive to increasing forcing. Large fractions of the northern and southern hemisphere mid-latitudes exhibit increasing probability of eclipsing the historically driest year and longest dry spell (Fig. 5). These include many areas that are currently heavily populated and highly vulnerable, such as the Mediterranean, southern Africa, Southeast Asia, and southern South America. Not only have increases in event probability

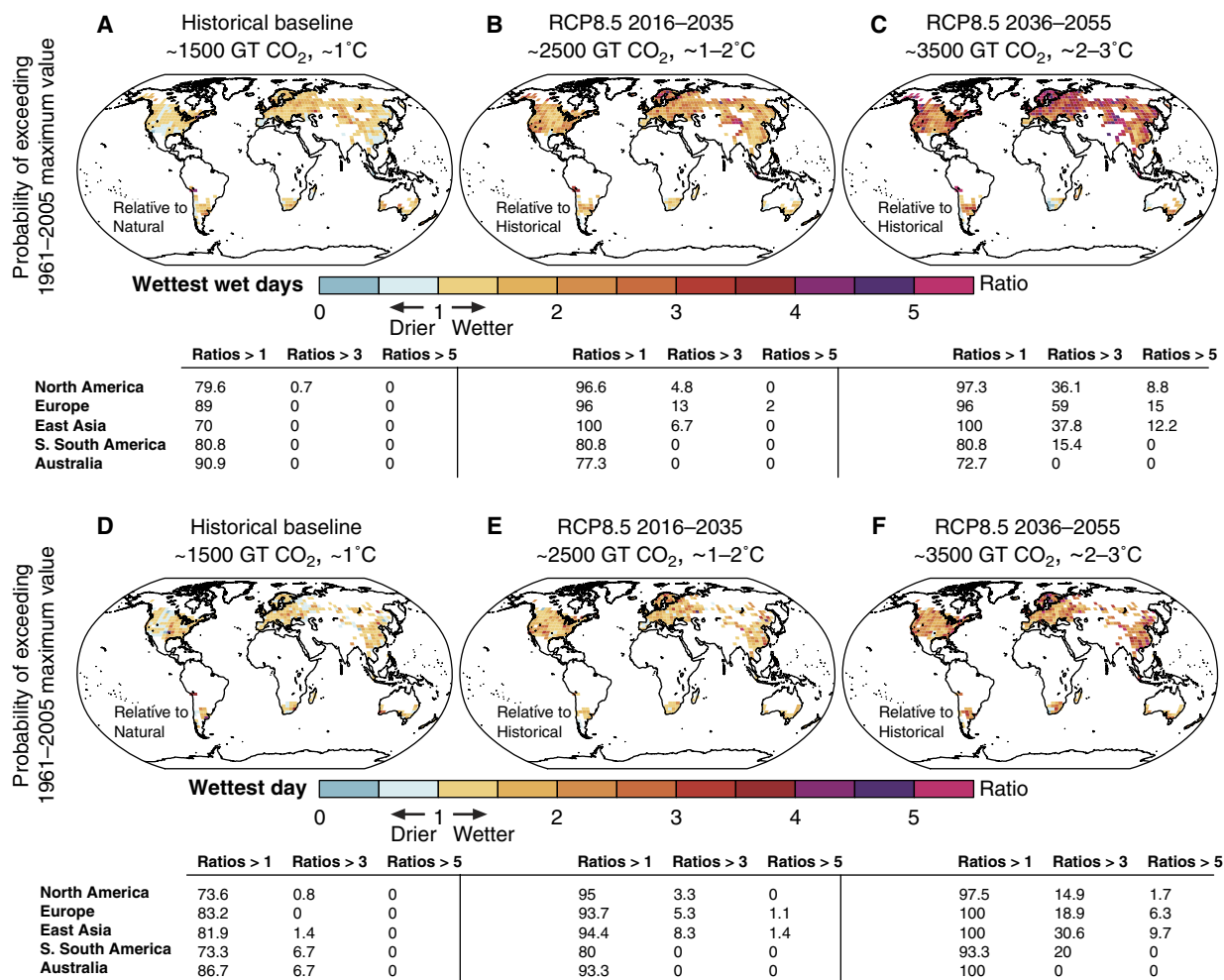


Fig. 4. The change in probability of exceeding the historically unprecedented wet event at three levels of forcing. As in Fig. 2, but for annual precipitation from days that exceed the 95th percentile (maximum R95p value; “wettest wet days”) and wettest day of the year (maximum Rx1day value; “wettest day”).

already emerged over most of these regions, but also continued emissions substantially intensify the regional increases. Regional intensification is particularly strong for the longest dry spell, with areas of North America, Europe, southern South America, and southern Africa exhibiting higher probability of record-setting events for cumulative emissions consistent with 2° to 3°C of global warming than 1° to 2°C of global warming (Fig. 5, E and F). The fact that increases in probability are generally more substantial and widespread for the longest dry spell of the year (“longest dry spell”) than for the minimum annual precipitation (“driest year”) suggests that the risk of increasing extreme dry conditions is greater at subannual than annual time scales and that the probability of prolonged dry conditions within the year can increase even if the probability of the driest year does not.

DISCUSSION

We note a number of important considerations when evaluating our results. One is that although the CMIP5 ensemble accurately simulates the observed variability of most of the extreme indices over most areas, there are areas of disagreement (fig. S1). Although our methodology does use the observed uncertainty in the probability of the record-setting event to implicitly correct errors in the climate model probability

(see Materials and Methods), the regions where the climate model ensemble does not accurately simulate the observed variability (fig. S1) should be treated with caution.

In addition, because our methodology is built around the observed statistics of each extreme climate indicator, analyses are limited to areas with observational coverage in the CLIMDEX data set (22). Areas that lack observational coverage could exhibit substantial changes in the probability of record-setting events, particularly in the tropics, where the mean warming has been large relative to the historical variability (21, 34, 35). Not only would inclusion of these areas alter the global-scale CDFs shown in Fig. 1, but also many of these areas coincide with large human populations, high human vulnerability, and/or high biodiversity, whose exposure to changing extreme event probabilities is not represented in our results due to the lack of observational coverage.

We can provide some estimation of the change in probability in these regions by calculating how often the maximum/minimum value of the CMIP5 natural forcing (“HistoricalNat”) simulations is exceeded in the CMIP5 historical and future scenarios (figs. S3 to S6). These occurrence frequencies suggest that areas lacking observational coverage are also likely to exhibit substantial increases in the probability of events that fall outside of the historical range. For example, for

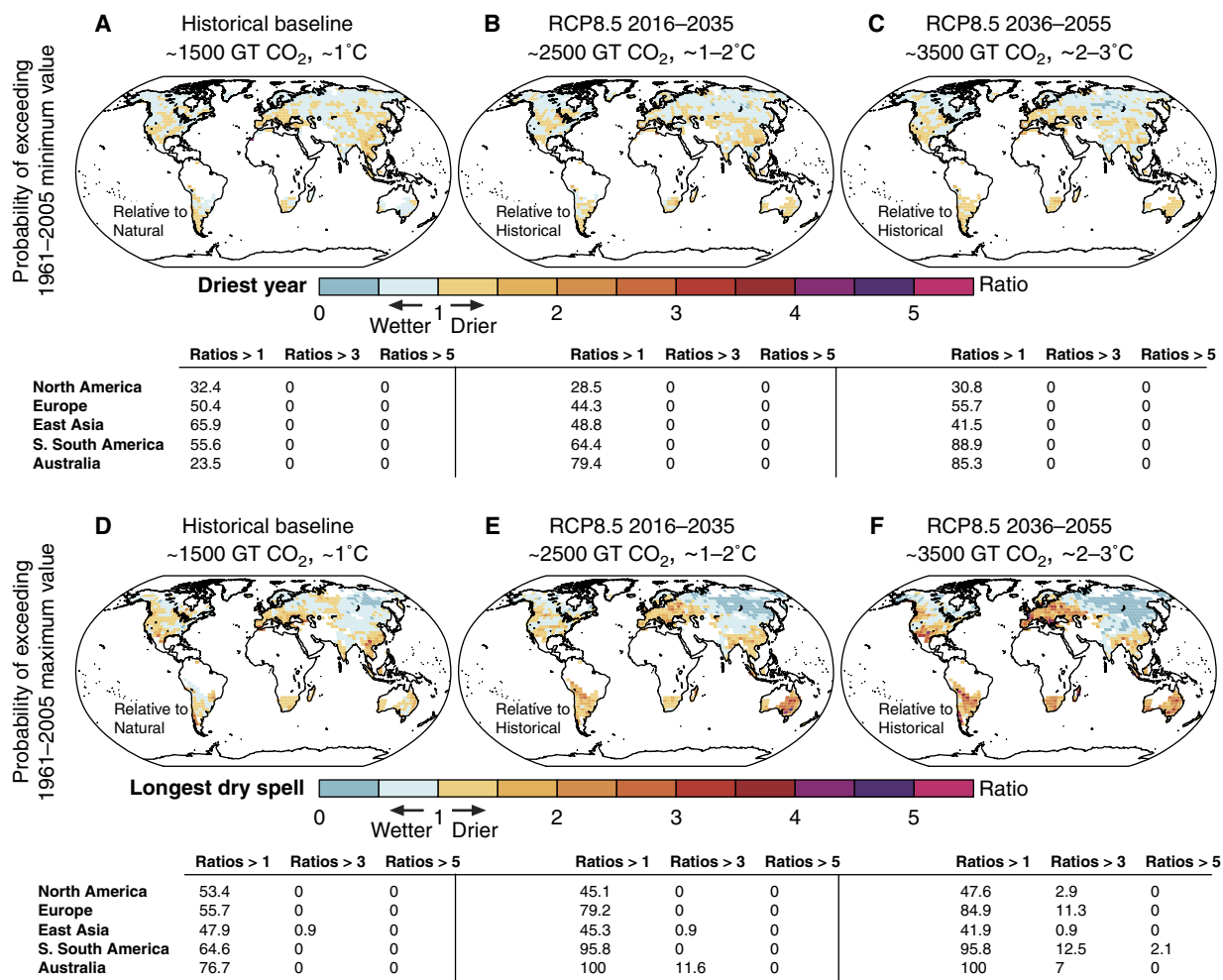


Fig. 5. The change in probability of exceeding the historically unprecedented dry event at three levels of forcing. As in Fig. 2, but for total annual precipitation (minimum PRCPTOT value; “driest year”) and longest consecutive dry spell of the year (maximum CDD value; “longest dry spell”).

cumulative emissions consistent with 2° to 3°C of global warming, the occurrence of the hottest day and wettest day is more than five times the recent historical occurrence over most of tropical South America and tropical Africa (figs. S3 and S5). Likewise, for cumulative emissions consistent with both 2° to 3°C and 1° to 2°C, the occurrence of the driest year and longest dry spell is more than three times the recent historical occurrence over substantial fractions of tropical South America and tropical Africa (fig. S6).

We also note that our analysis of cumulative emissions windows within transient climate model simulations is likely to yield conservative estimates of the ultimate climate response, because further regional climate change is likely to occur after emissions are terminated (36). The occurrence frequencies of the maximum/minimum HistoricalNat value in the CMIP5 Representative Concentration Pathway (RCP) simulations (figs. S3 to S6) provide a test of the sensitivity to the pathway of cumulative emissions. For example, the cumulative emissions are similar in RCP8.5 and RCP2.6 in the first three decades of the 21st century, after which they diverge sharply, with the mid-21st century cumulative emissions of RCP8.5 exceeding the late-21st century cumulative emissions of RCP2.6 (3). The rapid decline in annual emissions in RCP2.6 means that the global temperature remains approximately between 1° and 2.5°C above the pre-industrial for the second half of the 21st century of

RCP2.6 (3, 33). Therefore, comparison of the mid-century of RCP2.6 with the late century of RCP2.6 provides an approximation of the sensitivity of the event probability to changes in regional climate that occur after near stabilization of the global temperature. We find that the changes in occurrence between the mid- and late-century of RCP2.6 are broadly similar (figs. S3 to S6). However, a comprehensive quantification of the sensitivity of event probabilities to cumulative emissions pathway will require multiple simulations of multiple stabilization trajectories using multiple climate models.

The conservativeness of our statistical methodology is another reason that our results provide a lower bound on the probability of unprecedented climate events at different levels of forcing identified by global policy-makers. In particular, our methodology selects a parametric distribution that minimizes the return interval ratio (22). Comparing our results with the simple occurrence frequencies in the CMIP5 simulations (figs. S3 to S6) provides a comparison of our probability quantification with the kind of ensemble frequency quantification that has been used in previous studies and assessments (19, 29–31). This comparison shows that our results do exhibit smaller changes than those calculated based on thresholds from the models themselves. However, it should be reiterated that our method allows calculation of the uncertainty in the probability of the actual observed record-setting

event based on the statistics of the observed distribution (22), which is distinct from approaches that have analyzed the frequency of occurrence of the simulated quantiles (19, 29–31).

Our analyses also provide an important comparison with the historical attribution analyses of Diffenbaugh *et al.* (22). First, we extend the number of extreme event metrics from four in the study of Diffenbaugh *et al.* to eight in the current analysis. Second, whereas Diffenbaugh *et al.* did not differentiate human and natural forcings during the historical period, our analysis isolates the human component of the historical climate forcing. Third, whereas Diffenbaugh *et al.* used many realizations of a single climate model [the National Center for Atmospheric Research (NCAR) “Large Ensemble”], our analysis spans a larger range of uncertainty by analyzing results from multiple climate models.

A high priority of the proof-of-concept study of Diffenbaugh *et al.* (22) was to isolate the “irreducible uncertainty” arising from internal climate system variability. In contrast, our emphasis on quantitatively comparing historical and future changes makes spanning both internal variability and model structural uncertainty a key requirement. As shown by Diffenbaugh *et al.*, the historical global warming in the NCAR Large Ensemble falls in the lower half of the CMIP5 multimodel ensemble. Therefore, by using many climate models, our current analysis spans a far greater range of climate sensitivity, which is crucial for comparing climate risks associated with the UN targets versus the UN NDC commitments. Likewise, given the potential for systematic errors in the simulation of the atmosphere and ocean circulation to create errors in the simulated response of temperature and precipitation to changes in forcing (37, 38), the use of multiple climate models also enables our analysis to span a broader range of regional uncertainty.

CONCLUSIONS

Our results provide the first quantitative comparison of the probability of unprecedented climate events in cumulative emissions windows that are consistent with both historical changes and the UN aspirational targets and pledged national commitments. Analysis of cumulative emissions consistent with global warming of 2° to 3°C shows that the commitments outlined in the UN Paris Agreement are likely to lead to substantial and widespread increases in the probability of historically unprecedented extreme events. For example, 15 to 60% of observed locations in North America, Europe, East Asia, and southern South America exhibit return interval ratios of >3 for most of the extreme indices analyzed here. In contrast, analysis of cumulative emissions consistent with global warming of 1° to 2°C shows that achieving the more aspirational UN targets is likely to substantially limit those increases.

However, even if cumulative emissions are sufficiently constrained to ensure that global warming is held to 1° to 2°C, many areas are still likely to experience substantial increases in the probability of unprecedented events. At the global scale, hot, cold, wet, and dry extremes all exhibit prominent changes in event probability within the 2°C target, including more than fivefold increases at ~25% of the observed area for warmest night and wettest wet days and more than twofold increases at ~25% of the observed area for hottest day. These changes encompass substantial fractions of the United States, Europe, East Asia, and the southern hemisphere mid-latitudes. For example, >90% of observed locations in those regions exhibit increases in the probability of record-hot days and/or record-warm nights relative to the current climate, and 45 to 100% exhibit increases in probability of the longest dry spell. Further, although much of the tropics lack long-term observational

coverage, analyses of climate simulations indicate increases in record hot, wet, and dry events that are at least as substantial as the increases seen over the mid-latitude regions.

Together, our results suggest that the aspirational UN emissions targets are likely to yield substantial reductions in climate risk relative to the changes arising from pledged national commitments but also that those aspirational targets are likely to produce substantial—and potentially high-impact—increases in the probability of unprecedented extremes relative to the current climate.

MATERIALS AND METHODS

Observations and models

The CLIMDEX project has archived globally gridded extreme event indices for both historical observations and climate model simulations of historical and future forcing trajectories (29, 32). We analyzed eight of the CLIMDEX indices: (i) hottest maximum daily temperature of the year (TXx), (ii) warmest minimum daily temperature of the year (TNx), (iii) coldest minimum daily temperature of the year (TNn), (iv) number of days with maximum temperature below 0°C (ID0), (v) annual precipitation from days that exceed the 95th percentile (R95p), (vi) wettest day of the year (Rx1day), (vii) total annual precipitation (PRCPTOT), and (viii) longest consecutive dry spell of the year (CDD).

We applied the methods of Diffenbaugh *et al.* (22) to calculate the probability of exceeding the most extreme observed value of each of these eight indices. For these indices, “exceeding the most extreme observed value” means hotter than the maximum TXx value (“hottest day”), warmer than the maximum TNx value (“warmest night”), warmer than the maximum TNn value (“mildest cold night”), fewer days than the minimum ID0 value (“mildest freeze length”), wetter than the maximum R95p value (“wettest wet days”), wetter than the maximum Rx1day value (“wettest day”), drier than the minimum PRCPTOT value (“driest year”), and longer than the maximum CDD value (“longest dry spell”).

CLIMDEX calculated the simulated extreme event indices using output from CMIP5 (39). CLIMDEX has archived indices for the CMIP5 Historical, HistoricalNat, and RCP simulations. We analyzed the climate models for which there are matching realizations in the Historical, HistoricalNat, and RCP8.5 simulations. Following the Intergovernmental Panel on Climate Change (IPCC), we used the “r1i1p1” realization from each model (40), yielding a total of 15 realizations from 15 models.

Analysis

We followed the analysis of Diffenbaugh *et al.* (22), who compared four attribution metrics during the historical period. To extend the historical analysis of Diffenbaugh *et al.* to periods of elevated climate forcing, we focused on their fourth metric, which is the ratio of return intervals at lower and higher levels of climate forcing. (For example, an event that has a probability of 0.01—or a return interval of 100 years—in the lower forcing and a probability of 0.05—or a return interval of 20 years—in the higher forcing has a return interval ratio of 5). To account for uncertainty in the return interval of the observed record-level event, a distribution of return interval ratios was calculated at each grid point. To do so, we block bootstrapped the grid point time series at the lower and higher forcing levels to generate two distributions of return intervals; we then calculated ratios between all combinations of bootstrapped return intervals at lower and higher forcing, yielding a distribution of return interval ratios (22).

Some modifications are necessary to apply the methods of Diffenbaugh *et al.* (22) to the multimodel CMIP5 ensemble under

both historical and elevated levels of forcing. First, because CLIMDEX archived the extreme indices for the CMIP5 HistoricalNat simulations rather than the CMIP5 Pre-Industrial Control simulations, we used the HistoricalNat experiment as the “counterfactual” world without human influence. (The Pre-Industrial Control and HistoricalNat simulations are similar, but whereas the Pre-Industrial Control simulations use constant pre-industrial forcing, the HistoricalNat simulations add the volcanic and solar forcing that occurred during the historical period; the HistoricalNat simulations therefore enable isolation of the anthropogenic forcing during the historical period). We used the 1961–2005 period to calculate the return interval of the most extreme event in both the observations and the HistoricalNat simulations [see the study of Diffenbaugh *et al.* (22)].

We compared the return interval of the most extreme observed value between the HistoricalNat forcing and three anthropogenic forcing windows: the 1986–2005 period of the Historical simulations, the 2016–2035 period of the RCP8.5 simulations, and the 2036–2055 period of the RCP8.5 simulations. The 1986–2005 period of the Historical simulations is the baseline period used by the IPCC (3, 13), at the end of which there were ~1500 GT CO₂ emitted and ~1°C of global warming above the pre-industrial (3); comparing the return interval of the most extreme observed value between the HistoricalNat simulations and the 1986–2005 period of the Historical simulations quantifies the influence of historical anthropogenic forcing on the probability of the most extreme historical event. The 2016–2035 period of RCP8.5 encompasses a scenario in which there are ~2500 GT CO₂ emitted and ~1° to 2°C of global warming above the pre-industrial (3); comparing the return interval of the most extreme observed value between the 1986–2005 period of the Historical simulations and the 2016–2035 period of RCP8.5 thereby quantifies the change in event probability for a future in which the emissions and global warming targets outlined in the Paris Agreement are met. In contrast, the 2036–2055 period of RCP8.5 encompasses a scenario in which there are ~3500 GT CO₂ emitted and ~2° to 3°C of global warming above the pre-industrial (3); comparing the return interval of the most extreme observed value between the 1986–2005 period of the Historical simulations and the 2036–2055 period of RCP8.5 thereby quantifies the change in event probability for a future in which the UN NDC emissions commitments—but not the UN emissions targets—are met (3, 24, 28, 41).

We note that Millar *et al.* (42) have provided a more recent update of the cumulative emissions-temperature relationship shown in the IPCC Fifth Assessment Report (AR5). Because they are based on the same underlying CMIP5 simulations that were used to generate the findings in the IPCC AR5, the cumulative emissions windows are similar between the periods presented here and those by Millar *et al.* For example, the cumulative emissions that Millar *et al.* identify as having a 66% chance of staying below 1.5°C above the pre-industrial fall close to 2030 of RCP8.5, and the cumulative emissions that Millar *et al.* identify as having a 66% chance of staying below 0.6°C above the recent decade occur near 2040 of RCP8.5. Further, the cumulative emissions that Millar *et al.* identify as having a 66% chance of exceeding 1.1°C above the recent decade fall close to 2050 of RCP8.5.

In addition, whereas the proof-of-concept study of Diffenbaugh *et al.* (22) analyzed many realizations of a single climate model, the CLIMDEX archive contains output from many climate models but at most a few realizations of each model. Given the importance of sufficient population size for quantifying the probability of rare events (23), we pooled the CMIP5 realizations, yielding a total of 300 simulated years in each 20-year forcing period. We found that the pooled climate model output

generally agrees with the CLIMDEX observational data (that is, the *P* value using the Anderson-Darling test comparing distributions is >0.10, indicating that the null hypothesis that the simulated and observed values are drawn from the same underlying distribution cannot be rejected at the 1, 5, or 10% significance levels; fig. S1).

Note that the method of Diffenbaugh *et al.* (22) includes a bias correction step. As described by Diffenbaugh *et al.*, to evaluate each model’s simulation of interannual variability in each climate index, this bias correction is based on the differences between the detrended observations and the climate simulation without human forcings. First, the climate model mean is corrected to be equal to the observational mean (that is, by subtracting the difference between the climate model mean and the observational mean from the climate model time series). In the current analysis, we corrected each CMIP5 realization individually and then pooled the corrected data into a single “bias-corrected” CMIP5 population. This approach allows us to leverage the variability across the full CMIP5 ensemble while simultaneously controlling for the mean biases of the individual climate models. In addition, the method of Diffenbaugh *et al.* also controls for errors in the climate model variability by defining the simulated sample of event return intervals to be identical to the observed sample of event return intervals. That sample of event return intervals is then used to define the sample of event magnitudes in the pool of climate model simulations. This approach of defining the sample of simulated event magnitudes based on the sample of observed event return intervals helps to control for the effect of variability biases on event magnitudes in the tail of the simulated distribution.

SUPPLEMENTARY MATERIALS

Supplementary material for this article is available at <http://advances.sciencemag.org/cgi/content/full/4/2/eaao3354/DC1>

fig. S1. Statistical comparison of observed and simulated climate indices during the historical period.

fig. S2. Regions used in regional summary calculations.

fig. S3. Frequency of occurrence of the maximum “HistoricalNat” hot event value in the CMIP5 RCP8.5 and RCP2.6 simulations.

fig. S4. As in fig. S3, but for mild cold events.

fig. S5. As in fig. S3, but for wet events.

fig. S6. As in fig. S3, but for dry events.

REFERENCES AND NOTES

- H. D. Matthews, K. Caldeira, Stabilizing climate requires near-zero emissions. *Geophys. Res. Lett.* **35**, L04705 (2008).
- H. D. Matthews, N. P. Gillett, P. A. Stott, K. Zickfeld, The proportionality of global warming to cumulative carbon emissions. *Nature* **459**, 829–832 (2009).
- Intergovernmental Panel on Climate Change, *IPCC, 2013: Summary for Policymakers in Climate Change 2013: The Physical Science Basis. Contribution of Working Group I to the Fifth Assessment Report of the Intergovernmental Panel on Climate Change* (Cambridge Univ. Press, 2013).
- K. Zickfeld, M. Eby, H. D. Matthews, A. J. Weaver, Setting cumulative emissions targets to reduce the risk of dangerous climate change. *Proc. Natl. Acad. Sci. U.S.A.* **106**, 16129–16134 (2009).
- G. P. Peters, R. M. Andrew, S. Solomon, P. Freidlingstein, Measuring a fair and ambitious climate agreement using cumulative emissions. *Environ. Res. Lett.* **10**, 105004 (2015).
- United Nations Framework Convention on Climate Change, *Adoption of the Paris Agreement* (United Nations Framework Convention on Climate Change, 2015).
- R. Winkelmann, A. Levermann, A. Ridgwell, K. Caldeira, Combustion of available fossil fuel resources sufficient to eliminate the Antarctic Ice Sheet. *Sci. Adv.* **1**, e1500589 (2015).
- D. R. Easterling, G. A. Meehl, C. Parmesan, S. A. Changnon, T. R. Karl, L. O. Mearns, Climate extremes: Observations, modeling, and impacts. *Science* **289**, 2068–2074 (2000).

9. C. Parmesan, T. L. Root, M. R. Willig, Impacts of extreme weather and climate on terrestrial biota. *Bull. Am. Meteorol. Soc.* **81**, 443–450 (2000).
10. IPCC, *Managing the Risks of Extreme Events and Disasters to Advance Climate Change Adaptation* (Cambridge Univ. Press, 2012).
11. M. A. White, N. S. Diffenbaugh, G. V. Jones, J. S. Pal, F. Giorgi, Extreme heat reduces and shifts United States premium wine production in the 21st century. *Proc. Natl. Acad. Sci. U.S.A.* **103**, 11217–11222 (2006).
12. D. S. Battisti, R. L. Naylor, Historical warnings of future food insecurity with unprecedented seasonal heat. *Science* **323**, 240–244 (2009).
13. IPCC, Summary for policymakers, in *Climate Change 2014: Impacts, Adaptation, and Vulnerability. Part A: Global and Sectoral Aspects. Contribution of Working Group II to the Fifth Assessment Report of the Intergovernmental Panel on Climate Change*, C. B. Field, V. R. Barros, D. J. Dokken, K. J. Mach, M. D. Mastrandrea, T. E. Bilir, M. Chatterjee, K. L. Ebi, Y. O. Estrada, R. C. Genova, B. Girma, E. S. Kissel, A. N. Levy, S. MacCracken, P. R. Mastrandrea, L. L. White, Eds. (Cambridge Univ. Press, 2014), pp. 1–32.
14. N. S. Diffenbaugh, M. A. White, G. V. Jones, M. Ashfaq, Climate adaptation wedges: A case study of premium wine in the western United States. *Environ. Res. Lett.* **6**, 024024 (2011).
15. N. S. Diffenbaugh, T. W. Hertel, M. Scherer, M. Verma, Response of corn markets to climate volatility under alternative energy futures. *Nat. Clim. Change* **2**, 514–518 (2012).
16. N. S. Diffenbaugh, D. L. Swain, D. Touma, Anthropogenic warming has increased drought risk in California. *Proc. Natl. Acad. Sci. U.S.A.* **112**, 3931–3936 (2015).
17. R. M. Horton, J. S. Mankin, C. Lesk, E. Coffel, C. Raymond, A review of recent advances in research on extreme heat events. *Curr. Clim. Chang. Rep.* **2**, 242–259 (2016).
18. D. Singh, M. Tsiang, B. Rajaratnam, N. S. Diffenbaugh, Precipitation extremes over the continental United States in a transient, high-resolution, ensemble climate model experiment. *J. Geophys. Res. Atmos.* **118**, 7063–7086 (2013).
19. S. I. Seneviratne, M. G. Donat, A. J. Pitman, R. Knutti, R. L. Wilby, Allowable CO₂ emissions based on regional and impact-related climate targets. *Nature* **529**, 477–483 (2016).
20. A. Ciavarella, P. Stott, J. Lowe, Early benefits of mitigation in risk of regional climate extremes. *Nat. Clim. Change* **7**, 326–330 (2017).
21. N. S. Diffenbaugh, A. Charland, Probability of emergence of novel temperature regimes at different levels of cumulative carbon emissions. *Front. Ecol. Environ.* **14**, 418–423 (2016).
22. N. S. Diffenbaugh, D. Singh, J. S. Mankin, D. E. Horton, D. L. Swain, D. Touma, A. Charland, Y. Liu, M. Haugen, M. Tsiang, B. Rajaratnam, Quantifying the influence of global warming on unprecedented extreme climate events. *Proc. Natl. Acad. Sci. U.S.A.* **114**, 4881–4886 (2017).
23. W. K. Huang, M. L. Stein, D. J. McInerney, E. J. Moyer, Estimating changes in temperature extremes from millennial scale climate simulations using generalized extreme value (GEV) distributions. *Adv. Stat. Climatol. Meteorol. Oceanogr.* **2**, 79–103 (2016).
24. B. M. Sanderson, B. C. O'Neill, C. Tebaldi, What would it take to achieve the Paris temperature targets? *Geophys. Res. Lett.* **43**, 7133–7142 (2016).
25. E. Hawkins, R. Sutton, The potential to narrow uncertainty in regional climate predictions. *Bull. Am. Meteorol. Soc.* **90**, 1095–1107 (2009).
26. C. Deser, R. Knutti, S. Solomon, A. S. Phillips, Communication of the role of natural variability in future North American climate. *Nat. Clim. Change* **2**, 775–779 (2012).
27. J. S. Mankin, N. S. Diffenbaugh, Influence of temperature and precipitation variability on near-term snow trends. *Clim. Dyn.* **45**, 1099–1116 (2015).
28. J. Rogelj, M. den Elzen, N. Höhne, T. Fransen, H. Fekete, H. Winkler, R. Schaeffer, F. Sha, K. Riahi, M. Meinshausen, Paris Agreement climate proposals need a boost to keep warming well below 2°C. *Nature* **534**, 631–639 (2016).
29. J. Sillmann, V. V. Kharin, F. W. Zwiers, X. Zhang, D. Bronaugh, Climate extremes indices in the CMIP5 multimodel ensemble: Part 2. Future climate projections. *J. Geophys. Res. Atmos.* **118**, 2473–2493 (2013).
30. E. M. Fischer, R. Knutti, Anthropogenic contribution to global occurrence of heavy-precipitation and high-temperature extremes. *Nat. Clim. Change* **5**, 560–564 (2015).
31. M. Collins, R. Knutti, J. Arblaster, J.-L. Dufresne, T. Fichet, P. Friedlingstein, X. Gao, W. J. Gutowski, T. Johns, G. Krinner, M. Shongwe, C. Tebaldi, A. J. Weaver, M. Wehner, Long-term climate change: Projections, commitments and irreversibility, in *Climate Change 2013: The Physical Science Basis. Contribution of Working Group I to the Fifth Assessment Report of the Intergovernmental Panel on Climate Change*, T. F. Stocker, D. Qin, G.-K. Plattner, M. Tignor, S. K. Allen, J. Boschung, A. Nauels, Y. Xia, V. Bex, P. M. Midgley, Eds. (Cambridge Univ. Press, 2013).
32. J. Sillmann, V. V. Kharin, X. Zhang, F. W. Zwiers, D. Bronaugh, Climate extremes indices in the CMIP5 multimodel ensemble: Part 1. Model evaluation in the present climate. *J. Geophys. Res. Atmos.* **118**, 1716–1733 (2013).
33. N. S. Diffenbaugh, D. A. Stone, P. Thorne, F. Giorgi, B. C. Hewitson, R. G. Jones, G. J. van Oldenborgh, Cross-chapter box on the regional climate summary figures, in *Climate Change 2014: Impacts, Adaptation, and Vulnerability. Part A: Global and Sectoral Aspects. Contribution of Working Group II to the Fifth Assessment Report of the Intergovernmental Panel on Climate Change*, C. B. Field, V. R. Barros, D. J. Dokken, K. J. Mach, M. D. Mastrandrea, T. E. Bilir, M. Chatterjee, K. L. Ebi, Y. O. Estrada, R. C. Genova, B. Girma, E. S. Kissel, A. N. Levy, S. MacCracken, P. R. Mastrandrea, L. L. White, Eds. (Cambridge Univ. Press, 2014), pp. 137–141.
34. N. S. Diffenbaugh, M. Scherer, Observational and model evidence of global emergence of permanent, unprecedented heat in the 20th and 21st centuries. *Clim. Change* **107**, 615–624 (2011).
35. I. Mahlstein, R. Knutti, S. Solomon, R. W. Portmann, Early onset of significant local warming in low latitude countries. *Environ. Res. Lett.* **6**, 034009 (2011).
36. N. P. Gillett, V. K. Arora, K. Zickfeld, S. J. Marshall, W. J. Merryfield, Ongoing climate change following a complete cessation of carbon dioxide emissions. *Nat. Geosci.* **4**, 83–87 (2011).
37. M. Ashfaq, C. B. Skinner, N. S. Diffenbaugh, Influence of SST biases on future climate change projections. *Clim. Dyn.* **36**, 1303–1319 (2010).
38. I. R. Simpson, R. Seager, M. Ting, T. A. Shaw, Causes of change in Northern Hemisphere winter meridional winds and regional hydroclimate. *Nat. Clim. Change* **6**, 65–70 (2015).
39. K. E. Taylor, R. J. Stouffer, G. A. Meehl, An overview of CMIP5 and the experiment design. *Bull. Am. Meteorol. Soc.* **93**, 485–498 (2012).
40. IPCC, in *Climate Change 2013: The Physical Science Basis. Contribution of Working Group I to the Fifth Assessment Report of the Intergovernmental Panel on Climate Change* (Cambridge Univ. Press, 2013), pp. 1311–1394.
41. A. A. Fawcett, G. C. Iyer, L. E. Clarke, J. A. Edmonds, N. E. Hultman, H. C. McJeon, J. Rogelj, R. Schuler, J. Alsalam, G. R. Asrar, J. Creason, M. Jeong, J. McFarland, A. Mundra, W. Shi, Can Paris pledges avert severe climate change? *Science* **350**, 1168–1169 (2015).
42. R. J. Millar, J. S. Fuglested, P. Friedlingstein, J. Rogelj, M. J. Grubb, H. D. Matthews, R. B. Skeie, P. M. Forster, D. J. Frame, M. R. Allen, Emission budgets and pathways consistent with limiting warming to 1.5°C. *Nat. Geosci.* **10**, 741–747 (2017).

Acknowledgments: We thank Y. Liu for assistance with the data analysis. We thank CLIMDEX for calculating and archiving the observed and simulated extreme event indices. We acknowledge the World Climate Research Programme's Working Group on Coupled Modelling, which is responsible for CMIP, and we thank the climate modeling groups for producing and making available their model output. Computational facilities were provided by Center for Computational Earth and Environmental Science and Stanford Research Computing Center at Stanford University. Lamont contribution #8183. **Funding:** We acknowledge funding support from the School of Earth, Energy & Environmental Sciences and the Woods Institute for the Environment at Stanford University; the Earth Institute and Lamont-Doherty Earth Observatory of Columbia University; and the U.S. Department of Energy. **Author contributions:** N.S.D. designed the analysis, analyzed data, interpreted results, and wrote the paper. D.S. and J.S.M. contributed to the design of the analysis, interpretation of results, and writing of the paper. **Competing interests:** The authors declare that they have no competing interests. **Data and materials availability:** All data needed to evaluate the conclusions in the paper are present in the paper and/or the Supplementary Materials or are available from the CLIMDEX archive.

Submitted 9 July 2017

Accepted 12 January 2018

Published 14 February 2018

10.1126/sciadv.aao3354

Citation: N. S. Diffenbaugh, D. Singh, J. S. Mankin, Unprecedented climate events: Historical changes, aspirational targets, and national commitments. *Sci. Adv.* **4**, eao3354 (2018).

Unprecedented climate events: Historical changes, aspirational targets, and national commitments

Noah S. Diffenbaugh, Deepti Singh and Justin S. Mankin

Sci Adv 4 (2), eaao3354.
DOI: 10.1126/sciadv.aao3354

ARTICLE TOOLS	http://advances.sciencemag.org/content/4/2/eaao3354
SUPPLEMENTARY MATERIALS	http://advances.sciencemag.org/content/suppl/2018/02/12/4.2.eaao3354.DC1
REFERENCES	This article cites 35 articles, 8 of which you can access for free http://advances.sciencemag.org/content/4/2/eaao3354#BIBL
PERMISSIONS	http://www.sciencemag.org/help/reprints-and-permissions

Use of this article is subject to the [Terms of Service](#)

Science Advances (ISSN 2375-2548) is published by the American Association for the Advancement of Science, 1200 New York Avenue NW, Washington, DC 20005. 2017 © The Authors, some rights reserved; exclusive licensee American Association for the Advancement of Science. No claim to original U.S. Government Works. The title *Science Advances* is a registered trademark of AAAS.

CLIMATOLOGY

Verification of extreme event attribution: Using out-of-sample observations to assess changes in probabilities of unprecedented events

Noah S. Diffenbaugh^{1,2*}

Independent verification of anthropogenic influence on specific extreme climate events remains elusive. This study presents a framework for such verification. This framework reveals that previously published results based on a 1961–2005 attribution period frequently underestimate the influence of global warming on the probability of unprecedented extremes during the 2006–2017 period. This underestimation is particularly pronounced for hot and wet events, with greater uncertainty for dry events. The underestimation is reflected in discrepancies between probabilities predicted during the attribution period and frequencies observed during the out-of-sample verification period. These discrepancies are most explained by increases in climate forcing between the attribution and verification periods, suggesting that 21st-century global warming has substantially increased the probability of unprecedented hot and wet events. Hence, the use of temporally lagged periods for attribution—and, more broadly, for extreme event probability quantification—can cause underestimation of historical impacts, and current and future risks.

INTRODUCTION

The field of extreme event attribution has burgeoned since the seminal work of Stott *et al.* (1). In that time, numerous event attribution frameworks have been developed (2). Although there is heterogeneity in the design of these frameworks, most use a combination of instrumental observations and climate model simulations to quantify the influence of historical anthropogenic climate forcing on the probability and/or severity of individual events. The purpose of this study is to examine whether independent “out-of-sample” observations can be used to assess the accuracy of changes in extreme event return intervals that are either explicitly or implicitly predicted by attribution frameworks.

Since Stott *et al.* (1), attribution analyses have been published for many types of events (2), including heatwaves [e.g., (3–8)], cold snaps [e.g., (3, 5, 9)], heavy rainfall [e.g., (3–6, 10)], floods [e.g., (11)], droughts [e.g., (12)], tropical cyclone precipitation [e.g., (13, 14)], storm surge flooding [e.g., (15)], and extremely low Arctic sea ice [e.g., (4, 16)]. In addition, event attribution frameworks have been applied to the underlying physical causes of extremes (2, 17, 18), including atmospheric circulation patterns [e.g., (4, 19–22)], atmospheric water vapor (4), ocean heat content (23), and wildfire risk factors [e.g., (24)]. In recent years, attribution analyses have been applied increasingly quickly following an event [e.g., (10, 25)], with some techniques using forecasts generated before the event [e.g., (26, 27)]. “Precomputed” approaches (7) have likewise been used to quantify the influence of global warming on a particular type of event at each area of the globe, using observational data (4, 28), climate model simulations (6, 7), or a combination of the two (4, 5).

Independent verification of event attribution poses a particular challenge. In addition to the reliability of observational data and climate model simulations [e.g., (29, 30)], there are fundamental questions about the appropriate scientific framing through which causation

can be measured [e.g., (2, 31–34)]. One inherent challenge is that single event attribution is conducted for conditions at one specific place and time; the event only occurs once, and by construction, the attribution quantification pertains only to that event. Further, because extreme events are by definition rare, the available population of events with which to independently verify attribution results is limited, a challenge that is exacerbated for events that are unprecedented in the observational record.

One approach to resolving these challenges is to frame the attribution result as a falsifiable prediction, and then test that prediction using independent observations. Such an approach draws on the many aspects of climate and weather research that routinely use independent verification. For example, daily- and seasonal-scale forecasts are verified after the forecast period has passed [e.g., (35)]. This forecast verification includes daily fields such as temperature, precipitation, and winds, as well as extreme event phenomena such as tropical cyclones, severe thunderstorms, and river and storm surge flooding. Further, scientists have been making long-term climate projections for decades (36, 37). Older projections can be verified using current observations [e.g., (38)], and such comparisons are now made for global temperature anomalies in quasi-real time.

It is important to emphasize the distinction between verification of falsifiable predictions and evaluation of methodological uncertainty. Researchers have for years taken great care to thoroughly evaluate various aspects of uncertainty within climate attribution systems (2). This includes (i) assessing the robustness of the observational record and the fidelity of climate model simulations for different types of events [e.g., (2–4, 30)]; (ii) quantifying uncertainty in the climate model simulations, including the sensitivity to historical emissions (4), the ability to simulate the statistical properties of the historical observations [e.g., (4, 21, 39, 40)], and the ability to simulate the underlying physical processes that cause different types of events [e.g., (21, 41)]; (iii) quantifying uncertainty in the statistical analysis, including the appropriateness of the underlying statistical assumptions (4, 42–45); and (iv) applying different attribution methodologies to the same event (4, 16, 46, 47), including systematic

Copyright © 2020
The Authors, some
rights reserved;
exclusive licensee
American Association
for the Advancement
of Science. No claim to
original U.S. Government
Works. Distributed
under a Creative
Commons Attribution
NonCommercial
License 4.0 (CC BY-NC).

Downloaded from <http://advances.sciencemag.org/> on March 18, 2020

¹Department of Earth System Science, Stanford University, Stanford, CA, USA.

²Woods Institute for the Environment, Stanford University, Stanford, CA, USA.

*Corresponding author. Email: difflenbaugh@stanford.edu

reanalysis of multiple published results (3, 33). However, despite this emphasis on uncertainty quantification, independent observational verification of specific, quantitative attribution results remains elusive.

Central to the analysis presented in this study is the idea that attribution results that are generated from estimates of return intervals in previous historical time periods can be verified using the frequency of extreme events that occur over large geographic domains during subsequent, multi-year, out-of-sample time periods (see Materials and Methods). For example, many attribution analyses have used global climate model simulations from the Coupled Model Inter-comparison Project (CMIP5) [e.g., (4–8, 20, 38)]. Because the CMIP5 Historical and Natural simulations were only run through 2005 (48, 49), simulations using the actual climate forcings do not cover the most recent period of observations. Attribution analyses that use CMIP5 can thus either restrict the historical analyses to this pre-2006 period [e.g., (4–6, 12, 20)] or use the early period of the CMIP5 future projections to extend the historical simulations (in which case the anthropogenic and non-anthropogenic simulations cover different time periods) [e.g., (8, 38)]. In the case of previously published global attribution analyses, which used the CMIP5 Historical and Natural simulations to quantify the influence of historical forcing on the probability of unprecedented hot, wet, and dry extremes at each area of the globe, the attribution analysis was limited to the pre-2006 period (5). However, this limitation also presents an opportunity, because the frequency of record-setting events during 2006–2017 can now be used to independently verify the published results that used data from 1961 to 2005.

Previous global attribution analyses (4) examined four different attribution metrics: (i) the contribution of the observed trend to the event magnitude, (ii) the contribution of the observed trend to the event probability, (iii) the probability of the observed trend in the historical forcing, and (iv) the contribution of the historical forcing to the event probability. This work was recently extended (5), using CMIP5 data to quantify the fourth metric for natural and anthropogenic forcing during the historical period, and for future levels of forcing consistent with the United Nations Paris Agreement goals and commitments.

The current study focuses on verifying the second and fourth metrics using out-of-sample observations. The contribution of historical climate change to the event probability is measured using an “attribution ratio” (AR), which is calculated as the ratio between the return interval in a counterfactual world without climate change and the return interval in the actual observed world with climate change (4, 5). For the contribution of the observed trend to the event probability, observational data are used to estimate the return intervals of extreme events, with the attribution ratio (AR_{Obs-dt}) calculated from the return interval in the actual time series (RI_{Obs}) and the return interval in the detrended time series (RI_{Obs-dt})

$$AR_{Obs-dt} = (RI_{Obs-dt}) \div (RI_{Obs})$$

For the contribution of the historical forcing to the event probability, observational data are used to correct systematic biases in the climate model simulations, which are then used to estimate the change in return intervals under historical (HIST) and natural (NAT) climate forcing

$$AR_{Forcing} = (RI_{Obs-dt}) \div (RI_{(HIST-NAT) + Obs-dt})$$

An attribution ratio of 1 indicates equal probability with and without global warming. Because return intervals are the inverse of event probabilities, larger ratios indicate greater influence of global warming (e.g., a ratio of 2 indicates that the probability of an event is twice as large with global warming). Block bootstrapping of the time series at each location is used to quantify a distribution describing the uncertainty in the event probabilities at each location (4, 5).

The present study is focused on two objectives. The first phase of the analysis uses specific, previously published predictions to demonstrate the framework for verifying extreme event attribution results. Independent data (i.e., observations over the 2006–2017 time period) are used to derive the return intervals of unprecedented events over different regions, based on the regional frequency of record-setting events. These out-of-sample return intervals are then compared with the regional-mean distributions of return intervals (e.g., 5th, 25th, 50th, 75th, and 95th percentiles) that were predicted from the detrended 1961–2005 observational data at each grid point in the region. The ratio is referred to as a “verification ratio” (VR)

$$VR_{Obs:2006-2017} = RI_{Obs-dt:1961-2005} \div RI_{Obs:2006-2017}$$

where $RI_{Obs-dt:1961-2005}$ is the regional-mean of the return intervals in the detrended 1961–2005 time series at each grid point, and $RI_{Obs:2006-2017}$ is the regional-mean return interval implied by the frequency of record-setting events in the region during the out-of-sample 2006–2017 verification period. These verification ratios are compared with attribution ratios that quantify the contribution of historical climate change during the 1961–2005 attribution period, calculated from both the observational record (AR_{Obs-dt}) and the CMIP5 global climate model ensemble ($AR_{Forcing}$). Thus, by construction, the out-of-sample comparison tests the stability of the attribution results over time, within the context of a nonstationary climate.

The second phase of the analysis attempts to understand discrepancies between the verification and attribution ratios. This analysis tests whether any such discrepancies are due to structural mismatches between the attribution and verification methods. It also tests whether there have been changes in the frequency of record-setting events between the attribution and verification periods, and whether any changes are due primarily to external climate forcing or to internal climate variability. Understanding discrepancies in the predicted probabilities of record-setting events and the actual out-of-sample occurrence is important not only for verifying extreme event attribution but also for evaluating the durability of design and planning guidelines that use similar return interval quantification when conducting risk analysis (such as for infrastructure design, land use planning, and disaster management).

In principle, this verification framework could be applied to any type of extreme event. The focus of this initial application is on events that are unprecedented in the baseline historical period (1961–2005). Unprecedented events pose important challenges for event attribution (4). First, statistical uncertainty increases as values reach further into the tails of the distribution. Events that fall outside of the historical range are, by definition, in the extreme tail, amplifying the challenges posed by small samples. Second, climate change is increasing the probability of unprecedented events (4). Quantifying the effects of this nonstationarity is a general challenge for risk assessment [e.g., (50, 51)] and poses specific challenges for event attribution (4). Third, climate models are the only available tool for systematically testing the influence of global warming on the physical processes that

shape extremes, making climate models a necessary component of event attribution frameworks (2). However, because historically unprecedented events often arise from rare combinations of physical ingredients, they generally pose the greatest challenge for accurate climate model simulation (2, 17, 18, 30).

Despite these potential barriers, events that fall outside of the historical experience are critical for a suite of design and management decisions [e.g., (50, 52–54)], as well as climate change mitigation and adaptation considerations [e.g., (4, 5, 54, 55)]. Given both the societal relevance and methodological challenges, this initial verification study focuses on the attribution of events that are unprecedented in the historical observations.

RESULTS

The regional verification ratios for 2006–2017 frequently exceed the published attribution ratios calculated from the 1961–2005 data (Fig. 1), suggesting that the attribution framework underestimates the influence of historical global warming. For example, for the influence of anthropogenic forcing, the median attribution ratio is less than 2.0 for all three extreme indices (hottest days, wettest days, and longest dry spell) over the United States, Europe, and East Asia. In contrast, the median verification ratio for the hottest days exceeds 4.0 over Europe and 2.5 over East Asia, with >95% of the verification ratio distribution exceeding the median attribution ratio. Likewise, the median verification ratio for the wettest days exceeds 3.0 over the United States and Europe, with >95% of the verification ratio distribution again exceeding the median attribution ratio.

Although the trend-based attribution ratio is generally larger than the forcing-based attribution ratio (Fig. 1), the verification ratio for 2006–2017 still frequently exceeds the trend-based attribution ratio (Fig. 1). For example, for the hottest days, >95% of the verification ratio distribution exceeds the median trend-based attribution ratio over Europe, and ~75% exceeds the median trend-based attribution ratio over East Asia. Similarly, for the wettest days, >95% of the verification ratio distribution exceeds the median trend-based attribution ratio over the United States and Europe.

In a number of cases, the median values of both the attribution and verification ratios are close to 1.0 (Fig. 1). For the hottest days, both the forcing- and trend-based attribution ratios exhibit median values just above 1.0 over the United States, while the median verification ratio is just below 1.0. Likewise, for the longest dry spells, the attribution and verification ratios are near 1.0 over the United States, Europe, and East Asia. In these cases, the range of values is larger for the attribution ratios than for the verification ratios, including greater likelihood of large increases in extreme event probability. However, the attribution and verification distributions largely overlap.

The discrepancies between the attribution and verification ratios for record-setting events (Fig. 1) are reflected in discrepancies between the probabilities predicted from the 1961–2005 observations and the frequencies observed in 2006–2017. For example, the 2006–2017 frequency of record-setting hottest days exceeds the 99th percentile of predicted probabilities over both Europe and East Asia (Fig. 2). Similarly, the 2006–2017 frequency of record-setting wettest days exceeds the 99th percentile of predicted probabilities over both the United States and Europe (Fig. 3). Further, in cases where the discrepancies between the verification and attribution ratios are less pronounced, such as the hottest days over the United States and wettest

Verification of anthropogenic influence on exceedance of 1961–2005 record using the 2006–2017 period

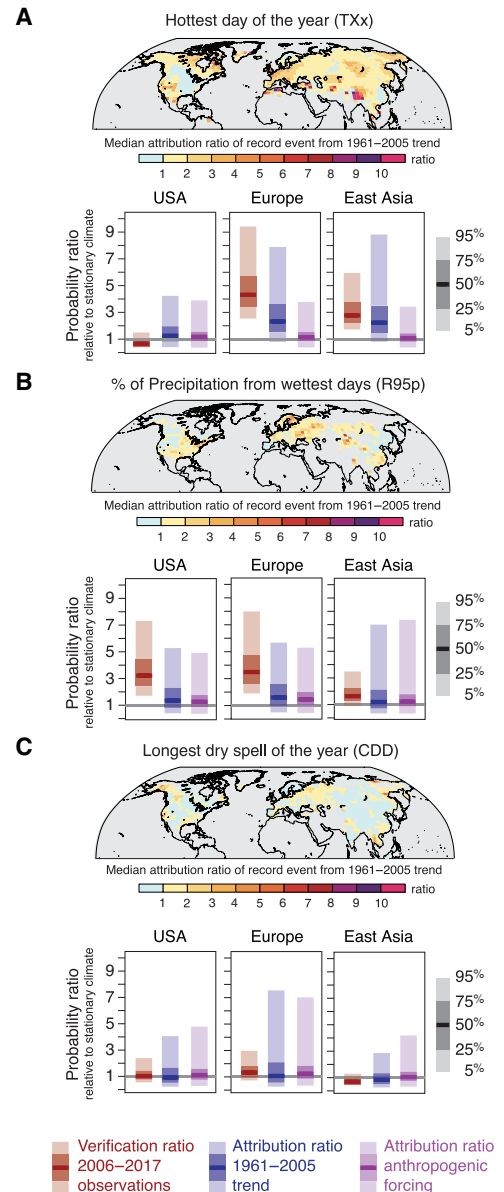


Fig. 1. Verification of the anthropogenic influence on unprecedented hot, wet, and dry events. The verification framework is based on the probability, during the out-of-sample verification period (2006–2017), of exceeding the most extreme value found in the period for which the attribution metrics were calculated (1961–2005). The framework is used to verify the attribution metrics published in (4) and (5), for (A) hottest day of the year (TXx), (B) percentage of annual precipitation falling in days that are wetter than the 95th percentile of the 1961–1990 period (R95p), and (C) longest consecutive dry spell of the year (CDD). Maps show the median attribution ratio calculated from the 1961–2005 trend at each northern hemisphere grid point for which there are continuous data in the CLIMDEX dataset (see Materials and Methods). The blue distribution shows the uncertainty in the attribution ratio calculated from the 1961–2005 trend (i.e., the metric shown in the map) over the United States, Europe, and East Asia. The purple distribution shows the uncertainty in the regional attribution ratio calculated from anthropogenic climate forcing. The red distribution shows the uncertainty in the regional verification ratio calculated from the 2006–2017 observations. Uncertainty in each ratio is depicted by the 5th, 25th, 50th, 75th, and 95th percentile values of the bootstrapping described in (4) and (5).

days over East Asia (Fig. 1), the 2006–2017 frequency still falls in the tail of predicted probabilities (Figs. 2 and 3).

There are at least two possible explanations for these discrepancies between the probabilities predicted during the attribution period (1961–2005) and the frequencies observed during the verification period (2006–2017). The first possibility is a structural discrepancy in the comparison, such as if the regional-mean of the probabilities calculated from the 1961–2005 grid-point time series did not accurately predict the regional frequencies during an overlapping time period. A second possibility is that there have been changes in the probabilities of record-setting events between the attribution and verification periods.

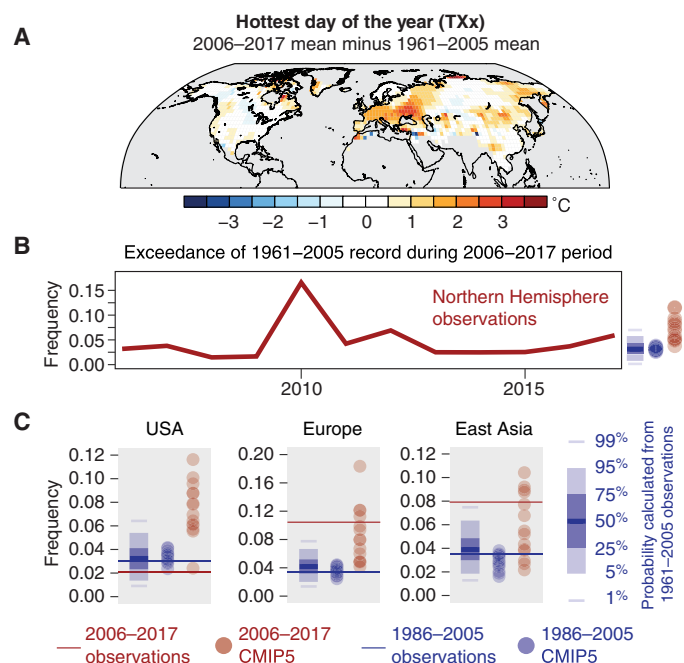


Fig. 2. Observed and simulated regional extreme event frequencies for the hottest day of the year (TXx). (A) The map shows the difference in the mean value between the out-of-sample verification period (2006–2017) and the period for which the attribution metrics were calculated (1961–2005). (B) The red line shows, for each year of the 2006–2017 verification period, the observed northern hemisphere frequency of events in which the grid-point value exceeded the maximum grid-point value during the period for which the attribution metrics were calculated (1961–2005). The blue distribution shows the uncertainty in the hemispheric mean probability of exceeding the most extreme value found in the period for which the attribution metrics were calculated (1961–2005). The probability of the record-setting event is calculated by fitting an extreme value distribution to the 1961–2005 time series at each grid point, as described in (4); uncertainty is depicted by the percentile values of the bootstrapping described in (4). The blue circles show the regional frequency simulated by the CMIP5 climate model ensemble during the IPCC’s baseline period (1986–2005). The red circles show the regional frequency simulated by the CMIP5 climate model ensemble during the verification period (2006–2017). (C) The blue distribution shows the uncertainty in the regional-mean probability of exceeding the most extreme value found in the period for which the attribution metrics were calculated (1961–2005). The blue horizontal line shows the observed regional frequency during the IPCC’s baseline period (1986–2005); blue circles show the regional frequency simulated by the CMIP5 climate model ensemble during the IPCC’s baseline period. The red horizontal line shows the observed regional frequency during the out-of-sample verification period (2006–2017); red circles show the regional frequency simulated by the CMIP5 climate model ensemble during the verification period.

The results favor the second possibility. For example, the actual regional frequencies that occurred during the Intergovernmental Panel on Climate Change (IPCC’s) baseline period (1986–2005) all fall within the 5th to 95th percentile uncertainty range predicted from the 1961–2005 observations, and the majority fall within the 25th to 75th percentile uncertainty range (Figs. 2 to 4). Further, the CMIP5 climate model ensemble, which is an independent dataset with which to predict the frequency of record-setting events at a given level of climate forcing, exhibits close overlap with the predicted probabilities and the observed 1986–2005 regional frequencies (Figs. 2 to 4). Even in the cases where the 1986–2005 CMIP5 ensemble spread is furthest from the median of the predicted probabilities (such as the longest dry spells over the United States, Europe, and East Asia), the ensemble range still falls within the distribution of predicted probabilities (Fig. 4). The fact that the observed and simulated 1986–2005 frequencies fall well within the distributions of probabilities predicted from the 1961–2005 observations (Figs. 2 to 4) suggests that discrepancies between the attribution and verification ratios (Fig. 1) are not caused by structural discrepancies between the underlying metrics.

In contrast, there are substantial differences in the observed frequency of record-setting events between 1986–2005 and 2006–2017. For example, the observed frequency is at least ~50% higher in 2006–2017 for hottest days over Europe and East Asia (Fig. 2), wettest days over the United States and Europe (Fig. 3), and longest dry spells over East Asia (Fig. 4). Likewise, with the exception of the longest dry spells over the United States and East Asia (Fig. 4), the frequency observed during 2006–2017 falls further from the median predicted probability, while the frequency observed during 1986–2005 falls closer to the median (Figs. 2 to 4). These comparisons quantify a substantial increase in the risk of unprecedented events between the attribution and verification periods, particularly for hot and wet events.

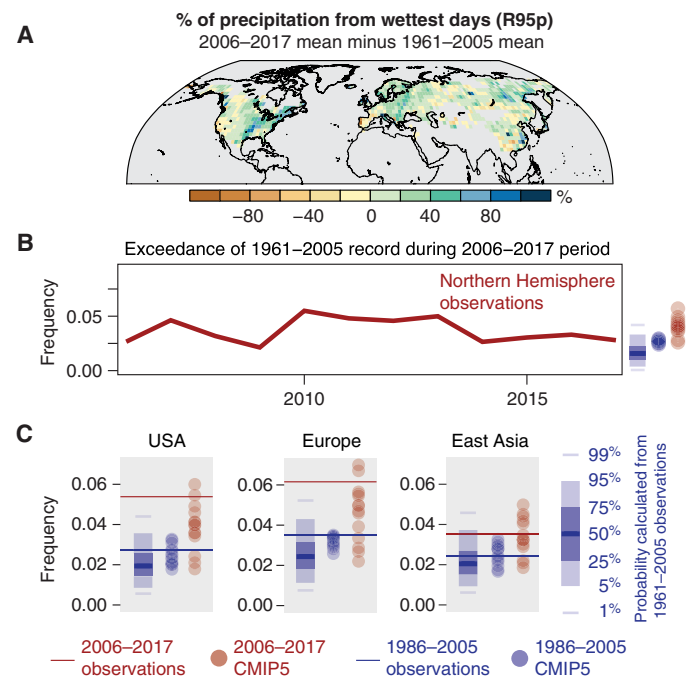


Fig. 3. Observed and simulated regional extreme event frequencies for the wettest days. As in Fig. 2, but for the percentage of annual precipitation falling in days that are wetter than the 95th percentile of the 1961–1990 baseline period (R95p).

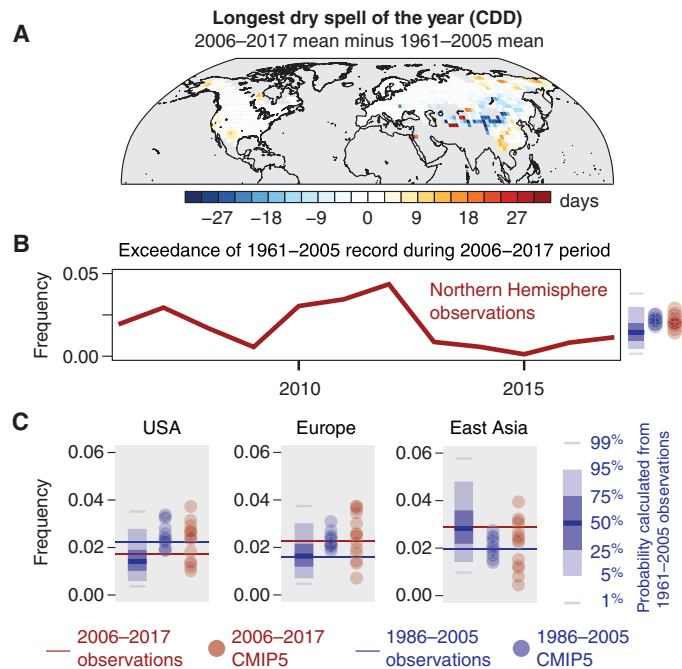


Fig. 4. Observed and simulated regional extreme event frequencies for the longest dry spell. As in Fig. 2, but for the longest consecutive dry spell of the year (CDD).

One concern about this analysis is that the verification period is relatively short (12 years) compared to a standard climatological baseline period (nominally 30 years). To test the robustness of the results to a longer period, the verification period can be extended to include the period from the beginning of the IPCC baseline (1986) to the end of the out-of-sample verification period (2017). As would be expected, mixing the out-of-sample verification period (2006–2017) with the end of the attribution period (1961–2005) to form an extended verification period (1986–2017) yields verification results that generally fall between the original attribution results and the out-of-sample verification results (tables S1 to S3). However, in a number of cases, the verification results for this modified period still exceed the original attribution results, including hot events over Europe (table S1) and wet events over the United States and Europe (table S3).

By generating multiple realizations of the climate system within a given level of forcing, the CMIP5 simulations can also provide an independent evaluation of whether the change in frequency of record-setting events is due primarily to climate variability, or has instead been influenced by the increase in climate forcing between the attribution and verification periods. For the hottest days over Europe and East Asia (Fig. 2) and the wettest days over the United States, Europe, and East Asia (Fig. 3), both the observations and the CMIP5 ensemble exhibit higher probability of record-breaking events in 2006–2017 than in 1986–2005. Likewise, for the hottest days over Europe and East Asia (Fig. 2), wettest days over the United States, Europe, and East Asia (Fig. 3), and longest dry spells over the United States and East Asia (Fig. 4), the frequency of record-breaking events observed in 2006–2017 has a higher likelihood of occurring in 2006–2017 of CMIP5 than in 1986–2005 of CMIP5. These patterns are also true at the scale of the northern hemisphere for both the hottest and wettest days, where the CMIP5 ensemble exhibits higher frequency

of record-setting events in 2006–2017 than in 1986–2005, and the observed 2006–2017 frequencies have a higher likelihood of occurring in 2006–2017 of CMIP5 than in 1986–2005 of CMIP5 (Figs. 2 and 3). The fact that the frequency of record-setting hot and wet events observed during the 2006–2017 verification period generally falls within the CMIP5 ensemble spread for 2006–2017 and generally outside the CMIP5 ensemble spread for 1986–2005 suggests that the observed increase in occurrence was likely influenced by the increase in forcing between the attribution and verification periods.

In contrast, the verification of record-setting longest dry spells suggests that, at both the regional and hemispheric scales, global warming has not had a clear influence on the probability of record-setting events. This lack of attribution was already suggested by the high fraction of attribution ratios near 1.0 (Fig. 1) (5). The fact that the verification ratios are also clustered near 1.0 (Fig. 1) strengthens that conclusion. Further, the close overlap between the observed and simulated frequencies for 1986–2005 and 2006–2017 (Fig. 4) suggests that, in contrast to hot and wet events (Figs. 2 and 3), the recent increase in climate forcing has not altered the probability of record-setting longest dry spells over the analysis regions. However, it is important to note that other areas of the globe may have experienced verifiable increases in the probability and/or intensity of dry spells [e.g., (4)].

DISCUSSION

The fact that the verification framework reveals the published global attribution results to be overly conservative for hot and wet events carries a number of implications. For example, those attribution results suggested that global warming had already influenced the magnitude and probability of unprecedented events at large fractions of the globe, including >80% for hot events and >50% for wet events (4). This includes 71% of North America, 77% of Europe, and 56% of East Asia for the record hottest day of the year, and 80% of North America, 89% of Europe, and 70% of East Asia for the record percentage of annual precipitation falling in the wettest days (5). The verification results presented here suggest that the influence of global warming on these events has been even more pervasive than suggested by those original attribution results.

Likewise, because many of the impacts of global warming are felt through extremes (54), attribution of the influence of global warming on record-setting events is highly relevant for quantifying the impacts of historical anthropogenic climate forcing on natural and human systems. In revealing previously published attribution results to be largely conservative, the verification results suggest that the impacts of global warming have been even larger than originally implied (4, 5). Further, attribution quantification is now being used to assign specific responsibility for the damages resulting from individual events (55). The results presented here highlight the importance of independent verification of the attribution frameworks that are used to assign responsibility for damages.

The underestimation of the probability of record hot and wet events during the verification period implies a rapid intensification of extreme event probability—and therefore risk—resulting from relatively small increases in climate forcing. This intensification has important implications both for extreme event attribution and for accurately quantifying probabilities of extreme values in the current and near-term climate. Although the calculation of record-setting probabilities attempts to account for nonstationarity in the observational

time series (4), the verification results suggest that even one to two additional decades of global-scale climate forcing can lead to substantial underestimation of the probability of record-setting hot and wet events (Figs. 2 and 3).

The fact that the observed and simulated frequencies of record-setting events exhibit such large nonstationarities between the baseline period (ending in 2005) and the verification period (2006–2017) suggests that extreme event attribution assessments—as well as other risk assessments—should take particular care to use techniques that capture conditions in the current time period. Researchers have used a number of approaches to extend the period of the attribution analysis. For metrics that rely only on observational data, researchers have used the period of available data at the time of the event [e.g., (4, 10, 28, 46)]. Other researchers have calculated statistical relationships between the event probability and the global mean temperature (10, 13, 14). For metrics that rely on climate model simulations (including coordinated archived experiments such as CMIP5), researchers have used climate model projections to extend the period of analysis up to the time of the event [e.g., (38)] or to generate attribution results for different levels of global warming (including projected future levels) [e.g., (5, 6, 8, 13)]. For the attribution results evaluated here, the original study (5) included projections of return interval ratios for 2016–2035 and 2036–2055 in the CMIP5 RCP8.5 experiment, enabling comparisons with 1° to 2°C and 2° to 3°C of global warming.

Extending probability predictions under higher levels of global warming has been less common in other applications that rely on extreme event probability quantification, such as infrastructure design and risk assessment [e.g., (52)]. The verification results suggest that those applications could benefit from such approaches, particularly given that those planning decisions are more explicitly future-oriented than attribution analysis. For example, the underprediction of occurrence of record-setting events during the out-of-sample verification period provides evidence in support of dynamic design guidelines that can be updated as new observational data become available [e.g., (50, 52–54)]. Likewise, the fact that the CMIP5 projections for 2006–2017 most accurately capture the actual 2006–2017 frequency of record-setting hot and wet events (Figs. 2 and 3) suggests that ensemble climate model projections could be used to improve probability quantification for applications that have traditionally relied solely on historical observations.

In addition to capturing the response of extreme events to increasing climate forcing, ensemble climate model projections can also help to quantify the influence of variability on future extreme event probabilities. For example, the 1961–2005 attribution metrics suggest >50% likelihood that global warming has increased the probability of record-setting hottest days over the United States (Fig. 1). Further, comparison of the CMIP5 simulations for 2006–2017 and 1986–2005 predicts very high likelihood of a substantial increase in the frequency of record-setting hot events in the later period (Fig. 2). However, 75% of the verification ratio distribution is less than 1.0 over the United States (Fig. 1), driven by a 2006–2017 frequency that is in the lowest quartile predicted from the 1961–2005 observations (Fig. 2).

This relatively low frequency of record-setting hottest days over the United States is consistent with the well-documented “warming hole,” a pattern of reduced warming over the central and southeastern United States that has been attributed alternatively to atmosphere-soil moisture feedbacks (56), the aerosol-indirect effect (57), and

internal ocean-atmosphere variability (58). Although high levels of global warming are projected to cause substantial warming throughout North America, the lower rates of warming associated with the warming hole are projected to persist over the near-term decades, with relatively high summer temperature variability over the central and southeastern United States persisting throughout the 21st century (59). Although there is some indication that the mechanisms causing the warming hole may have reversed early in the 21st century (58), the pattern of reduced warming over the central and southeastern United States is present in the mean hottest day of the year for 2006–2017 relative to 1961–2005 (including negative anomalies over the central United States; Fig. 2). Notably, although the observed frequency of record-setting hottest days is lower over the United States in 2006–2017 compared to 1986–2005 (Fig. 2), the 2006–2017 frequency does overlap with the lowest CMIP5 value, highlighting the importance of climate variability within the context of increasing forcing.

CONCLUSIONS

The motivation for this study is to introduce and demonstrate a framework for independent verification of extreme event attribution results. The field of extreme event attribution has expanded rapidly in the past two decades. Results are now the subject of frequent public interest (2). This interest has extended into various public decision-making processes, both as motivation for incorporating climate change into decisions [e.g., (52)] and as a basis for assigning responsibility for damages (55). The use of attribution results raises the burden for scientists to independently verify those results, particularly for events that are unprecedented in the historical experience (and therefore pose the most acute risks).

Numerous methods for event attribution have been developed (2). Although different dimensions of methodological uncertainty have been thoroughly evaluated, and in some cases the results of different methods have been systematically intercompared, extreme event attribution results have not yet been independently verified within a framework of scientific falsifiability. To fulfill that need, this study presents a framework for using the attribution calculation to create falsifiable predictions of the frequency of record-setting events and then uses out-of-sample observations to test those predictions. As an initial proof of concept, the verification framework is applied to previously published attribution results for record-setting hot, wet, and dry events at different areas of the globe (4, 5).

Independent verification suggests that those published attribution results frequently underestimate the influence of global warming on the probability of unprecedented hot and wet extremes, with greater uncertainty for dry extremes. The discrepancy between the attribution and verification ratios can be most explained by the increase in climate forcing since the end of the period in which the attribution ratios were generated. This is particularly true for hot events and wet events, for which the discrepancies between the attribution and verification ratios are greatest. Overall, the verification results suggest not only that historical global warming has increased the probability of unprecedented hot and wet events over the northern hemisphere but also that the magnitude of this effect has increased during the 21st century.

Although this study focuses on record-setting hot, wet, and dry events over land areas of the northern hemisphere, the verification framework could also be applied to a suite of other extreme climate

variables [e.g., (49)] and physical ingredients [e.g., (4)], with different data sources providing coverage for different areas of the globe. Further development and application of this and other frameworks will provide a more comprehensive verification of the magnitude of anthropogenic influence on different types of extreme events in different regions of the world.

The verification of previously published results from one attribution method does offer some generalizable lessons. The first is that although many attribution analyses have leveraged the unique insights available from multi-institution climate model archives such as CMIP5 [e.g., (4–8, 20, 38)], such “ensembles of opportunity” also present limitations. For example, because the coordinated experiments require multiple years to plan and run, the simulations that use historical forcings do not extend to the present at the time that a new event occurs (48). This means that analyses must either cover historical periods that do not extend to the present [e.g., (4–6, 12, 20)] (which, as this study shows, results in an underestimation of the influence of global warming on hot and wet events) or use approaches to extend the calculation past the period of the historical simulations [e.g., (8, 10, 14, 38)]. The commonly implemented approach of using the early period of climate model projections to extend the calculation still presents limitations, both because researchers must compare the extended simulations with counterfactual simulations that do not reach up to the present [e.g., (8, 38)] and because the early period of the climate model projections does not include the actual forcings that occurred, which can hamper accurate attribution (60).

Another generalizable conclusion is that although precomputed approaches remove bias in the selection of events that are studied and enable unified analysis of multiple types of events across multiple regions of the world, the fact that the precalculation necessarily limits the analysis to an earlier baseline period likely leads to an underestimation of current probabilities. As a result, other precomputed calculations [e.g., (6, 7)] are likely also subject to a similar underestimation of the influence of historical forcing on the probability of events in the current climate. The verification results presented in this study highlight the importance for precomputed event attribution analyses to include calculations for higher levels of forcing [e.g., (5, 6, 8)] and to update the precomputed results as new observations become available. These results also suggest that “rapid” attribution approaches [which produce analyses soon after a specific event has occurred; e.g., (10, 14, 25)] should likewise continue to use methods that align the climate forcing in the attribution analysis with the forcing at the time of the event. Efforts to develop and deploy “operational” attribution systems [e.g., (27)] that update observations and simulations in real time will also help to address this limitation.

Last, the verification results have general implications beyond extreme event attribution. Historical climate observations are widely used as the basis for risk management decisions in areas as diverse as land use, infrastructure, water resources, supply chain management, disaster relief, finance, insurance, and liability. In many of these cases, decisions must be robust to both current and future probabilities of extreme events. Although decision-makers have been aware of the challenges posed by climate nonstationarity for a number of years [e.g., (50, 51)], many of these decisions still rely primarily on historical observations for calculating extreme event probability [e.g., (52)]. The methods for calculating those probabilities from historical data are closely linked to the methods used in the attribu-

tion framework evaluated here (4, 5). The out-of-sample verification results presented in this study thus highlight the importance of incorporating present and future nonstationarity into the extreme event probability quantification that underlies a broad suite of climate-sensitive risk management decisions.

MATERIALS AND METHODS

Data

The analysis uses data from the CLIMDEX project, which has archived observational and climate model values for multiple extreme climate indices (49). The observational values are calculated from station observations and gridded to a global grid, based on data continuity criteria. The climate model values are calculated from the CMIP5 climate model experiments (48).

The current study uses the observational data, along with the Historical and Natural climate model simulations. The Historical simulations include both natural forcings (such as volcanic aerosols and variations in solar output) and anthropogenic forcings (such as greenhouse gases and aerosols); the Natural simulations include only the natural forcings. The Historical and Natural simulations were run through the year 2005 (48). Comparison of the Historical and Natural simulations thus quantifies the influence of anthropogenic forcings during the historical climate period through 2005.

Attribution metrics

This study evaluates the extreme event attribution analyses that were published by Diffenbaugh *et al.* (5). The study focuses on three of the CLIMDEX indices included in that analysis, which together measure hot, wet, and dry events: the hottest day of the year (TXx; “hottest day”), the percentage of annual precipitation falling in days that are wetter than the 95th percentile of the 1961–1990 period (R95p; “wettest days”), and the longest consecutive dry spell of the year (CDD; “longest dry spell”).

Diffenbaugh *et al.* (5) calculated the attribution ratio described in (4), using the CMIP5 Historical and Natural simulations over the 1961–2005 period. This attribution ratio ($AR_{\text{Forcing:1961–2005}}$) quantifies the influence of anthropogenic forcing on the probability of exceeding the most extreme value observed at each grid point during the 1961–2005 period. The metric is calculated as the ratio between the return interval of the observed record value in the lower level of forcing ($RI_{\text{NAT:1961–2005}}$) and the return interval of the observed record value in the higher level of forcing ($RI_{\text{HIST:1961–2005}}$). For example, if the most extreme observed value has a return interval of 100 years in the Natural forcing (probability = 0.01) and a return interval of 50 years in the Historical forcing (probability = 0.02), then the attribution ratio ($AR_{\text{Forcing:1961–2005}}$) is 2, suggesting that anthropogenic forcing has doubled the probability of exceeding the most extreme observed value.

Diffenbaugh *et al.* (4) also calculated the contribution of the historical trend at each grid point to the probability of exceeding that grid point’s most extreme observed value. This metric ($AR_{\text{Obs-dt:1961–2005}}$) is calculated as the ratio of the return interval of the observed record value in the detrended historical time series ($RI_{\text{Obs-dt:1961–2005}}$) and the return interval of the observed record value in the actual historical time series ($RI_{\text{Obs:1961–2005}}$)

$$AR_{\text{Obs-dt:1961–2005}} = (RI_{\text{Obs-dt:1961–2005}}) \div (RI_{\text{Obs:1961–2005}})$$

This second metric ($AR_{\text{Obs-dt:1961-2005}}$) thus relies only on observational data (without any climate model simulations) and is agnostic about the cause of the historical trend.

The current study evaluates both the attribution ratio due to anthropogenic forcing ($AR_{\text{Forcing:1961-2005}}$) and the attribution ratio due to the observed trend ($AR_{\text{Obs-dt:1961-2005}}$). Both attribution metrics report an uncertainty distribution of attribution ratios. These distributions are based on the uncertainty distribution of return intervals for the record setting event ($RI_{\text{Obs:1961-2005}}$), which are calculated from the observational time series using a block bootstrap approach.

Verification framework

To verify the previously published attribution ratios, the uncertainty distributions calculated for 1961–2005 are compared with the frequency of occurrence of record-setting events observed during 2006–2017. This verification approach is conceptually similar to the attribution calculation of Coumou *et al.* (28), except here the verification data are kept out of sample (i.e., the verification data are not used in the calculation of the counterfactual time series from which the counterfactual probabilities are quantified).

First, the maximum value of each climate index is calculated at each grid point during the 1961–2005 period of the CLIMDEX observations. Then, for each grid point, all events during 2006–2017 that exceed the respective 1961–2005 grid-point maximum are identified. The frequency of occurrence of record-setting events in 2006–2017 ($F_{\text{Obs:2006-2017}}$) is then calculated over the Northern Hemisphere, the United States (30–50°N, 120–60°W), Europe (30–60°N, 0–50°E), and East Asia (20–45°N, 90–135°E), where

$$F_{\text{Obs:2006-2017}} = \frac{\text{[the total number of exceedances in the region in 2006-2017]} \div \text{[(the number of grid points in the region)} \times \text{(the number of years in 2006-2017)]}$$

This regional frequency of occurrence ($F_{\text{Obs:2006-2017}}$) is then converted to a regional verification ratio ($VR_{\text{Obs:2006-2017}}$) that can be compared with the attribution ratios described in (5) and (4). First, the regional frequency of occurrence is converted to a “regional return interval” ($RI_{\text{Obs:2006-2017}}$) using the formula for the return interval

$$RI = 1 \div (1 - P)$$

but using the regional frequency of occurrence ($F_{\text{Obs:2006-2017}}$) as the measure of probability

$$RI_{\text{Obs:2006-2017}} = 1 \div (F_{\text{Obs:2006-2017}})$$

The regional-mean return interval of the observed record value in the detrended historical time series ($RI_{\text{Obs-dt:1961-2005}}$) is then computed by first calculating the mean of the grid-point probabilities in the detrended time series ($P_{\text{Obs-dt:1961-2005}}[i,j]$) and then calculating the regional-mean return interval from that regional-mean probability. (Note that the order of operations matters: It is important to first calculate the regional-mean of the grid-point probabilities to avoid the regional-mean return interval being dominated by any single grid-point return interval value.) The uncertainty in the regional-mean return interval ($RI_{\text{Obs-dt:1961-2005}}$) is quantified by calculating

the regional-mean at each quantile of the uncertainty distribution of grid-point probabilities ($P_{\text{Obs-dt:1961-2005}}[i,j]$).

Last, the uncertainty distribution of regional-mean return intervals in the detrended 1961–2005 time series ($RI_{\text{Obs-dt:1961-2005}}$) is divided by the regional-mean 2006–2017 return interval ($RI_{\text{Obs:2006-2017}}$), generating an uncertainty distribution of verification ratios ($VR_{\text{Obs:2006-2017}}$) for each region

$$VR_{\text{Obs:2006-2017}} = RI_{\text{Obs-dt:1961-2005}} \div RI_{\text{Obs:2006-2017}}$$

This distribution of verification ratios ($VR_{\text{Obs:2006-2017}}$) is compared with the regional-means of the grid-point distributions of attribution ratios from anthropogenic forcing ($AR_{\text{Forcing:1961-2005}}$) and attribution ratios from the observed trend ($AR_{\text{Obs-dt:1961-2005}}$).

To understand the comparisons between the published attribution ratios and the regional verification ratios, a number of regional extreme event frequencies are calculated using the IPCC’s baseline period (1986–2005). These include the regional frequency of events that exceed the observed 1961–2005 maximum during the 1986–2005 period of the observations ($F_{\text{Obs:1986-2005}}$), the regional frequency of events that exceed the simulated 1961–2005 maximum during the 1986–2005 period of the CMIP5 Historical simulations ($F_{\text{CMIP5:1986-2005}}$), and the regional frequency of events that exceed the simulated 1961–2005 maximum during the 2006–2017 period of the CMIP5 RCP8.5 simulations ($F_{\text{CMIP5:2006-2017}}$). For each observed or simulated climate realization, the regional frequency is calculated as the number of times during the evaluation period (1986–2005 or 2006–2017) that a grid-point value within the region exceeds the respective 1961–2005 grid-point maximum, divided by the number of grid points in the region, divided by the number of years in the evaluation period.

SUPPLEMENTARY MATERIALS

Supplementary material for this article is available at <http://advances.sciencemag.org/cgi/content/full/6/12/eaay2368/DC1>

Table S1. Verification metrics for the hottest day of the year (TXx), calculated for different time periods.

Table S2. Verification metrics for the percent of precipitation from wettest days (R95p), calculated for different time periods.

Table S3. Verification metrics for the longest dry spell of the year (CDD), calculated for different time periods.

REFERENCES AND NOTES

1. P. A. Stott, D. A. Stone, M. R. Allen, Human contribution to the European heatwave of 2003. *Nature* **432**, 610–614 (2004).
2. The National Academies Press, *Attribution of Extreme Weather Events in the Context of Climate Change* (The National Academies Press, 2016).
3. O. Angélli, D. Stone, M. Wehner, C. J. Paciorek, H. Krishnan, W. Collins, An independent assessment of anthropogenic attribution statements for recent extreme temperature and rainfall events. *J. Climate* **30**, 5–16 (2017).
4. N. S. Diffenbaugh, D. Singh, J. S. Mankin, D. E. Horton, D. L. Swain, D. Touma, A. Charland, Y. Liu, M. Haugen, M. Tsiang, B. Rajaratnam, Quantifying the influence of global warming on unprecedented extreme climate events. *Proc. Natl. Acad. Sci. U.S.A.* **114**, 4881–4886 (2017).
5. N. S. Diffenbaugh, D. Singh, J. S. Mankin, Unprecedented climate events: Historical changes, aspirational targets, and national commitments. *Sci. Adv.* **4**, eaao3354 (2018).
6. E. M. Fischer, R. Knutti, Anthropogenic contribution to global occurrence of heavy-precipitation and high-temperature extremes. *Nat. Clim. Chang.* **5**, 560–564 (2015).
7. N. Christidis, P. A. Stott, F. W. Zwiers, Fast-track attribution assessments based on pre-computed estimates of changes in the odds of warm extremes. *Climate Dynam.* **45**, 1547–1564 (2015).
8. M. M. Vogel, J. Zscheischler, R. Wartenburger, D. Dee, S. I. Seneviratne, Concurrent 2018 hot extremes across northern hemisphere due to human-induced climate change. *Earth’s Futur.* **7**, 692–703 (2019).

9. D. Singh, D. L. Swain, J. S. Mankin, D. E. Horton, L. N. Thomas, B. Rajaratnam, N. S. Diffenbaugh, Recent amplification of the North American winter temperature dipole. *J. Geophys. Res. Atmos.* **121**, 9911–9928 (2016).
10. K. van der Wiel, S. B. Kapnick, G. J. van Oldenborgh, K. Whan, S. Philip, G. A. Vecchi, R. K. Singh, J. Arrighi, H. Cullen, Rapid attribution of the August 2016 flood-inducing extreme precipitation in south Louisiana to climate change. *Hydrol. Earth Syst. Sci.* **21**, 897–921 (2017).
11. P. Pall, T. Aina, D. A. Stone, P. A. Stott, T. Nozawa, A. G. J. Hilberts, D. Lohmann, M. R. Allen, Anthropogenic greenhouse gas contribution to flood risk in England and Wales in autumn 2000. *Nature* **470**, 382–385 (2011).
12. N. S. Diffenbaugh, D. L. Swain, D. Touma, Anthropogenic warming has increased drought risk in California. *Proc. Natl. Acad. Sci. U.S.A.* **112**, 3931–3936 (2015).
13. K. Emanuel, Assessing the present and future probability of Hurricane Harvey's rainfall. *Proc. Natl. Acad. Sci. U.S.A.* **114**, 12681–12684 (2017).
14. G. J. van Oldenborgh, K. van der Wiel, A. Sebastian, R. Singh, J. Arrighi, F. Otto, K. Haustein, S. Li, G. Vecchi, H. Cullen, Attribution of extreme rainfall from Hurricane Harvey, August 2017. *Environ. Res. Lett.* **12**, 124009 (2017).
15. N. Lin, R. E. Kopp, B. P. Horton, J. P. Donnelly, Hurricane Sandy's flood frequency increasing from year 1800 to 2100. *Proc. Natl. Acad. Sci. U.S.A.* **113**, 12071–12075 (2016).
16. M. C. Kirchmeier-Young, F. W. Zwiers, N. P. Gillett, Attribution of extreme events in Arctic sea ice extent. *J. Climate* **30**, 553–571 (2017).
17. K. E. Trenberth, J. T. Fasullo, T. G. Shepherd, Attribution of climate extreme events. *Nat. Clim. Chang.* **5**, 725–730 (2015).
18. T. G. Shepherd, A common framework for approaches to extreme event attribution. *Curr. Clim. Chang. Rep.* **2**, 28–38 (2016).
19. D. Coumou, V. Petoukhov, S. Rahmstorf, S. Petri, H. J. Schellnhuber, Quasi-resonant circulation regimes and hemispheric synchronization of extreme weather in boreal summer. *Proc. Natl. Acad. Sci. U.S.A.* **111**, 12331–12336 (2014).
20. M. E. Mann, S. Rahmstorf, K. Kornhuber, B. A. Steinman, S. K. Miller, D. Coumou, Influence of anthropogenic climate change on planetary wave resonance and extreme weather events. *Sci. Rep.* **7**, 45242 (2017).
21. D. L. Swain, M. Tsiang, M. Haugen, D. Singh, A. Charland, B. Rajaratnam, N. S. Diffenbaugh, The extraordinary California drought of 2013–2014: Character, context, and the role of climate change [in “Explaining Extremes of 2013 from a Climate Perspective”]. *Bull. Am. Meteorol. Soc.* **95**, S3–S7 (2014).
22. S. Wang, L. Hipps, R. R. Gillies, J.-H. Yoon, Probable causes of the abnormal ridge accompanying the 2013–2014 California drought: ENSO precursor and anthropogenic warming footprint. *Geophys. Res. Lett.* **41**, 3220–3226 (2014).
23. K. E. Trenberth, L. Cheng, P. Jacobs, Y. Zhang, J. Fasullo, Hurricane Harvey links to ocean heat content and climate change adaptation. *Earth's Futur.* **6**, 730–744 (2018).
24. M. C. Kirchmeier-Young, N. P. Gillett, F. W. Zwiers, A. J. Cannon, F. S. Anslow, Attribution of the influence of human-induced climate change on an extreme fire season. *Earth's Futur.* **7**, 2–10 (2019).
25. F. E. L. Otto, K. van der Wiel, G. J. van Oldenborgh, S. Philip, S. F. Kew, P. Uhe, H. Cullen, Climate change increases the probability of heavy rains in Northern England/Southern Scotland like those of storm Desmond—A real-time event attribution revisited. *Environ. Res. Lett.* **13**, 24006 (2018).
26. K. Haustein, F. E. L. Otto, P. Uhe, N. Schaller, M. R. Allen, L. Hermanson, N. Christidis, P. McLean, H. Cullen, Real-time extreme weather event attribution with forecast seasonal SSTs. *Environ. Res. Lett.* **11**, 64006 (2016).
27. A. Hannart, A. Carrassi, M. Bocquet, M. Ghil, P. Naveau, M. Pulido, J. Ruiz, P. Tandeo, DADA: Data assimilation for the detection and attribution of weather and climate-related events. *Clim. Change* **136**, 155–174 (2016).
28. D. Coumou, A. Robinson, S. Rahmstorf, Global increase in record-breaking monthly-mean temperatures. *Clim. Change* **118**, 771–782 (2013).
29. F. C. Lott, M. Gordon, R. J. Graham, A. A. Scaife, M. Vellinga, Reliability of African climate prediction and attribution across timescales. *Environ. Res. Lett.* **9**, 104017 (2014).
30. T. C. Peterson, R. R. Heim Jr., R. Hirsch, D. P. Kaiser, H. Brooks, N. S. Diffenbaugh, R. M. Dole, J. P. Giovannetone, K. Guirguis, T. R. Karl, R. W. Katz, K. Kunkel, D. Lettenmaier, G. J. McCabe, C. J. Paciorek, K. R. Ryberg, S. Schubert, V. B. S. Silva, B. C. Stewart, A. V. Vecchia, G. Villarini, R. S. Vose, J. Walsh, M. Wehner, D. Wolock, K. Wolter, C. A. Woodhouse, D. Wuebbles, Monitoring and understanding changes in heat waves, cold waves, floods and droughts in the United States: State of knowledge. *Bull. Am. Meteorol. Soc.* **94**, 821–834 (2013).
31. M. E. Mann, E. A. Lloyd, N. Oreskes, Assessing climate change impacts on extreme weather events: The case for an alternative (Bayesian) approach. *Clim. Change* **144**, 131–142 (2017).
32. A. Hannart, J. Pearl, F. E. L. Otto, P. Naveau, M. Ghil, Causal counterfactual theory for the attribution of weather and climate-related events. *Bull. Am. Meteorol. Soc.* **97**, 99–110 (2015).
33. A. Jézéquel, V. Dépoues, H. Guillemot, M. Troillet, J.-P. Vanderlinden, P. Yiou, Behind the veil of extreme event attribution. *Clim. Change* **149**, 367–383 (2018).
34. P. A. Stott, D. J. Karoly, F. W. Zwiers, Is the choice of statistical paradigm critical in extreme event attribution studies? *Clim. Change* **144**, 143–150 (2017).
35. R. B. Alley, K. A. Emanuel, F. Zhang, Advances in weather prediction. *Science* **363**, 342–344 (2019).
36. W. S. Broecker, Climatic change: Are we on the brink of a pronounced global warming? *Science* **189**, 460–463 (1975).
37. J. Hansen, I. Funck, A. Laci, D. Rind, S. Lebedeff, R. Ruedy, G. Russell, P. Stone, Global climate changes as forecast by Goddard Institute for Space Studies three-dimensional model. *J. Geophys. Res. Atmos.* **93**, 9341–9364 (1988).
38. T. R. Knutson, J. Kam, F. Zeng, A. T. Wittenberg, CMIP5 model-based assessment of anthropogenic influence on record global warmth during 2016. *Bull. Am. Meteorol. Soc.* **99**, S11–S15 (2018).
39. O. Bellprat, F. Doblas-Reyes, Attribution of extreme weather and climate events overestimated by unreliable climate simulations. *Geophys. Res. Lett.* **43**, 2158–2164 (2016).
40. O. Bellprat, V. Guemas, F. Doblas-Reyes, M. G. Donat, Towards reliable extreme weather and climate event attribution. *Nat. Commun.* **10**, 1732 (2019).
41. A. Weisheimer, N. Schaller, C. O'Reilly, D. A. MacLeod, T. Palmer, Atmospheric seasonal forecasts of the twentieth century: Multi-decadal variability in predictive skill of the winter North Atlantic Oscillation (NAO) and their potential value for extreme event attribution. *Q. J. Roy. Meteorol. Soc.* **143**, 917–926 (2017).
42. S. Jeon, C. J. Paciorek, M. F. Wehner, Quantile-based bias correction and uncertainty quantification of extreme event attribution statements. *Weather Clim. Extrem.* **12**, 24–32 (2016).
43. S. Sippel, D. Mitchell, M. T. Black, A. J. Dittus, L. Harrington, N. Schaller, F. E. L. Otto, Combining large model ensembles with extreme value statistics to improve attribution statements of rare events. *Weather Clim. Extrem.* **9**, 25–35 (2015).
44. B. Christiansen, The role of the selection problem and non-Gaussianity in attribution of single events to climate change. *J. Climate* **28**, 9873–9891 (2015).
45. C. J. Paciorek, D. A. Stone, M. F. Wehner, Quantifying statistical uncertainty in the attribution of human influence on severe weather. *Weather Clim. Extrem.* **20**, 69–80 (2018).
46. L. J. Wilcox, P. Yiou, M. Hauser, F. C. Lott, G. J. van Oldenborgh, I. Cofrescu, B. Dong, G. Hegerl, L. Shaffrey, R. Sutton, Multiple perspectives on the attribution of the extreme European summer of 2012 to climate change. *Climate Dynam.* **50**, 3537–3555 (2018).
47. M. Hauser, L. Gudmundsson, R. Orth, A. Jézéquel, K. Haustein, R. Vautard, G. J. van Oldenborgh, L. Wilcox, S. I. Seneviratne, Methods and model dependency of extreme event attribution: The 2015 European drought. *Earth's Futur.* **5**, 1034–1043 (2017).
48. K. E. Taylor, R. J. Stouffer, G. A. Meehl, An overview of CMIP5 and the experiment design. *Bull. Am. Meteorol. Soc.* **93**, 485–498 (2012).
49. J. Sillmann, V. V. Kharin, X. Zhang, F. W. Zwiers, D. Bronaugh, Climate extremes indices in the CMIP5 multimodel ensemble: Part 1. Model evaluation in the present climate. *J. Geophys. Res. Atmos.* **118**, 1716–1733 (2013).
50. P. C. D. Milly, J. Betancourt, M. Falkenmark, R. M. Hirsch, Z. W. Kundzewicz, D. P. Lettenmaier, R. J. Stouffer, Stationarity is dead: Whither water management? *Science* **319**, 573–574 (2008).
51. L. Cheng, A. AghaKouchak, E. Gilleland, R. W. Katz, Non-stationary extreme value analysis in a changing climate. *Clim. Change* **127**, 353–369 (2014).
52. Climate-Safe Infrastructure Working Group, *Paying It forward: The Path Toward Climate-Safe Infrastructure in California* (California Natural Resources Agency, 2018).
53. E. Mills, Insurance in a climate of change. *Science* **309**, 1040–1044 (2005).
54. IPCC, *Managing the Risks of Extreme Events and Disasters to Advance Climate Change Adaptation* (Cambridge Univ. Press, 2012).
55. C. Huggel, D. Stone, H. Eicken, G. Hansen, Potential and limitations of the attribution of climate change impacts for informing loss and damage discussions and policies. *Clim. Change* **133**, 453–467 (2015).
56. Z. T. Pan, R. W. Arritt, E. S. Takle, W. J. Gutowski Jr., C. J. Anderson, M. Segal, Altered hydrologic feedback in a warming climate introduces a “warming hole”. *Geophys. Res. Lett.* **31**, L17109 (2004).
57. S. Yu, K. Alapaty, R. Mathur, J. Pleim, Y. Zhang, C. Nolte, B. Eder, K. Foley, T. Nagashima, Attribution of the United States “warming hole”: Aerosol indirect effect and precipitable water vapor. *Sci. Rep.* **4**, 6929 (2014).
58. G. A. Meehl, J. M. Arblaster, C. T. Y. Chung, Disappearance of the southeast U.S. “warming hole” with the late 1990s transition of the Interdecadal Pacific Oscillation. *Geophys. Res. Lett.* **42**, 5564–5570 (2015).
59. N. S. Diffenbaugh, M. Ashfaq, M. Scherer, Transient regional climate change: Analysis of the summer climate response in a high-resolution, century-scale ensemble experiment over the continental United States. *J. Geophys. Res. Atmos.* **116**, D24111 (2011).
60. B. D. Santer, C. Bonfils, J. F. Painter, M. D. Zelinka, C. Mears, S. Solomon, G. A. Schmidt, J. C. Fyfe, J. N. S. Cole, L. Nazarenko, K. E. Taylor, F. J. Wentz, Volcanic contribution to decadal changes in tropospheric temperature. *Nat. Geosci.* **7**, 185–189 (2014).

Acknowledgments: I thank the editor and three anonymous reviewers for insightful and constructive feedback. I thank the CLIMDEX project for access to the observational and climate model data, as well as DOE's PCMDI and the participating climate modeling groups (which made the climate model data available to CLIMDEX and the broader community). I also thank the CEES and SRCC at Stanford University for access to computational resources. **Funding:** I acknowledge funding support from Stanford University. **Author contributions:** N.S.D. is the sole author. **Competing interests:** The author declares no competing interests. **Data and materials availability:** All data are available from the CLIMDEX archive.

Submitted 31 May 2019
Accepted 20 December 2019
Published 18 March 2020
10.1126/sciadv.aay2368

Citation: N. S. Diffenbaugh, Verification of extreme event attribution: Using out-of-sample observations to assess changes in probabilities of unprecedented events. *Sci. Adv.* **6**, eaay2368 (2020).

Verification of extreme event attribution: Using out-of-sample observations to assess changes in probabilities of unprecedented events

Noah S. Diffenbaugh

Sci Adv 6 (12), eaay2368.
DOI: 10.1126/sciadv.aay2368

ARTICLE TOOLS	http://advances.sciencemag.org/content/6/12/eaay2368
SUPPLEMENTARY MATERIALS	http://advances.sciencemag.org/content/suppl/2020/03/16/6.12.eaay2368.DC1
REFERENCES	This article cites 57 articles, 10 of which you can access for free http://advances.sciencemag.org/content/6/12/eaay2368#BIBL
PERMISSIONS	http://www.sciencemag.org/help/reprints-and-permissions

Use of this article is subject to the [Terms of Service](#)

Science Advances (ISSN 2375-2548) is published by the American Association for the Advancement of Science, 1200 New York Avenue NW, Washington, DC 20005. The title *Science Advances* is a registered trademark of AAAS.

Copyright © 2020 The Authors, some rights reserved; exclusive licensee American Association for the Advancement of Science. No claim to original U.S. Government Works. Distributed under a Creative Commons Attribution NonCommercial License 4.0 (CC BY-NC).

Environmental Research Letters



LETTER

OPEN ACCESS

RECEIVED
20 August 2019

REVISED
25 February 2020

ACCEPTED FOR PUBLICATION
26 March 2020





PUBLISHED
20 August 2020

Original content from this work may be used under the terms of the [Creative Commons Attribution 4.0 licence](#).

Any further distribution of this work must maintain attribution to the author(s) and the title of the work, journal citation and DOI.



Climate change is increasing the likelihood of extreme autumn wildfire conditions across California

Michael Goss^{1,10} , Daniel L Swain^{2,3,4} , John T Abatzoglou^{5,6} , Ali Sarhadi¹ , Crystal A Kolden^{5,7} , A Park Williams⁸  and Noah S Diffenbaugh^{1,9} 

¹ Department of Earth System Science, Stanford University, Stanford, CA, United States of America

² Institute of the Environment and Sustainability, University of California, Los Angeles, CA, United States of America

³ The Nature Conservancy of California, San Francisco, CA, United States of America

⁴ Capacity Center for Climate and Weather Extremes, National Center for Atmospheric Research, Boulder, CO, United States of America

⁵ Management of Complex Systems Department, University of California, Merced, CA, United States of America

⁶ Department of Geography, University of Idaho, Moscow, ID, United States of America

⁷ College of Natural Resources, University of Idaho, Moscow, ID, United States of America

⁸ Lamont-Doherty Earth Observatory of Columbia University, Palisades, NY 10964, United States of America

⁹ Woods Institute for the Environment, Stanford University, Stanford, CA, United States of America

E-mail: goss@stanford.edu

Keywords: climate change, attribution, wildfires, california, CMIP5, global warming

Supplementary material for this article is available [online](#)

Abstract

California has experienced devastating autumn wildfires in recent years. These autumn wildfires have coincided with extreme fire weather conditions during periods of strong offshore winds coincident with unusually dry vegetation enabled by anomalously warm conditions and late onset of autumn precipitation. In this study, we quantify observed changes in the occurrence and magnitude of meteorological factors that enable extreme autumn wildfires in California, and use climate model simulations to ascertain whether these changes are attributable to human-caused climate change. We show that state-wide increases in autumn temperature (~ 1 °C) and decreases in autumn precipitation ($\sim 30\%$) over the past four decades have contributed to increases in aggregate fire weather indices ($+20\%$). As a result, the observed frequency of autumn days with extreme (95th percentile) fire weather—which we show are preferentially associated with extreme autumn wildfires—has more than doubled in California since the early 1980s. We further find an increase in the climate model-estimated probability of these extreme autumn conditions since ~ 1950 , including a long-term trend toward increased same-season co-occurrence of extreme fire weather conditions in northern and southern California. Our climate model analyses suggest that continued climate change will further amplify the number of days with extreme fire weather by the end of this century, though a pathway consistent with the UN Paris commitments would substantially curb that increase. Given the acute societal impacts of extreme autumn wildfires in recent years, our findings have critical relevance for ongoing efforts to manage wildfire risks in California and other regions.

1. Introduction

California has recently endured a multi-year period of unprecedented wildfire activity. The state's single deadliest wildfire, two largest contemporary wildfires, and two most destructive wildfires all occurred during 2017 and 2018 [1]. Over 150 fatalities were directly

attributed to these fires [2]—a total greater than during any California earthquake since San Francisco's 'Great Quake' of 1906 [3]. Over 30 000 structures and >1.2 million ha burned in 2017–2018, including nearly the entire Sierra Nevada foothill town of Paradise (population 27 000). State-level fire suppression expenditures exceeded \$1.6 billion in 2017–2018 [1], and estimated economic losses exceeded \$40 billion [2]. Wildfire smoke was transported across the state, exposing millions to prolonged periods of degraded

¹⁰ Author to whom any correspondence should be addressed.

air quality, leading to public health emergencies and the extended closure of thousands of schools and businesses [4]. In the wake of these events, California's largest electricity utility has implemented a policy of pre-emptive 'Public Safety Power Shut-Offs' during periods of severe wildfire risk to reduce the probability of ignitions—resulting in widespread and disruptive California power outages in autumn 2019 [5, 6].

The recent California wildfires have garnered widespread attention, with an especially high level of interest from policymakers and emergency responders seeking to understand the multiple contributors to the increase in wildfire disasters. Quantitative assessments of changing wildfire risk factors have thus become critical as California moves beyond the initial stages of short-term disaster recovery and begins to develop risk mitigation, land management, and resource allocation strategies.

Changing demographic factors have undoubtedly played a substantial role in community exposure and vulnerability [7]—including the expansion of urban and suburban developments into the 'wildland-urban interface' [8]. In many forested regions that historically experienced frequent, low-intensity fire, a century-long legacy of fire suppression has promoted the accumulation of fuels, likely contributing to the size and intensity of some fires [9, 10]. Nevertheless, the broad geographic extent of increased burned area in California and the western United States (U.S.)—across geographies and biomes [11, 12], and even when limited to lightning-caused fires [13, 14]—suggests that demographic and forest management factors alone are insufficient to explain the magnitude of the observed increase in wildfire extent over the past half-century.

California's climate has changed considerably over the past several decades [15]. The state's five warmest years on record occurred in 2014–2018 (figure S1 (stacks.iop.org/ERL/15/094016/mmedia)). In addition, over the past century, robust state-wide warming occurred during all 12 months, with the most pronounced warming in the late summer and early autumn (figure S1). This warming has increased the likelihood and magnitude of hydrological drought [16–18], decreased mountain snowpack [19], and increased vegetation moisture stress and forest mortality [20]. Rising temperatures and declining snowpack—in combination with precipitation deficits that are consistent with emerging evidence of mechanisms that support decreasing precipitation in autumn and spring [21–23]—have acted to extend California's fire season [13, 24, 25]. As global warming continues in the future, regional warming and snowpack loss are expected to accelerate [26–28], concurrent with a regional increase in the frequency of both wet and dry precipitation extremes [17, 21, 29–32]. Therefore, even absent substantial changes in average precipitation, warming and seasonal shifts in

hydroclimate will likely yield pronounced aridification across most of California [16].

Over the past decade, numerous studies have provided substantial insight into the influence of historical climate change on wildfire risk (e.g. [12, 33, 34]). Studies have identified spring and summer warming and earlier melting of snowpack [13, 24]—accompanied by declines in precipitation and wetting rain days during the fire season [35]—as important influences on large wildfires in the western U.S., and demonstrated a 'detectable influence' of historical anthropogenic climate forcing on long-term increases in area burned in Canada [36]. Additional recent studies have attributed approximately half of the increase in annual forest fire area in the western U.S. since the early 1980s to warming-induced increases in fuel aridity [37, 38], and found that anthropogenic climate forcing has greatly enhanced the probability of recent extreme fire seasons (e.g. [39–41]).

Recent autumns have been characterized by multiple large and fast-spreading wildfires burning simultaneously across California. This simultaneous occurrence can quickly compromise the efficacy of local, regional, and even national suppression efforts. Indeed, autumn fires in particular may expose an additional vulnerability: many of the temporary firefighting resources deployed during the core summer fire season—including personnel, vehicles, and aircraft—become unavailable as winter approaches. This is because funding for fire suppression activities has historically been aligned with the 20th century seasonality of wildfire, which typically decreases across most of the American West in the autumn (e.g. [42]). As the seasonality of the fire season broadens in a warming climate, a mismatch can emerge between firefighting resource availability and actual needs [43].

The consequences of such a confluence of events were starkly evidenced in 2018, when large late-autumn fires burning simultaneously in northern and southern California created major logistical challenges, and the heavy commitment of resources simultaneously in both regions required national resources to be ordered [44]. The scope of the resulting wildfire disasters motivates formal analysis of possible changes in the likelihood of warm, dry autumns that enable widespread late season fire activity simultaneously in both northern and southern California.

We therefore focus primarily on climatic factors that contribute to extreme wildfire conditions during autumn, including during two particularly devastating November 2018 events: the Camp Fire, which occurred in a transitional oak woodland in the northern Sierra Nevada foothills; and the Woolsey Fire, which occurred in the coastal chaparral shrub regime near Los Angeles. Both fires ignited during strong and dry 'offshore' downslope wind events, known locally as the Santa Ana winds in Southern California and

Diablo winds in parts of Northern California. The frequency and strength of Santa Ana winds peaks in winter [45], but such winds in autumn that co-occur with dry fuels are responsible for a disproportionate fraction of both area burned [46] and wildfire losses in much of California [47, 48]. While offshore winds in November are not unusual, much of interior northern California and coastal southern California experienced the hottest summer on record in 2018, and autumn rainfall did not arrive across much of the state until mid-to-late November—thus predisposing the region to extreme fire danger conditions.

Motivated by the conditions that led to extreme autumn wildfire activity in 2018, we investigate changes in autumn temperature, precipitation, and daily fire weather indices, with a particular emphasis on the simultaneous co-occurrence of extreme conditions in northern and southern portions of the state. Analyzing both observational and climate model evidence, we seek to quantify (i) whether the occurrence of climate conditions contributing to extreme autumn wildfire potential has changed in recent decades; (ii) whether anthropogenic climate forcing has contributed to any detected changes in extreme fire weather; and (iii) how continued global warming could alter the probability of extreme fire weather in the future. We emphasize that the present investigation only considers changes in climatic contributions to wildfire risk, irrespective of changes in fire ignitions, vegetation, land use or management strategies.

2. Materials and methods

2.1. Historical observations of climate, fire weather, and area burned

We analyze gridded meteorological data ($1/24^\circ$ spatial resolution) from the gridMET database [49] during 1979–2018. We calculate seasonal-mean temperature, precipitation, and Fire Weather Index ('FWI') for each autumn season (September through November; 'SON') from 1979 to 2018 (shown in figures 1 and 2).

The FWI (from the Canadian Forest Fire Danger Weather Index System) is a widely-used generalized measure of fire potential that incorporates both fuel aridity and fire weather (using maximum temperature, minimum relative humidity, wind speed, and precipitation), irrespective of fuel type and abundance [51]. FWI closely tracks interannual variability of other commonly used fire danger metrics such as Energy Release Component (ERC) [37], and exhibits strong empirical links to individual high-intensity fire events (e.g. [48]) and interannual variability in burned area for much of the globe (e.g. [52]).

At each grid point in California, we calculate (i) seasonal-mean temperature by averaging the daily maximum and minimum temperatures in SON of each year; (ii) seasonal total precipitation by summing the daily precipitation accumulation in SON

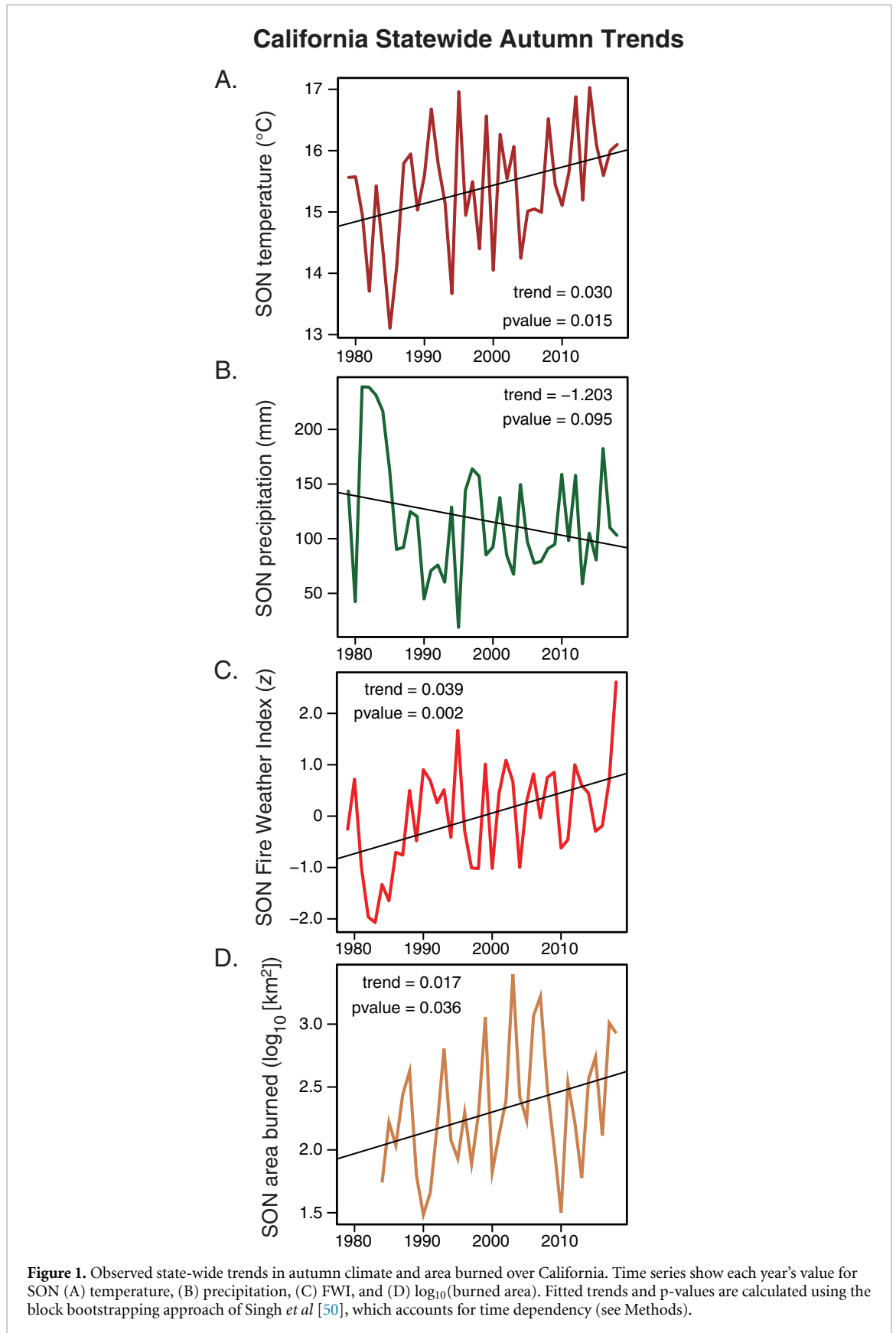
of each year; and (iii) seasonal-mean FWI by averaging the daily FWI values in SON of each year (shown in the maps in figure 2). In addition, we calculate spatially averaged values of SON temperature, precipitation and FWI over the land grid points of three domains: (i) state-wide, encompassing land grid points in California (shown in figure 1); (ii) a Northern Sierra region ($38.75\text{--}40.75^\circ\text{N}$, $122.875\text{--}120.375^\circ\text{W}$) encompassing the city of Paradise and the Camp Fire footprint (shown in figure 2); and (iii) a South Coast region ($33\text{--}35^\circ\text{N}$, $120\text{--}117.5^\circ\text{W}$) encompassing the city of Malibu and the Woolsey Fire footprint (shown in figure 2).

In addition to these climate observations, we analyze burned area data from the Monitoring Trends in Burn Severity dataset during 1984–2016 [53] that includes all large fires >404 ha; these data have been extended through 2018 using burned area from MODIS [54] and applying bias adjustments to the MODIS records [37]. Data include burned area by wildfires that had fire discovery dates between September 1 and November 30, and do not include wildfire events that began prior to September. It is possible to separate burned area by vegetation class (e.g. [12]), and because we find that only 43% of SON burned area over the period of record occurred in forests, we use total burned area for the state-wide analysis shown in figure 1.

For each of the regional-mean climate and area burned time series, we quantify the linear trend and statistical significance using the nonparametric bootstrap resampling approach described in Singh *et al* [50], using $n = 10\,000$ iterations. This resampling approach has two key strengths. First, as a nonparametric resampling method, it is applicable even in cases where the underlying distribution is non-Gaussian. Second, it allows us to account for potential temporal autocorrelation in the raw time series by using a block length greater than that of any statistically significant autocorrelation. The resampling approach, along with the calculation of statistical significance, is described in detail in the supplementary materials of Singh *et al*.

2.2. Relationship between extreme autumn fire weather and area burned

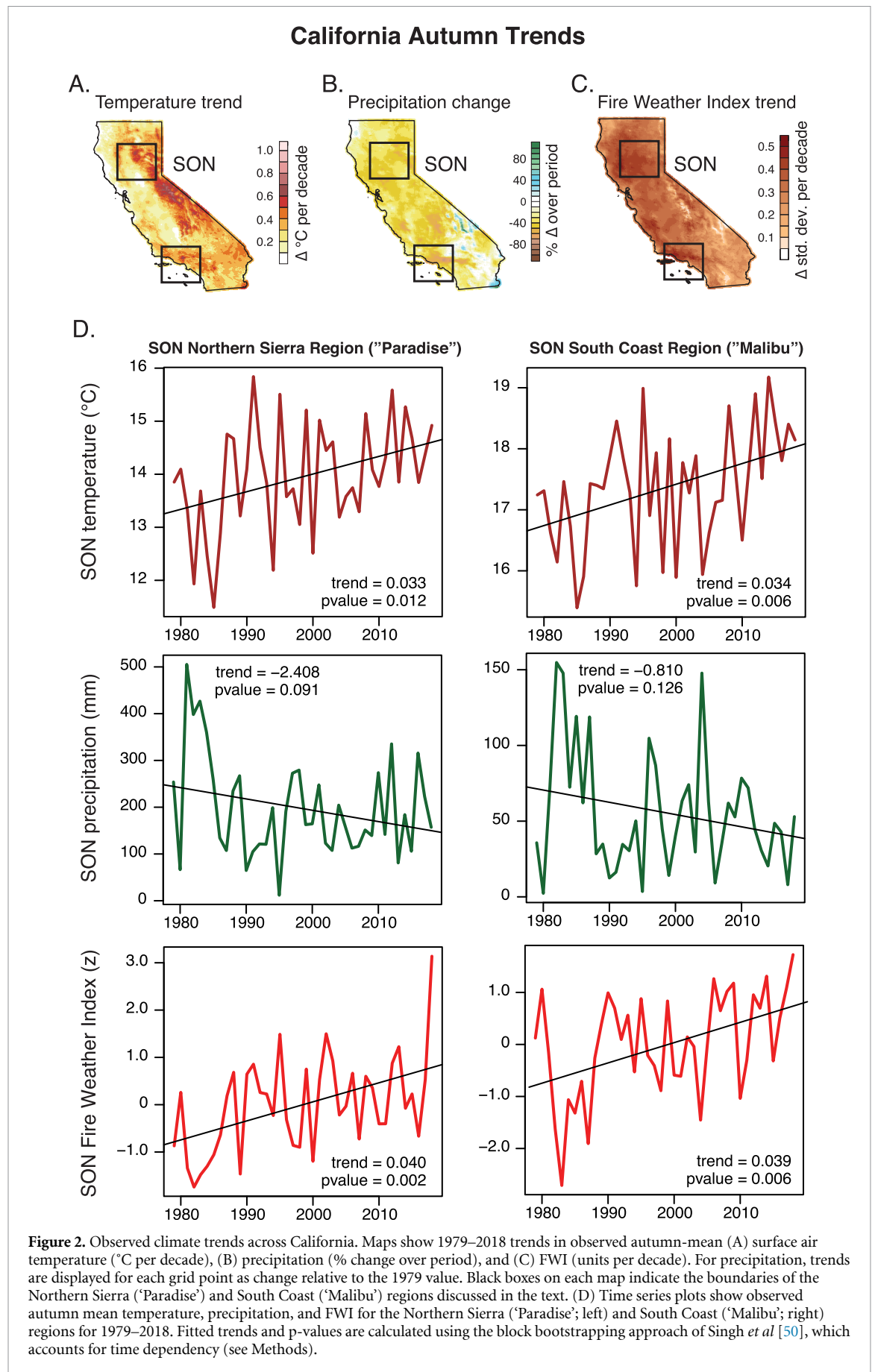
The area burned dataset described in the previous section allows us to quantify the trend and interannual climate-burned area relationships. In addition, to quantify the relationship between extreme daily-scale autumn fire weather and the area burned by individual wildfires, we use the fire database of individual wildfires occurring in non-desert and non-agricultural regions of California from Williams *et al* [12]. We query this dataset from 1979–2018 to identify relationships between daily FWI exceeding the locally-defined 95th percentile (FWI_{95} ; 'extreme fire weather') and the occurrence of very large autumn fires (herein defined as the largest 1%



of autumn fires, or 54.25 km²). We calculate the 95th percentile threshold using data pooled over the calendar year during 1979–2018. We tabulate the maximum FWI over the first three days of each fire at the

fire ignition location, as this often comprises a critical period where fires escape initial attack [55].

In addition, we quantify seasonal relationships between autumn area burned and the number of



FWI₉₅ days. Both measures are aggregated state-wide over the geographic region from Williams *et al* [12] to create annual time series. We calculate bivariate interannual correlations between the logarithm of autumn burned area and the number of FWI₉₅ during 1984–2018 using both Pearson and Spearman correlation coefficients. As in previous studies, we use logarithms of burned area to overcome the exponential distribution of burned area records. Correlations are additionally calculated using detrended data to assess whether interannual relationships were strongly contingent on trends. Finally, we estimate average annual SON burned area for years where the state-wide FWI₉₅ was above and below the 1984–2018 median (approximately 5.5 d). Given the heavily right skewed nature of burned area, we quantify uncertainty of these estimates through bootstrap resampling with replacement ($n = 1000$).

2.3. Simulated occurrence of extreme fire weather during the 20th and 21st centuries

We calculate daily FWI using the statistically down-scaled (1/24th degree) maximum temperature, minimum relative humidity, wind speed, and precipitation fields from 18 CMIP5 models, described in [56]. These high-resolution fields are available for 1950–2005 in the CMIP5 Historical forcing, and 2006–2099 in the CMIP5 RCP4.5 and RCP8.5 forcing pathways. Together, they represent a unique, extremely high-resolution, daily-scale version of the CMIP5 ensemble. Although these high-resolution fields do not extend back to the late-19th/early-20th century (and therefore cannot be used to calculate changes in the probability of extreme autumn fire weather conditions since the Industrial Revolution), they do enable an unprecedented analysis of the spatial response of extreme fire weather to increases in climate forcing over the past half century, and projection of changes in multiple future climate forcing scenarios.

This high-resolution version of the CMIP5 dataset allows us to examine responses to two distinct future anthropogenic emissions scenarios: (i) a ‘high emission’ scenario (RCP8.5, which is the forcing most closely matching actual emissions over the past decade [57]), and (ii) a ‘stabilization’ scenario (RCP4.5, which is a forcing scenario slightly lower than that which would result from adherence to existing national commitments made as part of the Paris Agreement [58, 59]). While the RCP8.5 ‘high emissions’ scenario is viewed by some as implausible, we include it in our analysis because, while the underlying socioeconomic assumptions and resultant energy portfolio underpinning the RCP8.5 scenario may be implausible, attainment of ‘RCP8.5-like’ warming may be possible even under lower emission trajectories if carbon cycle feedbacks are stronger than anticipated (e.g. [60]), and/or if climate sensitivity is

higher than had previously been projected—as preliminary results from new CMIP6 simulations suggest is possible [61].

We harmonize this CMIP5 analysis with the analysis of observed extreme daily FWI (see previous section) by calculating the 95th percentile FWI value at each grid point across all calendar days during the CMIP5-simulated 1979–2018 period. We then calculate the mean frequency of occurrence of SON days that exceed the respective grid-point FWI₉₅ threshold during 1950–2005 of the CMIP5 Historical simulations, along with 2006–2099 of the CMIP5 RCP4.5 and RCP8.5 simulations.

We use these high-resolution grid-point time series of autumn FWI₉₅ days to conduct four analyses (shown in figures 4 and 5):

First, for each of the individual CMIP5 realizations, we calculate the 1979–2018 trend in autumn FWI₉₅ days over the Northern Sierra (Paradise) and South Coast (Malibu) regions. As described in [62], we use a binomial test to compare the frequency of positive trends with the null hypothesis that in a stationary climate the probability of a positive multi-decadal trend is 0.5.

Second, for each year between 1950 and 2099 in the CMIP5 Historical, RCP4.5 and RCP8.5 simulations, we calculate the number of autumn FWI₉₅ days in the Northern Sierra region, and the number of autumn FWI₉₅ days in the South Coast region. Then, for each region, we calculate the mean of the CMIP5 values in each year, yielding an annual time series of CMIP5-mean autumn FWI₉₅ occurrence for the Northern Sierra and South Coast regions.

Third, for each year between 1950 and 2099 in the CMIP5 Historical, RCP4.5 and RCP8.5 simulations, we identify each of the CMIP5 realizations for which both the Northern Sierra and South Coast regions experience >5 FWI₉₅ days during autumn. We then calculate the fraction of the CMIP5 realizations meeting this criterion in each year, yielding an annual time series of the probability that both the Northern Sierra and South Coast regions experience >5 FWI₉₅ days in the same autumn season.

Fourth, we calculate the mean occurrence of autumn FWI₉₅ days at each of the high-resolution grid points during three 30-year periods of the CMIP5 RCP4.5 and RCP8.5 simulations: 2006–2035, 2036–2065 and 2066–2095. Together, these three periods span the cumulative emissions and global temperature changes of similar periods in RCP2.6 and RCP6.0, with all four RCPs overlapping closely during the early period [63].

3. Results and discussion

3.1. Observed trends in climate, fire weather, and area burned

Between 1979 and 2018, state-wide autumn trends were +0.30 °C/decade ($p = 0.015$) for

temperature, -12.03 mm/decade ($p = 0.095$) for precipitation, and $+0.39$ standard deviations/decade ($p = 0.002$) for FWI (figure 1). Likewise, the trend in state-wide autumn burned area corresponded to an increase of $\sim 40\%$ per decade during 1984–2018 ($p = 0.036$).

These state-wide trends are reflected more broadly throughout California, with most areas having experienced positive temperature trends (figure 2(A)), negative autumn precipitation trends, and positive autumn FWI trends (figure 2(C)) during 1979–2018. The Northern Sierra (Paradise) and South Coast (Malibu) regions have exhibited autumn temperature trends of $+0.33$ °C/decade ($p = 0.012$) and $+0.34$ °C/decade ($p = 0.006$), respectively, along with autumn precipitation trends of -24.08 mm/decade ($p = 0.091$) and -8.10 mm/decade ($p = 0.126$) (figure 2(D)). Further, strongly positive FWI trends have been observed for both the Northern Sierra ($+0.40$ standard deviations/decade; $p = 0.002$) and South Coast ($+0.39$ standard deviations/decade; $p = 0.006$) regions.

The autumn 2018 FWI value was the highest in the observed record for both the Northern Sierra and South Coast regions (figure 2(D)). However, those record FWI values were not associated with record SON temperature or precipitation in either region (figure 2(D)). This discrepancy highlights the fact that FWI incorporates build-up factors (e.g. summer aridity) that entrain some memory of summer conditions into early autumn, as well as the multivariate and nonlinear nature of FWI calculations.

The seasonal mean precipitation from the full October–November period may also not always represent on-the-ground moisture conditions coincident with fire activity, since individual large storms during mid-late November can occasionally offset critically dry antecedent conditions. In 2018, a series of Pacific storm systems brought widespread heavy rainfall and anomalously cool temperatures to California in the final ~ 10 d of November. However, conditions from September through the first half of November were very warm and dry, which produced a period of extraordinarily high wildfire potential (figure 2(D)) during which both the Camp and Woolsey fires ignited and spread. Additionally, the record downslope-wind-driven Thomas Fire in 2017 ignited in early December [46], suggesting that future analyses may need to consider September–December, as the later onset of precipitation extends the autumn fire season later into the year. Although further research is needed to fully assess changes in the precise timing of cool-season precipitation onset, recent work suggests that projected sub-seasonal shifts in California precipitation ([17, 21–23, 29]; figure S2) have significant potential to interact non-linearly with changes in the seasonality of autumn offshore winds [64].

3.2. Observed relationships between extreme autumn fire weather and area burned

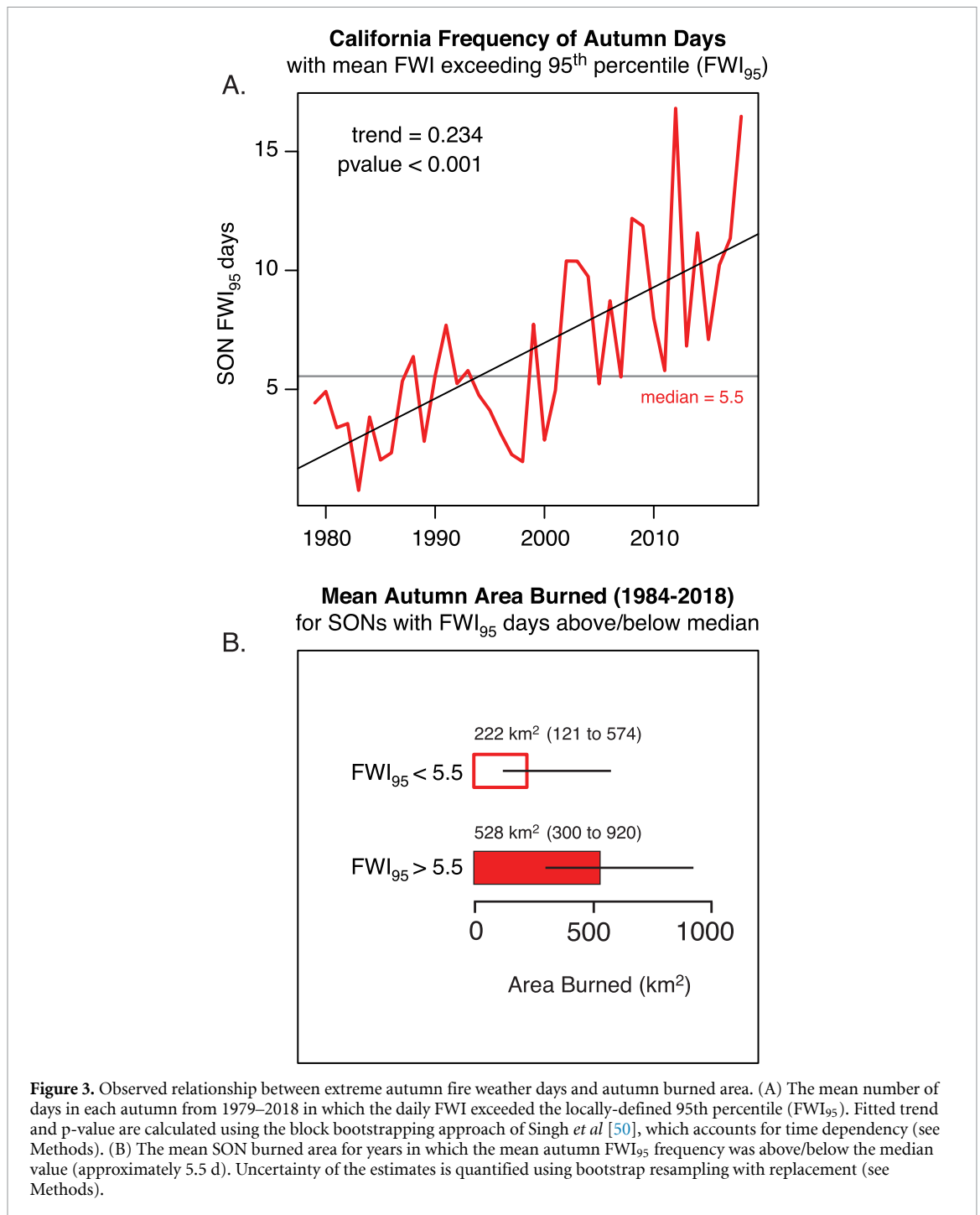
We find moderate interannual correlations between SON area burned and the mean number of SON days in which FWI exceeds the locally-defined 95th percentile (FWI_{95}) (e.g. $r > 0.35$ for forest and non-forest area; Table S1). Correlations between SON burned area and FWI_{95} days are stronger than those between SON burned area and seasonal FWI, temperature, or precipitation. These weaker relationships to total SON burned area are consistent with prior studies [12, 65]. A matrix of additional factors ultimately shape autumn fire potential and realized fire activity, including live fuel moistures; sensitivity of short-term fuel abundance in grassland regions to the preceding winter/spring moisture availability (e.g. [66]); and the stochastic nature of synchronization between predominantly human-caused ignitions, critical fire weather conditions, and dry fuels.

Given the inherent limitations of the relationships between seasonal-scale climate variables and wildfire activity, we also analyze relationships with daily-scale fire weather conditions at the individual fire event level. Approximately 60% of the largest 1% of autumn fires during 1979–2018 started or were immediately followed within the first two days by extreme fire weather conditions. Further, we find substantially more area burned in SON seasons with greater frequency of FWI_{95} days. For instance, over the 1984–2018 period, the mean area burned for SON seasons in which the number of FWI_{95} days exceeded the median FWI_{95} frequency (5.5 d) was 528 km² (95% range: 300–920 km²), compared with 222 km² (95% range: 121–574 km²) for SON seasons in which the number of FWI_{95} days was less than the median frequency (figure 3(B)).

The occurrence of autumn FWI_{95} days has increased substantially in recent decades (figure 3(A)). Over the 1979–2018 period, the regional average number of SON FWI_{95} days exhibits a trend of $+2.34$ d/decade ($p < 0.001$). As a result, the mean number of days with extreme fire weather during the autumn season has more than doubled since the late 1970s. Further, 2005 was the last year in which the regional average fell below the 1979–2018 median value.

3.3. Response of extreme autumn fire weather to historical and future changes in climate forcing

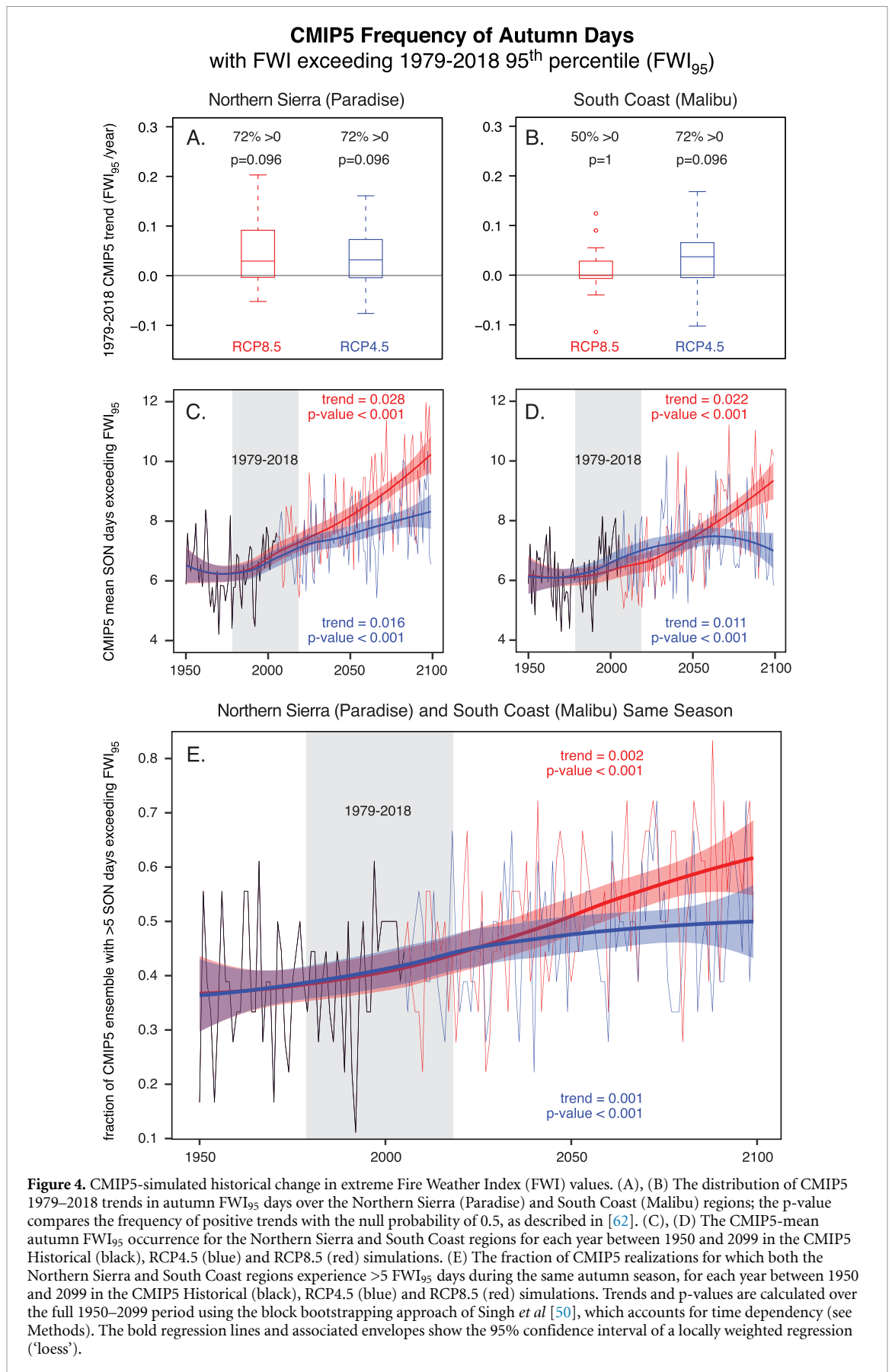
Given the elevated probability of extensive area burned for autumn seasons with >5 FWI_{95} days (figure 3), we compare the frequency of FWI_{95} days—and seasons with >5 FWI_{95} days—for different periods of the CMIP5 historical and future climate simulations. During the 1979–2018 period, both the Northern Sierra and South Coast regions exhibit simulated increases in frequency of autumn FWI_{95} days, both in the mean of the CMIP5 realizations (fig-

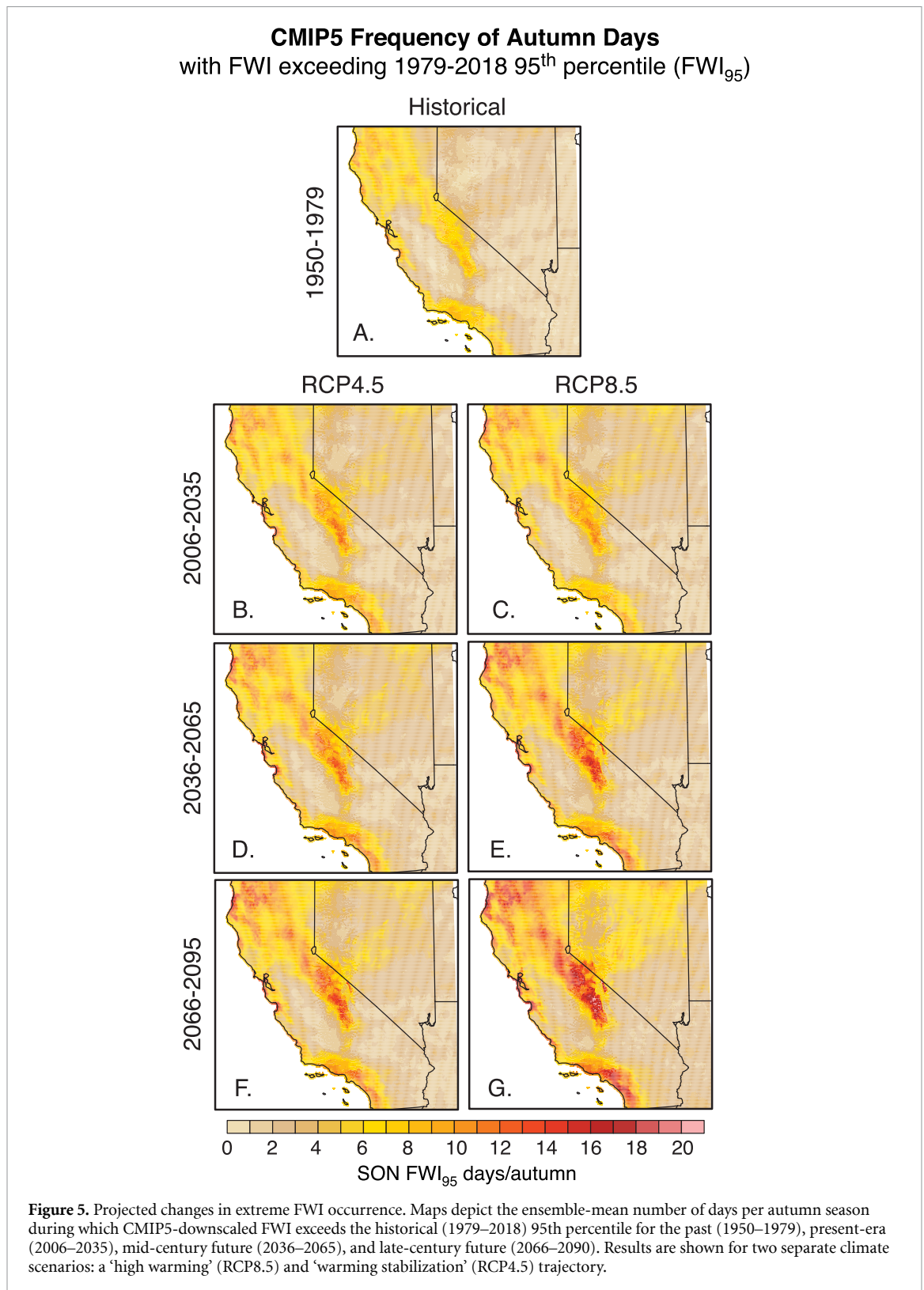


ures 4(C), (D)), and in a majority of the individual realizations (figures 4(A), (B)). These increases in FWI₉₅ days result in increases in the joint occurrence of years in which both the Northern Sierra and South Coast regions experience high FWI₉₅ occurrence during the same autumn (figure 4(E)). For example, the CMIP5-mean simulated fraction of SON seasons in which there are >5 FWI₉₅ days in both the Northern Sierra and South Coast regions increases from ~0.35 to >0.40 between 1950 and 2018.

Simulated future changes in extreme FWI days are projected in both ‘high warming’ (RCP8.5) and ‘warming stabilization’ (RCP4.5) scenarios. Both the

Northern Sierra and South Coast regions exhibit increases in mean FWI₉₅ occurrence of >25% over the remainder of the 21st century in RCP8.5, reaching a mean of ~10 d/autumn over the Northern Sierra and ~9 d/autumn over the South Coast (figure 4(B)). The multi-model mean increases are reduced in RCP4.5, reaching a mean of ~8 d/autumn over the Northern Sierra and ~7 d/autumn over the South Coast (figure 4(B)). As a result, the projected fraction of autumn seasons in which both the Northern Sierra and South Coast experience >5 FWI₉₅ days is reduced from ~0.6 at the end of the 21st century in RCP8.5 to below 0.5 in RCP4.5.





The greater intensification of extreme wildfire weather in the ‘high warming’ RCP8.5 scenario is also reflected in much of the rest of California (figure 5). During the present era (2006–2035), RCP8.5 and RCP4.5 show similar increases in FWI₉₅ occurrence, with the area experiencing >10 FWI₉₅ days/autumn expanding over northern California, the Sierra Nevada, and the Pacific coast relative to the mid-20th

century (1950–1979). By the mid-21st century (2036–2065), RCP8.5 exhibits a higher frequency of FWI₉₅ days over many of the high-FWI regions, including much of northern California, the Sierra Nevada and the South Coast. These differences between RCP4.5 and RCP8.5 are further exacerbated in the late-21st century. Specifically, the frequency of FWI₉₅ days is projected to remain below 15 d/autumn

throughout almost all of the state in 2066–2095 of RCP4.5, but it is projected to exceed 15 d/autumn over many of the high-FWI regions in 2066–2095 of RCP8.5.

We emphasize that although the projected increases in extreme FWI are not spatially uniform, they are essentially ubiquitous across vegetated areas of California. In particular, we note ‘hotspots’ of extreme projected FWI increases in regions with very different vegetation regimes. For example, relative increases in extreme FWI frequency are broadly projected to exceed 50% by the late-21st century of RCP4.5 (relative to 1950–1979), and approach 100% in some regions by the late-21st century of RCP8.5 (figure 5). This finding strongly suggests that—at least from an extreme fire weather perspective—the direct influence of climate change on wildfire risk is not limited to California’s forested regions, and instead extends across a diverse range of microclimates and ecoregions as long as fuel abundance is not limiting.

4. Conclusions

We report a substantial and statistically significant historical trend toward autumns which are increasingly conducive to enhanced wildfire risk across most of California. This observed increase in weather-driven autumn wildfire risk coincides with a strong and robust warming trend ($+0.30$ °C/decade; $p = 0.015$), and a modest negative precipitation trend (-12.03 mm/decade; $p = 0.095$) over the 1979–2018 period. Observations and climate model simulations suggest that the likelihood of Northern and Southern California simultaneously experiencing extreme autumn fire weather conditions has increased since the mid-20th century. Climate model simulations further suggest that continued warming and strengthening of seasonal drying trends in the future will likely result in further increases in extreme autumn fire weather conditions throughout California—even for a future climate scenario similar to that which would result from adherence to commitments made in the UN Paris Agreement [58, 59]. Collectively, this analysis offers strong evidence for a human fingerprint on the observed increase in meteorological preconditions necessary for extreme wildfires in California. Absent a strong decrease in autumn wind patterns, observed and projected temperature and precipitation trends portend increasing risk that autumn offshore wind events will coincide with critically dry fuels—increasing the potential for wildfire catastrophes when fires affect populated areas.

We note several caveats. First, the increases in wildfire probability that we quantify are based on links with FWI, but not on simulations of wildfire frequency. However, there are physical and empirical bases for the relationship with FWI (e.g. [67–69]) and our results help to further refine the linkage

between the occurrence of extreme autumn fire weather and autumn area burned (figure 3; table S1). Second, although the high-resolution climate datasets enable analysis of historical and projected changes in extreme fire weather potential, gridded datasets are imperfect approximations of real-world weather conditions, climate trends, and the response of local climate to changes in forcing (including the mesoscale atmospheric dynamics that generate strong wind events). Third, there are uncertainties associated with internal low-frequency climate variability apparent in multi-decadal climate observations of simulations (e.g. [70]), especially with respect to precipitation trends [26], that may alter past and future multi-decadal trajectories of autumn extreme fire weather from those dictated by anthropogenic climate forcing alone. Additionally, we do not account for feedback mechanisms between climate, wildfire, and the biosphere. These could include negative climate-fire feedbacks that result from dynamic vegetation processes that lessen future fuel loads [71]—although positive climate-fire feedbacks are also plausible in some higher-frequency fire regimes and in regions where invasive grasses proliferate [72].

We also emphasize that climate change is only one of several factors driving California’s multi-year wildfire disaster. Nearly 88% of fires and 92% of burned area from autumn wildfires in California are human-caused [73], highlighting human ignition sources as key contributors. However, the number of ignitions has declined over the past several decades [74]. In the present study, we do not quantify the relative role of increased urban and suburban incursion into the high-risk wildland-urban interface, nor the contribution of historical land/vegetation management practices to increasing wildfire risk or possible future climate-fire feedbacks. We note, however, that although demographics and vegetation exhibit high spatial heterogeneity, observed and projected climate trends relevant to wildfire risk (including temperature, precipitation, and FWI) are pervasive across California’s major ecological zones, vegetation types, and fire regimes (e.g. [75]). California’s mean climate is aridifying from a net water balance perspective [12]—primarily due to rising temperatures, but also with some contribution from the potentially narrowing seasonality and shifting temporal characteristics of precipitation [21, 30–32]. Increased aridity in semi-arid landscapes in California may alter fire-climate relationships, resulting in fuel-limited regimes in regions that become increasingly sensitive to interannual variations in biomass abundance, and less sensitive to the aridity of the vegetation itself (e.g. [76, 77]). A key consequence of climate change-driven aridification is that vegetation throughout the state is becoming increasingly flammable, setting the stage for extreme burning conditions given an ignition source and otherwise conducive weather conditions.

Climate change can thus be viewed as a wildfire ‘threat multiplier’ amplifying natural and human risk factors that are already prevalent throughout California.

Observed and projected trends suggest that anthropogenic climate change has already facilitated conditions that are increasingly conducive to wildfire activity, and that continued global warming will continue to intensify those conditions in the future. Increased synchronicity of extreme fire danger between northern and southern California has the potential to hamper fire suppression and risk-reduction efforts, particularly as longer fire seasons increase fatigue among firefighters and evacuated residents alike. Absent substantial interventions, our results portend even greater potential for future wildfire disasters in California, placing further burdens on an already stressed global fire suppression network. In the long-term, reduction of global greenhouse gas emissions is the most direct path to reducing this risk, though the near-term impacts of these reductions may be limited given the many sources of inertia in the climate system [78]. Fortunately, a broad portfolio of options already exists, including the use of prescribed burning to reduce fuel loads and improve ecosystem health [79], upgrades to emergency communications and response systems, community-level development of protective fire breaks and defensible space, and the adoption of new zoning rules and building codes to promote fire-resilient construction [80]. Assessment of those options will require integration of perspectives from multiple disciplines in order to fully understand the complex ecological, meteorological and human interactions revealed during the recent wildfires in California.

Acknowledgments

We thank the editor and five anonymous reviewers for insightful and constructive feedback. We acknowledge the World Climate Research Programme’s Working Group on Coupled Modelling, the U.S. Department of Energy’s Program for Climate Model Diagnosis and Intercomparison, and the climate modeling groups for contributing their model output to CMIP5. Goss and Duffenbaugh were supported by Stanford University and the Department of Energy. Swain was supported by a joint collaboration between the Institute of the Environment and Sustainability at the University of California, Los Angeles; the Center for Climate and Weather Extremes at the National Center for Atmospheric Research; and the Nature Conservancy of California. Kolden and Abatzoglou were partially supported by the National Science Foundation under DMS-1520873. Williams was supported by the Zegar Family Foundation.

Data availability

The data that support the findings of this study are available from the corresponding author upon reasonable request. Observed temperature, precipitation and FWI data were obtained from the gridMET dataset (www.climatologylab.org/gridmet.html). Climate model temperature and precipitation data, as well as all other underlying variables required to calculate FWI, were obtained from the CMIP5 archive (accessible via the Earth System grid at <https://esgf-node.llnl.gov/projects/cmip5/>). Downscaled climate data used to calculate FWI were obtained from the Multivariate Adaptive Constructed Analogs archive (www.climatologylab.org/maca.html). A database of daily downscaled FWI covering the region 32.5–42N, 113–125W will be made available at www.climatologylab.org. Time series of temperature, precipitation, Fire Weather Index and burned area plotted in figures 1 and 2 are available in supplementary data file 1 of this paper.

ORCID iDs

Michael Goss  <https://orcid.org/0000-0003-2106-9210>

Daniel L Swain  <https://orcid.org/0000-0003-4276-3092>

John T Abatzoglou  <https://orcid.org/0000-0001-7599-9750>

Ali Sarhadi  <https://orcid.org/0000-0001-9038-9619>

Crystal A Kolden  <https://orcid.org/0000-0001-7093-4552>

A Park Williams

 <https://orcid.org/0000-0001-8176-8166>

Noah S Duffenbaugh  <https://orcid.org/0000-0002-8856-4964>

References

- [1] CAL FIRE 2019 (Accessed: 10 April 2019) (available at: <https://calfire.ca.gov>)
- [2] Kolden C A, Williamson G J, Abatzoglou J T, Steuer M and Bowman D M J S 2019 A global increase in wildfire disasters in preparation
- [3] NOAA 2018 National Geophysical Data Center/World Data Service (NGDC/WDS): Significant Earthquake Database. NOAA Natl Geophys Data Cent 1755(April):711657 (available at: www.ngdc.noaa.gov/hazard/earthqk.shtml)
- [4] Mull A 2018 Smoke Days Are Now California’s Snow Days. *The Atlantic* (Accessed: 17 November 2018) pp 1–5 (available at: www.theatlantic.com/health/archive/2018/11/california-wildfires-smoke-days/576112/)
- [5] Penn I 2019 PG&E Begins Power Shut-Off to 179,000 California Customers *The New York Times* (Accessed: 12 November 2019) (available at: www.nytimes.com/2019/10/23/business/energy-environment/california-power.html)
- [6] Tollefson J California wildfires and power outages cause disruptions for scientists *Nature* 575 2019 (Accessed: 12

- November 2019) p16 (available at: www.nature.com/articles/d41586-019-03302-z)
- [7] Radeloff V C, Helmers D P, Anu Kramer H, Mockrin M H, Alexandre P M Bar-Massada A et al 2018 Rapid growth of the US wildland-urban interface raises wildfire risk *Proc. Natl Acad. Sci. USA* **115** 3314–19
 - [8] Kramer H A, Mockrin M H, Alexandre P M and Radeloff V C 2019 High wildfire damage in interface communities in California *Int. J. Wildl and Fire* **28** 641–50
 - [9] Marlon J R, Bartlein P J, Gavin D G, Long C J, Anderson R S, Briles C E et al 2012 Long-term perspective on wildfires in the western USA *Proc. Natl Acad. Sci. USA* **109** 9
 - [10] Stephens S L, Agee J K, Fulé P Z, North M P, Romme W H, Swetnam T W et al 2013 Managing forests and fire in changing climates *Science* **342** 41–42
 - [11] Dennison P E, Brewer S C, Arnold J D and Moritz M A 2014 Large wildfire trends in the western United States, 1984–2011 *Geophys Res. Lett.* **41** 2928–33
 - [12] Williams A P, Abatzoglou J T, Gershunov A, Guzman-Morales J, Bishop D A Balch J K et al 2019 Observed impacts of anthropogenic climate change on wildfire in California *Earth's Futur.* **7** 892–910
 - [13] Westerling A L 2016 Increasing western US forest wildfire activity: sensitivity to changes in the timing of spring *Philos. Trans. R Soc. B: Biol. Sci.* **371** 20150178
 - [14] Balch J K, Bradley B A, Abatzoglou J T, Chelsea Nagy R, Fusco E J and Mahood A L 2017 Human-started wildfires expand the fire niche across the United States *Proc. Natl Acad. Sci. USA* **114** 2946–51
 - [15] Mooney H and Zavaleta E 2019 Part one: drivers. Chapter 14: climate change impacts *Ecosystems of California*, ed M C Chapin (Oakland, CA: University of California Press) pp 251–64
 - [16] Barnett T P, Pierce D W, Hidalgo H G, Bonfils C, Santer B D, Das T et al 2008 Human-induced changes in the hydrology of the Western United States *Science* **319** 1080–3
 - [17] Diffenbaugh N S, Swain D L, Touma D and Lubchenco J 2015 Anthropogenic warming has increased drought risk in California *Proc. Natl Acad. Sci. USA* **112** 3931–6
 - [18] Williams A P, Seager R, Abatzoglou J T, Cook B I, Smerdon J E and Cook E R 2015 Contribution of anthropogenic warming to California drought during 2012–2014 *Geophys Res. Lett.* **42** 6819–28
 - [19] Mote P W, Li S, Lettenmaier D P, Xiao M and Engel R 2018 Dramatic declines in snowpack in the western US *npj Clim. Atmos. Sci.* **1** 2
 - [20] Van Mantgem P J, Stephenson N L, Byrne J C, Daniels L D, Franklin J F Fulé P Z et al 2009 Widespread increase of tree mortality rates in the Western United States *Science* **323** 521–4
 - [21] Swain D L, Langenbrunner B, Neelin J D and Hall A 2018 Increasing precipitation volatility in twenty-first-century California *Nat. Clim. Chang.* **8** 427–33
 - [22] Dong L, Leung L R, Lu J and Song F 2019 Mechanisms for an amplified precipitation seasonal cycle in the u.s. west coast under global warming *J. Clim.* **32** 4681–98
 - [23] Dong L, Leung L R, Lu J and Gao Y 2019 Contributions of extreme and non-extreme precipitation to California precipitation seasonality changes under warming *Geophys Res. Lett.* **46** 13470–8
 - [24] Westerling A L, Hidalgo H G, Cayan D R and Swetnam T W 2006 Warming and earlier spring increase Western U.S. forest wildfire activity *Science* **313** 940–3
 - [25] Westerling A L 2018 Wildfire simulations for California's fourth climate change assessment: projecting changes in extreme wildfire events with a warming climate California's Fourth Climate Change Assessment, California Energy Commission (available at: www.climateassessment.ca.gov/techreports/docs/20180827-Projections_CCCA4-CEC-2018-014.pdf)
 - [26] Ashfaq M, Ghosh S, Kao S C, Bowling L C, Mote P, Touma D et al 2013 Near-term acceleration of hydroclimatic change in the western U.S. *J. Geophys Res. Atmos.* **118** 10676–93
 - [27] Walton D B, Hall A, Berg N, Schwartz M and Sun F 2017 Incorporating snow albedo feedback into downscaled temperature and snow cover projections for California's Sierra Nevada *J. Clim.* **30** 1417–38
 - [28] Schwartz M, Hall A, Sun F, Walton D and Berg N 2017 Significant and inevitable end-of-twenty-first-century advances in surface runoff timing in California's Sierra Nevada *J. Hydrometeorol.* **18** 3181–97
 - [29] Diffenbaugh N S and Giorgi F 2012 Climate change hotspots in the CMIP5 global climate model ensemble *Clim. Change* **114** 813–22
 - [30] Berg N and Hall A 2015 Increased interannual precipitation extremes over California under climate change *J. Clim.* **28** 6324–34
 - [31] Dettinger M D 2016 Historical and future relations between large storms and droughts in California *San. Fr. Estuary Watershed Sci.* **14**
 - [32] Dong L, Leung L R and Song F 2018 Future changes of subseasonal precipitation variability in North America during winter under global warming *Geophys Res. Lett.* **45** 12467–76
 - [33] Williams A P and Abatzoglou J T 2016 Recent advances and remaining uncertainties in resolving past and future climate effects on global fire activity *Curr. Clim. Change Reports* **2** 1–14
 - [34] Abatzoglou J T, Williams A P and Barbero R 2019 Global emergence of anthropogenic climate change in fire weather indices *Geophys Res. Lett.* **46** 326–36
 - [35] Holden Z A, Swanson A, Luce C H, Jolly W M, Maneta M, Oyster J W et al 2018 Decreasing fire season precipitation increased recent western US forest wildfire activity *Proc. Natl Acad. Sci. USA* **115** E8349–57
 - [36] Gillett N P, Weaver A J, Zwiers F W and Flannigan M D 2004 Detecting the effect of climate change on Canadian forest fires *Geophys Res. Lett.* **31**
 - [37] Abatzoglou J T and Williams A P 2016 Impact of anthropogenic climate change on wildfire across western US forests *Proc. Natl Acad. Sci. USA* **113** 11770–5
 - [38] Duffy P B, Field C B, Diffenbaugh N S, Doney S C, Dutton Z, Goodman S et al 2019 Strengthened scientific support for the Endangerment Finding for atmospheric greenhouse gases *Science* **363** eaat5982
 - [39] Kirchmeier-Young M C, Zwiers F W, Gillett N P and Cannon A J 2017 Attributing extreme fire risk in Western Canada to human emissions *Clim. Change* **144** 365–79
 - [40] Kirchmeier-Young M C, Gillett N P, Zwiers F W, Cannon A J and Anslow F S 2019 Attribution of the influence of human-induced climate change on an extreme fire season *Earth's Futur.* **7** 2–10
 - [41] Yoon J H, Simon Wang S Y, Gillies R R, Hipps L, Kravitz B and Rasch P J 2015 Extreme fire season in California: a glimpse into the future? *Bull. Am. Meteorol. Soc.* **96** S5–9
 - [42] Westerling A L, Gershunov A, Brown T J, Cayan D R and Dettinger M D 2003 Climate and wildfire in the western United States *Bull. Am. Meteorol. Soc.* **84** 595–604+548
 - [43] Corringham T W, Westerling A L and Morehouse B J 2008 Exploring use of climate information in wildland fire management: A decision calendar study *J. For.* **106** 71–77 (<https://academic.oup.com/jof/article/106/2/71/4734833>)
 - [44] NIFC. Incident Management Situation Report National Interagency Coordination Center. (Accessed: 19 August 2019) (available at: www.predictiveservices.nifc.gov/IMSR/2018/20181112IMSR.pdf)
 - [45] Guzman-Morales J, Gershunov A, Theiss J, Li H and Cayan D 2016 Santa Ana Winds of Southern California: their climatology, extremes, and behavior spanning six and a half decades *Geophys Res. Lett.* **43** 2827–34
 - [46] Kolden C and Abatzoglou J 2018 Spatial distribution of wildfires ignited under katabatic versus non-katabatic winds in mediterranean Southern California USA *Fire* **1** 19
 - [47] Jin Y, Goulden M L, Faivre N, Veraverbeke S, Sun F, Hall A et al 2015 Identification of two distinct fire regimes in Southern California: implications for economic impact and future change *Environ. Res. Lett.* **10**

- [48] Bowman D M J S, Williamson G J, Abatzoglou J T, Kolden C A, Cochrane M A and Smith A M S 2017 Human exposure and sensitivity to globally extreme wildfire events *Nat. Ecol. Evol.* **1**
- [49] Abatzoglou J T 2013 Development of gridded surface meteorological data for ecological applications and modelling *Int. J. Climatol.* **33** 121–31
- [50] Singh D, Tsiang M, Rajaratnam B and Diffenbaugh N S 2014 Observed changes in extreme wet and dry spells during the south Asian summer monsoon season *Nat. Clim. Chang.* **4** 456–61
- [51] Flannigan M, Cantin A S, De Groot W J, Wotton M, Newbery A and Gowman L M 2013 Global wildland fire season severity in the 21st century *For. Ecol. Manage.* **294** 54–61
- [52] Abatzoglou J T, Williams A P, Boschetti L, Zubkova M and Kolden C A 2018 Global patterns of interannual climate–fire relationships *Glob. Chang. Biol.* **24** 5164–75
- [53] Eidenshink J, Schwind B, Brewer K, Zhu Z-L, Quayle B and Howard S 2007 A project for monitoring trends in burn severity *Fire Ecol.* **3** 3–21
- [54] Boschetti L, Roy D P, Giglio L, Huang H, Zubkova M and Humber M L 2019 Global validation of the collection 6 MODIS burned area product *Remote Sens. Environ.* **235**
- [55] Abatzoglou J T, Balch J K, Bradley B A and Kolden C A 2018 Human-related ignitions concurrent with high winds promote large wildfires across the USA *Int. J. Wildl and Fire* **27** 377–86
- [56] Abatzoglou J T and Brown T J 2012 A comparison of statistical downscaling methods suited for wildfire applications *Int. J. Climatol.* **32** 772–80
- [57] Fuss S, Canadell J G, Peters G P, Tavoni M, Andrew R M, Ciais P et al 2014 COMMENTARY: betting on negative emissions *Nat. Clim. Chang.* **4** 850–3
- [58] Rogelj J, Den Elzen M, Höhne N, Fransen T, Fekete H, Winkler H et al 2016 Paris agreement climate proposals need a boost to keep warming well below 2 °C *Nature* **534** 631–9
- [59] Gütschow J, Jeffery M L, Schaeffer M and Hare B 2018 Extending near-term emissions scenarios to assess warming implications of Paris agreement NDCs *Earth's Futur.* **6** 1242–59
- [60] Natali S M, Watts J D, Rogers B M, Potter S, Ludwig S M, Selbmann A K et al 2019 Large loss of CO₂ in winter observed across the northern permafrost region *Nat. Clim. Chang.* **9** 852–7
- [61] Forster P M, Maycock A C, McKenna C M and Smith C J 2020 Latest climate models confirm need for urgent mitigation *Nat. Clim. Chang.* **10** 7–10
- [62] Diffenbaugh N S, Singh D, Mankin J S, Horton D E, Swain D L, Touma D et al 2017 Quantifying the influence of global warming on unprecedented extreme climate events *Proc. Natl Acad. Sci. USA* **114** 4881–6
- [63] Pachauri R K, Meyer L, Van Ypersele J-P, Brinkman S, Van Kesteren L, Leprince-Ringuet N and Van Boxmeer F 2014 Climate Change 2014: Synthesis Report. Contribution of Working Groups I, II and III to the Fifth Assessment Report of the Intergovernmental Panel on Climate Change. IPCC p 151
- [64] Guzman-Morales J and Gershunov A 2019 Climate Change Suppresses Santa Ana Winds of Southern California and Sharpens Their Seasonality *Geophys Res. Lett.* **46** 2772–80
- [65] Jin Y, Randerson J T, Faivre N, Capps S, Hall A and Goulden M L 2014 Contrasting controls on wildland fires in Southern California during periods with and without Santa Ana winds *J. Geophys Res. Biogeosci.* **119** 432–50
- [66] Keeley J E 2004 Impact of antecedent climate on fire regimes in coastal California *Int. J. Wildl and Fire* **13** 173–82
- [67] Jolly W M 2007 Sensitivity of a surface fire spread model and associated fire behaviour fuel models to changes in live fuel moisture *Int. J. Wildl and Fire* **16** 503–9
- [68] Flannigan M D, Wotton B M, Marshall G A, de Groot W J, Johnston J, Jurko N et al 2016 Fuel moisture sensitivity to temperature and precipitation: climate change implications *Clim. Change* **134** 59–71
- [69] Williams A P, Gentile P, Moritz M A, Roberts D A and Abatzoglou J T 2018 Effect of reduced summer cloud shading on evaporative demand and wildfire in coastal Southern California *Geophys Res. Lett.* **45** 5653–62
- [70] Deser C, Phillips A S, Alexander M A and Smoliak B V 2014 Projecting North American climate over the next 50 years: uncertainty due to internal variability *J. Clim.* **27** 2271–96
- [71] Hurteau M D, Liang S, Westerling A L R and Wiedinmyer C 2019 Vegetation–fire feedback reduces projected area burned under climate change *Sci. Rep.* **9**
- [72] Fusco E J, Finn J T, Balch J K, Chelsea Nagy R and Bradley B A 2019 Invasive grasses increase fire occurrence and frequency across US ecoregions *Proc. Natl Acad. Sci. USA* **116** 23594–9
- [73] Short K C 2014 A spatial database of wildfires in the United States, 1992–2011 *Earth Syst. Sci. Data* **6** 1–27
- [74] Keeley J E and Syphard A D 2018 Historical patterns of wildfire ignition sources in California ecosystems *Int. J. Wildl and Fire* **27** 781
- [75] Pierce D W, Kalansky J F and Cayan D R 2018 Climate, Drought, and Sea Level Rise Scenarios for the Fourth California Climate Assessment. California's Fourth Climate Change Assessment, California Energy Commission. Publication Number: CNRA-CEC-2018-006. California's Fourth Climate Change Assessment, California Energy Commission (August 2018) (available at: www.climateassessment.ca.gov)
- [76] Pausas J G and Paula S 2012 Fuel shapes the fire–climate relationship: evidence from Mediterranean ecosystems *Glob. Ecol. Biogeogr.* **21** 1074–82
- [77] Littell J S, McKenzie D, Wan H Y and Cushman S A 2018 Climate change and future wildfire in the Western United States: an ecological approach to nonstationarity *Earth's Futur.* **6** 1097–111
- [78] IPCC 2018 Global Warming of 1.5 °C *IPCC Report SR15* p 32 (www.ipcc.ch/report/sr15/)
- [79] Kolden C A 2019 We're not doing enough prescribed fire in the Western United States to mitigate wildfire risk *Fire* **2** 30
- [80] Kolden C A and Henson C 2019 A socio-ecological approach to mitigating wildfire vulnerability in the wildland urban interface: a case study from the 2017 Thomas fire *Fire* **2** 9



Contribution of historical precipitation change to US flood damages

Frances V. Davenport^{a,1}, Marshall Burke^{a,b,c}, and Noah S. Diffenbaugh^{a,d}

^aDepartment of Earth System Science, Stanford University, Stanford, CA 94305; ^bCenter on Food Security and the Environment, Stanford University, Stanford, CA 94305; ^cEnvironment and Energy Economics, National Bureau of Economic Research, Cambridge, MA 02138; and ^dWoods Institute for the Environment, Stanford University, Stanford, CA 94305

Edited by Kerry A. Emanuel, Massachusetts Institute of Technology, Cambridge, MA, and approved December 16, 2020 (received for review August 18, 2020)

Precipitation extremes have increased across many regions of the United States, with further increases anticipated in response to additional global warming. Quantifying the impact of these precipitation changes on flood damages is necessary to estimate the costs of climate change. However, there is little empirical evidence linking changes in precipitation to the historically observed increase in flood losses. We use >6,600 reports of state-level flood damage to quantify the historical relationship between precipitation and flood damages in the United States. Our results show a significant, positive effect of both monthly and 5-d state-level precipitation on state-level flood damages. In addition, we find that historical precipitation changes have contributed approximately one-third of cumulative flood damages over 1988 to 2017 (primary estimate 36%; 95% CI 20 to 46%), with the cumulative impact of precipitation change totaling \$73 billion (95% CI 39 to \$91 billion). Further, climate models show that anthropogenic climate forcing has increased the probability of exceeding precipitation thresholds at the extremely wet quantiles that are responsible for most flood damages. Climate models project continued intensification of wet conditions over the next three decades, although a trajectory consistent with UN Paris Agreement goals significantly curbs that intensification. Taken together, our results quantify the contribution of precipitation trends to recent increases in flood damages, advance estimates of the costs associated with historical greenhouse gas emissions, and provide further evidence that lower levels of future warming are very likely to reduce financial losses relative to the current global warming trajectory.

precipitation | flooding | climate change

Flooding is one of the most costly natural hazards, causing billions of dollars in damage each year (1). Both the total cost of flood-related damages and the frequency of “billion-dollar disasters” have been growing over time (2–4) (Fig. 1*A*). Simultaneously, extreme, short-duration precipitation has been increasing in many areas (5–7). Many historical trends in precipitation intensity—including of individual extreme events—have been attributed to climate change (8–11), and continued global warming is very likely to yield further increases in extreme precipitation (12–15). Quantifying the impact of these precipitation changes on flood damages is a critical step toward evaluating the costs of climate change and informing adaptation and resilience planning (16).

However, the effect of changes in precipitation on historical flood damages—and the potential attribution of these damages to anthropogenic climate change—remains poorly quantified (17, 18). Such attribution requires isolating the impact of changes in precipitation from changes in other factors such as exposure and vulnerability, as well as from changes in reporting of damages. Previous studies have argued that increases in exposure (e.g., increases in property values or the number of structures) could explain most or all trends in disaster losses (19–22). While much of the research on trends in the cost of flood damage has been conducted at the national scale (2, 4, 19, 20), both the processes that cause damaging precipitation and the factors that control exposure and vulnerability occur at

smaller spatial scales. Analyzing the national precipitation trend is thus not sufficient to understand historical drivers of flood damage, which result from regionally varying trends in flood hazard, exposure, and/or vulnerability. As a result, there remains critical uncertainty in the contribution of historical precipitation trends to the observed national-level increase in flood damages.

“Bottom-up” flood risk assessments (23–25)—which integrate higher-resolution socioeconomic and flood hazard information—can provide greater detail, but are often limited in temporal and geographic extent. Further, these approaches may require assumptions about the relationship between flood hazard and damage that cannot be easily verified. For example, existing flood depth–damage curves are often poor predictors of observed flood damage (26) but are commonly used in flood risk assessments. The attribution of historical precipitation trends also becomes more uncertain at finer spatial scales because of the progressively stronger influence of climate variability (27), particularly over the United States, where there is uncertainty in the signal-to-noise ratio of mean precipitation change during the historical period (17).

Here we quantify the impact of historical global warming on flood damages by combining 1) empirical approaches that integrate historical flood damages and precipitation at the subnational scale, 2) an analysis of historical changes in precipitation, and 3) ensemble climate model simulations that quantify the contribution of anthropogenic forcing to historical and future

Significance

Precipitation extremes have increased in many regions of the United States, suggesting that climate change may be exacerbating the cost of flooding. However, the impact of historical precipitation change on the cost of US flood damages remains poorly quantified. Applying empirical analysis to historical precipitation and flood damages, we estimate that approximately one-third (36%) of the cost of flood damages over 1988 to 2017 is a result of historical precipitation changes. Climate models show that anthropogenic climate change has increased the probability of heavy precipitation associated with these costs. Our results provide information quantifying the costs of climate change, and suggest that lower levels of future warming would very likely reduce flooding losses relative to the current global warming trajectory.

Author contributions: F.V.D., M.B., and N.S.D. designed research; F.V.D. performed research; F.V.D. contributed new analytic tools; F.V.D., M.B., and N.S.D. analyzed data; and F.V.D., M.B., and N.S.D. wrote the paper.

The authors declare no competing interest.

This article is a PNAS Direct Submission.

This open access article is distributed under [Creative Commons Attribution-NonCommercial-NoDerivatives License 4.0 \(CC BY-NC-ND\)](https://creativecommons.org/licenses/by-nc-nd/4.0/).

¹To whom correspondence may be addressed. Email: fvdav@stanford.edu.

This article contains supporting information online at <https://www.pnas.org/lookup/suppl/doi:10.1073/pnas.2017524118/-DCSupplemental>.

Published January 11, 2021.

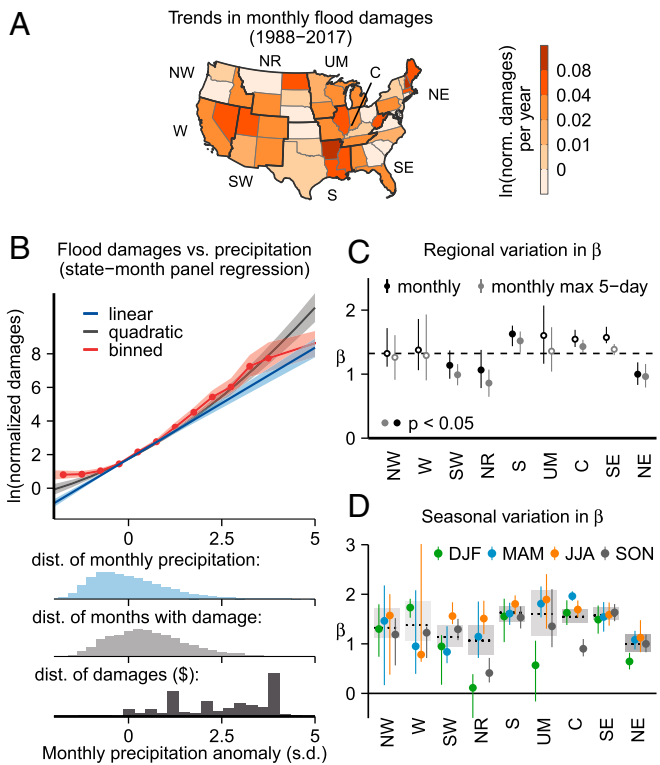


Fig. 1. Effect of state-level precipitation on flood damages. (A) Historical state-level trends in monthly flood damages. The nine National Centers for Environmental Information (NCEI) climate regions are outlined in dark gray: Northwest (NW), West (W), Southwest (SW), Northern Rockies and Plains (NR), South (S), Upper Midwest (UM), Central (C), Northeast (NE), and Southeast (SE). (B) Relationship between normalized flood damages and monthly precipitation at the state level using linear (blue line), quadratic (gray line), and binned (red line) models. Shading indicates the 95% CI estimated by bootstrapping states. Response functions are centered at mean monthly precipitation (0.04 SD) and mean log-normalized damage (1.8). Histograms show the distribution of monthly precipitation anomalies across all state-months (blue), the distribution of monthly precipitation anomalies during months with flood damage (light gray), and the distribution of total damages (in 2017 dollars) across monthly precipitation anomalies (dark gray). (C) Effect of precipitation on flood damages within each NCEI climate region (shown in A), for two precipitation variables: total monthly precipitation (black) and monthly maximum 5-d precipitation (gray). Effects are measured as the change in $\ln(\text{normalized damages})$ per SD change in precipitation. Points show median coefficient estimates and vertical lines show the 95% CI around each point estimate. Filled circles indicate statistically significant ($P < 0.05$) differences between the regional coefficients and a pooled model (shown as a black dashed line for total monthly precipitation, same as the blue line in B). (D) Seasonal variations in the effect of monthly precipitation on flood damages for each region. Points show the median coefficient estimates for each season and region, and vertical lines show the 95% CI around each point estimate. Seasons are defined as December–January–February (DJF), March–April–May (MAM), June–July–August (JJA), and September–October–November (SON). Black dotted lines show the median coefficient estimate for each region (the same as black points in C), and gray shading shows the 95% CI (black lines in C).

precipitation change within the context of climate variability (*SI Appendix, Text*).

We use historical observations from 1988 to 2017 to model the relationship between precipitation and flood damages at the state-month level using fixed-effects panel regression analyses. We control explicitly for changes in income in each state, and include fixed effects that account for 1) year-to-year variations in precipitation and flood damages within each state and 2) state-specific seasonality in precipitation and flooding. In essence, we

compare the effect of a relatively wet month in one state with a relatively dry month in the same calendar month and state, while accounting for year-to-year changes in average flood damage in that state. Over shorter (i.e., monthly or submonthly) timescales, variations in precipitation within each state are plausibly uncorrelated with variations in exposure or vulnerability, meaning that the regression analyses isolate the effect of a precipitation anomaly from other confounding variables that also affect flood damages.

Results and Discussion

We find a significant, positive relationship between monthly precipitation and flood damages, with a 1-SD increase in the monthly precipitation anomaly corresponding to a >3-fold increase in flood damages (Fig. 1B). Variation in monthly, state-level precipitation (after accounting for state-month and state-year fixed effects) explains 21% of the observed variation in monthly flood damages. The log-linear response suggests exponential growth in flood damages for a given increase in monthly precipitation, and we find a similar shape and magnitude of response using either a quadratic or nonparametric binned model (Fig. 1B). We also show that the presence of reporting errors in the data (such as missing damages) is unlikely to cause an overestimation of the effect of precipitation on flood damage (*SI Appendix, Text and Fig. S1*).

Although months with flood damages occur at a range of precipitation anomalies, the largest damages primarily occur at precipitation anomalies >2 SDs (Fig. 1B). As expected, the slope of the relationship is flatter across negative monthly precipitation anomalies when using a nonlinear functional form. Smaller flood damages do occur during months with negative statewide precipitation anomalies (Fig. 1B), possibly due to lagged effects from snowmelt, precipitation in adjacent states, or short-duration and/or localized precipitation during months that are relatively dry at the state-month scale. (We include additional models to test for some of these effects, as described below.)

Given the range of temporal and spatial scales at which flooding occurs, we compare our primary monthly, state-level regression model with regression models that use shorter- or longer-duration precipitation, or precipitation over large watersheds that span multiple states. Monthly maximum 5-d precipitation has a positive effect on monthly flood damages, but the effect is smaller compared with that of total monthly precipitation (Fig. 1C). Using a lagged precipitation model, we find that precipitation in previous months has a positive effect on flood damages (*SI Appendix, Fig. S24*) but that these effects are much smaller than the effect of the current-month precipitation. Further, although there are additional effects from precipitation that occurs out-of-state (*SI Appendix, Fig. S3*), these effects are small compared with that of within-state precipitation. Combined, these analyses indicate that results based on the state-month regression are consistent with models that account for the effects of shorter- or longer-duration precipitation, or large-scale flooding processes.

We do find regional differences in the magnitude of the effect of monthly precipitation on flood damages (Fig. 1C), reflecting both regional differences in the conditions creating flood hazards (e.g., the type of weather events associated with extreme precipitation, and the primary flooding processes) and regionally specific patterns of exposure and vulnerability (e.g., patterns of land use and development). Additionally, some regions show seasonal variations in the effect of precipitation on flood damages (Fig. 1D). For example, there are smaller effects of precipitation on flood damages during the winter (December through February) season in the Northern Rockies, Upper Midwest, and Northeast regions. This result could reflect the fact that these cold regions receive snow in the winter, which would not have the same immediate impact on flooding as rain during

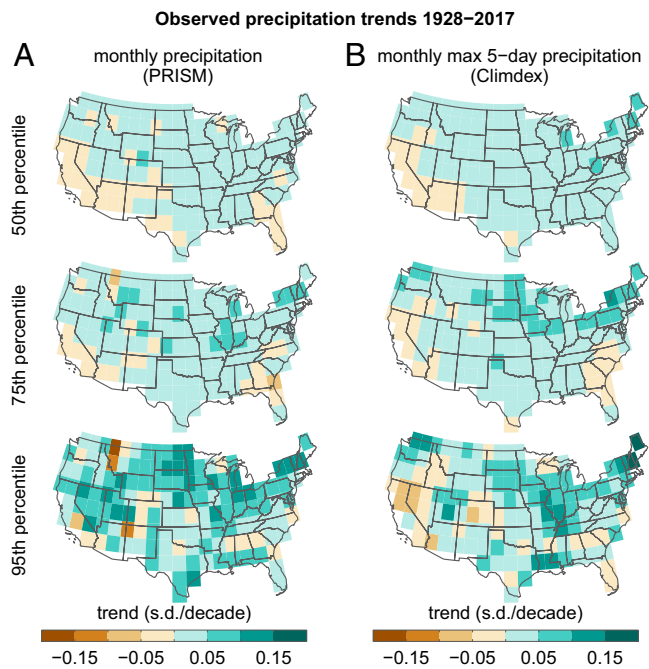


Fig. 2. Observed trends in monthly total and maximum 5-d precipitation. (A) Observed 1928-to-2017 trends in the 50th, 75th, and 95th percentiles of monthly precipitation, measured in SDs per decade. Trends are calculated on a $2.5 \times 2.5^\circ$ grid using quantile regression and the PRISM monthly precipitation product. (B) Same as A, but for monthly maximum 5-d precipitation. Trends are calculated on a $2.5 \times 2.5^\circ$ grid using quantile regression and the Climdex HadEX3 monthly Rx5day product.

warmer seasons. We use the regional, monthly regression model (Fig. 1C) as our primary model for later analyses, but we test the sensitivity of our results to these seasonal effects (see Fig. 3B).

We use our regression model results as a framework to understand the effect of historical precipitation changes on flood damages. Because monthly total and maximum 5-d precipitation have a similar effect on monthly flood damages (Fig. 1C), and because previous studies have detected changes in short-duration (e.g., daily or 5-d) precipitation extremes (5, 28), we analyze trends in both monthly total (Fig. 2A) and maximum 5-d precipitation (Fig. 2B). Further, given existing evidence that trends in extreme precipitation are larger and sometimes of opposite sign compared with trends in mean precipitation (29), we calculate trends at multiple quantiles within the distributions of monthly total and maximum 5-d precipitation. This approach allows us to distinguish between changes in the wettest months (which are associated with the largest flood damages; Fig. 1B) and changes in the median or drier months.

Fig. 2 shows trends in the 50th, 75th, and 95th percentiles of the monthly total and maximum 5-d precipitation distributions from 1928 to 2017. These analyses confirm that historical precipitation trends are not uniform across the distribution, with the 95th percentile exhibiting the largest trends. The spatial pattern of changes in monthly precipitation is very similar to that of monthly maximum 5-d precipitation. Most of the northwestern, central, and eastern United States have seen increases in median (50th percentile) monthly precipitation, whereas the Southwest has experienced decreases in median monthly precipitation. This spatial pattern is very similar to reported changes in annual mean precipitation over the United States, which results from changes that vary by region and season, including increases in fall precipitation in the Southeast, Northeast, and Great Plains and decreases in spring precipitation in the Southwest (29).

Precipitation during the wettest months (i.e., the 95th percentile) has increased across most of the country, even in some areas where median monthly precipitation is decreasing (Fig. 2). This pattern is also true for monthly maximum 5-d precipitation, and is consistent with previously identified increases in short-duration (e.g., daily or 5-d) precipitation extremes (29). The largest increases in the 95th percentile have occurred in the Midwest and Northeast.

Based on the regional regression coefficients, expected state-level flood damages have increased by an average of 35, 50, and 70% for precipitation at the 50th, 75th, and 95th percentiles, respectively (SI Appendix, Text and Fig. S4). In some states, we calculate that damages from the wettest 5% of months are now more than three times what would be expected in the absence of the observed precipitation changes (SI Appendix, Fig. S4).

Removing the historical quantile-specific monthly precipitation trends in each state allows us to estimate the effect of state-level precipitation changes on cumulative national-level damages (Fig. 3A and Methods). We find that precipitation changes have contributed 36% (\$73 billion) of the 1988-to-2017 cumulative US flood damages. Uncertainty in the regional regression coefficients (Fig. 1C) and observed precipitation trends (SI Appendix, Figs. S4 and S5) yields a 95% confidence range of 20 to 46% (39 to \$91 billion) contributed by state-level precipitation trends.

Our results are robust to using alternative regression models that account for lagged and seasonal effects (Fig. 3B), and to calculating precipitation trends over different time periods

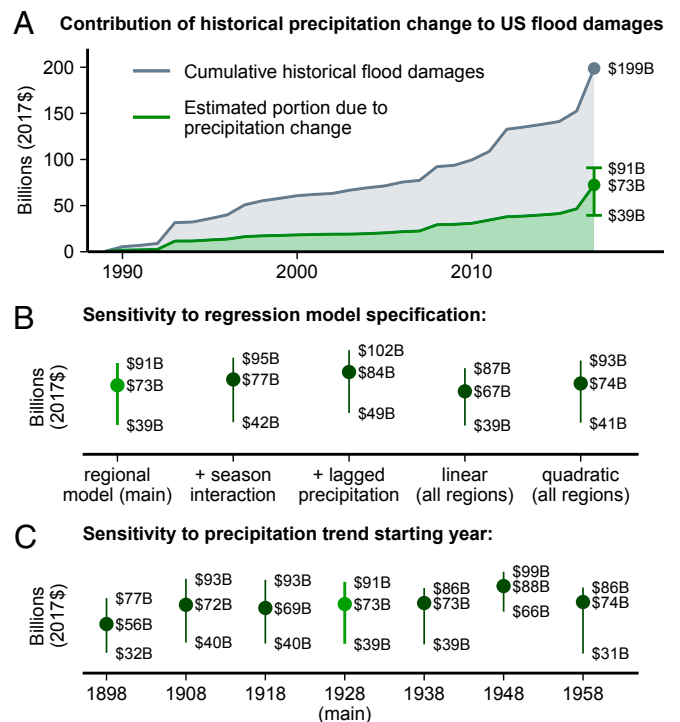


Fig. 3. Cumulative damages due to historical precipitation change. (A) Cumulative observed flood damages (gray) and estimated portion due to historical precipitation change (green) from 1988 to 2017. Error bars show the 95% CI for cumulative damages in 2017 (based on precipitation trends from 1928 to 2017). (B) Impact of historical precipitation change on cumulative flood damages in 2017 using various regression model specifications. From left to right, the models are the regional model (same as A), the regional-seasonal model (Fig. 1D), a regional model with lagged precipitation (SI Appendix, Fig. S2A), a linear model (Fig. 1B), and a quadratic model (Fig. 1B). (C) Sensitivity of cumulative damages from precipitation change to starting year of precipitation trend calculation. All estimates use the same regional regression model used in A.

(Fig. 3C). They are also robust to using different assumptions about possible unreported damages (*SI Appendix, Fig. S6*); further, the fact that the historical flood damage values are likely underestimated and/or unreported in earlier years (1) would cause the effect of precipitation on damages to be underestimated, and thus make our estimate of the contribution of historical precipitation change conservative (*SI Appendix, Text and Fig. S14*).

There are limitations to using the state-month as the unit of analysis, because flooding can occur on shorter or longer timescales, and over smaller or larger areas. However, we find that our primary regression model yields a similar (although slightly lower) estimate of the contribution of historical precipitation change compared with versions of the model that include effects of precipitation over longer timescales (Fig. 3B) or larger spatial scales (*SI Appendix, Fig. S3*). The strong similarity between historical trends in monthly total and monthly maximum 5-d precipitation (Fig. 2), as well as similarity in their effect on damages (Fig. 1C), indicate that an analysis based on 5-d precipitation would yield a similar estimated contribution of historical precipitation change. Together, these sensitivity analyses suggest that our primary estimate of the contribution of historical precipitation trends to total US flood damages is both robust and conservative.

Prior studies have attributed increases in short-duration precipitation extremes over the United States to anthropogenic climate forcing by comparing historical trends with climate model simulations (10, 30), isolating forced changes from those driven by modes of natural climate variability (31–34), or calculating the probability of extreme events (i.e., “risk ratio”) with and without anthropogenic climate forcing (9, 35, 36). While the general circulation models that comprise the Coupled Model Intercomparison Project (CMIP5) ensemble show a thermodynamic response to warming (37, 38) (Figs. 4 and 5), they do not explicitly resolve the precipitation processes that cause flood damages (such as severe thunderstorms and tropical cyclones), and may underestimate the magnitude of extreme precipitation change (10, 28, 29, 31). Given the large uncertainties in modeled precipitation trends, particularly at the spatial scale of individual events, we do not use our regression analysis to explicitly separate the contributions of forced climate change and unforced climate variability to cumulative flood damages.

However, we do use the CMIP5 global climate model simulations to assess changes in the probability of monthly total and maximum 5-d precipitation thresholds over the recent historical period (1988 to 2017) compared with an early-industrial baseline (1860 to 1920; *SI Appendix, Text*). The probability of exceeding the baseline 50th and 75th percentiles of monthly precipitation has increased slightly across the central and eastern United States in the recent historical period, and decreased slightly across the Southwest (Fig. 4). In contrast, the probability of exceeding the baseline 95th or 99th percentiles has increased across most of the United States, especially for monthly maximum 5-d precipitation (Fig. 4). This analysis suggests that anthropogenic climate forcing has increased the frequency of extreme monthly precipitation, with the ensemble mean response (Fig. 4) showing many similarities to the observations (Fig. 2). However, despite the mean wetting in response to anthropogenic forcing, there is some disagreement across models on the direction of change over the recent historical period, particularly at the higher-percentile thresholds (Fig. 4). We must therefore conclude that the estimated flood damages due to precipitation change (Fig. 3) represent the combined effects of anthropogenic forcing and natural variability, and cannot be entirely attributed to anthropogenic climate change.

To understand the implications of additional global warming for the cost of future flood damages, we evaluate future precipitation change in the “high-” (RCP8.5) and “low-” (RCP2.6)

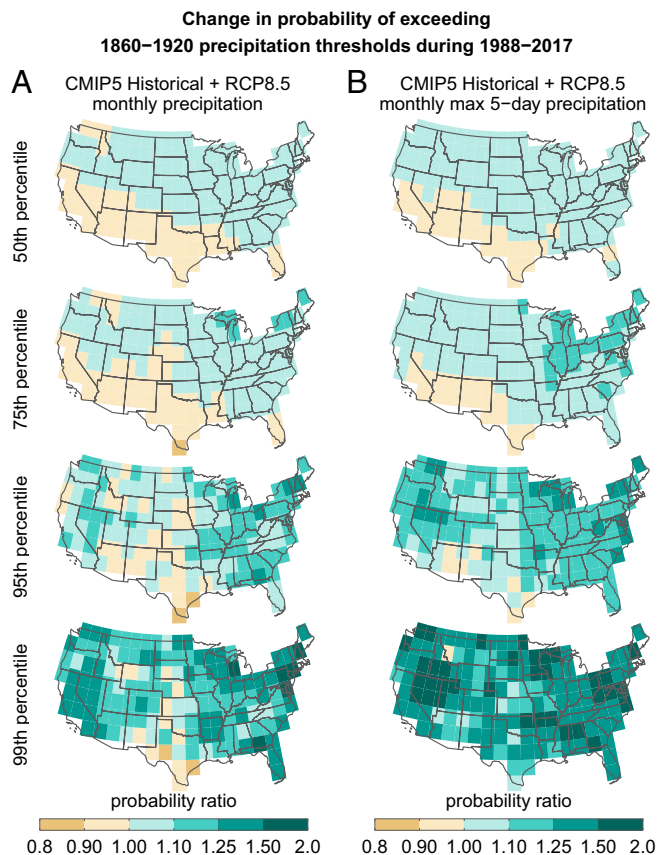


Fig. 4. Change in probability of exceeding early industrial baseline precipitation thresholds during the recent historical period, simulated by the CMIP5 global climate model ensemble. (A) Probability of exceeding the early industrial baseline (1860 to 1920) 50th, 75th, 95th, and 99th percentile monthly precipitation thresholds during the recent historical period (1988 to 2017). Probabilities are shown as a ratio relative to the probability during the baseline period, and are based on a 24-model ensemble (*SI Appendix*). Solid colors indicate strong model agreement (following the IPCC AR5 definition, when $\geq 66\%$ of models agree with the direction of change shown on the map). Black stippling indicates $< 66\%$ of models agree with the direction of change shown. (B) Same as A but for monthly maximum 5-d precipitation.

emissions scenarios analyzed in the assessment of impacts, adaptation, and vulnerability in the Intergovernmental Panel on Climate Change (IPCC) Fifth Assessment Report [IPCC AR5 (16)]. In both scenarios, the 95th and 99th percentiles of monthly total and maximum 5-d precipitation are projected to increase across most of the United States by midcentury (2046 to 2065) relative to the recent historical period (*SI Appendix, Fig. S7*). Under the high-emissions scenario (RCP8.5), there is strong model agreement that the wettest months (both in total precipitation and maximum 5-d precipitation) will continue to intensify through the end of the century (Fig. 5). In some parts of the northeastern and western United States, the 99th percentile of monthly maximum 5-d precipitation is projected to increase by more than 1 SD (Fig. 5B). Combined with our regression model, these analyses suggest that—absent changes in exposure or vulnerability—future global warming is very likely to increase the costs of flooding, but that those increases could be greatly reduced under a low-emissions scenario consistent with the UN Paris Agreement.

Overall, our findings are consistent with prior conclusions that flood damages are sensitive to variations in weather (39–41), and that climate change has likely increased historical damages from

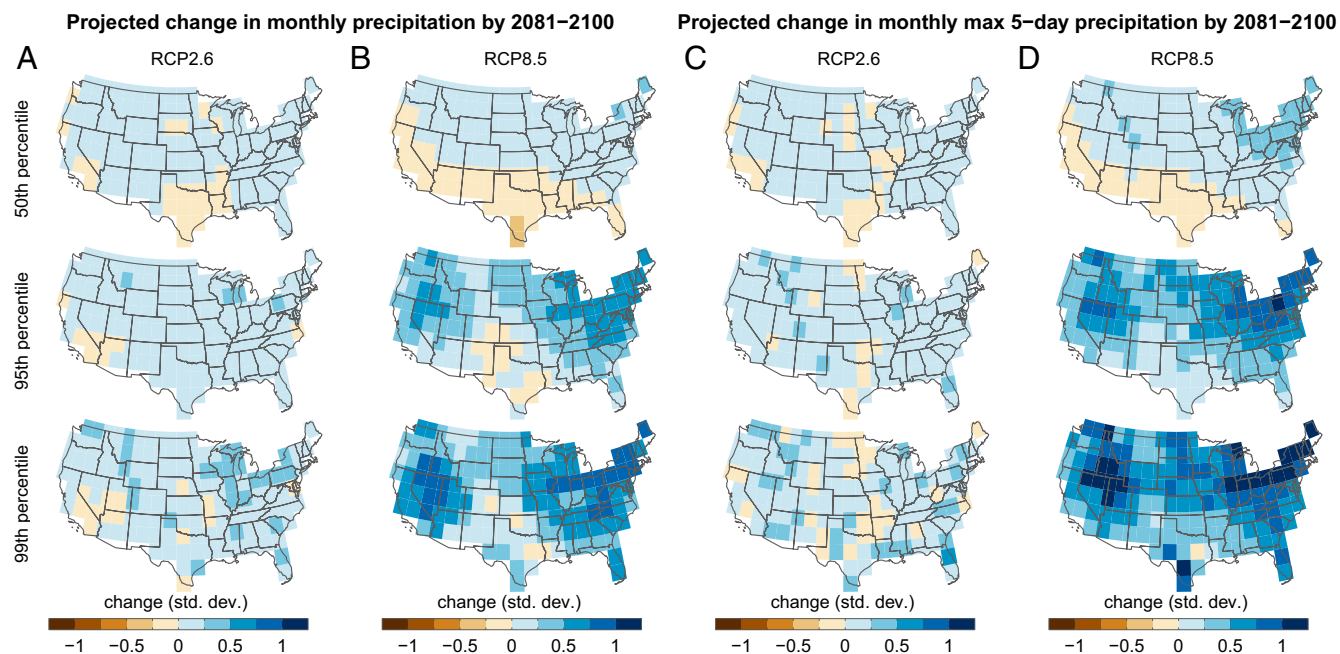


Fig. 5. Projected changes in monthly total and maximum 5-d precipitation. (A) Projected change in the 50th, 95th, and 99th percentiles of monthly precipitation by 2081 to 2100 for RCP2.6. Changes are relative to the recent historical (1988 to 2017) period. Maps show the mean change across a 17-model ensemble (*Methods*). Solid colors indicate strong model agreement (following the IPCC AR5 definition, when $\geq 66\%$ of models agree with the direction of change shown on the map). Black stippling indicates $< 66\%$ of models agree with the direction of change shown. (B) Same as A but for RCP8.5. (C) Same as A but for monthly maximum 5-d precipitation. (D) Same as B but for monthly maximum 5-d precipitation.

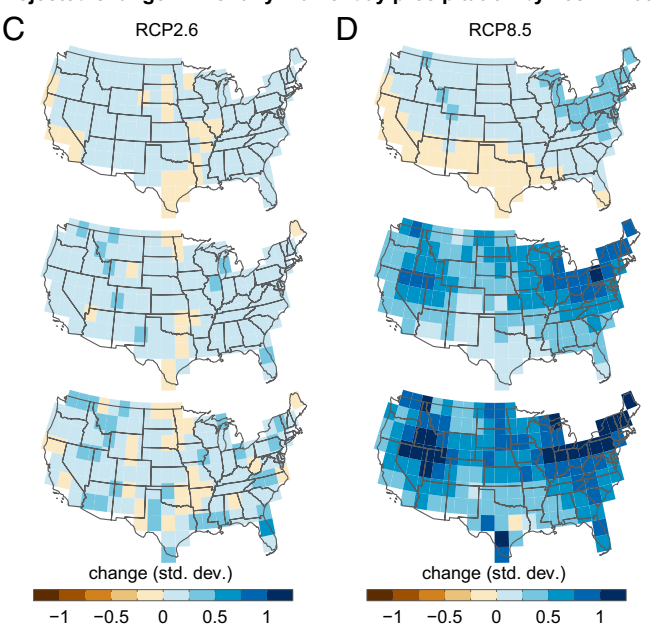
flooding and/or tropical cyclones (42, 43). While some studies have not found an impact of climate change on historical flood damages (20, 21), this contrast may be explained by different methodology, including 1) the scale of the analysis (for example, country-year in previous studies vs. state-month in our study); 2) our use of fixed effects to isolate precipitation variation from the many other time-invariant and time-varying factors that might also affect flood damages (such as variations in exposure and vulnerability); and 3) our use of precipitation trends at different percentiles of the distribution to isolate trends affecting the wettest months (in which damages are most likely to occur).

Conclusions

Our results show that historical increases in precipitation are very likely responsible for a substantial fraction of recent increases in US flood damages. Not only does precipitation in the upper tail of the distribution cause the largest historical damages (Fig. 1B) but the most intense precipitation has also shown the greatest increase over the historical period (Fig. 2), along with the strongest imprint of anthropogenic climate forcing (Fig. 4). Our panel regression models, combined with our analyses of quantile-specific precipitation trends, provide an empirical framework for quantifying the contribution of historical precipitation changes to recent increases in flood damages, and more broadly the costs associated with global warming.

This framework provides empirical evidence that climate change has affected the cost of flood damages at the national scale, along with comprehensive quantification of the magnitude and uncertainty of that impact. The framework could be extended to calculate the costs due to changes in other natural hazards, or to calculate the global costs of regional precipitation change. Given the importance of evaluating the costs of climate change versus the costs of mitigation options (44), the empirical quantification of losses due to changing natural hazards provides critical information to inform policy and decision making.

Projected change in monthly max 5-day precipitation by 2081–2100



Methods

Precipitation and Flood Damage Data. We calculate historical monthly precipitation in each state using 4-km gridded monthly precipitation observations from the PRISM (parameter-elevation regressions on independent slopes model) Climate Group (45, 46) and state boundaries from the US Census Bureau. Monthly precipitation for each state is calculated as the average of all grid cells within each state boundary. We standardize the precipitation time series in each state by subtracting the mean monthly precipitation and dividing the anomaly by the SD of monthly precipitation, with the mean and SD for each state calculated over the IPCC's 1986-to-2005 baseline period (16). To test the regression model with shorter-duration precipitation, we also calculate monthly maximum 5-d precipitation in each state using the PRISM daily precipitation data. The maximum 5-d precipitation in each month is defined as the maximum total precipitation over 5 consecutive days within each calendar month. We standardize the monthly maximum 5-d precipitation time series in each state using the same procedure described above.

We analyze monthly, state-level flood damage estimates over 1988 to 2017 from the Spatial Hazard Events and Losses Database for the United States (SHELDUS) version 17.0 (47). SHELDUS compiles flood damage estimates from the National Climatic Data Center *Storm Data* publications. Details of the SHELDUS dataset, including a comparison with other flood damage datasets and discussion of how uncertainty in reported damages could impact our results, are included in *SI Appendix*.

Regression Model. To estimate the relationship between monthly precipitation and flood damages (Fig. 1B), we use a least-squares log-linear regression model:

$$\ln(y_{ilm}) = \beta P_{ilm} + \delta_{il} + \mu_{im} + \varepsilon_{ilm}, \quad [1]$$

where y_{ilm} is normalized flood damages in state i during month m of year l , P_{ilm} is the standardized precipitation anomaly during the same state-month, δ_{il} and μ_{im} are state-year fixed effects and state-calendar month fixed effects, respectively, and ε_{ilm} is an error term. We normalize flood damages by annual state income, which is strongly correlated with exposure (see details in *SI Appendix*). The fixed effects in Eq. 1 subtract out year-to-year and seasonal variations in average damages in each state, allowing us to estimate the effect of monthly precipitation on flood damages after controlling for

long-term changes in flood damage in each state. In other words, we can directly compare flood damages during a relatively wet month in a given state (e.g., June 2008 in Iowa) with flood damages during a relatively dry month in the same calendar month and state (e.g., June 2012 in Iowa), after accounting for average differences in flood damages and precipitation between the two different years (e.g., 2008 and 2012) that could have arisen from simultaneous changes in exposure or vulnerability. We calculate CIs around the estimated coefficients using bootstrap resampling (SI Appendix).

We test a number of variations of Eq. 1 by including additional interaction terms and testing nonlinear functional forms. The remaining regression models (including those shown in Figs. 1 C and D and 3B) are described in SI Appendix, Text.

Impact of Historical Precipitation Trends on Flood Damages. Following the approach of Diffenbaugh and Burke (48), we estimate the impact of historical precipitation trends on cumulative flood damages by calculating the “counterfactual” flood damages that would have occurred in the absence of precipitation changes. To create the counterfactual monthly precipitation time series, we remove observed trends at each decile of the distribution, which allows us to account for nonuniform changes in the distribution of monthly precipitation (SI Appendix). We next estimate counterfactual flood damages associated with this counterfactual precipitation time series. For each month with flood damages, we calculate the difference between the observed and detrended precipitation. While there are limitations to using counterfactual “treatments” and fixed-effects regression models to extrapolate impacts of large within-unit changes (49), in this case the changes in precipitation due to the historical trends are much smaller than the historical precipitation variability within each state (SI Appendix, Fig. S9). Because many of the observed trends are positive (Fig. 2), the detrended precipitation anomalies in the counterfactual scenario are less extreme than the observed precipitation anomalies, and this analysis does not require extrapolating the regression model beyond the observed data.

Based on the difference between the observed and detrended precipitation anomalies, we estimate counterfactual damages using the regional regression coefficients (SI Appendix, Eq. S4). We calculate the cumulative damages due to precipitation change as the sum of all observed damages minus the sum of the counterfactual damages. We calculate a 95% confidence range for our estimate of cumulative counterfactual damages based on 1) uncertainty in the regional regression coefficients and 2) uncertainty in the observed precipitation trends (SI Appendix, Text). We also evaluate the sensitivity of the counterfactual damage analysis to using other regression models, or using precipitation trends over shorter or longer time periods (SI Appendix, Text). The various alternatives lead to slightly higher or lower estimates of counterfactual damage, with our main result falling in the middle of the distribution (Fig. 3 B and C and SI Appendix, Fig. S6).

Climate Model Analysis. We analyze historical and future climate model simulations from CMIP5 (50) to understand the impacts of anthropogenic climate forcing on extreme monthly and 5-d precipitation. To assess the

influence of anthropogenic climate forcing on historical changes, we calculate risk ratios (i.e., changes in the probability of exceeding various monthly total or maximum 5-d precipitation thresholds) for 24 simulations over the recent historical period (1988 to 2017) compared with an early-industrial baseline (1860 to 1920). To understand the impact of additional global warming on the future costs of flooding, we analyze changes in monthly total and maximum 5-d precipitation by 2046 to 2065 and by 2081 to 2100 in 34 simulations and two future emissions scenarios (17 simulations with the RCP2.6 forcing and 17 simulations with the RCP8.5 forcing). A detailed description of the CMIP5 simulations and analyses, including the limiting factors on the number of simulations analyzed, is provided in SI Appendix, Text.

Data Availability. The PRISM monthly and daily precipitation products are available from the PRISM Climate Group (<http://www.prism.oregonstate.edu>). The SHELUS dataset is a subscription-based dataset available from the Center for Emergency Management and Homeland Security at Arizona State University (<https://cemhs.asu.edu/sheldus>). State boundary files are available from the US Census Bureau (<https://www.census.gov/geographies/mapping-files/time-series/geo/tiger-line-file.html>). Watershed boundary files can be downloaded from the Watershed Boundary Dataset (<https://www.usgs.gov/core-science-systems/ngp/national-hydrography/watershed-boundary-dataset>). Data on annual state income and national net stock of reproducible fixed assets are available from the US Bureau of Economic Analysis (<https://www.bea.gov>). Data on state-level housing values and number of housing units are available from the US Census Housing Tables (<https://www.census.gov/topics/housing/data/tables.html>) and the American Community Survey (<https://www.census.gov/programs-surveys/acs>). The Climdex HadEX3 gridded monthly Rx5day product is available from the Climdex project archive (<https://www.climdex.org/access/>), and the Climdex CMIP5 data are available through Environment Canada (<https://crd-data-donnees-rdc.ec.gc.ca/CCCMA/products/CLIMDEX/>). CMIP5 data are available from the Program for Climate Model Diagnosis & Intercomparison through the Earth System Grid Federation data portal (<https://esgf-node.llnl.gov/projects/cmip5/>). Code and data supporting the findings of the study are available in GitHub at <https://github.com/fdavenport/DBD2021>.

ACKNOWLEDGMENTS. We thank the editor and two anonymous reviewers for insightful and constructive comments, which greatly improved the manuscript. We thank the PRISM Climate Group for access to the PRISM monthly precipitation product, the Center for Emergency Management and Homeland Security at Arizona State University for access to SHELUS 17.0, the US Bureau of Economic Analysis for providing access to state income data, Climdex for calculating and archiving the observed and simulated Rx5day climate indices, and the Program for Climate Model Diagnosis & Intercomparison for access to CMIP5 data. Computational resources were provided by the Center for Computational Earth & Environmental Sciences and the Stanford Research Computing Center at Stanford University. Funding was provided by Stanford University.

1. M. Gall, K. A. Borden, C. T. Emrich, S. L. Cutter, The unsustainable trend of natural hazard losses in the United States. *Sustainability* 3, 2157–2181 (2011).
2. A. B. Smith, R. W. Katz, US billion-dollar weather and climate disasters: Data sources, trends, accuracy and biases. *Nat. Hazards* 67, 387–410 (2013).
3. L. Cartwright, An examination of flood damage data trends in the United States. *J. Contemp. Water Res. Educ.* 130, 20–25 (2010).
4. S. L. Cutter, C. Emrich, Are natural hazards and disaster losses in the U.S. increasing? *Eos (Wash. D.C.)* 86, 381–388 (2005).
5. K. E. Kunkel et al., Monitoring and understanding trends in extreme storms: State of knowledge. *Bull. Am. Meteorol. Soc.* 94, 499–514 (2013).
6. A. T. DeGaetano, Time-dependent changes in extreme-precipitation return-period amounts in the continental United States. *J. Appl. Meteorol. Climatol.* 48, 2086–2099 (2009).
7. S. C. Pryor, J. A. Howe, K. E. Kunkel, How spatially coherent and statistically robust are temporal changes in extreme precipitation in the contiguous USA? *Int. J. Climatol.* 29, 31–45 (2009).
8. M. D. Risser, M. F. Wehner, Attributable human-induced changes in the likelihood and magnitude of the observed extreme precipitation during Hurricane Harvey. *Geophys. Res. Lett.* 44, 12457–12464 (2017).
9. N. S. Diffenbaugh et al., Quantifying the influence of global warming on unprecedented extreme climate events. *Proc. Natl. Acad. Sci. U.S.A.* 114, 4881–4886 (2017).
10. S. K. Min, X. Zhang, F. W. Zwiers, G. C. Hegerl, Human contribution to more-intense precipitation extremes. *Nature* 470, 378–381 (2011).
11. S. M. Papalexiou, A. Montanari, Global and regional increase of precipitation extremes under global warming. *Water Resour. Res.* 55, 4901–4914 (2019).
12. D. Singh, M. Tsiang, B. Rajaratnam, N. S. Diffenbaugh, Precipitation extremes over the continental United States in a transient, high-resolution, ensemble climate model experiment. *J. Geophys. Res. Atmos.* 118, 7063–7086 (2013).
13. K. E. Trenberth, Conceptual framework for changes of extremes of the hydrological cycle with climate change. *Clim. Change* 42, 327–339 (1999).
14. P. Y. Groisman et al., Trends in intense precipitation in the climate record. *J. Clim.* 18, 1326–1350 (2005).
15. M. R. Allen, W. J. Ingram, Constraints on future changes in climate and the hydrologic cycle. *Nature* 419, 224–232 (2002).
16. Intergovernmental Panel on Climate Change, “2014: Summary for policymakers” in *Climate Change 2014: Impacts, Adaptation, and Vulnerability. Contribution of Working Group II to the Fifth Assessment Report of the Intergovernmental Panel on Climate Change*, C. B. Field et al., Eds. (Cambridge University Press, 2014), pp. 1–32.
17. P. Romero-Lankao et al., “North America” in *Climate Change 2014: Impacts, Adaptation, and Vulnerability. Part B: Regional Aspects. Contribution of Working Group II to the Fifth Assessment Report of the Intergovernmental Panel on Climate Change*, V. R. Barros et al., Eds. (Cambridge University Press, 2014), pp. 1439–1498.
18. K. Hayhoe et al., “Our changing climate” in *Impacts, Risks, and Adaptation in the United States: Fourth National Climate Assessment*, D. R. Reidmiller, Ed. et al. (US Global Change Research Program, Washington, DC, 2018), vol. II, pp. 72–144.
19. F. Barthel, E. Neumayer, A trend analysis of normalized insured damage from natural disasters. *Clim. Change* 113, 215–237 (2012).
20. P. J. Klotzbach, S. G. Bowen, R. Pielke Jr, M. Bell, Continental US hurricane landfall frequency and associated damage: Observations and future risks. *Bull. Am. Meteorol. Soc.* 99, 1359–1376 (2018).
21. L. M. Bouwer, Have disaster losses increased due to anthropogenic climate change? *Bull. Am. Meteorol. Soc.* 92, 39–46 (2011).
22. M. W. Downton, J. Z. B. Miller, R. A. Pielke Jr, Reanalysis of U.S. National Weather Service flood loss database. *Nat. Hazards Rev.* 6, 13–22 (2005).

23. A. H. Thieken, M. Müller, H. Kreibich, B. Merz, Flood damage and influencing factors: New insights from the August 2002 flood in Germany. *Water Resour. Res.* **41**, 1–16 (2005).
24. S. Brody, R. Blessing, A. Sebastian, P. Bedient, Examining the impact of land use/land cover characteristics on flood losses. *J. Environ. Plann. Manage.* **57**, 1252–1265 (2014).
25. Y. O. Kim, S. B. Seo, O. J. Jang, Flood risk assessment using regional regression analysis. *Nat. Hazards* **63**, 1203–1217 (2012).
26. O. E. J. Wing, N. Pinter, P. D. Bates, C. Kousky, New insights into US flood vulnerability revealed from flood insurance big data. *Nat. Commun.* **11**, 1444 (2020).
27. E. Hawkins, R. Sutton, The potential to narrow uncertainty in regional climate predictions. *Bull. Am. Meteorol. Soc.* **90**, 1095–1108 (2009).
28. E. Janssen, D. J. Wuebbles, K. E. Kunkel, S. C. Olsen, A. Goodman, Observational- and model-based trends and projections of extreme precipitation over the contiguous United States. *Earths Future* **2**, 99–113 (2014).
29. D. R. Easterling *et al.*, “Precipitation change in the United States” in *Climate Science Special Report: Fourth National Climate Assessment*, D. J. Wuebbles, Ed. *et al.* (US Global Change Research Program, Washington, DC, 2017), vol. I, pp. 207–230.
30. N. S. Diffenbaugh, Verification of extreme event attribution: Using out-of-sample observations to assess changes in probabilities of unprecedented events. *Sci. Adv.* **6**, eaay2368 (2020).
31. F. H. Lambert, N. P. Gillett, D. A. Stone, C. Huntingford, Attribution studies of observed land precipitation changes with nine coupled models. *Geophys. Res. Lett.* **32**, 1–4 (2005).
32. S. Armal, N. Devineni, R. Khanbilvardi, Trends in extreme rainfall frequency in the contiguous United States: Attribution to climate change and climate variability modes. *J. Clim.* **31**, 369–385 (2018).
33. C. J. W. Bonfils *et al.*, Relative contributions of mean-state shifts and ENSO-driven variability to precipitation changes in a warming climate. *J. Clim.* **28**, 9997–10013 (2015).
34. H. Wang *et al.*, Attribution of the seasonality and regionality in climate trends over the United States during 1950–2000. *J. Clim.* **22**, 2571–2590 (2009).
35. P. A. Stott *et al.*, Attribution of extreme weather and climate-related events. *Wiley Interdiscip. Rev. Clim. Change* **7**, 23–41 (2016).
36. D. R. Easterling, K. E. Kunkel, M. F. Wehner, L. Sun, Detection and attribution of climate extremes in the observed record. *Weather Clim. Extrem.* **11**, 17–27 (2016).
37. I. M. Held, B. J. Soden, Robust responses of the hydrologic cycle to global warming. *J. Clim.* **19**, 5686–5699 (2006).
38. C. Tebaldi, K. Hayhoe, J. M. Arblaster, G. A. Meehl, Going to the extremes: An intercomparison of model-simulated historical and future changes in extreme events. *Clim. Change* **79**, 185–211 (2006).
39. O. Choi, A. Fisher, The impacts of socioeconomic development and climate change on severe weather catastrophe losses: Mid-Atlantic region (MAR) and the U.S. *Clim. Change* **58**, 149–170 (2003).
40. J. Pielke, A. Roger, M. W. Downton, Precipitation and damaging floods: Trends in the United States, 1932–97. *J. Clim.* **13**, 3625–3637 (2000).
41. M. H. Spekkers, M. Kok, F. H. L. R. Clemens, J. A. E. Ten Veldhuis, A statistical analysis of insurance damage claims related to rainfall extremes. *Hydrol. Earth Syst. Sci.* **17**, 913–922 (2013).
42. F. Estrada, W. J. W. Botzen, R. S. J. Tol, Economic losses from US hurricanes consistent with an influence from climate change. *Nat. Geosci.* **8**, 880–884 (2015).
43. S. Schmidt, C. Kemfert, P. Höppe, Tropical cyclone losses in the USA and the impact of climate change—A trend analysis based on data from a new approach to adjusting storm losses. *Environ. Impact Assess. Rev.* **29**, 359–369 (2009).
44. M. Burke, W. M. Davis, N. S. Diffenbaugh, Large potential reduction in economic damages under UN mitigation targets. *Nature* **557**, 549–553 (2018).
45. PRISM Climate Group, Recent years (Jan 1981–Jun 2020). <https://prism.oregonstate.edu/recent/>. Accessed 31 July 2020.
46. PRISM Climate Group, Historical past (1895–1980). <https://prism.oregonstate.edu/historical/>. Accessed 31 July 2020.
47. Center for Emergency Management and Homeland Security, The Spatial Hazard Events and Losses Database for the United States, Version 17.0. <https://cemhs.asu.edu/sheldus>. Accessed 10 February 2019.
48. N. S. Diffenbaugh, M. Burke, Global warming has increased global economic inequality. *Proc. Natl. Acad. Sci. U.S.A.* **116**, 9808–9813 (2019).
49. J. Mummolo, E. Peterson, Improving the interpretation of fixed effects regression results. *Political Sci. Res. Methods* **6**, 829–835 (2018).
50. K. E. Taylor, R. J. Stouffer, G. A. Meehl, An overview of CMIP5 and the experiment design. *Bull. Am. Meteorol. Soc.* **93**, 485–498 (2012).

REVIEW SUMMARY

GREENHOUSE GASES

Strengthened scientific support for the Endangerment Finding for atmospheric greenhouse gases

Philip B. Duffy*†, Christopher B. Field*, Noah S. Diffenbaugh*, Scott C. Doney, Zoe Dutton, Sherri Goodman, Lisa Heinzerling, Solomon Hsiang, David B. Lobell, Loretta J. Mickley, Samuel Myers, Susan M. Natali, Camille Parmesan, Susan Tierney, A. Park Williams

BACKGROUND: The Clean Air Act requires the Environmental Protection Agency (EPA) to regulate air pollutants when the EPA Administrator finds that they “cause, or contribute to, air pollution which may reasonably be anticipated to endanger public health or welfare.” In *Massachusetts v. EPA*, the U.S. Supreme Court held that the EPA has the authority to regulate greenhouse gases (GHGs) under the Clean Air Act and that the EPA may not refuse to regulate once it has made a finding of endangerment.

In December 2009, the EPA released its “Endangerment and Cause or Contribute Findings for Greenhouse Gases under Section 202(a) of the Clean Air Act,” known informally as the Endangerment Finding (EF). The EF found that six long-lived GHGs, in combination, should be defined as “air pollution” under the Clean Air Act and may reasonably be anticipated to endanger the health and welfare of current and future generations.

The EF is an essential element of the legal basis for regulating GHG emissions under the Clean Air Act. It provides foundational support for important aspects of U.S. climate policy, including vehicle mileage standards for cars and light trucks and the emissions standards for electricity generation known as the “Clean Power Plan.”

The EF was rooted in careful evaluation of observed and projected effects of GHGs, with assessments from the U.S. Global Change Research Program, the Intergovernmental Panel on Climate Change, and the U.S. National Research Council providing primary evidence. The EF was clear that, although many aspects of climate change were still uncertain, the evidence available in 2009 was strong. Since the original EF, scientific information about the causes, historical impacts, and future risks of climate change has continued to accumulate. This Review assesses that new information in the context of the EF.

ADVANCES: The EF was structured around knowledge related to public health and public welfare, with a primary focus on impacts in the United States. The information on public welfare was grouped into sections on air quality; food production and agriculture; forestry; water resources; sea level rise and coastal areas; energy, infrastructure, and settlements; and ecosystems and wildlife.

In this Review, we assess new evidence in the impact areas addressed in the EF, as well as emergent areas that were not addressed in the EF but in which there have been important advances in understanding the risks of climate change. For each area, we characterize

changes since the EF in terms of the strength of evidence for a link with anthropogenic climate change, the severity of observed and projected impacts, and the risk of additional categories of impact beyond those considered in the EF.

For each of the areas addressed in the EF, the amount, diversity, and sophistication of the evidence has increased markedly, clearly strengthening the case for endangerment (see Fig. 1 in the full article). New evidence about

ON OUR WEBSITE

Read the full article at <http://dx.doi.org/10.1126/science.aat5982>

the extent, severity, and interconnectedness of impacts detected to date and projected for the future reinforces the case that climate change endangers the health and welfare of

current and future generations. For the sectors analyzed in the 2009 EF, new evidence expands the range of case studies, deepens the understanding of mechanisms, and analyzes the contribution of climate change to particular types of extreme events. In many cases, new evidence points to the risk of impacts that are more severe or widespread than those anticipated in 2009. Further, several categories of climate change impacts, including effects on ocean acidification, violence, national security, and economic well-being, are now supported by such broad evidence that they warrant inclusion in the framing of endangerment.

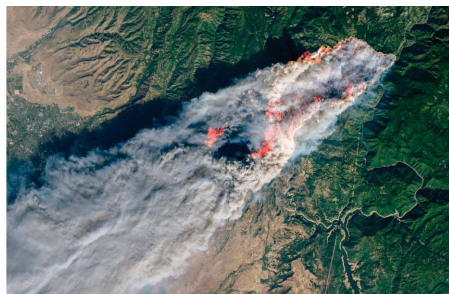
OUTLOOK: The EPA Administrator found in 2009 that the EF for six long-lived GHGs was “compellingly” supported by “strong and clear” scientific evidence. Our review of evidence published since the EF shows that the case for endangerment, which was already overwhelming in 2009, is even more strongly justified in 2018. ■

The list of author affiliations is available in the full article online.
*These authors contributed equally to this work.
†Corresponding author. Email: pduffy@whrc.org
Cite this article as P. B. Duffy *et al.*, *Science* **363**, eaat5982 (2019). DOI: [10.1126/science.aat5982](https://doi.org/10.1126/science.aat5982)



TOMORROW'S EARTH

Read more articles online at scim.ag/TomorrowsEarth



New evidence relevant to the EF. New evidence strengthens the link with anthropogenic climate change (category 1); suggests more severe observed and/or projected impacts (category 2); or identifies new types of risks beyond those considered in the EF (category 3). Examples discussed in this Review include, for category 1, wildfire (left); for category 2, coastal flooding (center); and for category 3, ocean acidification (right).

REVIEW

GREENHOUSE GASES

Strengthened scientific support for the Endangerment Finding for atmospheric greenhouse gases

Philip B. Duffy^{1,*†}, Christopher B. Field^{2,3*}, Noah S. Diffenbaugh^{2,3*}, Scott C. Doney⁴, Zoe Dutton⁵, Sherri Goodman⁵, Lisa Heinzerling⁶, Solomon Hsiang^{7,8}, David B. Lobell^{2,3}, Loretta J. Mickley⁹, Samuel Myers^{10,11}, Susan M. Natali¹, Camille Parmesan^{12,13,14}, Susan Tierney¹⁵, A. Park Williams¹⁶

We assess scientific evidence that has emerged since the U.S. Environmental Protection Agency's 2009 Endangerment Finding for six well-mixed greenhouse gases and find that this new evidence lends increased support to the conclusion that these gases pose a danger to public health and welfare. Newly available evidence about a wide range of observed and projected impacts strengthens the association between the risk of some of these impacts and anthropogenic climate change, indicates that some impacts or combinations of impacts have the potential to be more severe than previously understood, and identifies substantial risk of additional impacts through processes and pathways not considered in the Endangerment Finding.

The Clean Air Act (CAA) requires the U.S. Environmental Protection Agency (EPA) to regulate air pollutants when the EPA Administrator finds that they “cause, or contribute to, air pollution which may reasonably be anticipated to endanger public health or welfare” (1). In *Massachusetts v. EPA*, the U.S. Supreme Court held that the EPA has the authority to regulate greenhouse gases (GHGs) under the CAA and that the EPA may not refuse to regulate these pollutants once it has made a finding of endangerment (2). In this decision, the Supreme Court characterized an endangerment finding on GHGs as a “scientific judgment”

about “whether greenhouse gas emissions contribute to climate change.”

The courts have long held that the CAA embraces a precautionary approach to findings of endangerment. For example, the federal court of appeals in Washington, DC, has held that “evidence of potential harm as well as actual harm” meets the endangerment threshold and that the EPA’s degree of certitude may be lower where the hazards are most grave (3). Moreover, public health and welfare are broad concepts under the act, encompassing not only human morbidity and mortality but also effects on soils, water, crops, vegetation, animals, wildlife, weather, and climate (4).

In December 2009, the EPA released its “Endangerment and Cause or Contribute Findings for Greenhouse Gases under Section 202(a) of the Clean Air Act,” known informally as the Endangerment Finding (EF). The EF found that six long-lived GHGs, in combination, should be defined as “air pollution” under the CAA and may reasonably be anticipated to endanger the health and welfare of current and future generations. In addition, the EPA explained that “it is fully reasonable and rational to expect that events occurring outside our borders can affect the U.S. population” (5).

The EF is an essential element of the legal basis for regulating GHG emissions under the CAA. It provides foundational support for important aspects of U.S. climate policy, including vehicle mileage standards for cars and light trucks and the emissions standards for fossil fuel-fired electric utility generating units (the “Clean Power Plan”).

As the DC Circuit held in affirming the EF, the EPA may not decline to find endangerment

on the basis of the perceived effectiveness or ineffectiveness of the regulations that may follow in the wake of an endangerment finding or on the basis of predictions about the potential for societal adaptation to climate change (6). The DC Circuit held that arguments to the contrary were “foreclosed by the language of the [Clean Air Act] and the Supreme Court’s decision in *Massachusetts v. EPA*.” The court also rejected the argument that the EPA must find that the air pollutants it regulates are the dominant source of the harms it identifies, as the act provides that the pollutants being regulated need only contribute to (or, under some provisions of the statute, “significantly” contribute to) (7) harmful air pollution.

The EF was rooted in careful evaluation of the observed and projected effects of GHGs, with assessments from the U.S. Global Change Research Program, the Intergovernmental Panel on Climate Change (IPCC), and the U.S. National Research Council providing primary scientific evidence. The EF was clear that, although many aspects of climate change were still uncertain, the evidence available in 2009 strongly supported the finding. Since the original EF, scientific information about the causes, historical impacts, and future risks of climate change has continued to accumulate. This Review assesses that new information in the context of the EF. We find that the case for endangerment, which was already overwhelming in 2009, is even stronger now.

The EF was structured around knowledge related to public health and public welfare, with a primary focus on effects in the United States. The information on public welfare was grouped into sections on air quality; food production and agriculture; forestry; water resources; sea level rise (SLR) and coastal areas; energy, infrastructure, and settlements; and ecosystems and wildlife. We follow that organization here. In addition, some of the most important advances in understanding the risks of climate change involve sectors or impact types not highlighted in the EF. We summarize the evidence for four of these that are broadly important: ocean acidification, violence and social instability, national security, and economic well-being. We characterize changes since the EF in terms of the strength of the evidence for a link with anthropogenic climate change, the potential severity of observed and projected impacts, and the risks of additional kinds of impacts beyond those considered in the EF (Fig. 1).

Our focus is on the evidence for endangerment rather than the potential for adaptation. Although evidence that a risk might be reduced by some future action is certainly relevant for developing an effective portfolio of responses, the DC Circuit has affirmed that such evidence does not change the core question of whether long-lived GHGs endanger public health and welfare (6). In addition, adaptation options are often limited or impose economic costs that reduce adoption (8). Even ambitious adaptation rarely eliminates risk. For 32 specific risks evaluated by the IPCC in its recent special report,

¹Woods Hole Research Center, Falmouth, MA 02540, USA.

²Stanford Woods Institute for the Environment, Stanford University, Stanford, CA 94305, USA. ³Department of Earth System Science, Stanford University, Stanford, CA 94305, USA.

⁴Department of Environmental Sciences, University of Virginia, Charlottesville, VA 22904, USA. ⁵Woodrow Wilson International Center for Scholars, Washington, DC 20004, USA.

⁶Georgetown University Law Center, Washington, DC 20001, USA. ⁷Global Policy Laboratory, Goldman School of Public Policy, University of California, Berkeley, CA 94720, USA.

⁸National Bureau of Economic Research, Cambridge, MA 02138, USA. ⁹John A. Paulson School of Engineering and Applied Sciences, Harvard University, Cambridge, MA 02138, USA.

¹⁰Harvard University Center for the Environment, Harvard University, Cambridge, MA 02138, USA. ¹¹Harvard T. H. Chan School of Public Health, Boston, MA 02115, USA.

¹²SETe, CNRS, and University P-Sabatier, Moulis 09200, France. ¹³School of Biological and Marine Sciences, University of Plymouth, Plymouth, Devon PL4 8AA, UK.

¹⁴Department of Geological Sciences, University of Texas at Austin, Austin, TX 78712, USA. ¹⁵Analysis Group, Denver, CO 80202, USA. ¹⁶Lamont-Doherty Earth Observatory, Columbia University, Palisades, NY 10964, USA.

*These authors contributed equally to this work. †Corresponding author. Email: pduffy@whrc.org

Summary of New Evidence Since the Endangerment Finding new evidence for impacts in areas included in and emergent beyond the EF

	Impacts Areas Included in EF		
	Confidence in Impacts	Evidence of More Severe or Pervasive Impacts	Emergent Impacts Beyond the EF
Public Health	↑	↑	↑
Air Quality	↑	↑	↑
Food Production and Agriculture	↑	↑	↑
Forestry	↑	↑	
Water Resources	↑	↑	↑
Sea Level Rise and Coastal Areas	↑	↑	
Energy, Infrastructure and Settlements	↑		
Ecosystems and Wildlife	↑	↑	
Ocean Acidification			↑
Violence			↑
National Security			↑
Economic Wellbeing			↑

Fig. 1. New evidence since the EF. The columns summarize changes in the amount and implications of new evidence since the EF for each of the impact areas discussed in the EF and four additional impact areas where evidence of climate sensitivity has matured since the EF. An upward-pointing arrow indicates increasing evidence of endangerment. A downward-pointing arrow would indicate decreasing evidence of endangerment. A plain red arrow indicates that the new evidence is abundant and robust. An outlined arrow indicates that the new evidence, in addition, comes from multiple approaches, is derived from independent lines of information, or builds on a new level of mechanistic understanding. The left column refers to confidence in the impacts discussed in the EF. The middle column refers to impact areas that are discussed in the EF but where new evidence points to specific impacts that are fundamentally more severe or pervasive than those discussed in the EF. The right column refers to types of impacts not discussed in the EF.

the potential for adaptation was assessed as low or very low for 25% of risks at a warming of 1.5°C and 53% of risks at 2°C (9).

One area of scientific progress since the EF is the attribution of extreme weather events (and some of their consequences) to human-caused climate change. This includes observed effects on human health and security, agriculture, and ecosystems (see below), as well as the probability and/or intensity of specific extreme weather events (10, 11). For extreme event attribution in North America, this includes more than 70% of recent record-setting hot, warm, and wet events and ~50% of record-setting dry spells (12), along

with the recent California drought (13, 14), the storm-surge flooding during Superstorm Sandy (15) and Hurricane Katrina (16), and heavy precipitation during Hurricane Harvey (17–19). Although the realization of risk is not required for a finding of endangerment, cases where extreme events can be confidently attributed to historical emissions reinforce the understanding that we are already seeing impacts and the risks they bring.

Public health

Since the EF, numerous scientific reports, reviews, and assessments have strengthened our understanding of the global health threats

posed by climate change [e.g., (20, 21)] (Fig. 1, left column). New evidence validates and deepens the understanding of threats, including increased exposure to extreme heat, reduced air quality, more frequent and/or intense natural hazards, and increased exposure to infectious diseases and aeroallergens. New evidence also highlights additional health-related threats not discussed in the EF, including reduced nutritional security, effects on mental health, and increased risk of population displacement and conflict (Fig. 1, right column).

Extreme heat is the most direct health impact (Fig. 2). With future warming, >200 U.S. cities face increased risk of aggregated premature mortality (22). In addition, extreme heat is linked to rising incidence of sleep loss (23), kidney stones (24), low birth weight (25), violence (26), and suicide (27) (Fig. 1, middle column).

New studies also strengthen evidence for health impacts via increased exposure to ozone and other air pollutants (28), including smoke from forest fires (29). Likewise, evidence for links among climate change, extreme weather, and climate-related disasters is growing rapidly (30). These events often lead to physical trauma, reduced air quality, infectious disease outbreaks, interruption of health service delivery, under-nutrition, and both acute and chronic mental health effects (31).

Changes in temperature, precipitation, and soil moisture are also altering habitats, life cycles, and feeding behaviors of vectors for most vector-borne diseases (32), with recent research documenting changes in exposure to malaria (33), dengue (34), West Nile virus (35), and Lyme disease (36), among others. Recent work also reinforces the evidence that increased outbreaks of waterborne (37) and foodborne (38) illnesses are likely to follow increasing temperatures and extreme precipitation. Likewise, recent research reinforces the conclusion that rising temperatures and carbon dioxide (CO₂) levels will increase pollen production and lengthen the pollen season for many allergenic plants (39, 40), leading to increased allergic respiratory disease (41).

One area of new understanding not covered in the EF is threats to global nutrition. Staple crops grown at 550 parts of CO₂ per million have lower amounts of zinc, iron, and protein than the same cultivars grown at ambient CO₂ (42). These nutrient losses could push hundreds of millions of people into deficiencies of zinc (43), protein (44), and iron (45), in addition to aggravating existing deficiencies in more than one billion people. These effects on nutritional quality exacerbate the impacts of climate change on agricultural yield, discussed below. Together, these effects underscore a substantial headwind in assuring access to nutritious diets for the global population (46).

Mental health impacts represent another area of new understanding (47). In particular, increased exposure to climate and weather disasters is associated with posttraumatic stress, anxiety, depression, and suicide (27, 48).

Downloaded from <http://science.sciencemag.org/> on February 10, 2019

Extreme Seasonal Temperature Conditions

2080-2099 seasons that are hotter than the 1986-2005 maximum

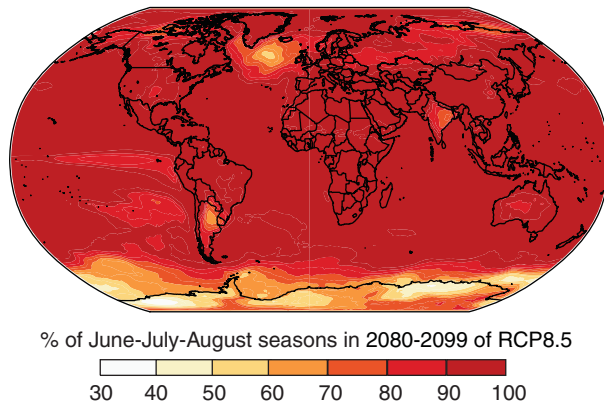


Fig. 2. The frequency of years from 2080 to 2099 of the RCP8.5 scenario in which the June-July-August (JJA) seasonal temperature equals or exceeds the warmest JJA value in the period from 1986 to 2005. [Adapted from (282)]

Lastly, climate change is increasingly understood to function as a threat magnifier, raising the risk of population displacement and armed conflict (discussed below), which can also amplify risks to human health.

Public welfare

Air quality

Evidence for the climate penalty on air quality stressed in the EF has strengthened (Fig. 1, left column). Mechanisms include extreme heat, leading to amplified production of surface ozone (49, 50); strong temperature inversions, leading to increased concentrations of particulate matter (PM) (51, 52); and stagnant atmospheric conditions (53). The most persistent and extreme episodes of elevated temperature, ozone, and PM in the United States have a high incidence of co-occurrence (54). Further global warming is likely to cause air stagnation events to increase over many midlatitude regions, including the western United States (53).

Recent studies confirm the increased risk of higher surface ozone concentrations as climate changes [e.g., (55–57)]. By the 2050s, the United States could experience more ozone episodes (days with 8-hour maximum daily averaged ozone concentrations greater than 75 parts per billion), including three to nine more episodes per year in the Northeast and California (58). By the 2090s, increases could reach 10 episodes per year across the Northeast (59). The U.S. ozone season, typically confined to summer, could also lengthen into spring and/or fall as climate warms (60) (Fig. 1, middle column).

Modeling studies of changes in PM present a mixed picture, arising from the complex responses of PM emissions and chemistry to meteorology [e.g., (61, 62)]. However, as the measurement record has lengthened, more robust estimates have come from observationally based statistical models. By using this approach and assuming no change in emissions

of anthropogenic PM sources, one study projected that the annual mean $PM_{2.5}$ (the concentration of particles $\leq 2.5 \mu m$ in diameter) could increase by 0.4 to $1.4 \mu g m^{-3}$ in the eastern United States by the 2050s, with small decreases in the West (58). However, summertime mean $PM_{2.5}$ was projected to increase as much as 2 to $3 \mu g m^{-3}$ in the East because of faster oxidation and greater biogenic emissions.

Warmer and drier conditions in the West and Southwest [e.g., (63)] have implications for wildfire smoke and dust storms, as discussed below. By the 2050s, increased wildfire activity could elevate the concentrations of organic particles across the West by 46 to 70%, depending on the ecoregion (64), and the frequency of smoke episodes could double in California (65) (Fig. 1, right column). Future projections of the frequency of dust storms are mixed [e.g., (66)]. However, seasonal means of fine dust particles are projected to increase 26 to 46% by the 2050s in the Southwest under a scenario of very high GHG emissions (67).

Taken together, these studies imply that the health impacts of changing air quality due to changing climate will vary across the United States, with greater effects from anthropogenic $PM_{2.5}$ in the East and greater effects from dust and wildfire smoke in the West. The effect of changing ozone on health is projected to be greatest in the Northeast and California. Even seasonal exacerbation in pollutants, though relatively short term, would likely have negative consequences for health (68). The projected degradation of air quality could be mitigated to some extent by more stringent restrictions on the anthropogenic emissions of pollution precursors [e.g., (57)].

Food production and agriculture

Research since the EF has confirmed the EF's conclusion that “the body of evidence points towards increasing risk of net adverse impacts

on U.S. food production and agriculture over time, with the potential for significant disruptions and crop failure in the future” (Fig. 1, left column). There is still an expectation that certain aspects of increasing CO_2 and temperature will be beneficial in the next few decades for some crops and locations within the United States but that these positive effects are likely to be outweighed by negative impacts, especially in the long term.

There is substantial new evidence quantifying and explaining the mechanisms behind crop yield losses that result from short periods of exposure to high growing-season temperatures (e.g., greater than $30^\circ C$, or $86^\circ F$) (69, 70) (Fig. 1, middle column). Likewise, warmer winter nights will also negatively affect perennial crops, such as apples and cherries, that require a certain amount of winter chill for high yields (71), an impact not included in the 2009 EF (Fig. 1, right column).

New understanding of weed and pest responses to climate and CO_2 highlights the risks from these biotic stresses [e.g., (72, 73)]. For example, weeds typically respond more quickly than crops to higher CO_2 , which “will contribute to increased risk of crop loss due to weed pressure” (70).

Understanding of agricultural vulnerability has also extended beyond the main commodity crops (Fig. 1, right column). For example, national aggregate agricultural total factor productivity (TFP) exhibits strong sensitivity to weather in regions having high-value crops or livestock production or specializing in commodity crops (74). Sensitivity was highest in recent time periods, and projected warming could reduce TFP at a rate faster than that of technological improvement.

Measurements since the EF enable more thorough characterization of ongoing impacts and adaptation responses. Climate changes since 1980 have had net negative impacts on yields of maize and wheat in most major producing regions globally, with less substantial impacts for rice and soybeans (69). Warming trends in the United States have been more muted than those in other regions, resulting in smaller impacts to date. Studies have also assessed the ability of farmers to adapt to ongoing changes, for example, by comparing regions with different rates of warming or by evaluating sensitivity to spatial gradients in temperature at different points in time. These studies generally indicate a limited ability of farmers to simultaneously raise yields and reduce yield sensitivity to warming (75, 76), which is consistent with the increased aggregate sensitivity of TFP. Other adaptations such as switching crops or adding irrigation have been less rigorously tested. Overall, the conclusion of the 2014 National Climate Assessment was that “although agriculture has a long history of successful adaptation to climate variability, the accelerating pace of climate change and the intensity of projected climate change represent new and unprecedented challenges to the sustainability of U.S. agriculture” (Fig. 1, middle column) (70).

Forestry

Evidence available at the time of the EF indicated that anthropogenic climate change would likely bring more harm than benefits for U.S. forests during the 21st century. Research since the EF broadly confirms that forest ecosystems are not in equilibrium with ongoing and projected trends in extreme heat and drought, making large ecological shifts in U.S. forests likely (77–81) (Fig. 1, left column).

Anthropogenic warming has reduced snowpack across the majority of the montane western United States (82, 83), and Earth system models project reduced summer soil moisture across most of the United States (63, 84). Warming also elevates plant respiration rates and atmospheric evaporative demand, aggravating drought stress and the risk of tree mortality. Further, projected increases in precipitation variability (85) are likely to promote increasingly severe droughts even in regions of increased mean precipitation (13, 86).

Whereas CO₂ fertilization, warming-induced lengthening of the growing season, and nitrogen deposition pose potential benefits to trees, models substantially overestimate CO₂-driven increases in global vegetation productivity over recent decades (87).

A large body of new evidence points to increasing risks of tree mortality or forest loss in the western United States from wildfire, insect outbreaks, and physiological failure due to drought stress (88) (Fig. 1, middle column). Although such disturbances occur naturally, increases in disturbance size, frequency, and severity can have long-term impacts on forest ecosystems (78, 89). Annual western U.S. forest-fire area increased by ~1000% from 1984 to 2017 (90, 91) (Fig. 3). Studies consistently attribute a substantial fraction of this trend to warming-induced fuel drying (92–94) and suggest continued increases in western U.S. forest-fire activity (95, 96) and resultant tree mortality (97) until fuels become limiting (98).

Land management has amplified the effects of warming on western U.S. forest-fire activity (Fig. 1, left column). A century of fire suppression caused fuels to accumulate, creating fire deficits in many forested areas (99). Accumulated fuels and warming combine to aggravate the risk of large, high-intensity wildfires (100–102). This risk may be further exacerbated where CO₂ fertilization or precipitation trends enhance biomass (103) or where humans add to natural ignitions (104).

Recent bark beetle outbreaks in western North America appear to be more massive than those in previous centuries (105), with new research since the EF documenting millions of hectares of tree mortality (106, 107) (Fig. 1, middle column). Warming may intensify bark beetle outbreaks by decreasing cold-season beetle mortality, accelerating the beetle life cycle, and weakening tree defenses (108). However, the full range of effects of climate change on bark beetle outbreaks remains unconstrained (109, 110).

Heat- and drought-driven tree mortality in western forests may be increasing even in the

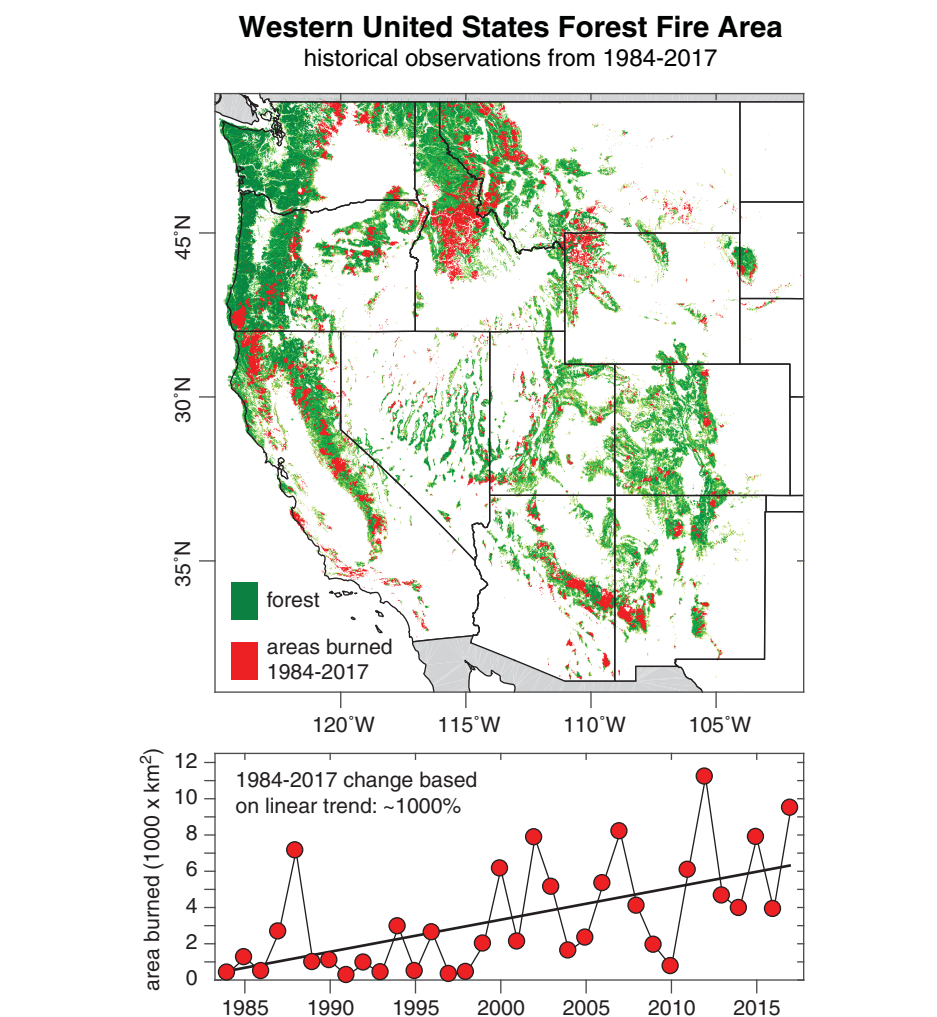


Fig. 3. Western U.S. forest-fire area for 1984 to 2017. (Top) Map of forest-fire areas. **(Bottom)** Annual forest-fire area according to the U.S. Forest Service Monitoring Trends in Burn Severity (MTBS) project for 1984 to 2016 (90) and the MODIS version 6 burned-area product for 2017 (91). The MODIS burned-area record was linearly calibrated to the MTBS record during overlapping years of 2001 to 2016. The linear trend is derived from least-squares regression.

absence of wildfire or insects, as more intense droughts can damage the water transporting xylem and reduce carbon reserves (111, 112). Quaking aspens in the Rocky Mountains have experienced particularly severe drought-driven mortality since 2002, with the risk of repeated events projected to rise throughout the century (113). Some of the impacts of drought intensification may be moderated by adaptation or enhanced capacity for postdrought injury repair (114, 115), but understanding of that potential is limited.

Climate change impacts on eastern forests have been more ambiguous because of the legacy effects of land management, complex competition dynamics, and in some locations, muted warming and/or increased precipitation. Nonetheless, eastern U.S. forests are vulnerable to extreme heat and drought (116, 117). Warming is implicated in the northward expansion of eastern forest pests, including the southern

pine beetle (108) and nonnative hemlock woolly adelgid (118). Recent drought-driven fires in the Southeast may portend warming-exacerbated fire activity in that region (119).

The current distributions and assemblages of vegetation species are not in equilibrium with future climate and CO₂ levels. Research over the past decade suggests that the velocity of climate change could exceed the rate of migration of some forest species (120, 121), enhancing the evidence in the EF that rapid 21st-century climate change will profoundly disrupt U.S. forest ecosystems (78) (Fig. 1, middle column).

Water resources

Climate change impacts on snow hydrology and water scarcity are especially pronounced in the western United States. Observed trends toward warming-induced reductions in snowpack were first widely reported by Mote *et al.* (122). Likewise, up to 60% of climate-related trends in

earlier river flow, warmer winter air temperature, and lower snowpack from 1950 to 1999 are attributed to human activities (82).

Since the EF, there has been substantial progress in quantifying trends in snowpack and associated impacts on water availability (Fig. 1, left column). Springtime warming over the past half century has resulted in a higher proportion of precipitation falling as rain versus snow in the western United States (123), earlier snowmelt onset by 1 to 2 weeks in the western United States (124), reductions in stream flow during the driest part of the year in the Pacific Northwest (125), earlier-in-the-year stream flow in snow-fed rivers in North America (126), and reductions in snow cover and snowpack over the Northern Hemisphere (127).

Climate models project accelerated changes in snow hydrology, both in the western United States and globally. Decreases in midlatitude snowfall (128, 129) are projected to reduce snow cover and depth (127, 128), accelerating hydroclimatic change in snow-dominated regions of the western United States (130), including losses in annual maximum water stored in snowpack of up to 60% in the next 30 years (131, 132). Losses of snow cover and water equivalent depth would fundamentally change the sources and timing of runoff in many midlatitude and mountainous regions (133), including the western (134), midwestern, and northeastern parts of the United States (135) (Fig. 1, middle column).

New research highlights risks from snowpack droughts (133, 136). These periods of very low snowpack negatively affect the water supply and other aspects of the Earth system, including rare and endangered species (e.g., salmon, trout, and wolverine) (137, 138) (Fig. 1, right column).

Research since the EF has highlighted the southwestern United States as a region of particular concern. On the Colorado River, elevated temperatures were an important contributor to the drought of 2000 to 2014, and continued warming is projected to drive greater reductions in river flows (139, 140) (Fig. 1, middle column). On the Rio Grande, warming temperatures are contributing to reductions in the fraction of precipitation that becomes river flow (141, 142).

Global urban freshwater availability is threatened by climate forcing and water management practices (143, 144), leading to a projected increase in the number of people living under absolute water scarcity (144, 145) (Fig. 1, right column). In addition, new evidence suggests that further global warming is likely to erode water quality in the United States by increasing nutrient loading and eutrophication, particularly in the Midwest and Northeast (146) (Fig. 1, right column).

Sea level rise and coastal areas

Understanding of the present rates of global and regional SLR, the role of contributing processes, the range of future rates, and the observed and projected impacts has improved since the EF (147). Evidence of the role of SLR in exacerbating impacts of recent hurricanes (15, 17, 19) further highlights the risks (Fig. 1, left column).

Recent studies project SLR at greater than 7 mm year⁻¹ after ~2050 (148). This is a global average SLR rate unprecedented in the last 7000 years (149). Recent acceleration of SLR in the U.S. Northeast and Gulf Coast adds to the longer-term trend (150). Annual exceedances of flood thresholds are increasing or accelerating at locations along the U.S. coastline (151), with the majority of tide gauge locations projected to pass a tipping point for flooding (more than 30 days year⁻¹ with water higher than 0.5 m above mean high tide) in the next several decades (152). With these rates of SLR, the stratigraphic record and modern analogs that serve as our traditional sources of insight are lacking, limiting our ability to predict the form, magnitude, and spatial extent of future changes to the coastal landscape (153, 154).

Research since the EF documents increased risks of SLR, especially for the higher levels of SLR now within the range of projections (155) (Fig. 1, middle column). SLR has and will increasingly expose coastal populations, economies, and infrastructure to hazards such as flooding, erosion, and extreme events. An SLR defined by the National Oceanic and Atmospheric Administration (NOAA) as an “Intermediate Low Scenario” of 0.5 m by 2100 results in tidally forced flooding approximately every other day for much of the East Coast and the Gulf of Mexico, whereas the “Intermediate Scenario” (1.0 m by 2100) leads to daily flooding in all U.S. coastal regions (156). In the United States, projected population growth approximately doubles the number of people at risk of inundation by 2100, to 4.2 million for an SLR of 0.9 m and 13.1 million for an SLR of 1.8 m (157). By 2110, a high SLR scenario results in the projected loss of more than 80% of West Coast tidal wetlands (158).

Coastal erosion and flooding risk are already affecting real estate values. For example, in Miami-Dade County, property subject to high-tide flooding is appreciating at a lower rate than properties at higher elevations, causing displacement through “climate gentrification” (159) (Fig. 1, left column). Furthermore, as older and less resilient residential structures are damaged or destroyed by coastal storms and chronic shoreline retreat, they are typically replaced by more resilient but also more expensive structures (159, 160).

New evidence since the EF highlights interactions between the SLR and other sectors (Fig. 1, middle column). The SLR and extreme events threaten the movement of goods among major port cities (161), which can lead to economic disruption (162), with cascading impacts far from the coastal zone, as well as opportunity costs associated with ensuring the viability of ports and other coastal infrastructure. Likewise, the domestic and international missions of the U.S. military, including disaster relief and humanitarian assistance, are increasingly affected by SLR, as discussed below.

Energy, infrastructure, and settlements

The EF found that “the evidence strongly supports the view that climate change presents risks

of serious adverse impacts on public welfare from the risk to energy production and distribution as well as risks to infrastructure and settlements.” This evidence has become stronger and broader since the EF, especially on the basis of increased understanding of the relationship between human-caused climate change and extreme events (10, 11) (Fig. 1, left column).

On the basis of analysis by Wilbanks *et al.* (163), Dell *et al.* reported that “changes in water availability, both episodic and long-lasting, will constrain different forms of energy production [including those] from fossil fuels (coal, oil, and natural gas), nuclear power, biofuels, hydropower, and some solar power systems ...” (164). Recent studies indicate that warming water bodies and the reduced availability of water for cooling power plant operations and for hydropower will continue to constrain power production at existing facilities and permitting of new power plants (163, 165). In some parts of the country, electric utilities and energy companies compete with farmers and ranchers, other industries, and municipalities for water rights and availability (166).

Recent work documents an increase in energy demand for cooling buildings, with a shift from predominantly heating to predominantly cooling in some regions and a greater reliance on electricity relative to other energy sources (163, 167).

Given that a substantial fraction of America’s energy and transportation infrastructure is located in low-lying coastal and riverine areas, much of that infrastructure is vulnerable to flooding from extreme weather events (168). Likewise, adverse effects on U.S. military infrastructure and surrounding communities have resulted most notably from drought and flooding, as discussed below.

The Third U.S. National Climate Assessment concluded that “in parts of Alaska, Louisiana, the Pacific Islands, and other coastal locations, climate change impacts ... are so severe that some communities are already relocating from historical homelands to which their traditions and cultural identities are tied” (169, 170, 171). In particular, “physical isolation, limited economic diversity, and higher poverty rates, combined with an aging population, increase the vulnerability of rural communities” (172).

The effects of rising temperatures are perhaps most severe in the Arctic, which is warming more than twice as fast as the global average (173) (Fig. 1, left column). Communities across the Arctic are experiencing impacts, including effects from the loss of sea ice, SLR, erosion, and permafrost thaw. These changes have been under way for decades, but much of the documentation has occurred since the EF. Arctic warming is endangering human health, destroying public infrastructure, and threatening water resources, cultural resources, and access to subsistence resources and traditional food storage (174, 175).

The risk and severity of climate impacts are particularly high for coastal communities in Alaska, where loss of land-fast sea ice is increasing storm impacts and permafrost thaw is

exacerbating coastal erosion rates (176) (Fig. 1, left column). Thirty-one Alaskan villages face imminent threats from flooding, erosion, and permafrost thaw (177). None of these villages have yet relocated, largely because of the lack of a governance framework to facilitate relocation efforts (178).

Permafrost thaw has a substantial economic cost, quantified mainly since the EF. Ground subsidence and collapse, particularly in ice-rich areas, negatively impact the structural integrity of buildings, roads, and industrial infrastructure, including gas and oil development (175). Cumulative projected costs of climate change damages to public infrastructure in the state of Alaska are estimated at \$5.5 billion for a high-emissions scenario [Representative Concentration Pathway 8.5 (RCP8.5)] and \$4.2 billion for a medium-emissions scenario (RCP4.5) for 2015 to 2099 (179). The greatest economic impact is expected to result from road flooding, followed by building damage as a result of near-surface permafrost thaw.

Ecosystems and wildlife

The first global meta-analyses of climate change impacts on wild species, mostly from terrestrial ecosystems, estimated that about half had responded by shifting their ranges poleward and upward and about two-thirds had responded by advancing their timing of spring events such as tree budburst and bird nesting (180). New studies since the EF have clarified and extended these findings, expanded documentation for marine systems, and illuminated responses at all levels of biological organization (181) (Fig. 1, left column). This new evidence makes clear that prior global estimates underestimated the impacts of anthropogenic climate change on ecosystems and wildlife.

Research since 2009 illuminates new range boundary dynamics that are more complex than simple northward or poleward shifts (182). For example, terrestrial range limits are shifting faster where local warming is stronger (183). Likewise, lower elevation limits set by precipitation can expand downward in response to increased rainfall, despite regional warming (184). Changes in behavior, the timing of activities, or the use of habitat can complement range shifts as a means of matching activity to the range of preferred temperatures (185).

By contrast, marine limits are typically set by physiological thermal tolerances and thus respond more strongly and predictably than equivalent terrestrial limits (186). The mean rate of movement in marine systems (187) reflects the faster poleward movement of isotherms in the oceans than on land (188, 189). The rapid range shift of marine organisms covers many taxa, including phytoplankton (470 km per decade), bony fish (278 km per decade), and invertebrate zooplankton (142 km per decade) (189). Taxa on the move also include important disease organisms, such as *Vibrio* bacteria, which have recently caused unprecedented outbreaks of food poisoning and infection of wounds [reviewed in (190)].

Research since 2009 on the timing of spring events illuminates changes that defy simple expectations (Fig. 1, left column). In plants that require chilling (“vernalization”) to determine that winter is over, winter warming slows development whereas spring warming speeds development. Actual changes in timing reflect the combination of these opposing effects, potentially resulting in development that is accelerated, delayed, or unchanged (191).

Before the EF, it was predicted that biological responses would lag behind changes in climate (192). Studies since 2009 have documented that this lag is already occurring. Across Europe, species are responding more slowly than climate is warming, causing bird and butterfly communities to suffer a “climate debt” (193). Likewise, populations of yellow warbler with detectable climate debts had the lowest population growth rates across the United States (194). By contrast, plants that have advanced their timing most strongly have had more positive population growth rates (195).

Similarly, at the time of the EF, there was an assumption that a sensitivity to warming would be most important at the limits of species’ ranges. However, several newer studies demonstrate that life history trade-offs can cause species to be constrained by the limits of their climatic tolerances even in central areas of their ranges (196, 197) (Fig. 1, left column).

Biological diversity and the services that ecosystems provide to humans face risks from climate change. The magnitude and timing of these risks are influenced not only by direct effects of climate on organisms but also by compounding effects of other stresses (198, 199), especially land use by humans, changes in disturbance regimes, defaunation (200), and ocean acidification (see below). Biotic interactions related to pollination, food resources, competition, pests, diseases, and predators can also amplify the risks (201). Since the EF, new research has provided additional detail on many of these risks and on the groups of species and ecosystem services that are most vulnerable (202) (Fig. 1, left column).

Extinction risk from climate change is broadly distributed across taxonomic groups, with 21st-century warming threatening about 15% of all species in a world of continued high emissions (202). Risks are especially great for species with small ranges or in habitat types that are spatially limited or rapidly shrinking, including Arctic sea-ice ecosystems (203) and mountaintops (198). Recent large-scale bleaching in warm-water coral reefs (204) and forest mortality events (205) provide clear evidence of risk under current conditions. In the United States, national parks have warmed at twice the national average rate, with precipitation declines at four times the average, highlighting risks to areas of high conservation value (206). Research since the EF underscores risks of climate change for diverse ecosystem services, such as those associated with the role of coral reefs in supporting fisheries (207) (Fig. 1, middle column) and the contribution of forests and soils in GHG balance (208).

Ocean acidification

The removal of anthropogenic CO₂ emissions by air-sea gas exchange and chemical dissolution into the ocean alters the acid-base chemistry of the ocean. Since the EF, scientific understanding of this process and of its possible negative effects on marine life has improved (Fig. 1, right column).

Excess CO₂ gas in the ocean reacts with water, resulting in a series of chemical changes that include reductions in pH, carbonate ion (CO₃²⁻) concentrations, and the saturation state for carbonate minerals used by many organisms to construct shells and skeletons (209). Such chemical changes are now well documented in the upper ocean. Acidification in coastal waters can be exacerbated by local pollution sources (210). Over the next several decades, trends in near-surface acidification are likely to closely track atmospheric CO₂ trends (211), with acidification hot spots in coastal upwelling systems, the Arctic, and the Southern Ocean (212, 213).

Evidence since the EF reveals a wide range of biological responses to elevated CO₂ and ocean acidification (Fig. 1, right column). For all marine species, the effects of current and future ocean acidification must be framed in the context of a rapidly changing ocean environment with multiple human-driven stressors, particularly ocean warming (214). Warming is reducing open-ocean oxygen levels and exacerbating coastal hypoxia driven by excess nutrients (215), the same nutrient pollution that also causes estuarine and coastal acidification.

Model and data syntheses indicate that acidification may shift reef systems to net dissolution during the 21st century (216). Coral bleaching from ocean warming is already having negative consequences for biologically rich coral reef ecosystems that provide food, income, and other valuable ecosystem services to >500 million people around the world (217), and the combined effects of warming and acidification are expected to worsen in the future (207).

Different kinds of organisms vary substantially in their responses to acidification, with generally negative effects for many mollusks and some plankton to neutral and even positive effects for other species (218). Lower seawater carbonate saturation states reduce calcification and may restrict the geographic habitat for planktonic pteropods (219) that are prey for many fish, marine mammals, and seabirds.

Many shellfish, and perhaps some kinds of crustaceans, are vulnerable to acidification, especially in larval and juvenile stages, with possible repercussions for valuable U.S. and international fisheries (220, 221) (Fig. 1, right column). During the mid-2000s, low-pH waters associated with coastal upwelling led to reduced larval survival of Pacific oysters in some U.S. Pacific Northwest shellfish hatcheries, a problem that has been largely addressable so far through adaptive strategies (222). Wild-harvest fisheries may be more at risk, particularly in regions with combined social and ecological vulnerability (223). Less is known about acidification responses in fish, with most studies indicating weak or no effects

Economic Damage from Climate Change in United States Counties

damage projected for 2080-2099 of RCP8.5

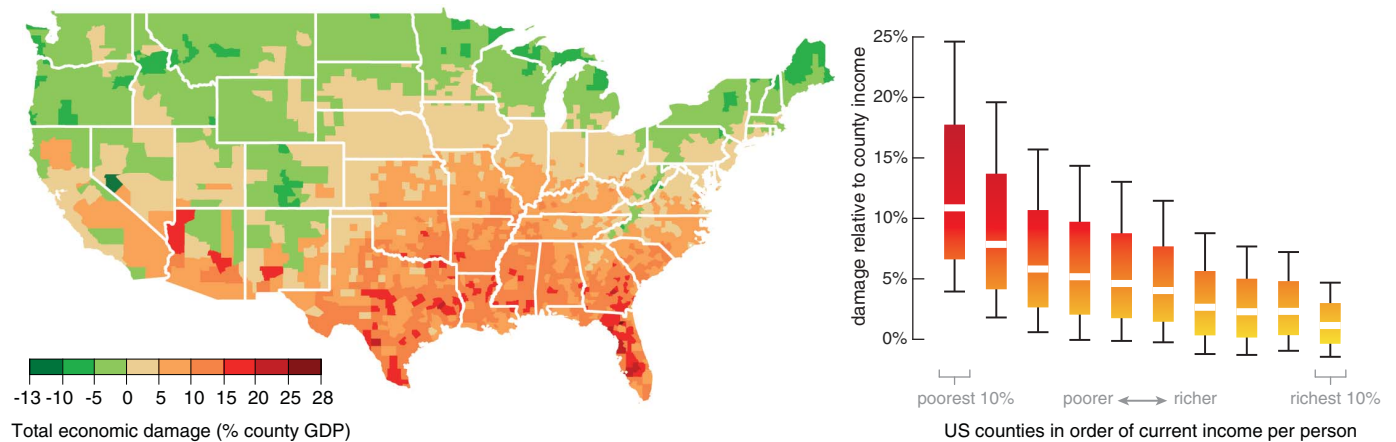


Fig. 4. Total direct economic damage integrated over agriculture, crime, coastal storms, energy, human mortality, and labor in 2080 to 2099 under a scenario of continued high emissions (RCP8.5). (Left) Damages in the median scenario for each county. Negative damages indicate benefits. (Right) Range of economic

damages per year for groupings of U.S. counties, on the basis of income (with 29,000 simulations for each of 3143 counties) as a fraction of county income (white lines, median; boxes, inner 66% of possible outcomes; outer whiskers, inner 90% of possible outcomes). [Adapted from (238)]

on growth and reproduction. However, a number of studies report negative effects on fish olfaction and behavior (224).

Taken as a whole, acidification will likely exacerbate many of the climate warming effects on marine ecosystems, including shifting species ranges, degrading coral reefs, and expanding low-oxygen zones.

Violence and social instability

Since the EF, a number of studies have used historical data to explore whether changes in environmental conditions influence the risk of violence or instability (225). In general, high temperatures and rainfall extremes amplify underlying risks (26) (Fig. 1, right column). These effects are not uniform (226). Many factors, including political institutions (227), income levels (228), and local economic structures (229), play a role in determining the structure of these effects.

A robust and generalizable finding is an increased risk of threatening and violent interactions between individuals under hot conditions (Fig. 1, right column). In the United States, exposure to high temperatures is associated with higher rates of domestic violence (230), rape, assault, and murder (231, 232), as well as greater use of threatening behaviors, such as aggressive language in social media posts (233) and horn honking in traffic (234), and higher rates of violent retaliation in sports (235). Emerging evidence also indicates that hot periods elevate the risk that individuals harm themselves, including by suicide (27, 236). U.S. data indicate no evidence of adaptation (27, 232).

Effects of temperature [$+2.4\%$ per SD (σ)] and rainfall (0.6% per σ) on interpersonal violence are both highly statistically significant, according to a meta-analysis (237). If these responses to historical fluctuations translate to future cli-

mate change, warming of 1°C could lead to an increase in national violent crime (rape, assault, and murder) by 0.88% ($\pm 0.04\%$) (238). Under RCP8.5, this trend projects to a warming-caused increase in violent crime of 1.7 to 5.4% by 2080 to 2099. Warming is projected to increase the national suicide rate by 0.6 to 2.6% by 2050 (27).

Many studies document a heightened risk of violence between groups of individuals when temperatures are hot and/or rainfall is extreme (26) (Fig. 1, right column). The patterns are similar for organized violence, such as civil conflicts (228, 239), and disorganized violence, such as ethnic riots (240), with highly statistically significant effects of temperature ($+11.3\%$ per σ) and rainfall (3.5% per σ , over 2 years) (237).

Political instability is heightened in hot periods, even in contexts where political institutions are sufficiently robust to avoid outright violence (Fig. 1, right column). The probability of political leadership changes, through both democratic process (241, 242) and “irregular” conditions (243, 244), rises in warm periods. Coups are more likely in hot years with extreme rainfall in agriculturally dependent countries (245).

By degrading economic conditions, climate events may contribute to out-migrations of populations seeking better opportunities. Drought and soil loss in the Dust Bowl induced mass out-migration from the rural Midwest (246), and young working-age individuals left the corn belt during periods of extreme heat in recent decades (247). Likewise, periods of high temperatures have been linked to migration from rural regions of Mexico to the United States (247, 248). Population movements after periods of extreme heat or dryness have been documented in multiple regions (249–251), and high temperatures in agrarian regions ele-

vate international applications for political asylum (252).

National security

Since the EF, the American military and intelligence communities have substantially increased their integration of climate change into national security strategies, policies, and plans. These considerations have been reflected in analyses of the national security implications of climate change by the U.S. Department of Defense, with almost 50 reports considering climate security impacts published between 2010 and 2018 (253) (Fig. 1, right column).

The National Intelligence Council (NIC) has warned Congress about the security risks of climate change every year since 2008, after the release of the landmark report by the CNA Military Advisory Board, “National Security and the Threat of Climate Change” (254). The NIC’s “Worldwide Threat Assessment,” which reflects the intelligence community’s consensus on the most substantial risks to national security, in 2018 for the first time included a robust section titled “Environment and climate change,” noting a range of security risks related to environmental concerns (255). The 2018 Defense Authorization Act, signed by President Donald J. Trump, stated that “climate change is a direct threat to the national security of the United States ...” (256). During the Trump presidency, 16 military leaders, including Secretary of Defense James Mattis (257), have voiced concerns about climate change and its security implications. Chairman of the Joint Chiefs of Staff General Joe Dunford stated, “Climate change ... is very much something that we take into account in our planning as we anticipate when, where and how we may be engaged in the future and what capabilities we should have” (258).

New studies strengthen the evidence that climate change causes weather patterns and extreme events that directly harm military installations and readiness through infrastructure damage, loss of utilities, and loss of operational capability (Fig. 1, right column). An SLR of 3.7 feet would threaten 128 military bases (259). Thawing permafrost exposes foundations to damage, whereas the loss of Arctic sea ice causes coastal erosion near critical facilities. Intensifying wildfires threaten facilities, transportation infrastructure, and utility lines. Fire-hazard days and inclement weather suspend outdoor training, and droughts limit the use of live-fire training. Greater storm frequency and strength put a strain on the resources of the defense support of civil authorities at home, as well as on assistance to humanitarian efforts and disaster relief around the world (260). As of 2018, 50% of military installations both at home and abroad had already reported damage due to climate change (260). Droughts or unpredictable rainfall could leave armed forces stationed abroad vulnerable to being disconnected from potable water supplies, a cause for concern given that protecting convoys for the “resupply of fuel and drinking water for troops in-theater costs lives” (261).

Climate change increasingly disrupts existing international security dynamics in geostrategic environments (Fig. 1, right column). Reduced Arctic sea-ice extent will open the way for more trade, as well as oil and gas extraction, turning a historically neutral territory into a potential political flashpoint. Moreover, the U.S. military now has to operate in an increasingly open water Arctic region as sea ice retreats. As Secretary of Defense Mattis recently stated, “America’s got to up its game in the Arctic” (262). Both China and Russia have been deepening their Arctic presence through investment and the development of ports. As much as 15 percent of China’s trade value could travel through the Arctic by 2030, and between 20 and 30 percent of Russia’s oil production will come from deposits in the Arctic shelf by 2050 (263). These interests will require further American military and coast guard activity in the region, as well as broader diplomatic and scientific engagement.

Indirectly, climate change has a major effect on national security by acting as a “threat multiplier” (254) or “accelerant of instability” (264) (Fig. 1, right column). This means that climate change heightens the risk posed by threats the United States is already facing and, in aggregate, fundamentally alters the security landscape (265). In both the 2010 and 2014 quadrennial defense reviews (264, 266), the Department of Defense emphasized how seriously the military takes this dangerous dynamic, a commitment that receives meaningful redress every year in its annual strategic sustainability performance plans (267).

As discussed in other parts of this Review, an expanding body of evidence reinforces how climate change fuels economic and social discontent, and even upheaval. This includes extreme weather events, which raise the risk of

humanitarian disasters, conflict, water and food shortages, population migration, labor shortfalls, price shocks, and power outages (255).

Economic well-being

Research on the economic consequences of climate change has advanced substantially since the EF, with important progress on understanding nonagricultural sectors and broad measures of well-being (225, 268) (Fig. 1, right column). In the United States, economic impacts of hot temperatures and changing tropical cyclone environments are clearly documented (238), and growing evidence indicates long-term adverse effects on the labor force (269–271). Other impacts, such as those from water availability or wildfire risks, are thought to be important but remain less well understood (272).

Since the EF, new “top-down” analyses of overall macroeconomic performance estimate that warming by an additional 1°C over 75 years can be expected to permanently reduce the U.S. gross domestic product (GDP) by ~3% through direct thermal effects (273) and that the U.S. GDP can be expected to be ~4% greater at 1.5°C than at 2°C above preindustrial temperatures (274) (Fig. 1, right column). The average projected alteration of cyclone activity under “business as usual” may cost the United States the equivalent of 29% of one year of current GDP (in net present value discounted at 3% annually) (275). In one study, the net cumulative market-based cost of thermal effects in RCP8.5 by 2100 should be valued at \$4.7 trillion to \$10.4 trillion (in net present value discounted at 3% annually) (276). Notably, in some cases these top-down analyses are able to account for both the opportunity costs and benefits of adaptations undertaken by populations as they adjust to new climatic conditions (276).

“Bottom-up” analyses examining impacts on individual sectors or industries have key advantages, including capturing the value of non-market impacts such as the loss of human life or biodiversity (238). Evidence from combining sector-specific analyses of impacts such as agricultural output (277), the quantity of labor supplied by workers (278), energy demand (167, 279), mortality rates (279), crime rates (232), SLR (280) and tropical cyclone damage (281) suggests U.S. costs equivalent to 1.2% of GDP for each 1°C of warming, with poorer counties experiencing an economic burden roughly five times that of wealthier counties (238) (Fig. 1, right column, and Fig. 4).

Conclusions

The EPA Administrator found in 2009 that the EF for six long-lived GHGs was “compellingly” supported by “strong and clear” scientific evidence (5). Since 2009, the amount, diversity, and sophistication of the evidence have increased markedly, clearly strengthening the case for endangerment. New evidence about the extent, severity, and interconnectedness of impacts detected to date and projected for the future reinforces the case that climate change may

reasonably be anticipated to endanger the health and welfare of current and future generations. For the sectors analyzed in the 2009 EF, new evidence expands the range of case studies, deepens the understanding of mechanisms, and analyzes the contribution of climate-related extremes. In many cases, new evidence points to the risk of impacts that are more severe or widespread than those anticipated in 2009. Several categories of climate-change impacts, including effects on ocean acidification, violence, national security, and economic well-being, are now supported by such broad evidence that they warrant inclusion in the framing of endangerment. In sum, the EF, fully justified in 2009, is much more strongly justified in 2018.

REFERENCES AND NOTES

- 42 U.S.C. (U.S.C.) § 7521(a)(1).
- U.S. Supreme Court, *Massachusetts v. EPA*, 549 U.S. 497 (2007).
- U.S. Court of Appeals DC Circuit, *Ethyl Corp. v. EPA*, 541 F.2d 1, 17–18 (1976).
- 42 U.S.C. § 7602(h).
- Environmental Protection Agency, Endangerment and cause or contribute findings for greenhouse gases under section 202(a) of the Clean Air Act. *Fed. Regist.* **74**, 66495–66546 (2009).
- U.S. Court of Appeals DC Circuit, *Coalition for Responsible Regulation v. EPA*, 684 F.3d 102, 117–18 (2012).
- 42 U.S.C. § 7411(b)(1)(A).
- S. Hsiang, D. Narita, Adaptation to cyclone risk: Evidence from the global cross-section. *Clim. Change Econ.* **3**, 1250011 (2012). doi: [10.1142/S201000781250011X](https://doi.org/10.1142/S201000781250011X)
- O. Hoegh-Guldberg et al., in “Global warming of 1.5°C, an IPCC special report on the impacts of global warming of 1.5°C above pre-industrial levels and related global greenhouse gas emission pathways, in the context of strengthening the global response to the threat of climate change, sustainable development, and efforts to eradicate poverty,” V. Masson-Delmotte et al., Eds. (IPCC, 2018).
- N. S. Diffenbaugh et al., Quantifying the influence of global warming on unprecedented extreme climate events. *Proc. Natl. Acad. Sci. U.S.A.* **114**, 4881–4886 (2017). doi: [10.1073/pnas.1618082114](https://doi.org/10.1073/pnas.1618082114); pmid: 28439005
- O. Angéil et al., An independent assessment of anthropogenic attribution statements for recent extreme temperature and rainfall events. *J. Clim.* **30**, 5–16 (2017). doi: [10.1175/JCLI-D-16-0077.1](https://doi.org/10.1175/JCLI-D-16-0077.1)
- N. S. Diffenbaugh, D. Singh, J. S. Mankin, Unprecedented climate events: Historical changes, aspirational targets, and national commitments. *Sci. Adv.* **4**, e3354 (2018). doi: [10.1126/sciadv.aao3354](https://doi.org/10.1126/sciadv.aao3354); pmid: 29457133
- N. S. Diffenbaugh, D. L. Swain, D. Touma, Anthropogenic warming has increased drought risk in California. *Proc. Natl. Acad. Sci. U.S.A.* **112**, 3931–3936 (2015). doi: [10.1073/pnas.1422385112](https://doi.org/10.1073/pnas.1422385112); pmid: 25733875
- A. P. Williams et al., Contribution of anthropogenic warming to California drought during 2012–2014. *Geophys. Res. Lett.* **42**, 6819–6828 (2015). doi: [10.1002/2015GL064924](https://doi.org/10.1002/2015GL064924)
- N. Lin, R. E. Kopp, B. P. Horton, J. P. Donnelly, Hurricane Sandy’s flood frequency increasing from year 1800 to 2100. *Proc. Natl. Acad. Sci. U.S.A.* **113**, 12071–12075 (2016). doi: [10.1073/pnas.1604386113](https://doi.org/10.1073/pnas.1604386113); pmid: 27790992
- A. Grinstead, J. C. Moore, S. Jevrejeva, Projected Atlantic hurricane surge threat from rising temperatures. *Proc. Natl. Acad. Sci. U.S.A.* **110**, 5369–5373 (2013). doi: [10.1073/pnas.1209980110](https://doi.org/10.1073/pnas.1209980110); pmid: 23509254
- K. Emanuel, Assessing the present and future probability of Hurricane Harvey’s rainfall. *Proc. Natl. Acad. Sci. U.S.A.* **114**, 12681–12684 (2017). doi: [10.1073/pnas.1716222114](https://doi.org/10.1073/pnas.1716222114); pmid: 29133388
- M. D. Risser, M. F. Wehner, Attributable human-induced changes in the likelihood and magnitude of the observed extreme precipitation during Hurricane Harvey. *Geophys. Res. Lett.* **44**, 12457–12464 (2017). doi: [10.1002/2017GL075888](https://doi.org/10.1002/2017GL075888)

19. G. J. van Oldenborgh *et al.*, Attribution of extreme rainfall from Hurricane Harvey, August 2017. *Environ. Res. Lett.* **12**, 124009 (2017). doi: [10.1088/1748-9326/aa9ef2](https://doi.org/10.1088/1748-9326/aa9ef2)
20. K. R. Smith *et al.*, in *Climate Change 2014: Impacts, Adaptation, and Vulnerability. Part A: Global and Sectoral Aspects. Contribution of Working Group II to the Fifth Assessment Report of the Intergovernmental Panel of Climate Change*, C. B. Field *et al.*, Eds. (Cambridge Univ. Press, 2014), chap. 11, pp. 709–754.
21. G. Luber *et al.*, in *Climate Change Impacts in the United States: The Third National Climate Assessment*, J. Melillo, T. T. C. Richmond, G. W. Yohe, Eds. (U.S. Global Change Research Program, 2014), pp. 220–256.
22. J. D. Schwartz *et al.*, Projections of temperature-attributable premature deaths in 209 U.S. cities using a cluster-based Poisson approach. *Environ. Health* **14**, 85 (2015). doi: [10.1186/s12940-015-0071-2](https://doi.org/10.1186/s12940-015-0071-2); pmid: [26537962](https://pubmed.ncbi.nlm.nih.gov/26537962/)
23. N. Obradovich, R. Migliorini, S. C. Mednick, J. H. Fowler, Nighttime temperature and human sleep loss in a changing climate. *Sci. Adv.* **3**, e1601555 (2017). doi: [10.1126/sciadv.1601555](https://doi.org/10.1126/sciadv.1601555); pmid: [28560320](https://pubmed.ncbi.nlm.nih.gov/28560320/)
24. G. E. Tasian *et al.*, Daily mean temperature and clinical kidney stone presentation in five U.S. metropolitan areas: A time-series analysis. *Environ. Health Perspect.* **122**, 1081–1087 (2014). doi: [10.1289/ehp.1307703](https://doi.org/10.1289/ehp.1307703); pmid: [25009122](https://pubmed.ncbi.nlm.nih.gov/25009122/)
25. O. Deschênes, M. Greenstone, J. Guryan, Climate change and birth weight. *Am. Econ. Rev.* **99**, 211–217 (2009). doi: [10.1257/aer.99.2.211](https://doi.org/10.1257/aer.99.2.211); pmid: [29505213](https://pubmed.ncbi.nlm.nih.gov/29505213/)
26. S. M. Hsiang, M. Burke, E. Miguel, Quantifying the influence of climate on human conflict. *Science* **341**, 1235367 (2013). doi: [10.1126/science.1235367](https://doi.org/10.1126/science.1235367); pmid: [24031020](https://pubmed.ncbi.nlm.nih.gov/24031020/)
27. M. Burke *et al.*, Higher temperatures increase suicide rates in the United States and Mexico. *Nat. Clim. Change* **9**, 723–729 (2018). doi: [10.1038/s41558-018-0222-x](https://doi.org/10.1038/s41558-018-0222-x)
28. B. J. Bloomer, J. W. Stehr, C. A. Piety, R. J. Salawitch, R. R. Dickerson, Observed relationships of ozone air pollution with temperature and emissions. *Geophys. Res. Lett.* **36**, L09803 (2009). doi: [10.1029/2009GL013708](https://doi.org/10.1029/2009GL013708)
29. B. J. Harvey, Human-caused climate change is now a key driver of forest fire activity in the western United States. *Proc. Natl. Acad. Sci. U.S.A.* **113**, 11649–11650 (2016). doi: [10.1073/pnas.1612926113](https://doi.org/10.1073/pnas.1612926113); pmid: [27791047](https://pubmed.ncbi.nlm.nih.gov/27791047/)
30. IPCC, in *A Special Report of Working Groups I and II of the Intergovernmental Panel on Climate Change*, C. B. Field *et al.*, Eds. (Cambridge Univ. Press, 2012), p. 592.
31. J. Bell *et al.*, “Ch. 4: Impacts of extreme events on human health” (U.S. Global Change Research Program, 2016).
32. S. Altizer, R. S. Ostfeld, P. T. Johnson, S. Kutz, C. D. Harvell, Climate change and infectious diseases: From evidence to a predictive framework. *Science* **341**, 514–519 (2013). doi: [10.1126/science.1239413](https://doi.org/10.1126/science.1239413); pmid: [23908230](https://pubmed.ncbi.nlm.nih.gov/23908230/)
33. V. Ermert, A. H. Fink, A. P. Morse, H. Paeth, The impact of regional climate change on malaria risk due to greenhouse forcing and land-use changes in tropical Africa. *Environ. Health Perspect.* **120**, 77–84 (2012). doi: [10.1289/ehp.1103681](https://doi.org/10.1289/ehp.1103681); pmid: [21900078](https://pubmed.ncbi.nlm.nih.gov/21900078/)
34. C. W. Morin, A. C. Comrie, K. Ernst, Climate and dengue transmission: Evidence and implications. *Environ. Health Perspect.* **121**, 1264–1272 (2013). doi: [10.1289/ehp.1306556](https://doi.org/10.1289/ehp.1306556); pmid: [24058050](https://pubmed.ncbi.nlm.nih.gov/24058050/)
35. S. Paz, Climate change impacts on West Nile virus transmission in a global context. *Philos. Trans. R. Soc. London Ser. B* **370**, 20130561 (2015). doi: [10.1098/rstb.2013.0561](https://doi.org/10.1098/rstb.2013.0561); pmid: [25688020](https://pubmed.ncbi.nlm.nih.gov/25688020/)
36. R. S. Ostfeld, J. L. Brunner, Climate change and Ixodes tick-borne diseases of humans. *Philos. Trans. R. Soc. London Ser. B* **370**, 20140051 (2015). doi: [10.1098/rstb.2014.0051](https://doi.org/10.1098/rstb.2014.0051); pmid: [25688022](https://pubmed.ncbi.nlm.nih.gov/25688022/)
37. L. Vezzulli, R. R. Colwell, C. Pruzzo, Ocean warming and spread of pathogenic vibrios in the aquatic environment. *Microb. Ecol.* **65**, 817–825 (2013). doi: [10.1007/s00248-012-0163-2](https://doi.org/10.1007/s00248-012-0163-2); pmid: [23280498](https://pubmed.ncbi.nlm.nih.gov/23280498/)
38. R. S. Hellberg, E. Chu, Effects of climate change on the persistence and dispersal of foodborne bacterial pathogens in the outdoor environment: A review. *Crit. Rev. Microbiol.* **42**, 548–572 (2016). pmid: [25612827](https://pubmed.ncbi.nlm.nih.gov/25612827/)
39. Y. Zhang *et al.*, Allergenic pollen season variations in the past two decades under changing climate in the United States. *Glob. Change Biol.* **21**, 1581–1589 (2015). doi: [10.1111/gcb.12755](https://doi.org/10.1111/gcb.12755); pmid: [25266307](https://pubmed.ncbi.nlm.nih.gov/25266307/)
40. L. Ziska *et al.*, Recent warming by latitude associated with increased length of ragweed pollen season in central North America. *Proc. Natl. Acad. Sci. U.S.A.* **108**, 4248–4251 (2011). doi: [10.1073/pnas.1014107108](https://doi.org/10.1073/pnas.1014107108); pmid: [21368130](https://pubmed.ncbi.nlm.nih.gov/21368130/)
41. N. Fann *et al.*, in *The Impacts of Climate Change on Human Health in the United States: A Scientific Assessment*, A. Crimmins *et al.*, Eds. (U.S. Global Change Research Program, 2016), p. 69.
42. S. S. Myers *et al.*, Increasing CO₂ threatens human nutrition. *Nature* **510**, 139–142 (2014). doi: [10.1038/nature13179](https://doi.org/10.1038/nature13179); pmid: [24805231](https://pubmed.ncbi.nlm.nih.gov/24805231/)
43. S. S. Myers, K. R. Wessells, I. Kloog, A. Zanobetti, J. Schwartz, Effect of increased concentrations of atmospheric carbon dioxide on the global threat of zinc deficiency: A modelling study. *Lancet Glob. Health* **3**, e639–e645 (2015). doi: [10.1016/S2214-109X\(15\)00093-5](https://doi.org/10.1016/S2214-109X(15)00093-5); pmid: [26189102](https://pubmed.ncbi.nlm.nih.gov/26189102/)
44. D. E. Medek, J. Schwartz, S. S. Myers, Estimated effects of future atmospheric CO₂ concentrations on protein intake and the risk of protein deficiency by country and region. *Environ. Health Perspect.* **125**, 087002 (2017). doi: [10.1289/EHP41](https://doi.org/10.1289/EHP41); pmid: [28885977](https://pubmed.ncbi.nlm.nih.gov/28885977/)
45. M. Smith, C. Golden, S. Myers, Potential rise in iron deficiency due to future anthropogenic carbon dioxide emissions. *Geofuture* **1**, 248–257 (2017). doi: [10.1002/2016GH000018](https://doi.org/10.1002/2016GH000018)
46. M. R. Smith, S. S. Myers, Impact of anthropogenic CO₂ emissions on global human nutrition. *Nat. Clim. Change* **8**, 834–839 (2018). doi: [10.1038/s41558-018-0253-3](https://doi.org/10.1038/s41558-018-0253-3)
47. S. Clayton, C. Manning, K. Krygman, M. Speiser, *Mental Health and Our Changing Climate: Impacts, Implications, and Guidance* (American Psychological Association and ecoAmerica, 2017).
48. E. Goldmann, S. Galea, Mental health consequences of disasters. *Annu. Rev. Public Health* **35**, 169–183 (2014). doi: [10.1146/annurev-publhealth-032013-182435](https://doi.org/10.1146/annurev-publhealth-032013-182435); pmid: [24159920](https://pubmed.ncbi.nlm.nih.gov/24159920/)
49. L. Camalier, W. Cox, P. Dolwick, The effects of meteorology on ozone in urban areas and their use in assessing ozone trends. *Atmos. Environ.* **41**, 7127–7137 (2007). doi: [10.1016/j.atmosenv.2007.04.061](https://doi.org/10.1016/j.atmosenv.2007.04.061)
50. E. M. Oswald, L.-A. Dupigny-Giroux, E. M. Leibensperger, R. Poirot, J. Merrell, Climate controls on air quality in the Northeastern US: An examination of summertime ozone statistics during 1993–2012. *Atmos. Environ.* **112**, 278–288 (2015). doi: [10.1016/j.atmosenv.2015.04.019](https://doi.org/10.1016/j.atmosenv.2015.04.019)
51. A. P. Tai, L. J. Mickley, D. J. Jacob, Correlations between fine particulate matter (PM_{2.5}) and meteorological variables in the United States: Implications for the sensitivity of PM_{2.5} to climate change. *Atmos. Environ.* **44**, 3976–3984 (2010). doi: [10.1016/j.atmosenv.2010.06.060](https://doi.org/10.1016/j.atmosenv.2010.06.060)
52. C. D. Whiteman, S. W. Hoch, J. D. Horel, A. Charland, Relationship between particulate air pollution and meteorological variables in Utah’s Salt Lake Valley. *Atmos. Environ.* **94**, 742–753 (2014). doi: [10.1016/j.atmosenv.2014.06.012](https://doi.org/10.1016/j.atmosenv.2014.06.012)
53. D. E. Horton, C. B. Skinner, D. Singh, N. S. Duffenbaugh, Occurrence and persistence of future atmospheric stagnation events. *Nat. Clim. Change* **4**, 698–703 (2014). doi: [10.1038/nclimate2272](https://doi.org/10.1038/nclimate2272); pmid: [25309627](https://pubmed.ncbi.nlm.nih.gov/25309627/)
54. J. L. Schnell, M. J. Prather, Co-occurrence of extremes in surface ozone, particulate matter, and temperature over eastern North America. *Proc. Natl. Acad. Sci. U.S.A.* **114**, 2854–2859 (2017). doi: [10.1073/pnas.1614453114](https://doi.org/10.1073/pnas.1614453114); pmid: [28242682](https://pubmed.ncbi.nlm.nih.gov/28242682/)
55. M. Lin, L. W. Horowitz, R. Payton, A. M. Fiore, G. Tonnesen, US surface ozone trends and extremes from 1980 to 2014: Quantifying the roles of rising Asian emissions, domestic controls, wildfires, and climate. *Atmos. Chem. Phys.* **17**, 2943–2970 (2017). doi: [10.5194/acp-17-2943-2017](https://doi.org/10.5194/acp-17-2943-2017)
56. A. Wilson *et al.*, Climate change impacts on projections of excess mortality at 2030 using spatially varying ozone-temperature risk surfaces. *J. Expo. Sci. Environ. Epidemiol.* **27**, 118–124 (2017). doi: [10.1038/jes.2016.14](https://doi.org/10.1038/jes.2016.14); pmid: [27005744](https://pubmed.ncbi.nlm.nih.gov/27005744/)
57. G. A. Meehl *et al.*, Future heat waves and surface ozone. *Environ. Res. Lett.* **13**, 064004 (2018). doi: [10.1088/1748-9326/aab0cd](https://doi.org/10.1088/1748-9326/aab0cd)
58. L. Shen, L. J. Mickley, L. T. Murray, Influence of 2000–2050 climate change on particulate matter in the United States: Results from a new statistical model. *Atmos. Chem. Phys.* **17**, 4355–4367 (2017). doi: [10.5194/acp-17-4355-2017](https://doi.org/10.5194/acp-17-4355-2017)
59. H. E. Rieder, A. M. Fiore, L. W. Horowitz, V. Naik, Projecting policy-relevant metrics for high summertime ozone pollution events over the eastern United States due to climate and emission changes during the 21st century. *J. Geophys. Res. Atmos.* **120**, 784–800 (2015). doi: [10.1002/2014JD022303](https://doi.org/10.1002/2014JD022303)
60. M. Trail *et al.*, Sensitivity of air quality to potential future climate change and emissions in the United States and major cities. *Atmos. Environ.* **94**, 552–563 (2014). doi: [10.1016/j.atmosenv.2014.05.079](https://doi.org/10.1016/j.atmosenv.2014.05.079)
61. H. Pye *et al.*, Effect of changes in climate and emissions on future sulfate-nitrate-ammonium aerosol levels in the United States. *J. Geophys. Res. Atmos.* **114** (D1), D01205 (2009). doi: [10.1029/2008JD010701](https://doi.org/10.1029/2008JD010701)
62. M. C. Day, S. N. Pandis, Effects of a changing climate on summertime fine particulate matter levels in the eastern US. *J. Geophys. Res. Atmos.* **120**, 5706–5720 (2015).
63. B. I. Cook, T. R. Ault, J. E. Smerdon, Unprecedented 21st century drought risk in the American Southwest and Central Plains. *Sci. Adv.* **1**, e1400082 (2015). doi: [10.1126/sciadv.1400082](https://doi.org/10.1126/sciadv.1400082); pmid: [26601131](https://pubmed.ncbi.nlm.nih.gov/26601131/)
64. X. Yue, L. J. Mickley, J. A. Logan, J. O. Kaplan, Ensemble projections of wildfire activity and carbonaceous aerosol concentrations over the western United States in the mid-21st century. *Atmos. Environ.* **77**, 767–780 (2013). doi: [10.1016/j.atmosenv.2013.06.003](https://doi.org/10.1016/j.atmosenv.2013.06.003); pmid: [24015109](https://pubmed.ncbi.nlm.nih.gov/24015109/)
65. J. C. Liu *et al.*, Particulate air pollution from wildfires in the Western US under climate change. *Clim. Change* **138**, 655–666 (2016). doi: [10.1007/s10584-016-1762-6](https://doi.org/10.1007/s10584-016-1762-6); pmid: [28642628](https://pubmed.ncbi.nlm.nih.gov/28642628/)
66. B. Pu, P. Ginoux, Projection of American dustiness in the late 21st century due to climate change. *Sci. Rep.* **7**, 5553 (2017). doi: [10.1038/s41598-017-05431-9](https://doi.org/10.1038/s41598-017-05431-9); pmid: [28717135](https://pubmed.ncbi.nlm.nih.gov/28717135/)
67. P. Achakulwisut, L. J. Mickley, S. C. Anenberg, Drought-sensitivity of fine dust in the US Southwest: Implications for air quality and public health under future climate change. *Environ. Res. Lett.* **13**, 054025 (2018). doi: [10.1088/1748-9326/aabf20](https://doi.org/10.1088/1748-9326/aabf20)
68. Q. Di *et al.*, Association of short-term exposure to air pollution with mortality in older adults. *JAMA* **318**, 2446–2456 (2017). doi: [10.1001/jama.2017.17923](https://doi.org/10.1001/jama.2017.17923); pmid: [29279932](https://pubmed.ncbi.nlm.nih.gov/29279932/)
69. J. R. Porter *et al.*, in *Climate Change 2014: Impacts, Adaptation, and Vulnerability. Part A: Global and Sectoral Aspects. Contribution of Working Group II to the Fifth Assessment Report of the Intergovernmental Panel of Climate Change*, C. B. Field *et al.*, Eds. (Cambridge Univ. Press, 2014), chap. 7, pp. 485–583.
70. J. Hatfield *et al.*, in *Climate Change Impacts in the United States: The Third National Climate Assessment*, J. Melillo, T. T. C. Richmond, G. W. Yohe, Eds. (U.S. Global Change Research Program, 2014), pp. 150–174.
71. J. A. Santos, R. Costa, H. Fraga, Climate change impacts on thermal growing conditions of main fruit species in Portugal. *Clim. Change* **140**, 273–286 (2017). doi: [10.1007/s10584-016-1835-6](https://doi.org/10.1007/s10584-016-1835-6)
72. C. A. Deutsch *et al.*, Increase in crop losses to insect pests in a warming climate. *Science* **361**, 916–919 (2018). doi: [10.1126/science.aat3466](https://doi.org/10.1126/science.aat3466); pmid: [30166490](https://pubmed.ncbi.nlm.nih.gov/30166490/)
73. R. Tito, H. L. Vasconcelos, K. J. Feeley, Global climate change increases risk of crop yield losses and food insecurity in the tropical Andes. *Glob. Change Biol.* **24**, e592–e602 (2018). doi: [10.1111/gcb.13959](https://doi.org/10.1111/gcb.13959); pmid: [29055170](https://pubmed.ncbi.nlm.nih.gov/29055170/)
74. X.-Z. Liang *et al.*, Determining climate effects on US total agricultural productivity. *Proc. Natl. Acad. Sci. U.S.A.* **114**, E2285–E2292 (2017). doi: [10.1073/pnas.1615922114](https://doi.org/10.1073/pnas.1615922114); pmid: [28265075](https://pubmed.ncbi.nlm.nih.gov/28265075/)
75. D. B. Lobell *et al.*, Greater sensitivity to drought accompanies maize yield increase in the U.S. Midwest. *Science* **344**, 516–519 (2014). doi: [10.1126/science.1251423](https://doi.org/10.1126/science.1251423); pmid: [24786079](https://pubmed.ncbi.nlm.nih.gov/24786079/)
76. M. Burke, K. Emerick, Adaptation to climate change: Evidence from US agriculture. *Am. Econ. J. Econ. Policy* **8**, 106–140 (2016). doi: [10.1257/pol.20130025](https://doi.org/10.1257/pol.20130025)
77. A. Park Williams *et al.*, Temperature as a potent driver of regional forest drought stress and tree mortality. *Nat. Clim. Change* **3**, 292–297 (2013). doi: [10.1038/nclimate1693](https://doi.org/10.1038/nclimate1693)
78. C. I. Millar, N. L. Stephenson, Temperate forest health in an era of emerging megadisturbance. *Science* **349**, 823–826 (2015). doi: [10.1126/science.aaa9933](https://doi.org/10.1126/science.aaa9933); pmid: [26293954](https://pubmed.ncbi.nlm.nih.gov/26293954/)
79. J. S. Clark *et al.*, The impacts of increasing drought on forest dynamics, structure, and biodiversity in the United States. *Glob. Change Biol.* **22**, 2329–2352 (2016). doi: [10.1111/gcb.13160](https://doi.org/10.1111/gcb.13160); pmid: [26898361](https://pubmed.ncbi.nlm.nih.gov/26898361/)
80. R. Seidl *et al.*, Forest disturbances under climate change. *Nat. Clim. Change* **7**, 395–402 (2017). doi: [10.1038/nclimate3303](https://doi.org/10.1038/nclimate3303); pmid: [28861124](https://pubmed.ncbi.nlm.nih.gov/28861124/)
81. C. Nolan *et al.*, Past and future global transformation of terrestrial ecosystems under climate change. *Science* **361**,

- 920–923 (2018). doi: [10.1126/science.aan5360](https://doi.org/10.1126/science.aan5360); pmid: [30166491](https://pubmed.ncbi.nlm.nih.gov/30166491/)
82. T. P. Barnett *et al.*, Human-induced changes in the hydrology of the western United States. *Science* **319**, 1080–1083 (2008). doi: [10.1126/science.1152538](https://doi.org/10.1126/science.1152538); pmid: [18239088](https://pubmed.ncbi.nlm.nih.gov/18239088/)
 83. P. W. Mote, S. Li, D. P. Lettenmaier, M. Xiao, R. Engel. Dramatic declines in snowpack in the western US. *npj Clim. Atmos. Sci.* **1**, 2 (2018). doi: [10.1038/s41612-018-0012-1](https://doi.org/10.1038/s41612-018-0012-1)
 84. A. Berg, J. Sheffield, P. C. Milly. Divergent surface and total soil moisture projections under global warming. *Geophys. Res. Lett.* **44**, 236–244 (2017). doi: [10.1002/2016GL071921](https://doi.org/10.1002/2016GL071921)
 85. A. G. Pendergrass, R. Knutti, F. Lehner, C. Deser, B. M. Sanderson. Precipitation variability increases in a warmer climate. *Sci. Rep.* **7**, 17966 (2017). doi: [10.1038/s41598-017-17966-y](https://doi.org/10.1038/s41598-017-17966-y); pmid: [29269737](https://pubmed.ncbi.nlm.nih.gov/29269737/)
 86. O. Mazdiyasi, A. AghaKouchak. Substantial increase in concurrent droughts and heatwaves in the United States. *Proc. Natl. Acad. Sci. U.S.A.* **112**, 11484–11489 (2015). doi: [10.1073/pnas.1422945112](https://doi.org/10.1073/pnas.1422945112); pmid: [26324927](https://pubmed.ncbi.nlm.nih.gov/26324927/)
 87. W. Kolby Smith *et al.*, Large divergence of satellite and Earth system model estimates of global terrestrial CO₂ fertilization. *Nat. Clim. Change* **6**, 306–310 (2016). doi: [10.1038/nclimate2879](https://doi.org/10.1038/nclimate2879)
 88. W. B. Cohen *et al.*, Forest disturbance across the conterminous United States from 1985–2012: The emerging dominance of forest decline. *For. Ecol. Manage.* **360**, 242–252 (2016). doi: [10.1016/j.foreco.2015.10.042](https://doi.org/10.1016/j.foreco.2015.10.042)
 89. J. S. Littell, D. L. Peterson, K. L. Riley, Y. Liu, C. H. Luce. A review of the relationships between drought and forest fire in the United States. *Glob. Change Biol.* **22**, 2353–2369 (2016). doi: [10.1111/gcb.13275](https://doi.org/10.1111/gcb.13275); pmid: [27090489](https://pubmed.ncbi.nlm.nih.gov/27090489/)
 90. J. Eidsenink *et al.*, A project for monitoring trends in burn severity. *Fire Ecol.* **3**, 3–21 (2007). doi: [10.4996/fireecology.0301003](https://doi.org/10.4996/fireecology.0301003)
 91. L. Giglio, W. Schroeder, C. O. Justice. The collection 6 MODIS active fire detection algorithm and fire products. *Remote Sens. Environ.* **178**, 31–41 (2016). doi: [10.1016/j.rse.2016.02.054](https://doi.org/10.1016/j.rse.2016.02.054); pmid: [30158718](https://pubmed.ncbi.nlm.nih.gov/30158718/)
 92. J. T. Abatzoglou, A. P. Williams. Impact of anthropogenic climate change on wildfire across western US forests. *Proc. Natl. Acad. Sci. U.S.A.* **113**, 11770–11775 (2016). doi: [10.1073/pnas.1607171113](https://doi.org/10.1073/pnas.1607171113); pmid: [27791053](https://pubmed.ncbi.nlm.nih.gov/27791053/)
 93. A. L. Westerling. Increasing western US forest wildfire activity: Sensitivity to changes in the timing of spring. *Philos. Trans. R. Soc. London Ser. B* **371**, 20150178 (2016). doi: [10.1098/rstb.2015.0178](https://doi.org/10.1098/rstb.2015.0178); pmid: [27216510](https://pubmed.ncbi.nlm.nih.gov/27216510/)
 94. M. Wehner, J. Arnold, T. Knutson, K. Kunkel, A. LeGrande, in *Climate Science Special Report: Fourth National Climate Assessment*, D. J. Wuebbles *et al.*, Eds. (U.S. Global Change Research Program, 2017), pp. 231–256.
 95. M. A. Moritz *et al.*, Climate change and disruptions to global fire activity. *Ecosphere* **3**, 1–22 (2012). doi: [10.1890/ES11-00345.1](https://doi.org/10.1890/ES11-00345.1)
 96. T. Kitzberger, D. A. Falk, A. L. Westerling, T. W. Swetnam. Direct and indirect climate controls predict heterogeneous early-mid 21st century wildfire burned area across western and boreal North America. *PLoS ONE* **12**, e0188486 (2017). doi: [10.1371/journal.pone.0188486](https://doi.org/10.1371/journal.pone.0188486); pmid: [29244839](https://pubmed.ncbi.nlm.nih.gov/29244839/)
 97. P. J. van Mantgem *et al.*, Climatic stress increases forest fire severity across the western United States. *Ecol. Lett.* **16**, 1151–1156 (2013). doi: [10.1111/ele.12151](https://doi.org/10.1111/ele.12151); pmid: [23869626](https://pubmed.ncbi.nlm.nih.gov/23869626/)
 98. D. McKenzie, J. S. Littell. Climate change and the ecohydrology of fire: Will area burned increase in a warming western USA? *Ecol. Appl.* **27**, 26–36 (2017). doi: [10.1002/eap.1420](https://doi.org/10.1002/eap.1420); pmid: [28001335](https://pubmed.ncbi.nlm.nih.gov/28001335/)
 99. J. R. Marlon *et al.*, Long-term perspective on wildfires in the western USA. *Proc. Natl. Acad. Sci. U.S.A.* **109**, E535–E543 (2012). doi: [10.1073/pnas.1112839109](https://doi.org/10.1073/pnas.1112839109); pmid: [22334650](https://pubmed.ncbi.nlm.nih.gov/22334650/)
 100. M. D. Hurteau, J. B. Bradford, P. Z. Fulé, A. H. Taylor, K. L. Martin. Climate change, fire management, and ecological services in the southwestern US. *For. Ecol. Manage.* **327**, 280–289 (2014). doi: [10.1016/j.foreco.2013.08.007](https://doi.org/10.1016/j.foreco.2013.08.007)
 101. S. A. Parks *et al.*, Wildland fire deficit and surplus in the western United States, 1984–2012. *Ecosphere* **6**, 1–13 (2015). doi: [10.1890/ES15-00294.1](https://doi.org/10.1890/ES15-00294.1)
 102. P. E. Higuera, J. T. Abatzoglou, J. S. Littell, P. Morgan. The changing strength and nature of fire-climate relationships in the northern Rocky Mountains, U.S.A., 1902–2008. *PLoS ONE* **10**, e0127563 (2015). doi: [10.1371/journal.pone.0127563](https://doi.org/10.1371/journal.pone.0127563); pmid: [26114580](https://pubmed.ncbi.nlm.nih.gov/26114580/)
 103. W. Knorr, L. Jiang, A. Arneth, Climate, CO₂, and demographic impacts on global wildfire emissions. *Biogeosci. Discuss.* **12**, 15011–15050 (2015). doi: [10.5194/bgd-12-15011-2015](https://doi.org/10.5194/bgd-12-15011-2015)
 104. J. K. Balch *et al.*, Human-started wildfires expand the fire niche across the United States. *Proc. Natl. Acad. Sci. U.S.A.* **114**, 2946–2951 (2017). doi: [10.1073/pnas.1617394114](https://doi.org/10.1073/pnas.1617394114); pmid: [28242690](https://pubmed.ncbi.nlm.nih.gov/28242690/)
 105. K. F. Raffa *et al.*, Cross-scale drivers of natural disturbances prone to anthropogenic amplification: The dynamics of bark beetle eruptions. *A.I.B.S. Bull.* **58**, 501–517 (2008).
 106. W. R. Anderegg *et al.*, Tree mortality from drought, insects, and their interactions in a changing climate. *New Phytol.* **208**, 674–683 (2015). doi: [10.1111/nph.13477](https://doi.org/10.1111/nph.13477); pmid: [26058406](https://pubmed.ncbi.nlm.nih.gov/26058406/)
 107. J. A. Hicke, A. J. Meddens, C. A. Kolden. Recent tree mortality in the western United States from bark beetles and forest fires. *For. Sci.* **62**, 141–153 (2016). doi: [10.5849/forsci.15-086](https://doi.org/10.5849/forsci.15-086)
 108. A. S. Weed, M. P. Ayres, B. J. Bentz, in *Bark Beetles* (Elsevier, 2015), pp. 157–176.
 109. B. J. Bentz, C. Boone, K. F. Raffa. Tree response and mountain pine beetle attack preference, reproduction and emergence timing in mixed whitebark and lodgepole pine stands. *Agric. For. Entomol.* **17**, 421–432 (2015). doi: [10.1111/afe.12124](https://doi.org/10.1111/afe.12124)
 110. D. L. Six, E. Biber, E. Long. Management for mountain pine beetle outbreak suppression: Does relevant science support current policy? *Forests* **5**, 103–133 (2014). doi: [10.3390/f501103](https://doi.org/10.3390/f501103)
 111. N. G. McDowell *et al.*, The interdependence of mechanisms underlying climate-driven vegetation mortality. *Trends Ecol. Evol.* **26**, 523–532 (2011). doi: [10.1016/j.tree.2011.06.003](https://doi.org/10.1016/j.tree.2011.06.003); pmid: [21802765](https://pubmed.ncbi.nlm.nih.gov/21802765/)
 112. H. D. Adams *et al.*, A multi-species synthesis of physiological mechanisms in drought-induced tree mortality. *Ecol. Evol.* **1**, 1285–1291 (2017). doi: [10.1038/s41559-017-0248-x](https://doi.org/10.1038/s41559-017-0248-x); pmid: [29046541](https://pubmed.ncbi.nlm.nih.gov/29046541/)
 113. W. R. Anderegg *et al.*, Tree mortality predicted from drought-induced vascular damage. *Nat. Geosci.* **8**, 367–371 (2015). doi: [10.1038/ngeo2400](https://doi.org/10.1038/ngeo2400)
 114. A. T. Trugman *et al.*, Tree carbon allocation explains forest drought-kill and recovery patterns. *Ecol. Lett.* **21**, 1552–1560 (2018). doi: [10.1111/ele.13136](https://doi.org/10.1111/ele.13136); pmid: [30125446](https://pubmed.ncbi.nlm.nih.gov/30125446/)
 115. I. Ibáñez, D. R. Zak, A. J. Burton, K. S. Pregitzer. Anthropogenic nitrogen deposition ameliorates the decline in tree growth caused by a drier climate. *Ecology* **99**, 411–420 (2018). doi: [10.1002/ecy.2095](https://doi.org/10.1002/ecy.2095); pmid: [29341107](https://pubmed.ncbi.nlm.nih.gov/29341107/)
 116. N. Pederson *et al.*, The legacy of episodic climatic events in shaping temperate, broadleaf forests. *Ecol. Monogr.* **84**, 599–620 (2014). doi: [10.1890/13-1025.1](https://doi.org/10.1890/13-1025.1)
 117. N. D. Charney *et al.*, Observed forest sensitivity to climate implies large changes in 21st century North American forest growth. *Ecol. Lett.* **19**, 1119–1128 (2016). doi: [10.1111/ele.12650](https://doi.org/10.1111/ele.12650); pmid: [27434040](https://pubmed.ncbi.nlm.nih.gov/27434040/)
 118. J. Kim *et al.*, Increased water yield due to the hemlock woolly adelgid infestation in New England. *Geophys. Res. Lett.* **44**, 2327–2335 (2017). doi: [10.1002/2016GL072327](https://doi.org/10.1002/2016GL072327)
 119. A. P. Williams *et al.*, The 2016 southeastern US drought: An extreme departure from centennial wetting and cooling. *J. Geophys. Res. Atmos.* **122**, 10888–10905 (2017). doi: [10.1029/2017JD027077](https://doi.org/10.1029/2017JD027077); pmid: [29780677](https://pubmed.ncbi.nlm.nih.gov/29780677/)
 120. N. S. Diffenbaugh, C. B. Field. Changes in ecologically critical terrestrial climate conditions. *Science* **341**, 486–492 (2013). doi: [10.1126/science.1237123](https://doi.org/10.1126/science.1237123); pmid: [23908225](https://pubmed.ncbi.nlm.nih.gov/23908225/)
 121. S. R. Loarie *et al.*, The velocity of climate change. *Nature* **462**, 1052–1055 (2009). doi: [10.1038/nature08649](https://doi.org/10.1038/nature08649); pmid: [20033047](https://pubmed.ncbi.nlm.nih.gov/20033047/)
 122. P. W. Mote, A. F. Hamlet, M. P. Clark, D. P. Lettenmaier. Declining mountain snowpack in western North America. *Bull. Am. Meteorol. Soc.* **86**, 39–50 (2005). doi: [10.1175/BAMS-86-1-39](https://doi.org/10.1175/BAMS-86-1-39)
 123. J. T. Abatzoglou. Influence of the PNA on declining mountain snowpack in the Western United States. *Int. J. Climatol.* **31**, 1135–1142 (2011). doi: [10.1002/joc.2137](https://doi.org/10.1002/joc.2137)
 124. S. Kapnick, A. Hall. Causes of recent changes in western North American snowpack. *Clim. Dyn.* **38**, 1885–1899 (2012). doi: [10.1007/s00382-011-1089-y](https://doi.org/10.1007/s00382-011-1089-y)
 125. C. H. Luce, Z. A. Holden. Declining annual streamflow distributions in the Pacific Northwest United States, 1948–2006. *Geophys. Res. Lett.* **36**, L16401 (2009). doi: [10.1029/2009GL039407](https://doi.org/10.1029/2009GL039407)
 126. H. Fritze, I. T. Stewart, E. Pebesma. Shifts in western North American snowmelt runoff regimes for the recent warm decades. *J. Hydrometeorol.* **12**, 989–1006 (2011). doi: [10.1175/2011JHM1360.1](https://doi.org/10.1175/2011JHM1360.1)
 127. R. D. Brown, P. W. Mote. The response of Northern Hemisphere snow cover to a changing climate. *J. Clim.* **22**, 2124–2145 (2009). doi: [10.1175/2008JCL12665.1](https://doi.org/10.1175/2008JCL12665.1)
 128. S. B. Kapnick, T. L. Delworth. Controls of global snow under a changed climate. *J. Clim.* **26**, 5537–5562 (2013). doi: [10.1175/JCLI-D-12-00528.1](https://doi.org/10.1175/JCLI-D-12-00528.1)
 129. J. P. Krasting, A. J. Broccoli, K. W. Dixon, J. R. Lanzante. Future changes in Northern Hemisphere snowfall. *J. Clim.* **26**, 7813–7828 (2013). doi: [10.1175/JCLI-D-12-00832.1](https://doi.org/10.1175/JCLI-D-12-00832.1)
 130. M. Ashfaq *et al.*, Near-term acceleration of hydroclimatic change in the western US. *J. Geophys. Res. Atmos.* **118**, 10676–10693 (2013). doi: [10.1002/jgrd.50816](https://doi.org/10.1002/jgrd.50816)
 131. J. C. Fyfe *et al.*, Large near-term projected snowpack loss over the western United States. *Nat. Commun.* **8**, 14996 (2017). doi: [10.1038/ncomms14996](https://doi.org/10.1038/ncomms14996); pmid: [28418406](https://pubmed.ncbi.nlm.nih.gov/28418406/)
 132. A. M. Rhoades, P. A. Ullrich, C. M. Zarzycki. Projecting 21st century snowpack trends in western USA mountains using variable-resolution CESM. *Clim. Dyn.* **50**, 261–288 (2018). doi: [10.1007/s00382-017-3606-0](https://doi.org/10.1007/s00382-017-3606-0)
 133. N. S. Diffenbaugh, M. Scherer, M. Ashfaq. Response of snow-dependent hydrologic extremes to continued global warming. *Nat. Clim. Change* **3**, 379–384 (2013). doi: [10.1038/nclimate1732](https://doi.org/10.1038/nclimate1732); pmid: [24015153](https://pubmed.ncbi.nlm.nih.gov/24015153/)
 134. D. Li, M. L. Wrzesien, M. Durand, J. Adam, D. P. Lettenmaier. How much runoff originates as snow in the western United States, and how will that change in the future? *Geophys. Res. Lett.* **44**, 6163–6172 (2017). doi: [10.1002/2017GL073551](https://doi.org/10.1002/2017GL073551)
 135. E. M. Demaria, J. K. Roundy, S. Wi, R. N. Palmer. The effects of climate change on seasonal snowpack and the hydrology of the northeastern and upper Midwest United States. *J. Clim.* **29**, 6527–6541 (2016). doi: [10.1175/JCLI-D-15-0632.1](https://doi.org/10.1175/JCLI-D-15-0632.1)
 136. A. Harpold, M. Dettinger, S. Rajagopal. Defining snow drought and why it matters. *EOS* **98**, 10.1029/2017EO068775 (2017). doi: [10.1029/2017EO068775](https://doi.org/10.1029/2017EO068775)
 137. D. Isaak, S. Wollrab, D. Horan, G. Chandler. Climate change effects on stream and river temperatures across the northwest US from 1980–2009 and implications for salmonid fishes. *Clim. Change* **113**, 499–524 (2012). doi: [10.1007/s10584-011-0326-z](https://doi.org/10.1007/s10584-011-0326-z)
 138. K. S. McKelvey *et al.*, Climate change predicted to shift wolverine distributions, connectivity, and dispersal corridors. *Ecol. Appl.* **21**, 2882–2897 (2011). doi: [10.1890/10-2206.1](https://doi.org/10.1890/10-2206.1)
 139. B. Udall, J. Overpeck. The twenty-first century Colorado River hot drought and implications for the future. *Water Resour. Res.* **53**, 2404–2418 (2017). doi: [10.1002/2016WR019638](https://doi.org/10.1002/2016WR019638)
 140. M. Xiao, B. Udall, D. P. Lettenmaier. On the causes of declining Colorado River streamflows. *Water Resour. Res.* **54**, 6739–6756 (2018). doi: [10.1029/2018WR023153](https://doi.org/10.1029/2018WR023153)
 141. F. Lehner, E. R. Wahl, A. W. Wood, D. B. Blatchford, D. Llewellyn. Assessing recent declines in Upper Rio Grande runoff efficiency from a paleoclimate perspective. *Geophys. Res. Lett.* **44**, 4124–4133 (2017). doi: [10.1002/2017GL073253](https://doi.org/10.1002/2017GL073253)
 142. S. B. Chavarria, D. S. Gutzler. Observed changes in climate and streamflow in the upper Rio Grande Basin. *J. Am. Water Resour. Assoc.* **54**, 644–659 (2018). doi: [10.1111/1752-1688.12640](https://doi.org/10.1111/1752-1688.12640)
 143. R. I. McDonald *et al.*, Urban growth, climate change, and freshwater availability. *Proc. Natl. Acad. Sci. U.S.A.* **108**, 6312–6317 (2011). doi: [10.1073/pnas.1011615108](https://doi.org/10.1073/pnas.1011615108); pmid: [21444797](https://pubmed.ncbi.nlm.nih.gov/21444797/)
 144. J. Schewe *et al.*, Multimodel assessment of water scarcity under climate change. *Proc. Natl. Acad. Sci. U.S.A.* **111**, 3245–3250 (2014). doi: [10.1073/pnas.1222460110](https://doi.org/10.1073/pnas.1222460110); pmid: [24344289](https://pubmed.ncbi.nlm.nih.gov/24344289/)
 145. J. S. Mankin *et al.*, Influence of internal variability on population exposure to hydroclimatic changes. *Environ. Res. Lett.* **12**, 044007 (2017). doi: [10.1088/1748-9326/aa5efc](https://doi.org/10.1088/1748-9326/aa5efc)
 146. E. Sinha, A. M. Michalak, V. Balaji. Eutrophication will increase during the 21st century as a result of precipitation changes. *Science* **357**, 405–408 (2017). doi: [10.1126/science.aan2409](https://doi.org/10.1126/science.aan2409); pmid: [28751610](https://pubmed.ncbi.nlm.nih.gov/28751610/)
 147. S. C. Moser *et al.*, in *Climate Change Impacts in the United States: The Third National Climate Assessment*, J. M. Melillo, T. T. C. Richmond, G. W. Yohe, Eds. (U.S. Global Change Research Program, 2014), pp. 579–618.
 148. W. V. Sweet, R. E. Kopp, C. P. Weaver, J. Obeyesekere, R. M. Horton, E. R. Thieler, C. Zervas. “Global and regional sea level rise scenarios for the United States” (NOAA Tech. Rep. NOS CO-OPS 083, National Oceanic and Atmospheric Administration, National Ocean Service, Center for Operational Oceanographic Products and Services, 2017).
 149. K. Lambeck, H. Rouby, A. Purcell, Y. Sun, M. Sambridge. Sea level and global ice volumes from the Last Glacial Maximum to the Holocene. *Proc. Natl. Acad. Sci. U.S.A.* **111**, 15296–15303 (2014). doi: [10.1073/pnas.1411762111](https://doi.org/10.1073/pnas.1411762111); pmid: [25313072](https://pubmed.ncbi.nlm.nih.gov/25313072/)

150. J. D. Boon, M. Mitchell, Nonlinear change in sea level observed at North American tide stations. *J. Coast. Res.* **31**, 1295–1305 (2015). doi: [10.2112/JCOASTRES-D-15-00041.1](https://doi.org/10.2112/JCOASTRES-D-15-00041.1)
151. T. Ezer, L. P. Atkinson, Accelerated flooding along the US East Coast: On the impact of sea-level rise, tides, storms, the Gulf Stream, and the North Atlantic oscillations. *Earths Futur.* **2**, 362–382 (2014). doi: [10.1002/2014EF000252](https://doi.org/10.1002/2014EF000252)
152. W. V. Sweet, J. Park, From the extreme to the mean: Acceleration and tipping points of coastal inundation from sea level rise. *Earths Futur.* **2**, 579–600 (2014). doi: [10.1002/2014EF000272](https://doi.org/10.1002/2014EF000272)
153. E. E. Lentz et al., Evaluation of dynamic coastal response to sea-level rise modifies inundation likelihood. *Nat. Clim. Change* **6**, 696–700 (2016). doi: [10.1038/nclimate2957](https://doi.org/10.1038/nclimate2957)
154. A. D. Ashton, J. Lorenzo-Trueba, in *Barrier Dynamics and Response to Changing Climate*, L. J. Moore, A. B. Murray, Eds. (Springer International Publishing, Cham, 2018), pp. 277–304.
155. R. E. Kopp, R. L. Shwom, G. Wagner, J. Yuan, Tipping elements and climate-economic shocks: Pathways toward integrated assessment. *Earths Futur.* **4**, 346–372 (2016). doi: [10.1002/2016EF000362](https://doi.org/10.1002/2016EF000362)
156. W. V. Sweet, G. P. Dusek, J. Obeyseker, J. J. Marra, *Patterns and Projections of High Tide Flooding along the US Coastline Using a Common Impact Threshold* (U.S. Department of Commerce, National Oceanic and Atmospheric Administration, National Ocean Service, Center for Operational Oceanographic Products and Services, 2018), p. 56.
157. M. E. Hauer, J. M. Evans, D. R. Mishra, Millions projected to be at risk from sea-level rise in the continental United States. *Nat. Clim. Change* **6**, 691–695 (2016). doi: [10.1038/nclimate2961](https://doi.org/10.1038/nclimate2961)
158. K. Thorne et al., U.S. Pacific coastal wetland resilience and vulnerability to sea-level rise. *Sci. Adv.* **4**, e3270 (2018). doi: [10.1126/sciadv.aao3270](https://doi.org/10.1126/sciadv.aao3270); PMID: 29507876
159. J. M. Keenan, T. Hill, A. Gumber, Climate gentrification: From theory to empiricism in Miami-Dade County, Florida. *Environ. Res. Lett.* **13**, 054001 (2018). doi: [10.1088/1748-9326/aabb32](https://doi.org/10.1088/1748-9326/aabb32)
160. K. F. Nordstrom, N. L. Jackson, Constraints on restoring landforms and habitats on storm-damaged shorefront lots in New Jersey, USA. *Ocean Coast. Manage.* **155**, 15–23 (2018). doi: [10.1016/j.ocecoaman.2018.01.025](https://doi.org/10.1016/j.ocecoaman.2018.01.025)
161. S. Hallegatte, C. Green, R. J. Nicholls, J. Corfee-Morlot, Future flood losses in major coastal cities. *Nat. Clim. Change* **3**, 802–806 (2013). doi: [10.1038/nclimate1979](https://doi.org/10.1038/nclimate1979)
162. P. Chhetri, J. Corcoran, V. Gekara, C. Maddox, D. McEvoy, Seaport resilience to climate change: Mapping vulnerability to sea-level rise. *J. Spat. Sci.* **60**, 65–78 (2015). doi: [10.1080/14498596.2014.943311](https://doi.org/10.1080/14498596.2014.943311)
163. T. Wilbanks, D. Bilello, D. Schmalzer, M. Scott, “Climate change and energy supply and use: Technical report to the U.S. Department of Energy in support of the national climate assessment” (Oak Ridge National Laboratory, U.S. Department of Energy, Office of Science, 2012).
164. J. Dell et al., in *Climate Change Impacts in the United States: The Third National Climate Assessment*, J. Melillo, T. T. C. Richmond, G. W. Yohe, Eds. (U.S. Global Change Research Program, 2014), pp. 113–129.
165. J. Macknick, S. Sattler, K. Averyt, S. Clemmer, J. Rogers, The water implications of generating electricity: Water use across the United States based on different electricity pathways through 2050. *Environ. Res. Lett.* **7**, 045803 (2012). doi: [10.1088/1748-9326/7/4/045803](https://doi.org/10.1088/1748-9326/7/4/045803)
166. O.-D. Cardona et al., in *Managing the Risks of Extreme Events and Disasters to Advance Climate Change Adaptation: Determinants of Risk: Exposure and Vulnerability. A Special Report of Working Groups I and II of the Intergovernmental Panel on Climate Change*, C. B. Field et al., Eds. (Cambridge Univ. Press, 2012), pp. 65–108.
167. M. Auffhammer, P. Baylis, C. H. Hausman, Climate change is projected to have severe impacts on the frequency and intensity of peak electricity demand across the United States. *Proc. Natl. Acad. Sci. U.S.A.* **114**, 1886–1891 (2017). doi: [10.1073/pnas.1613193114](https://doi.org/10.1073/pnas.1613193114); PMID: 28167756
168. T. Wilbanks et al., “Climate change and infrastructure, urban systems, and vulnerabilities: Technical report to the U.S. Department of Energy in support of the national climate assessment” (Oak Ridge National Laboratory, U.S. Department of Energy, Office of Science, 2012).
169. J. M. Melillo, T. T. C. Richmond, G. W. Yohe, Eds., *Climate Change Impacts in the United States: The Third National Climate Assessment* (U.S. Global Change Research Program, 2014), p. 17.
170. T. M. B. Bennett et al., in *Climate Change Impacts in the United States: The Third National Climate Assessment*, J. Melillo, T. T. C. Richmond, G. W. Yohe, Eds. (U.S. Global Change Research Program, 2014), pp. 297–317.
171. J. K. Maldonado, C. Shearer, R. Bronen, K. Peterson, H. Lazrus, The impact of climate change on tribal communities in the US: Displacement, relocation, and human rights. *Clim. Change* **120**, 601–614 (2013). doi: [10.1007/s10584-013-0746-z](https://doi.org/10.1007/s10584-013-0746-z)
172. P. Lal, J. R. Alvalapati, E. D. Mercer, Socio-economic impacts of climate change on rural United States. *Mitig. Adapt. Strategies Glob. Change* **16**, 819–844 (2011). doi: [10.1007/s11027-011-9295-9](https://doi.org/10.1007/s11027-011-9295-9)
173. J. Huang et al., Recently amplified arctic warming has contributed to a continual global warming trend. *Nat. Clim. Change* **7**, 875–879 (2017). doi: [10.1038/s41558-017-0009-5](https://doi.org/10.1038/s41558-017-0009-5)
174. T. J. Brinkman et al., Arctic communities perceive climate impacts on access as a critical challenge to availability of subsistence resources. *Clim. Change* **139**, 413–427 (2016). doi: [10.1007/s10584-016-1819-6](https://doi.org/10.1007/s10584-016-1819-6)
175. E. Hong, R. Perkins, S. Trainor, Thaw settlement hazard of permafrost related to climate warming in Alaska. *Arctic* **67**, 93–103 (2014). doi: [10.14430/arctic4368](https://doi.org/10.14430/arctic4368)
176. A. E. Gibbs, B. M. Richmond, “National assessment of shoreline change: Historical change along the north coast of Alaska, US-Canadian border to Icy Cape” (U.S. Geological Survey, 2015).
177. U.S. Government Accountability Office, “Alaska native villages: Limited progress has been made on relocating villages threatened by flooding and erosion” (U.S. Government Accountability Office, 2009).
178. R. Bronen, F. S. Chapin 3rd, Adaptive governance and institutional strategies for climate-induced community relocations in Alaska. *Proc. Natl. Acad. Sci. U.S.A.* **110**, 9320–9325 (2013). doi: [10.1073/pnas.1210508110](https://doi.org/10.1073/pnas.1210508110); PMID: 23690592
179. A. M. Melvin et al., Climate change damages to Alaska public infrastructure and the economics of proactive adaptation. *Proc. Natl. Acad. Sci. U.S.A.* **114**, E122–E131 (2017). doi: [10.1073/pnas.1611056113](https://doi.org/10.1073/pnas.1611056113); PMID: 28028223
180. C. Parmesan, G. Yohe, A globally coherent fingerprint of climate change impacts across natural systems. *Nature* **421**, 37–42 (2003). doi: [10.1038/nature01286](https://doi.org/10.1038/nature01286); PMID: 12511946
181. B. R. Scheffers et al., The broad footprint of climate change from genes to biomes to people. *Science* **354**, aaf7671 (2016). doi: [10.1126/science.aaf7671](https://doi.org/10.1126/science.aaf7671); PMID: 27846577
182. J. Lenoir, J. C. Svenning, Climate-related range shifts—a global multidimensional synthesis and new research directions. *Ecography* **38**, 15–28 (2015). doi: [10.1111/ecog.00967](https://doi.org/10.1111/ecog.00967)
183. I.-C. Chen, J. K. Hill, R. Ohlemüller, D. B. Roy, C. D. Thomas, Rapid range shifts of species associated with high levels of climate warming. *Science* **333**, 1024–1026 (2011). doi: [10.1126/science.1206432](https://doi.org/10.1126/science.1206432); PMID: 21852500
184. M. W. Tingley, M. S. Koo, C. Moritz, A. C. Rush, S. R. Beissinger, The push and pull of climate change causes heterogeneous shifts in avian elevational ranges. *Glob. Change Biol.* **18**, 3279–3290 (2012). doi: [10.1111/j.1365-2486.2012.02784.x](https://doi.org/10.1111/j.1365-2486.2012.02784.x)
185. J. B. Socolar, P. N. Epanchin, S. R. Beissinger, M. W. Tingley, Phenological shifts conserve thermal niches in North American birds and reshape expectations for climate-driven range shifts. *Proc. Natl. Acad. Sci. U.S.A.* **114**, 12976–12981 (2017). doi: [10.1073/pnas.1705897114](https://doi.org/10.1073/pnas.1705897114); PMID: 29133415
186. J. M. Sunday, A. E. Bates, N. K. Dulvy, Thermal tolerance and the global redistribution of animals. *Nat. Clim. Change* **2**, 686–690 (2012). doi: [10.1038/nclimate1539](https://doi.org/10.1038/nclimate1539)
187. C. J. Brown et al., Ecological and methodological drivers of species’ distribution and phenology responses to climate change. *Glob. Change Biol.* **22**, 1548–1560 (2016). doi: [10.1111/gcb.13184](https://doi.org/10.1111/gcb.13184); PMID: 26661135
188. M. T. Burrows et al., The pace of shifting climate in marine and terrestrial ecosystems. *Science* **334**, 652–655 (2011). doi: [10.1126/science.1210288](https://doi.org/10.1126/science.1210288); PMID: 22053045
189. E. S. Poloczanska et al., Global imprint of climate change on marine life. *Nat. Clim. Change* **3**, 919–925 (2013). doi: [10.1038/nclimate1958](https://doi.org/10.1038/nclimate1958)
190. C. Parmesan, M. J. Attrill, in *Explaining Ocean Warming: Causes, Scale, Effects and Consequences*, D. Laffoley, J. M. Baxter, Eds. (IUCN Full Report, IUCN, 2016), pp. 439–450.
191. B. I. Cook, E. M. Wolkovich, C. Parmesan, Divergent responses to spring and winter warming drive community level flowering trends. *Proc. Natl. Acad. Sci. U.S.A.* **109**, 9000–9005 (2012). doi: [10.1073/pnas.1118364109](https://doi.org/10.1073/pnas.1118364109); PMID: 22615406
192. L. F. Pitelka et al., Plant migration and climate-change: A more realistic portrait of plant migration is essential to predicting biological responses to global warming in a world drastically altered by human activity. *Am. Sci.* **85**, 464–473 (1997).
193. V. Devictor et al., Differences in the climatic debts of birds and butterflies at a continental scale. *Nat. Clim. Change* **2**, 121–124 (2012). doi: [10.1038/nclimate1347](https://doi.org/10.1038/nclimate1347)
194. R. A. Bay et al., Genomic signals of selection predict climate-driven population declines in a migratory bird. *Science* **359**, 83–86 (2018). doi: [10.1126/science.aan4380](https://doi.org/10.1126/science.aan4380); PMID: 29302012
195. C. G. Willis et al., Favorable climate change response explains non-native species’ success in Thoreau’s woods. *PLOS ONE* **5**, e8878 (2010). doi: [10.1371/journal.pone.0008878](https://doi.org/10.1371/journal.pone.0008878); PMID: 20126652
196. M. C. Singer, C. Parmesan, Phenological asynchrony between herbivorous insects and their hosts: Signal of climate change or pre-existing adaptive strategy? *Philos. Trans. R. Soc. London Ser. B* **365**, 3161–3176 (2010). doi: [10.1098/rstb.2010.0144](https://doi.org/10.1098/rstb.2010.0144); PMID: 20819810
197. M. C. Singer, Shifts in time and space interact as climate warms. *Proc. Natl. Acad. Sci. U.S.A.* **114**, 12848–12850 (2017). doi: [10.1073/pnas.1718334114](https://doi.org/10.1073/pnas.1718334114); PMID: 29162689
198. J. Settele et al., in *Climate Change 2014: Impacts, Adaptation, and Vulnerability. Part A: Global and Sectoral Aspects. Contribution of Working Group I to the Fifth Assessment Report of the Intergovernmental Panel of Climate Change*, C. B. Field et al., Eds. (Cambridge Univ. Press, 2014), chap. 4, pp. 271–359.
199. H. O. Pörtner et al., in *Climate Change 2014: Impacts, Adaptation, and Vulnerability. Part A: Global and Sectoral Aspects. Contribution of Working Group II to the Fifth Assessment Report of the Intergovernmental Panel of Climate Change*, C. B. Field et al., Eds. (Cambridge Univ. Press, 2014), chap. 6, pp. 411–484.
200. R. Dirzo et al., Defaunation in the Anthropocene. *Science* **345**, 401–406 (2014). doi: [10.1126/science.1251817](https://doi.org/10.1126/science.1251817); PMID: 25061202
201. J. L. Blois, P. L. Zarnetske, M. C. Fitzpatrick, S. Finnegan, Climate change and the past, present, and future of biotic interactions. *Science* **341**, 499–504 (2013). doi: [10.1126/science.1237184](https://doi.org/10.1126/science.1237184); PMID: 23908227
202. M. C. Urban, Climate change. Accelerating extinction risk from climate change. *Science* **348**, 571–573 (2015). doi: [10.1126/science.aaa4984](https://doi.org/10.1126/science.aaa4984); PMID: 25931559
203. J. N. Larsen et al., in *Climate Change 2014: Impacts, Adaptation, and Vulnerability. Part B: Regional Aspects. Contribution of Working Group II to the Fifth Assessment Report of the Intergovernmental Panel of Climate Change*, V. R. Barros et al., Eds. (Cambridge Univ. Press, 2014), chap. 28, pp. 1567–1612.
204. T. P. Hughes et al., Global warming transforms coral reef assemblages. *Nature* **556**, 492–496 (2018). doi: [10.1038/s41586-018-0041-2](https://doi.org/10.1038/s41586-018-0041-2); PMID: 29670282
205. C. D. Allen et al., A global overview of drought and heat-induced tree mortality reveals emerging climate change risks for forests. *For. Ecol. Manage.* **259**, 660–684 (2010). doi: [10.1016/j.foreco.2009.09.001](https://doi.org/10.1016/j.foreco.2009.09.001)
206. P. Gonzalez, F. Wang, M. Notaro, D. J. Vimont, J. W. Williams, Disproportionate magnitude of climate change in United States national parks. *Environ. Res. Lett.* **13**, 104001 (2018). doi: [10.1088/1748-9326/aade09](https://doi.org/10.1088/1748-9326/aade09)
207. O. Hoegh-Guldberg, E. S. Poloczanska, W. Skirving, S. Dove, Coral reef ecosystems under climate change and ocean acidification. *Front. Mar. Sci.* **4**, 158 (2017). doi: [10.3389/fmars.2017.00158](https://doi.org/10.3389/fmars.2017.00158)
208. H. Tian et al., The terrestrial biosphere as a net source of greenhouse gases to the atmosphere. *Nature* **531**, 225–228 (2016). doi: [10.1038/nature16946](https://doi.org/10.1038/nature16946); PMID: 26961656
209. S. C. Doney, V. J. Fabry, R. A. Feely, J. A. Kleypas, Ocean acidification: The other CO₂ problem. *Annu. Rev. Mar. Sci.* **1**, 169–192 (2009). doi: [10.1146/annurev.marine.010908.163834](https://doi.org/10.1146/annurev.marine.010908.163834); PMID: 21141034
210. A. L. Strong, K. J. Kroeker, L. T. Teneva, L. A. Mease, R. P. Kelly, Ocean acidification 2.0: Managing our changing coastal ocean chemistry. *Bioscience* **64**, 581–592 (2014). doi: [10.1093/biosci/biu072](https://doi.org/10.1093/biosci/biu072)
211. L. Bopp et al., Multiple stressors of ocean ecosystems in the 21st century: Projections with CMIP5 models. *Biogeosciences* **10**, 6225–6245 (2013). doi: [10.5194/bg-10-6225-2013](https://doi.org/10.5194/bg-10-6225-2013)
212. C. Hauri et al., Ocean acidification in the California current system. *Oceanography* **22**, 60–71 (2009). doi: [10.5670/oceanog.2009.97](https://doi.org/10.5670/oceanog.2009.97)

213. J. T. Mathis, J. N. Cross, W. Evans, S. C. Doney, Ocean acidification in the surface waters of the Pacific-Arctic boundary regions. *Oceanography* **28**, 122–135 (2015). doi: [10.5670/oceanog.2015.36](https://doi.org/10.5670/oceanog.2015.36)
214. D. L. Breitburg *et al.*, And on top of all that... Coping with ocean acidification in the midst of many stressors. *Oceanography* **28**, 48–61 (2015). doi: [10.5670/oceanog.2015.31](https://doi.org/10.5670/oceanog.2015.31)
215. D. Breitburg *et al.*, Declining oxygen in the global ocean and coastal waters. *Science* **359**, eaam7240 (2018). doi: [10.1126/science.aam7240](https://doi.org/10.1126/science.aam7240); pmid: [29301986](https://pubmed.ncbi.nlm.nih.gov/29301986/)
216. B. D. Eyre *et al.*, Coral reefs will transition to net dissolving before end of century. *Science* **359**, 908–911 (2018). doi: [10.1126/science.aao1118](https://doi.org/10.1126/science.aao1118); pmid: [29472482](https://pubmed.ncbi.nlm.nih.gov/29472482/)
217. T. P. Hughes *et al.*, Spatial and temporal patterns of mass bleaching of corals in the Anthropocene. *Science* **359**, 80–83 (2018). doi: [10.1126/science.aan8048](https://doi.org/10.1126/science.aan8048); pmid: [29302011](https://pubmed.ncbi.nlm.nih.gov/29302011/)
218. K. J. Kroeker *et al.*, Impacts of ocean acidification on marine organisms: Quantifying sensitivities and interaction with warming. *Glob. Change Biol.* **19**, 1884–1896 (2013). doi: [10.1111/gcb.12179](https://doi.org/10.1111/gcb.12179); pmid: [23505245](https://pubmed.ncbi.nlm.nih.gov/23505245/)
219. N. Bednaršek *et al.*, Limacina helicina shell dissolution as an indicator of declining habitat suitability owing to ocean acidification in the California Current Ecosystem. *Proc. R. Soc. London Ser. B* **281**, 20140123 (2014). doi: [10.1098/rspb.2014.0123](https://doi.org/10.1098/rspb.2014.0123); pmid: [24789895](https://pubmed.ncbi.nlm.nih.gov/24789895/)
220. D. K. Gledhill *et al.*, Ocean and coastal acidification off New England and Nova Scotia. *Oceanography* **28**, 182–197 (2015). doi: [10.5670/oceanog.2015.41](https://doi.org/10.5670/oceanog.2015.41)
221. J. A. Hare *et al.*, A vulnerability assessment of fish and invertebrates to climate change on the northeast U.S. continental shelf. *PLOS ONE* **11**, e0146756 (2016). doi: [10.1371/journal.pone.0146756](https://doi.org/10.1371/journal.pone.0146756); pmid: [26839967](https://pubmed.ncbi.nlm.nih.gov/26839967/)
222. A. Barton *et al.*, Impacts of coastal acidification on the Pacific Northwest shellfish industry and adaptation strategies implemented in response. *Oceanography* **28**, 146–159 (2015). doi: [10.5670/oceanog.2015.38](https://doi.org/10.5670/oceanog.2015.38)
223. J. A. Ekstrom *et al.*, Vulnerability and adaptation of US shellfisheries to ocean acidification. *Nat. Clim. Change* **5**, 207–214 (2015). doi: [10.1038/nclimate2508](https://doi.org/10.1038/nclimate2508)
224. C. Cattaneo, J. Claudet, P. Domenici, M. Milazzo, Living in a high CO₂ world: A global meta-analysis shows multiple trait-mediated fish responses to ocean acidification. *Ecol. Monogr.* **88**, 320–335 (2018). doi: [10.1002/ecm.1297](https://doi.org/10.1002/ecm.1297)
225. T. A. Carleton, S. M. Hsiang, Social and economic impacts of climate. *Science* **353**, aad9837 (2016). doi: [10.1126/science.aad9837](https://doi.org/10.1126/science.aad9837); pmid: [27609899](https://pubmed.ncbi.nlm.nih.gov/27609899/)
226. T. Carleton, S. Hsiang, M. Burke, Conflict in a changing climate. *Eur. Phys. J. Spec. Top.* **225**, 489–511 (2016). doi: [10.1140/epjst/e2015-50100-5](https://doi.org/10.1140/epjst/e2015-50100-5)
227. J. O'Loughlin *et al.*, Climate variability and conflict risk in East Africa, 1990–2009. *Proc. Natl. Acad. Sci. U.S.A.* **109**, 18344–18349 (2012). doi: [10.1073/pnas.1205130109](https://doi.org/10.1073/pnas.1205130109); pmid: [23090992](https://pubmed.ncbi.nlm.nih.gov/23090992/)
228. S. M. Hsiang, K. C. Meng, M. A. Cane, Civil conflicts are associated with the global climate. *Nature* **476**, 438–441 (2011). doi: [10.1038/nature10311](https://doi.org/10.1038/nature10311); pmid: [21866157](https://pubmed.ncbi.nlm.nih.gov/21866157/)
229. E. McGuirk, M. Burke, “The economic impacts of conflict in Africa” (National Bureau of Economic Research, 2017).
230. D. Card, G. B. Dahl, Family violence and football: The effect of unexpected emotional cues on violent behavior. *Q. J. Econ.* **126**, 103–143 (2011). doi: [10.1093/qje/qjr001](https://doi.org/10.1093/qje/qjr001); pmid: [21853617](https://pubmed.ncbi.nlm.nih.gov/21853617/)
231. B. Jacob, L. Lefgren, E. Moretti, The dynamics of criminal behavior evidence from weather shocks. *J. Hum. Resour.* **42**, 489–527 (2007). doi: [10.3368/jhr.XLII.3.489](https://doi.org/10.3368/jhr.XLII.3.489)
232. M. Ranson, Crime, weather, and climate change. *J. Environ. Econ. Manage.* **67**, 274–302 (2014). doi: [10.1016/j.jeem.2013.11.008](https://doi.org/10.1016/j.jeem.2013.11.008)
233. P. Baylis, “Temperature and temperament: Evidence from a billion tweets” (Energy Institute at HAAS working paper, 2015).
234. D. T. Kenrick, S. W. MacFarlane, Ambient temperature and horn honking: A field study of the heat/aggression relationship. *Environ. Behav.* **18**, 179–191 (1986). doi: [10.1177/0013916586182002](https://doi.org/10.1177/0013916586182002)
235. R. P. Larrick, T. A. Timmerman, A. M. Carton, J. Abrevaya, Temper, temperature, and temptation: Heat-related retaliation in baseball. *Psychol. Sci.* **22**, 423–428 (2011). doi: [10.1177/0956797611399292](https://doi.org/10.1177/0956797611399292); pmid: [21350182](https://pubmed.ncbi.nlm.nih.gov/21350182/)
236. T. A. Carleton, Crop-damaging temperatures increase suicide rates in India. *Proc. Natl. Acad. Sci. U.S.A.* **114**, 8746–8751 (2017). doi: [10.1073/pnas.1701354114](https://doi.org/10.1073/pnas.1701354114); pmid: [28760983](https://pubmed.ncbi.nlm.nih.gov/28760983/)
237. M. Burke, S. M. Hsiang, E. Miguel, Climate and conflict. *Annu. Rev. Econ.* **7**, 577–617 (2015). doi: [10.1146/annurev-economics-080614-115430](https://doi.org/10.1146/annurev-economics-080614-115430)
238. S. Hsiang *et al.*, Estimating economic damage from climate change in the United States. *Science* **356**, 1362–1369 (2017). doi: [10.1126/science.aal4369](https://doi.org/10.1126/science.aal4369); pmid: [28663496](https://pubmed.ncbi.nlm.nih.gov/28663496/)
239. M. B. Burke, E. Miguel, S. Satyanath, J. A. Dykema, D. B. Lobell, Climate robustly linked to African civil war. *Proc. Natl. Acad. Sci. U.S.A.* **107**, E185, author reply E186–E187 (2010). doi: [10.1073/pnas.1014879107](https://doi.org/10.1073/pnas.1014879107); pmid: [21118990](https://pubmed.ncbi.nlm.nih.gov/21118990/)
240. A. T. Bohlken, E. J. Sergenti, Economic growth and ethnic violence: An empirical investigation of Hindu-Muslim riots in India. *J. Peace Res.* **47**, 589–600 (2010). doi: [10.1177/002234310373032](https://doi.org/10.1177/002234310373032)
241. P. J. Burke, A. Leigh, Do output contractions trigger democratic change? *Am. Econ. J. Macroecon.* **2**, 124–157 (2010). doi: [10.1257/mac.2.4.124](https://doi.org/10.1257/mac.2.4.124)
242. N. Obradovich, Climate change may speed democratic turnover. *Clim. Change* **140**, 135–147 (2017). doi: [10.1007/s10584-016-1833-8](https://doi.org/10.1007/s10584-016-1833-8)
243. M. Dell, B. F. Jones, B. A. Olken, Temperature shocks and economic growth: Evidence from the last half century. *Am. Econ. J. Macroecon.* **4**, 66–95 (2012). doi: [10.1257/mac.4.3.66](https://doi.org/10.1257/mac.4.3.66)
244. P. J. Burke, Economic growth and political survival. *B. E. J. Macroecon.* **12**, 10.1515/1935-1690.2398 (2012). doi: [10.1515/1935-1690.2398](https://doi.org/10.1515/1935-1690.2398)
245. N. K. Kim, Revisiting economic shocks and coups. *J. Conflict Resolut.* **60**, 3–31 (2016). doi: [10.1177/0022002713520531](https://doi.org/10.1177/0022002713520531)
246. R. Hornbeck, The enduring impact of the American Dust Bowl: Short-and long-run adjustments to environmental catastrophe. *Am. Econ. Rev.* **102**, 1477–1507 (2012). doi: [10.1257/aer.102.4.1477](https://doi.org/10.1257/aer.102.4.1477)
247. S. Feng, M. Oppenheimer, Applying statistical models to the climate-migration relationship. *Proc. Natl. Acad. Sci. U.S.A.* **109**, E2915 (2012). doi: [10.1073/pnas.121226109](https://doi.org/10.1073/pnas.121226109); pmid: [22908301](https://pubmed.ncbi.nlm.nih.gov/22908301/)
248. S. Feng, A. B. Krueger, M. Oppenheimer, Linkages among climate change, crop yields and Mexico-US cross-border migration. *Proc. Natl. Acad. Sci. U.S.A.* **107**, 14257–14262 (2010). doi: [10.1073/pnas.1002632107](https://doi.org/10.1073/pnas.1002632107); pmid: [20660749](https://pubmed.ncbi.nlm.nih.gov/20660749/)
249. P. Bohra-Mishra, M. Oppenheimer, S. M. Hsiang, Nonlinear permanent migration response to climatic variations but minimal response to disasters. *Proc. Natl. Acad. Sci. U.S.A.* **111**, 9780–9785 (2014). doi: [10.1073/pnas.1317166111](https://doi.org/10.1073/pnas.1317166111); pmid: [24958887](https://pubmed.ncbi.nlm.nih.gov/24958887/)
250. J. V. Henderson, A. Storeygard, U. Deinhammer, Has climate change driven urbanization in Africa? *J. Dev. Econ.* **124**, 60–82 (2017). doi: [10.1016/j.jdevco.2016.09.001](https://doi.org/10.1016/j.jdevco.2016.09.001); pmid: [28458445](https://pubmed.ncbi.nlm.nih.gov/28458445/)
251. F. D. Hidalgo, S. Naidu, S. Nichter, N. Richardson, Economic determinants of land invasions. *Rev. Econ. Stat.* **92**, 505–523 (2010). doi: [10.1162/REST_a_00007](https://doi.org/10.1162/REST_a_00007)
252. A. Missirian, W. Schlenker, Asylum applications respond to temperature fluctuations. *Science* **358**, 1610–1614 (2017). doi: [10.1126/science.aao0432](https://doi.org/10.1126/science.aao0432); pmid: [29269476](https://pubmed.ncbi.nlm.nih.gov/29269476/)
253. Center for Climate and Security, “Climate and security resources: U.S. government, defense” (Council on Strategic Risks, 2018); <https://climateandsecurity.org/resources/u-s-government/defense/>.
254. CNA Military Advisory Board, “National security and the threat of climate change” (CNA, 2007).
255. D. Coates, “Worldwide threat assessment of the U.S. intelligence community” (National Intelligence Council, 2018).
256. Congress of the United States, H.R.2810. National Defense Authorization Act (2018).
257. F. Femia, C. Werrell, “Chronology of U.S. military leadership on climate change and security: 2017–2018” (Center for Climate and Security, 2018).
258. Center for Climate and Security, “Chairman of the Joint Chiefs: Climate change a source of conflict around the world,” 6 November 2018; <https://climateandsecurity.org>.
259. Union of Concerned Scientists, “The U.S. military on the front lines of rising seas” (Union of Concerned Scientists, 2016).
260. U.S. Department of Defense, “Climate-related risk to DoD infrastructure initial vulnerability assessment survey (SLVAS) report” (Office of the Under Secretary of Defense for Acquisition, Technology, and Logistics, U.S. Department of Defense, 2018).
261. Army Environmental Policy Institute, “Sustain the mission project: Casualty factors for fuel and water resupply convoys” (Final Tech. Rep., Army Environmental Policy Institute, 2009); http://www.aepi.army.mil/docs/whatsnew/SMP_Casualty_Cost_Factors_Final_09.pdf.
262. P. Stewart, “America’s got to up its game in the Arctic”: Mattis,” *Reuters*, 25 June 2018; <https://www.reuters.com/article/us-usa-military-arctic/americas-got-to-up-its-game-in-the-arctic-mattis-idU5KBNJL2W4>.
263. Strategic Studies Institute Army War College, “Russia in the Arctic” (Strategic Studies Institute Army War College, 2011).
264. U.S. Department of Defense, “Quadrennial defense review report, February 2010” (U.S. Department of Defense, 2010).
265. CNA Military Advisory Board, “National security and the accelerating risks of climate change” (CNA, 2014).
266. U.S. Department of Defense, “Quadrennial defense review 2014” (U.S. Department of Defense, 2014).
267. U.S. Department of Defense, “Department of Defense strategic sustainability performance plan FY2015” (U.S. Department of Defense, 2015).
268. M. Burke *et al.*, Opportunities for advances in climate change economics. *Science* **352**, 292–293 (2016). doi: [10.1126/science.aad9634](https://doi.org/10.1126/science.aad9634); pmid: [27081055](https://pubmed.ncbi.nlm.nih.gov/27081055/)
269. A. Isen, M. Rossin-Slater, R. Walker, Relationship between season of birth, temperature exposure, and later life wellbeing. *Proc. Natl. Acad. Sci. U.S.A.* **114**, 13447–13452 (2017). doi: [10.1073/pnas.1702436114](https://doi.org/10.1073/pnas.1702436114); pmid: [29203654](https://pubmed.ncbi.nlm.nih.gov/29203654/)
270. T. Deryugina, The fiscal cost of hurricanes: Disaster aid versus social insurance. *Am. Econ. J. Econ. Policy* **9**, 168–198 (2017). doi: [10.1257/pol.20140296](https://doi.org/10.1257/pol.20140296)
271. K. Karbownik, A. Wray, Long-run consequences of exposure to natural disasters. *J. Labor Econ.*, in press.
272. T. Houser, S. Hsiang, R. Kopp, K. Larsen, *Economic Risks of Climate Change: An American Prospectus* (Columbia Univ. Press, 2015).
273. M. Burke, S. M. Hsiang, E. Miguel, Global non-linear effect of temperature on economic production. *Nature* **527**, 235–239 (2015). doi: [10.1038/nature15725](https://doi.org/10.1038/nature15725); pmid: [26503051](https://pubmed.ncbi.nlm.nih.gov/26503051/)
274. M. Burke, W. M. Davis, N. S. Diffenbaugh, Large potential reduction in economic damages under UN mitigation targets. *Nature* **557**, 549–553 (2018). doi: [10.1038/s41586-018-0071-9](https://doi.org/10.1038/s41586-018-0071-9); pmid: [29795251](https://pubmed.ncbi.nlm.nih.gov/29795251/)
275. S. M. Hsiang, A. S. Jina, “The causal effect of environmental catastrophe on long-run economic growth: Evidence from 6,700 cyclones” (National Bureau of Economic Research, 2014).
276. T. Deryugina, S. Hsiang, “The marginal product of climate” (National Bureau of Economic Research, 2017).
277. W. Schlenker, M. J. Roberts, Nonlinear temperature effects indicate severe damages to U.S. crop yields under climate change. *Proc. Natl. Acad. Sci. U.S.A.* **106**, 15594–15598 (2009). doi: [10.1073/pnas.0906865106](https://doi.org/10.1073/pnas.0906865106); pmid: [19171432](https://pubmed.ncbi.nlm.nih.gov/19171432/)
278. J. Graff Zivin, M. Neidell, Temperature and the allocation of time: Implications for climate change. *J. Labor Econ.* **32**, 1–26 (2014). doi: [10.1086/671766](https://doi.org/10.1086/671766)
279. O. Deschênes, M. Greenstone, Climate change, mortality, and adaptation: Evidence from annual fluctuations in weather in the US. *Am. Econ. J. Appl. Econ.* **3**, 152–185 (2011). doi: [10.1257/app.3.4.152](https://doi.org/10.1257/app.3.4.152)
280. R. E. Kopp *et al.*, Probabilistic 21st and 22nd century sea-level projections at a global network of tide-gauge sites. *Earths Futur.* **2**, 383–406 (2014). doi: [10.1002/2014EF000239](https://doi.org/10.1002/2014EF000239)
281. K. A. Emanuel, Downscaling CMIP5 climate models shows increased tropical cyclone activity over the 21st century. *Proc. Natl. Acad. Sci. U.S.A.* **110**, 12219–12224 (2013). doi: [10.1073/pnas.1301293110](https://doi.org/10.1073/pnas.1301293110); pmid: [23836646](https://pubmed.ncbi.nlm.nih.gov/23836646/)
282. N. S. Diffenbaugh, F. Giorgi, Climate change hotspots in the CMIP5 global climate model ensemble. *Clim. Change* **114**, 813–822 (2012). doi: [10.1007/s10584-012-0570-x](https://doi.org/10.1007/s10584-012-0570-x); pmid: [24014154](https://pubmed.ncbi.nlm.nih.gov/24014154/)

ACKNOWLEDGEMENTS

Funding: N.S.D. was supported by Stanford University. S.C.D. was supported by the University of Virginia Environmental Resilience Institute. S.M. was supported by the NSF through grants NSF-1417700 and NSF-1312402. **Competing interests:** L.J.M. received consulting fees from the EPA for contributions to the Integrated Science Assessment (ISA) on PM matter and for review of the ozone ISA. S.T. serves on the boards of directors of the ClimateWorks Foundation and the Energy Foundation. **Data and materials availability:** All data are available in the main text.

10.1126/science.aat5982

Strengthened scientific support for the Endangerment Finding for atmospheric greenhouse gases

Philip B. Duffy, Christopher B. Field, Noah S. Diffenbaugh, Scott C. Doney, Zoe Dutton, Sherri Goodman, Lisa Heinzerling, Solomon Hsiang, David B. Lobell, Loretta J. Mickley, Samuel Myers, Susan M. Natali, Camille Parmesan, Susan Tierney and A. Park Williams

Science **363** (6427), eaat5982.

DOI: 10.1126/science.aat5982originally published online December 13, 2018

The case for endangerment

In 2009, the U.S. Environmental Protection Agency (EPA) established the so-called "Endangerment Finding." This defined a suite of six long-lived greenhouse gases as "air pollution." Such air pollution was anticipated to represent a danger to the health and welfare of current and future generations. Thus, the EPA has the authority to regulate these gases under the rules of the U.S. Clean Air Act. Duffy *et al.* provide a comprehensive review of the scientific evidence gathered in the years since then. These findings further support and strengthen the basis of the Endangerment Finding. Thus, a compelling case has been made even more compelling with an enormous body of additional data.

Science, this issue p. eaat5982

ARTICLE TOOLS

<http://science.sciencemag.org/content/363/6427/eaat5982>

RELATED CONTENT

<http://science.sciencemag.org/content/sci/363/6427/578.fullfile/content>

REFERENCES

This article cites 227 articles, 56 of which you can access for free
<http://science.sciencemag.org/content/363/6427/eaat5982#BIBL>

PERMISSIONS

<http://www.sciencemag.org/help/reprints-and-permissions>

Use of this article is subject to the [Terms of Service](#)



Global warming has increased global economic inequality

Noah S. Diffenbaugh^{a,b,1} and Marshall Burke^{a,c,d}

^aDepartment of Earth System Science, Stanford University, Stanford, CA 94305; ^bWoods Institute for the Environment, Stanford University, Stanford, CA 94305; ^cCenter on Food Security and the Environment, Stanford University, Stanford, CA 94305; and ^dEnvironment and Energy Economics, National Bureau of Economic Research, Cambridge, MA 02138

Edited by Ottmar Edenhofer, Potsdam Institute for Climate Impact Research, Potsdam, Germany, and accepted by Editorial Board Member Hans J. Schellnhuber March 22, 2019 (received for review September 16, 2018)

Understanding the causes of economic inequality is critical for achieving equitable economic development. To investigate whether global warming has affected the recent evolution of inequality, we combine counterfactual historical temperature trajectories from a suite of global climate models with extensively replicated empirical evidence of the relationship between historical temperature fluctuations and economic growth. Together, these allow us to generate probabilistic country-level estimates of the influence of anthropogenic climate forcing on historical economic output. We find very high likelihood that anthropogenic climate forcing has increased economic inequality between countries. For example, per capita gross domestic product (GDP) has been reduced 17–31% at the poorest four deciles of the population-weighted country-level per capita GDP distribution, yielding a ratio between the top and bottom deciles that is 25% larger than in a world without global warming. As a result, although between-country inequality has decreased over the past half century, there is ~90% likelihood that global warming has slowed that decrease. The primary driver is the parabolic relationship between temperature and economic growth, with warming increasing growth in cool countries and decreasing growth in warm countries. Although there is uncertainty in whether historical warming has benefited some temperate, rich countries, for most poor countries there is >90% likelihood that per capita GDP is lower today than if global warming had not occurred. Thus, our results show that, in addition to not sharing equally in the direct benefits of fossil fuel use, many poor countries have been significantly harmed by the warming arising from wealthy countries' energy consumption.

economic inequality | global warming | climate change attribution | CMIP5

Detection of impacts caused by historical global warming has increased substantially in the past decade, including documented impacts on agriculture, human health, and ecosystems (1). Quantifying these historical impacts is critical for understanding the costs and benefits of global warming, and for designing and evaluating climate mitigation and adaptation measures (1).

The impact of historical warming on economic inequality is of particular concern (2). There is growing evidence that poorer countries or individuals are more negatively affected by a changing climate, either because they lack the resources for climate protection (3) or because they tend to reside in warmer regions where additional warming would be detrimental to both productivity and health (4–6). Furthermore, given that wealthy countries have been responsible for the vast majority of historical greenhouse gas emissions, any clear evidence of inequality in the impacts of the associated climate change raises critical questions of international justice.

More broadly, measuring and understanding the past and present evolution of global economic inequality is an area of active research and policy interest, with ongoing disagreement about the nature and causes of observed inequality trends (7–10). Quantifying any climatic influence on these trends thus has implications beyond climate risk management.

Recent research has identified pathways by which changes in climate can affect the fundamental building blocks of economic production (11, 12). Empirical work has included sector-specific

analyses of agriculture, labor productivity, and human health (12), as well as analyses of aggregate indicators such as gross domestic product (GDP) (4, 13). A key insight is the nonlinear response of many outcomes to temperature change, with the coolest regions often benefitting in warm years, and warmer regions being harmed. As a result, empirical evidence combined with projections of future climate change suggests that, although some wealthy countries in cooler regions could benefit from additional warming, most poor countries are likely to suffer (4, 14).

Efforts to apply empirical approaches to explicitly quantify the spatial pattern of aggregate impacts have primarily focused on future climate change (4–6, 14), with quantification of historical impacts being limited to specific economic sectors and outcomes (e.g., ref. 1), or to global GDP (12). Likewise, although a number of researchers have noted that the most robust regional warming has generally occurred in lower-latitude regions that are currently relatively poor (e.g., refs. 15–19), these analyses have not attempted to quantify the distributional impacts of historical temperature change.

Here, we build on past work linking economic growth and fluctuations in temperature (4, 14) to quantify the impact of historical anthropogenic climate forcing on the global distribution of country-level per capita GDP (*Materials and Methods* and Fig. 1). We use the Historical and Natural climate model simulations from the Coupled Model Intercomparison Project (CMIP5) (20) to quantify the temperature trajectory of different countries in the absence of anthropogenic forcing. We then combine these counterfactual country-level temperature trajectories

Significance

We find that global warming has very likely exacerbated global economic inequality, including ~25% increase in population-weighted between-country inequality over the past half century. This increase results from the impact of warming on annual economic growth, which over the course of decades has accumulated robust and substantial declines in economic output in hotter, poorer countries—and increases in many cooler, wealthier countries—relative to a world without anthropogenic warming. Thus, the global warming caused by fossil fuel use has likely exacerbated the economic inequality associated with historical disparities in energy consumption. Our results suggest that low-carbon energy sources have the potential to provide a substantial secondary development benefit, in addition to the primary benefits of increased energy access.

Author contributions: N.S.D. and M.B. designed research, performed research, contributed new reagents/analytic tools, analyzed data, and wrote the paper.

The authors declare no conflict of interest.

This article is a PNAS Direct Submission. O.E. is a guest editor invited by the Editorial Board.

This open access article is distributed under [Creative Commons Attribution-NonCommercial-NoDerivatives License 4.0 \(CC BY-NC-ND\)](https://creativecommons.org/licenses/by-nc-nd/4.0/).

¹To whom correspondence should be addressed. Email: difflenbaugh@stanford.edu.

This article contains supporting information online at www.pnas.org/lookup/suppl/doi:10.1073/pnas.1816020116/-DCSupplemental.

Published online April 22, 2019.

Country-level economic impact of historical global warming

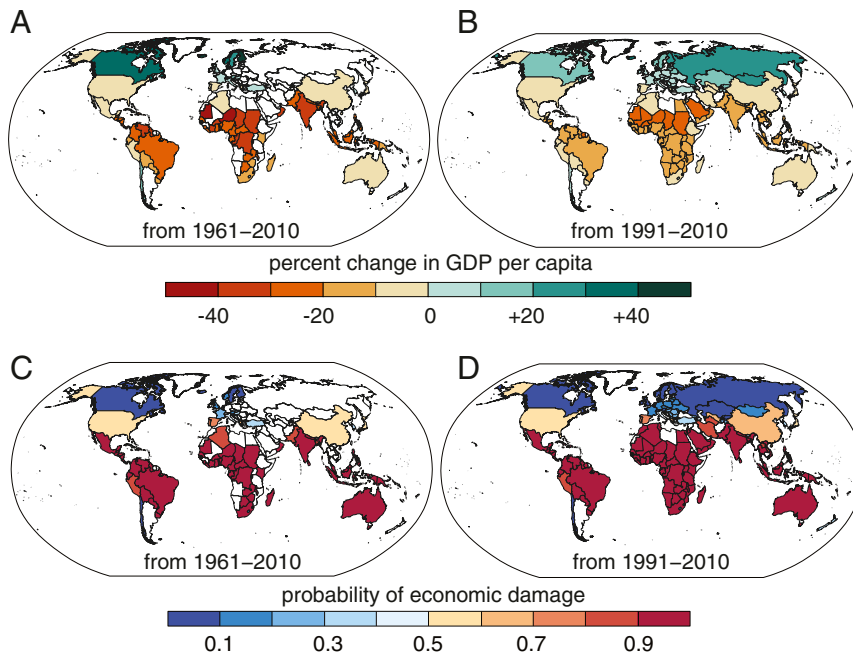


Fig. 2. Country-level economic response to global warming. (A) The median impact on country-level per capita GDP across the >20,000 realizations of the world without anthropogenic forcing, calculated for each country over the 1961–2010 period. (B) As in A, but for the 1991–2010 period. Differences in the presence/absence of countries between the 1961–2010 and 1991–2010 periods reflect differences in the availability of country-level economic data. Differences in the magnitude of country-level values between the 1961–2010 and 1991–2010 periods reflect the influence of accumulation time on the net accumulated economic impact. (C and D) The probability that historical anthropogenic forcing has resulted in economic damage, calculated as the percentage of the >20,000 realizations that show a decrease in per capita GDP relative to the counterfactual world without anthropogenic forcing.

without global warming, with ~90% likelihood that the ratio has increased (Fig. 4C). Likewise, the ratio between the top and bottom population-weighted quintiles [another common measure (9)] has become 45% larger (5th to 95th range of +10% to +99%), with ~99% likelihood that the ratio has increased. As a result, although overall between-country inequality has decreased substantially over the past half century (Fig. 4A, refs. 9 and 10), it is “very likely” (27) that global warming has slowed that decrease (Fig. 4A and C).

The increase in inequality between countries has resulted primarily from warming-induced penalties in poor countries, along with warming-induced benefits in some rich countries (Figs. 2A, 3B, and 4B). We find that the poorest half of the population-weighted country-level economic distribution has become relatively more poor over the 1961–2010 period, including a median impact of –17% at the poorest decile, and –30% to –31% at the next three poorest deciles (Fig. 4B). In contrast, the top half of the population-weighted country-level economic distribution has likely suffered much less—and has a much higher likelihood of having benefited—than the bottom half of the distribution (Fig. 4B).

Discussion

Although some canonical uncertainties in quantifying future economic impacts are largely removed when focusing on the historical period—such as future discounting uncertainty (e.g., refs. 14, 28, and 29) and the limits of accounting for future changes that fall well outside of historical experience (14)—other uncertainties must be considered.

For example, uncertainty in the exact magnitude of the temperature optimum creates uncertainty in the sign of the historical climate impact in some countries (Fig. 2C and SI Appendix, Table S1). However, the sign of the impact on inequality is robust (Fig. 4C), primarily because the mean temperature of so many poor countries lies in the extreme warm tail of uncertainty in the optimum (Fig. 3A and B). For these countries, it is “very likely” (27) that historical warming has reduced economic growth and lowered per capita GDP (Fig. 2C and SI Appendix, Table S1). As a result, although uncertainty in the magnitude of the response of regional temperature to historical forcing creates uncertainty in the magnitude of impact at a given decile of the country-level economic distribution (Fig. 4B), the sign of the impact on the lower deciles (Fig. 4B)—and therefore on inequality (Fig. 4C)—is robust.

Relationship between the economic impact of historical global warming and temperature, wealth, and cumulative carbon emissions

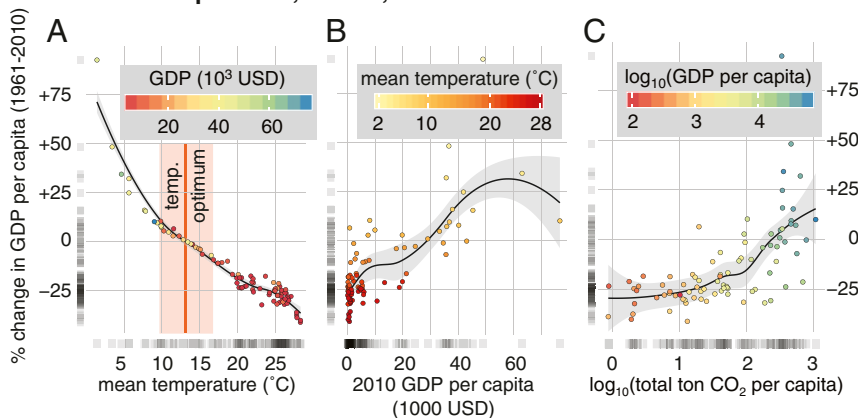


Fig. 3. Relationship between economic impact of global warming and country-level temperature, GDP, and cumulative CO₂ emissions. (A) The relationship between country-level mean annual temperature and median economic impact of anthropogenic forcing over the 1961–2010 period. The orange line shows the median temperature optimum reported by Burke et al. (14), and the orange envelope shows the 5–95% range. (B) The relationship between per capita GDP in 2010 and median economic impact of historical anthropogenic forcing over the 1961–2010 period. (C) The relationship between cumulative emissions over the 1961–2010 period (calculated from ref. 32) and median economic impact of historical anthropogenic forcing over the 1961–2010 period. (A–C) Gray strip plots show the density of points along the x and y axes. The black regression line and gray envelope show the 95% confidence interval of a locally weighted regression (“loess”).

A Impact of anthropogenic global warming on economic inequality

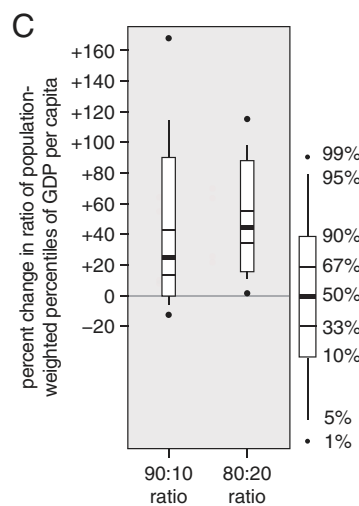
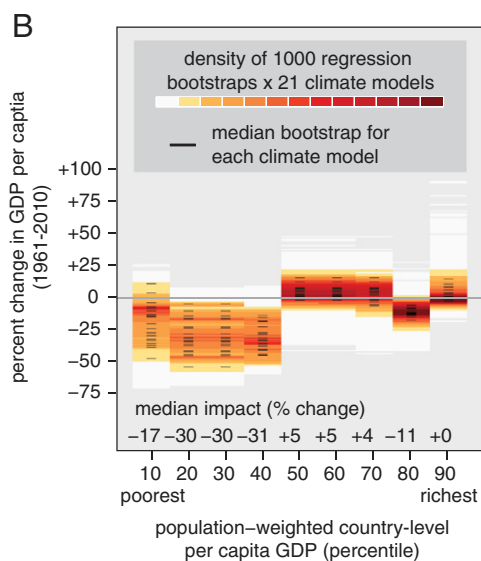
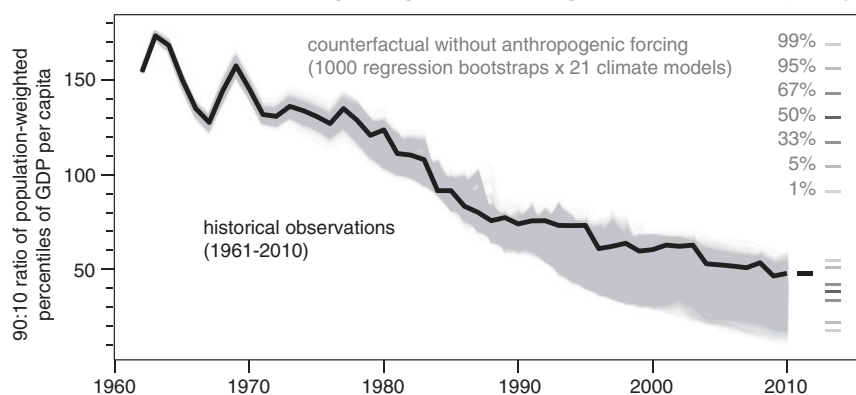


Fig. 4. Impact of global warming on country-level inequality over the past half century. (A) The ratio between the population-weighted 90th percentile and 10th percentile country-level per capita GDP for the historical observed time series and each of the >20,000 realizations of the world without anthropogenic forcing. (B) The density of the >20,000 realizations at each decile of the population-weighted country-level per capita GDP distribution. (C) The distribution across the >20,000 realizations of percent change in population-weighted 90:10 and 80:20 percentile ratios in the year 2010, relative to the present ratio. Calculations include only those countries that have continuous socioeconomic data from 1961 through 2010 ($n = 86$).

The sign of the inequality impact is also robust to the inclusion of lagged responses (*SI Appendix, Table S2*). Lagged responses can compensate the growth effects of temperature fluctuations, leading to decreases in both the growth benefit in cool countries and the growth penalty in warm countries (4). These lagged responses reduce the calculated magnitude and probability of warming-induced increases in economic inequality. However, even with a 5-y lag, there is still 66% likelihood that historical warming has increased country-level inequality.

The availability of socioeconomic data also creates uncertainty. Because growth effects cumulate, the length of time over which economic impacts are evaluated can meaningfully affect results (4, 12, 14). However, data availability creates an inherent tradeoff between evaluating fewer countries over a longer period and evaluating more countries over a shorter period. We repeat our primary analysis using a larger, shorter sample. Overall, the pattern of impact is robust, but the cumulative magnitude is larger over the longer period (Figs. 2 and 3 and *SI Appendix, Fig. S1*). This expansion over longer periods suggests that the full impact of warming since the Industrial Revolution has been even greater than the impact calculated over the past half century.

Our approach to quantifying the impact of global warming on economic inequality is also limited by its reliance on country-level relationships between temperature and economic growth. Our analysis focuses on country-level data because their wide availability (in both space and time) allows us to use empirical relationships to quantify how historical temperature changes have affected economic outcomes around the world. The impact of climate change on the evolution of within-country inequality is

a critical question (e.g., ref. 2), but would require either strong assumptions about how within-country income distributions respond to aggregate shocks at the country level, or comprehensive subnational data on incomes (which are currently unavailable for most country-years around the world). Although our population weighting provides some indication of global-scale individual-level inequality (9), documenting the impact of global warming on within-country inequality remains an important challenge.

Many countries in our sample have experienced rapid urbanization and economic development for reasons unrelated to climate, and such trends could plausibly alter how economies respond to subsequent climate change. Because past work did not find statistically significant evidence that higher incomes reduce temperature sensitivities (4), we do not attempt to model this moderating effect here. However, if increasing urbanization or economic development has reduced the temperature sensitivity of economies over our study period, this effect will be implicitly included in our estimated impact of temperature on GDP growth and inequality—that is, we have estimated the effect of temperature on growth for economies that are rapidly urbanizing. Explicitly quantifying the roles of these moderating influences is an important avenue for future work, as it will be critical for understanding how future climate change will affect the level and distribution of global income.

Trade between countries has likely already influenced the impacts of global warming on population-weighted inequality. First, a large part of the reduction in historical inequality during our sample period has been due to the unprecedented growth in incomes in East Asia [and particularly China (9, 10)], much of which was built on critical trading relationships with high-income countries. In

a no-trade counterfactual, China would likely grow much less rapidly. Thus, because of China's large population and small sensitivity to historical warming (Fig. 2), repeating our analysis in a no-trade counterfactual would likely result in smaller reductions in per capita GDP in the lower deciles of the population-weighted income distribution (Fig. 4B). However, trade can also serve as a buffer against climate shocks, particularly in poor countries (e.g., ref. 30). Thus, the economic impacts of global warming—which has substantially increased the occurrence of extremes (e.g., ref. 21)—would likely have been even greater in poor countries in a no-trade counterfactual, amplifying the impact on between-country inequality.

Conclusions

It has been frequently observed that wealthy countries have benefited disproportionately from the activities that have caused global warming, while poor countries suffer disproportionately from the impacts (e.g., refs. 16, 17, 19, 25, and 26). Our results show that, in addition to the direct benefits of fossil fuel use, many wealthy countries have likely been made even more wealthy by the resulting global warming. Likewise, not only have poor countries not shared in the full benefits of energy consumption, but many have already been made poorer (in relative terms) by the energy consumption of wealthy countries. Given the magnitude of the warming-induced growth penalties that poor countries have already suffered, expansion of low-carbon energy sources can be expected to provide a substantial secondary development benefit (by curbing future warming-induced growth penalties), in addition to the primary benefits of increased energy access.

Materials and Methods

Climate Model Experiments. We compare the Historical and Natural climate model simulations from the CMIP5 archive (20). As in Burke et al. (14), we analyze the subselection of CMIP5 realizations analyzed by the Intergovernmental Panel on Climate Change (IPCC) (31). For the Natural experiment, this includes one realization each from 21 of the participating global climate models, which are paired with the 21 corresponding Historical realizations. Note that although the socioeconomic data are available through 2010, the CMIP5 experimental protocol for the Historical and Natural experiments ends in 2005. Thus, as in Burke et al. (14), we use the IPCC's 20-y historical baseline period (1986–2005) as the baseline period for climate model bias correction.

For each country, we create 21 counterfactual historical temperature timeseries $T_{NoAnthro}$, which remove the influence of anthropogenic forcing simulated by each of the 21 climate models. Our approach to creating the counterfactual timeseries follows the widely applied "delta method" of climate model bias correction, in which the model-simulated change in the mean is applied to the observed timeseries. For each country c , we first calculate the observed country-level population-weighted mean annual temperature timeseries T_{Obs} for the 1961–2010 time period covered by the socioeconomic data, following Burke et al. (14). Then, for each country c and climate model m , we calculate the difference in country-level population-weighted mean temperature between the Historical and Natural CMIP5 simulations, both for the 20-y period centered on the beginning of the socioeconomic data (1951–1970), and for the 20-y historical baseline period used by the IPCC (1986–2005). We then linearize the difference between the Historical and Natural simulations over the 1961–2010 period, such that the difference in 1961 is equal to the difference in the Historical and Natural means during the 20-y period centered on 1961 (1951–1970), and the difference in 2010 is equal to the difference in the Historical and Natural means during the IPCC's 20-y baseline period (1986–2005). Finally, for each year t in the 1961–2010 observed temperature timeseries, we add the linearized *Natural* minus *Historical* difference ΔT for that year:

$$T_{NoAnthro}[t] = T_{Obs}[t] + \Delta T[t].$$

This process generates, for each country, an ensemble of 21 counterfactual timeseries $T_{NoAnthro}$. This 21-member ensemble reflects a combination of uncertainty in the climate response to external forcings and uncertainty arising from internal climate system variability, but removes biases in the climate model simulation of the absolute temperature magnitude and of the interannual temperature variability. [The $T_{NoAnthro}$ timeseries corresponds to the counterfactual timeseries used in Diffenbaugh et al. (21) to calculate the contribution of the observed trend to the extreme event magnitude, except that in this case the magnitude of the counterfactual trend is calculated from the CMIP5 Natural forcing simulation.]

Impact of Historical Temperature Change on Economic Growth. Burke et al. (4, 14) used historical data to quantify the empirical relationship between variations in country-level temperature and country-level annual growth in per capita GDP, allowing for the marginal effect of annual temperature deviations to vary nonlinearly as a function of country-level mean temperature. As described in detail in Burke et al. (4, 14), the equation for the panel fixed-effects model is as follows:

$$\Delta \log(Y_{it}) = \beta_1 T_{it} + \beta_2 T_{it}^2 + \lambda_1 P_{it} + \lambda_2 P_{it}^2 + \mu_i + \nu_t + \theta_{1i}t + \theta_{2i}t^2 + \varepsilon_{it},$$

where Y_{it} is per capita GDP in country i in year t , T is the average temperature in year t , P is the average precipitation in year t , μ_i are country-fixed effects, ν_t are year-fixed effects, and $\theta_{1i}t + \theta_{2i}t^2$ are country-specific linear and quadratic time trends.

In the current study, we repeat the primary regression calculation described in Burke et al. (14), using historical data from 1961 to 2010, and bootstrapping with replacement to estimate a separate response function for each of 1,000 resamples, which we denote f_b . The uncertainty in the magnitude of the temperature optimum (Fig. 1B) creates uncertainty in exactly which countries are likely to benefit or be penalized at different levels of warming, and is the largest source of uncertainty in the response of GDP growth to elevated levels of global climate forcing (14).

We quantify the uncertainty in economic damages arising from uncertainty in the temperature optimum (e.g., Figs. 2 and 4 and *SI Appendix, Table S1*), as well as the uncertainty arising from lagged responses to temperature fluctuations (*SI Appendix, Table S2*). We also explore additional aspects of the relationship between temperature and GDP growth. For example, we find that historical temperature fluctuations explain on average 8.6% of the overall variation in country-level annual income growth fluctuations during our study period (*SI Appendix, Fig. S2*). Likewise, given the shape of the temperature–growth response function (Fig. 1B), temperature fluctuations around a stable mean will induce a negative trend in per capita GDP. However, we find that the magnitude of this effect is small compared with the impact of long-term warming (*SI Appendix, Fig. S3*).

Whereas Burke et al. (4, 14) projected economic impacts under future emissions scenarios, we calculate the accumulated economic impacts of historical temperature change. For each country c in each year t , we compare economic growth under historical observed temperatures (T_{Obs}) with predicted growth under counterfactual temperatures ($T_{NoAnthro}$). We repeat this comparison for each climate model m and each bootstrap j , yielding more than 20,000 realizations of the impact of anthropogenic forcing on economic growth in each country.

We first initialize the analysis in each country with the observed per capita GDP from the starting year $t = 0$ of the socioeconomic data (e.g., $GDPcap_{Obs}[1961]$). Then, for each year t and using the temperature–growth response functions f estimated above, we calculate the difference in growth rate between the observed temperature and the counterfactual temperature (Fig. 1C and D):

$$\Delta Growth[t] = f(T_{NoAnthro}[t]) - f(T_{Obs}[t]).$$

We then add that difference $\Delta Growth[t]$ to the actual observed growth rate $Growth_{Obs}[t]$ to calculate the counterfactual growth rate $Growth_{NoAnthro}[t]$:

$$Growth_{NoAnthro}[t] = Growth_{Obs}[t] + \Delta Growth[t].$$

We then multiply this counterfactual growth $Growth_{NoAnthro}[t]$ by the accumulated counterfactual per capita GDP in the previous year ($GDPcap_{NoAnthro}[t - 1]$) to calculate current-year counterfactual per capita GDP:

$$GDPcap_{NoAnthro}[t] = GDPcap_{NoAnthro}[t - 1] + (GDPcap_{NoAnthro}[t - 1] * Growth_{NoAnthro}[t]).$$

We repeat this process through the last year of the socioeconomic data (2010), for each country in the GDP dataset.

Finally, we calculate the percent difference between the actual observed per capita GDP ($GDPcap_{Obs}$) and the per capita GDP calculated for the counterfactual temperature timeseries ($GDPcap_{NoAnthro}$) in the last year of the socioeconomic data (2010):

$$\Delta GDPcap = [(GDPcap_{Obs}[2010] - GDPcap_{NoAnthro}[2010]) / GDPcap_{NoAnthro}[2010]] \times 100\%.$$

For each country c , we calculate $GDPcap_{NoAnthro}$ and $\Delta GDPcap$ for each of the 1,000 bootstrapped response functions f_b , applied to the counterfactual temperature timeseries $T_{NoAnthro}$ from each of the 21 global climate models

(thus yielding more than 20,000 values of $GDPcap_{NoAnthro}$ and $\Delta GDPcap$ for each country).

Our primary analysis is focused on quantifying the impacts that historical global warming has had during the full period for which socioeconomic data are available (1961–2010). However, because the socioeconomic data do not extend to 1961 for a large number of countries, we repeat our analysis for the 1991–2010 period. For all analyses that start in 1961, we analyze only those countries that have continuous socioeconomic data from 1961 through 2010 ($n = 86$); for all analyses that start in 1991, we analyze only those countries that have continuous socioeconomic data from 1991 through 2010 ($n = 151$). Observed and estimated counterfactual temperatures and growth rates are the same for the years that overlap between the two periods, but growth rates are cumulated over 30 more years in the longer period, yielding larger (in absolute value) impacts on economic outcomes by the end of the period (Fig. 2).

Quantifying the Impact of Historical Global Warming on Economic Inequality. A number of measures of economic inequality have been developed (9). Given the limited availability of long timeseries of subnational economic data, investigations of changes in global inequality often rely on country-level metrics (e.g., refs. 9 and 10). However, when using country-level metrics, weighting by country-level population is critical to accurately capture trends in global inequality (9).

We measure global economic inequality using the ratio of the top and bottom decile (“90:10 ratio”) and top and bottom quintile (“80:20 ratio”) of the population-weighted country-level per capita GDP distribution. Both metrics are included among “eight of the most popular” indexes of income inequality identified by Sala-i-Martin (9). According to Sala-i-Martin (9), “The top-20-percent-to-bottom-20-percent is the ratio of the income of the person located at the top twentieth centile divided by the income of the corresponding person at the bottom twentieth centile. A similar definition applies to the top-10-percent-to-bottom-10-percent ratio.” Because of the lack of availability of long timeseries of subnational economic data, we calculate these ratios using the respective percentiles of the population-weighted empirical CDF of country-level per capita GDP values (SI Appendix, Fig. S4).

We first calculate the percent difference in per capita GDP for each decile of the population-weighted country-level GDP distribution. To do so, we calculate the deciles of country-level population-weighted per capita GDP, using the countries in the 1961–2010 dataset. For each year t in the observed country-level per capita GDP dataset ($GDPcap_{Obs}$), we calculate the p th percentile population-weighted GDP as the country-level per capita GDP

below which the sum of the country-level populations represents p percent of the total population of countries in the 1961–2010 dataset (SI Appendix, Fig. S4). For example, we calculate the 10th percentile population-weighted GDP as the country-level per capita GDP for which the total population of countries with lower per capita GDP is 10% of the total population of countries in the 1961–2010 dataset, and so on for each decile.

Next, we calculate the deciles of country-level population-weighted per capita GDP in each year t of each bootstrap j and climate model m of the counterfactual world without anthropogenic climate forcing ($GDPcap_{NoAnthro}$). Then, for the year 2010 in each bootstrap j and climate model m , we calculate the percent difference between the observed population-weighted decile value and the counterfactual population-weighted decile value (as described for $\Delta GDPcap$ above). For the differences in each population-weighted decile, we calculate the density distribution across all 1,000 bootstrap regressions from all 21 climate models, as well as the median value across the 1,000 bootstrap regressions for each climate model.

Finally, we quantify the between-country population-weighted economic inequality $GDPcapHigh:Low$ as the ratio between the higher percentile (e.g., 90th) and lower percentile (e.g., 10th) population-weighted per capita GDP. We first calculate $GDPcapHigh:Low$ in each year t of the observations ($GDPcapHigh:Low_{Obs}$), and in each year t of the counterfactual world without anthropogenic climate forcing ($GDPcapHigh:Low_{NoAnthro}$). Then, for each bootstrap j and climate model m , we calculate the percent difference between the observed population-weighted inequality $GDPcapHigh:Low_{Obs}$ and the counterfactual population-weighted inequality $GDPcapHigh:Low_{NoAnthro}$ in the year 2010:

$$\Delta GDPcapHigh:Low = \left[\frac{(GDPcapHigh:Low_{Obs}[2010] - GDPcapHigh:Low_{NoAnthro}[2010])}{GDPcapHigh:Low_{NoAnthro}[2010]} \right] \times 100\%.$$

ACKNOWLEDGMENTS. We thank the editor and two anonymous reviewers for insightful and constructive feedback. We acknowledge the World Climate Research Programme’s Working Group on Coupled Modelling (which is responsible for CMIP), the climate modeling groups for producing and making available their model output, and the Department of Energy’s Program for Climate Model Diagnosis and Intercomparison for access to the CMIP5 data. Computational facilities were provided by the Center for Computational Earth and Environmental Science and Stanford Research Computing Center at Stanford University. We acknowledge funding support from Stanford University.

- Intergovernmental Panel on Climate Change (2014) *Climate Change 2014: Impacts, Adaptation, and Vulnerability. Contribution of Working Group II to the Fifth Assessment Report of the Intergovernmental Panel on Climate Change*, eds Field CB, et al. (Cambridge Univ Press, Cambridge, UK), pp 1–32.
- Hallegraeve S, Rozenberg J (2017) Climate change through a poverty lens. *Nat Clim Chang* 7:250–256.
- Intergovernmental Panel on Climate Change (2012) *Managing the Risks of Extreme Events and Disasters to Advance Climate Change Adaptation*, eds Field CB, et al. (Cambridge Univ Press, Cambridge, UK).
- Burke M, Hsiang SM, Miguel E (2015) Global non-linear effect of temperature on economic production. *Nature* 527:235–239.
- Hsiang S, et al. (2017) Estimating economic damage from climate change in the United States. *Science* 356:1362–1369.
- Duffy PB, et al. (2019) Strengthened scientific support for the Endangerment Finding for atmospheric greenhouse gases. *Science* 363:eaat5982.
- Piketty T, Saez E (2014) Inequality in the long run. *Science* 344:838–843.
- Milanovic B (2016) *Global Inequality: A New Approach for the Age of Globalization* (Harvard Univ Press, Cambridge, MA).
- Sala-i-Martin X (2006) The world distribution of income: Falling poverty and... convergence, period. *Q J Econ* 121:351–397.
- Schultz TP (1998) Inequality in the distribution of personal income in the world: How it is changing and why. *J Popul Econ* 11:307–344.
- Dell M, Jones BF, Olken BA (2014) What do we learn from the weather? The new climate-economy literature. *J Econ Lit* 52:740–798.
- Carleton TA, Hsiang SM (2016) Social and economic impacts of climate. *Science* 353: aad9837.
- Dell M, Jones BF, Olken BA (2012) Temperature shocks and economic growth: Evidence from the last half century. *Am Econ J Macroecon* 4:66–95.
- Burke M, Davis WM, Diffenbaugh NS (2018) Large potential reduction in economic damages under UN mitigation targets. *Nature* 557:549–553.
- Harrington LJ, et al. (2016) Poorest countries experience earlier anthropogenic emergence of daily temperature extremes. *Environ Res Lett* 11:55007.
- Mahlstein I, Knutti R, Solomon S, Portmann RW (2011) Early onset of significant local warming in low latitude countries. *Environ Res Lett* 6:34009.
- Hansen J, Sato M (2016) Regional climate change and national responsibilities. *Environ Res Lett* 11:34009.
- King A, Harrington L (2018) The inequality of climate change from 1.5 to 2 °C of global warming. *Geophys Res Lett* 45:5030–5033.
- Davis SJ, Diffenbaugh NS (2016) Dislocated interests and climate change. *Environ Res Lett* 11:61001.
- Taylor KE, Stouffer RJ, Meehl GA (2012) An overview of CMIP5 and the experiment design. *Bull Am Meteorol Soc* 93:485–498.
- Diffenbaugh NS, et al. (2017) Quantifying the influence of global warming on unprecedented extreme climate events. *Proc Natl Acad Sci USA* 114:4881–4886.
- Deser C, Knutti R, Solomon S, Phillips AS (2012) Communication of the role of natural variability in future North American climate. *Nat Clim Chang* 2:775–779.
- Nordhaus WD (2006) Geography and macroeconomics: New data and new findings. *Proc Natl Acad Sci USA* 103:3510–3517.
- Woodard DL, Davis SJ, Randerson JT (2019) Economic carbon cycle feedbacks may offset additional warming from natural feedbacks. *Proc Natl Acad Sci USA* 116:759–764.
- Ravallion M, Heil M, Jalan J (2000) Carbon emissions and income inequality. *Oxf Econ Pap* 52:651–669.
- Duro JA, Padilla E (2006) International inequalities in per capita CO₂ emissions: A decomposition methodology by Kaya factors. *Energy Econ* 28:170–187.
- Mastrandrea MD, et al. (2011) The IPCC AR5 guidance note on consistent treatment of uncertainties: A common approach across the working groups. *Clim Change* 108: 675–691.
- Stern N (2006) *The Economics of Climate Change: The Stern Review* (Cambridge Univ Press, Cambridge, UK).
- Nordhaus WD (2007) A review of the Stern review on the economics of climate change. *J Econ Lit* 45:686–702.
- Ahmed SA, Diffenbaugh NS, Hertel TW (2009) Climate volatility deepens poverty vulnerability in developing countries. *Environ Res Lett* 4:034004.
- Intergovernmental Panel on Climate Change (2013) *Climate Change 2013: The Physical Science Basis. Contribution of Working Group I to the Fifth Assessment Report of the Intergovernmental Panel on Climate Change* (Cambridge Univ Press, Cambridge, UK), pp 1311–1394.
- Le Quéré C, et al. (2018) Global carbon budget 2018. *Earth Syst Sci Data* 10: 2141–2194.

Large potential reduction in economic damages under UN mitigation targets

Marshall Burke^{1,2,3*}, W. Matthew Davis² & Noah S. Diffenbaugh^{1,4}

International climate change agreements typically specify global warming thresholds as policy targets¹, but the relative economic benefits of achieving these temperature targets remain poorly understood^{2,3}. Uncertainties include the spatial pattern of temperature change, how global and regional economic output will respond to these changes in temperature, and the willingness of societies to trade present for future consumption. Here we combine historical evidence⁴ with national-level climate⁵ and socioeconomic⁶ projections to quantify the economic damages associated with the United Nations (UN) targets of 1.5 °C and 2 °C global warming, and those associated with current UN national-level mitigation commitments (which together approach 3 °C warming⁷). We find that by the end of this century, there is a more than 75% chance that limiting warming to 1.5 °C would reduce economic damages relative to 2 °C, and a more than 60% chance that the accumulated global benefits will exceed US\$20 trillion under a 3% discount rate (2010 US dollars). We also estimate that 71% of countries—representing 90% of the global population—have a more than 75% chance of experiencing reduced economic damages at 1.5 °C, with poorer countries benefiting most. Our results could understate the benefits of limiting warming to 1.5 °C if unprecedented extreme outcomes, such as large-scale sea level rise⁸, occur for warming of 2 °C but not for warming of 1.5 °C. Inclusion of other unquantified sources of uncertainty, such as uncertainty in secular growth rates beyond that contained in existing socioeconomic scenarios, could also result in less precise impact estimates. We find considerably greater reductions in global economic output beyond 2 °C. Relative to a world that did not warm beyond 2000–2010 levels, we project 15%–25% reductions in per capita output by 2100 for the 2.5–3 °C of global warming implied by current national commitments⁷, and reductions of more than 30% for 4 °C warming. Our results therefore suggest that achieving the 1.5 °C target is likely to reduce aggregate damages and lessen global inequality, and that failing to meet the 2 °C target is likely to increase economic damages substantially.

Anticipating the potential impacts of climate change is central to planning appropriate policy responses, including how to allocate resources among mitigation and adaptation options. By committing the international community to holding global warming to “well below 2 °C above pre-industrial levels” and pursuing a 1.5 °C target¹, the UN Paris Agreement increased the need for quantitative analysis of uncertainties in the costs and benefits of achieving highly resolved warming targets. In particular, because mitigation costs are thought to rise rapidly for more stringent targets⁹, understanding the value of avoided impacts (what we term ‘benefits’) is central to evaluating the 1.5 °C target. Quantification of these potential benefits and their uncertainties is needed at the aggregate global level to guide coordinated global policy, as well as at a more local level to understand the distributional impacts of global policy choices¹⁰. Further, because the current national commitments imply warming⁷ of 2.5–3 °C, quantifying the impact of exceeding the 1.5 °C and 2 °C targets is also critical to understanding the implications of policy choices.

Here we estimate the global and country-specific economic impacts of limiting warming to 1.5 °C relative to 2 °C, as well as the global impacts of projected warming under current mitigation commitments, separate from any mitigation costs incurred in achieving those targets. We measure potential global and country-level damages using gross domestic product (GDP), the total value of goods and services produced in a country in a given year. GDP is clearly an incomplete summary of the benefits of mitigation, and it cannot easily diagnose many sector-specific impacts (for example, in crop agriculture versus manufacturing). However, it does capture how sector-specific impacts interact and aggregate—a traditional challenge for sector-specific empirical work and model-based approaches to aggregation¹¹. GDP also remains highly relevant to policy discussions, and the level and uncertainty in GDP impacts associated with the UN temperature targets has not been formally quantified.

We construct a probabilistic framework (Fig. 1) that incorporates uncertainty in (1) the historical relationship between temperature variability and economic growth, (2) the spatial pattern of future mean annual temperature change associated with a given level of aggregate emissions, (3) the future rate and pattern of economic development absent climate change, and (4) how future damages should be discounted.

To estimate the historical relationship between temperature and GDP, we use annual measurements of average temperature and growth in GDP per capita from 165 countries over the years 1960–2010. Following Burke et al.⁴, we use a fixed-effects estimator that isolates the effect of temperature fluctuations from other time-invariant and time-varying factors that might be correlated with both temperature and economic output, and we estimate nonlinear response functions that allow the marginal effect of warming to differ as a function of countries’ average temperatures. To quantify uncertainty in this historical relationship, we employ multiple bootstrapping approaches, estimating a separate response function for each re-sample (see Methods).

All estimated response functions relating GDP growth to temperature display a similar concave shape (Fig. 1a), suggesting that additional warming accelerates growth in cooler regions and slows growth in warmer regions. These findings are consistent with a large body of work demonstrating nonlinear responses of economic outcomes to changes in temperature^{12–17}. However, there is uncertainty in the temperature at which additional warming begins to generate damages rather than benefits (the ‘temperature optimum’), with a median estimate of 13.1 °C but a 5%–95% range of 9.7–16.8 °C. Because much of today’s GDP is produced in areas just beyond the median estimated optimal temperature (density plot, bottom of Fig. 1a), uncertainty in this optimum leads to substantial overall uncertainty in both the magnitude and sign of the impact of additional warming.

We project impacts under different levels of future warming by combining these historical response functions with the Intergovernmental Panel on Climate Change (IPCC) projections of future climate¹⁸. The climate model experiments used by the IPCC involve dozens of general circulation models (GCMs) run under four forcing pathways (called

¹Department of Earth System Science, Stanford University, Stanford, CA, USA. ²Center on Food Security and the Environment, Stanford University, Stanford, CA, USA. ³National Bureau of Economic Research, Cambridge, MA, USA. ⁴Woods Institute for the Environment, Stanford University, Stanford, CA, USA. *e-mail: mburke@stanford.edu

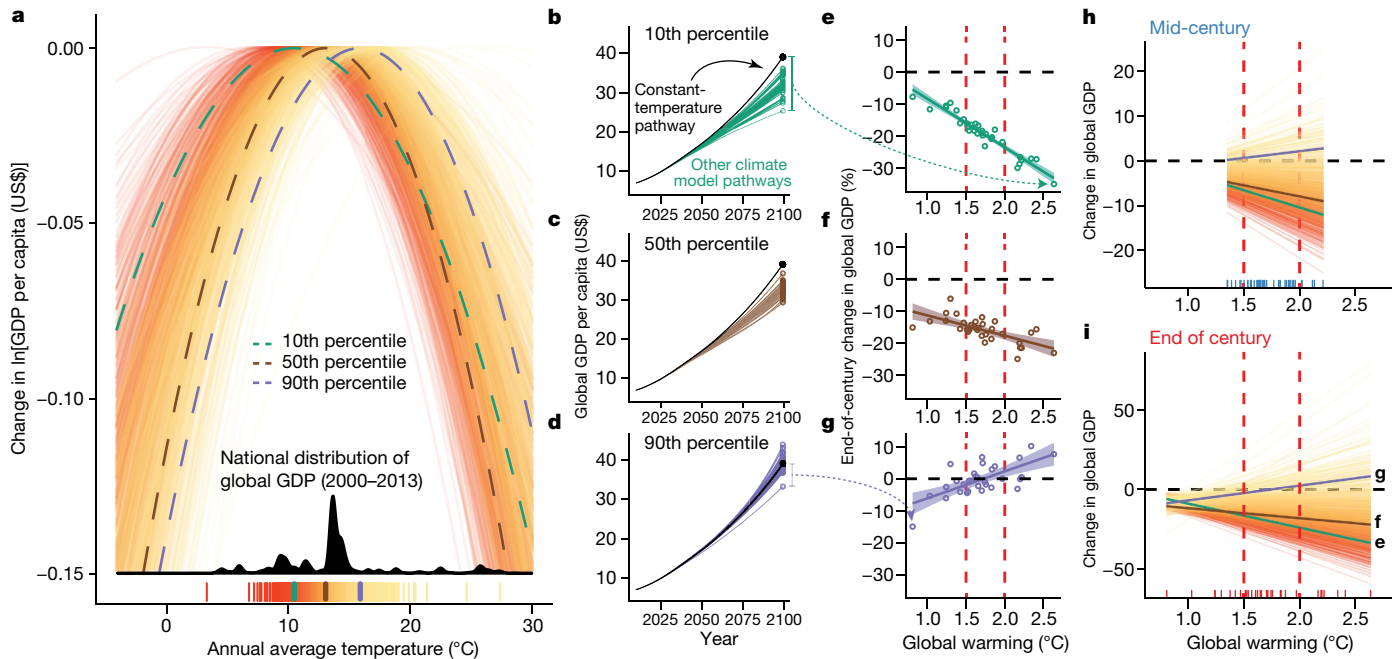


Fig. 1 | Deriving impact projections. **a**, Historical response of per capita GDP growth rates to temperature. Each curve is the response function estimated from one of 1,000 bootstraps of a historical regression with colour corresponding to the temperature at which it optimizes (redder colours for cooler optima). The green, brown and purple dashed curves highlight bootstraps at the 10th, 50th and 90th percentiles of optimizing temperatures, respectively. The rug plot at the bottom shows the distribution of optimizing temperatures across bootstraps using the same colour scheme. The density plot in black shows the GDP-weighted distribution of baseline average national temperatures. **b–d**, Projected future economic pathways under different historical response functions. Black lines represent the pathway of global GDP per capita, assuming no future warming. Coloured lines are pathways corresponding to the response functions at the 10th, 50th and 90th percentiles highlighted in **a**, under warming projections from 32 GCMs consistent with RCP2.6. Points represent values projected for 2099. **e–g**, Projected climate impact

on global GDP per capita by 2099 for the same response functions, equivalent to the percentage difference between the black points and coloured points in **b–d**. The warming on the *x* axes is the global warming projected for 2099 by GCMs running RCP2.6, relative to a pre-industrial benchmark. Red vertical dashed lines mark 1.5°C and 2.0°C warming. Linear ordinary least-squares models are fitted for each of the response functions, with the slope estimating the per-degree impact of global warming on global GDP per capita. Shaded areas represent the 95% confidence interval of the ordinary least-squares fit. **i**, The linear fits from **e–g**, but for all bootstrapped response functions instead of just the three highlighted in **b–g**. The colours correspond to the optimizing temperatures of the response functions, as in **a**. The rug plot at the bottom marks global warming for the end of the century (2099) projected by the 32 GCMs consistent with RCP2.6, equivalent to the *x*-axis values of points in **e–g**. **h**, Equivalent to **i** but for mid-century (2049) projections based on 42 GCMs consistent with RCP4.5.

representative concentration pathways, or RCPs). Each GCM realization contains a temperature trajectory for each country and, in aggregate, for the globe. Because temperature affects both the level and the growth rate of economic output^{4,11}, and because growth effects compound over time, the projected differential impacts of 1.5°C versus 2°C are a function of the time horizon. We calculate differential impacts under the two targets using temperature changes for the mid-century (2046–2065) and end-of-century (2081–2100) periods used by the IPCC, focusing on output from those RCPs whose ensemble range spans 1.5°C and 2°C for a given time period (Methods). We use projections from the relevant shared socioeconomic pathways (SSPs) to define the secular evolution of population and economic development^{6,19}, (Fig. 1b–d, Extended Data Fig. 2).

Economic impacts are calculated relative to a constant-temperature counterfactual and are then aggregated globally (weighting by population), resulting in a unique estimate of global impact for each bootstrap–GCM–SSP–year combination. We present two measures of these relative impacts: the percentage difference in annual GDP at the end of the chosen projection period and the discounted present value of absolute GDP differences accumulated over that span. For the second measure we employ a range of discounting schemes, including fixed rates of 2.5%–5% per annum (where a 5% discount rate assumes that society values a given amount of consumption in one year roughly 5% less than it values it today) and time-varying rates that depend on the levels of and uncertainty in realized growth (Methods).

We estimate the benefits of 1.5°C versus 2°C by fitting a linear least-squares regression relating either measure of relative economic impact

to the global warming projected by each GCM that archives the RCP (Fig. 1e–g). We repeat this procedure for every bootstrapped response function to arrive at a distribution of estimated impacts for the chosen combination of GCM, SSP and projection period. See Methods for a full derivation.

Most response functions generate more negative global impacts at 2°C than at 1.5°C (Fig. 1h–i, Extended Data Fig. 2). Cooler estimated historical optima (red colours) generate steeper negative responses to additional warming, implying greater benefits from more stringent mitigation. We estimate that limiting warming to 1.5°C instead of 2°C by mid-century would lead to an increase in global GDP of 1.5%–2.0% (median estimate; Fig. 2a) and US\$7.7–11.1 trillion in discounted avoided damages under a 3% fixed annual discount rate. Meeting these targets at the end of the century is estimated to lead to median gains in global GDP per capita of 3.4% and discounted avoided damages of US\$36.4 trillion.

We use the distributions of bootstrapped estimated impacts to quantify the probability that more stringent mitigation yields benefits of different magnitudes (Extended Data Table 1). We estimate that achieving the 1.5°C target at mid-century (2046–2065) would lead to a 68%–76% chance of overall cumulative net benefit relative to 2°C under a fixed 3% discount rate. Under the same discount rate, we estimate a 43%–53% chance of discounted cumulative benefits exceeding US\$10 trillion and a 4%–8% chance of exceeding \$30 trillion, which is about 40% of current global GDP. For the end of the century (2081–2100), we estimate a >75% chance of net gain in per capita global GDP, an approximately 38% chance that benefits exceed US\$50 trillion, and

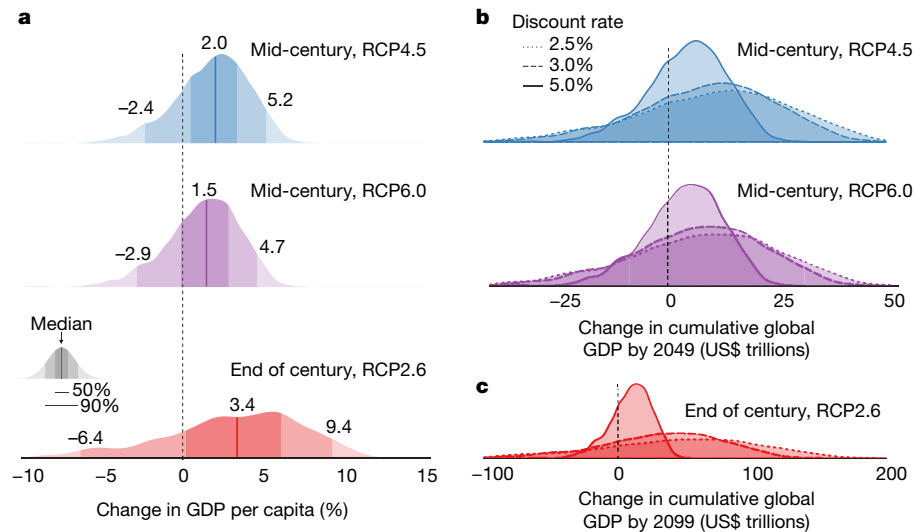


Fig. 2 | Global impact of limiting global warming to 1.5°C relative to 2°C. **a**, Probability distribution of the percentage change in global GDP per capita for 1.5°C versus 2°C by mid-century and by the end of the century, as derived from the slopes of the linear fits across response functions illustrated in Fig. 1h–i. Positive values indicate reduced damages at 1.5°C of global warming as compared to 2°C. Values above distribution

report percentage changes at the 10th, 50th and 90th percentiles of distribution. **b**, Probability distribution of the change in cumulative global GDP by mid-century, assuming discount rates of 2.5% (dotted line), 3% (dashed line) and 5% (filled line). **c**, The equivalent for the end of the century.

an approximately 5% chance that benefits exceed US\$100 trillion (3% discount rate; Extended Data Table 2).

While end-of-century estimates of the magnitude of absolute impacts are sensitive to choices about discounting (Extended Data Fig. 3, Extended Data Table 1), estimates of the probability of positive benefits

are much less so (Extended Data Tables 2 and 3). Results are also relatively insensitive to alternative bootstrap resampling approaches, to different SSPs, and to alternative assumptions about the time path of future warming for a given RCP (Extended Data Figs. 4, 5). Inclusion of additional lags of temperature in the historical regression—a common

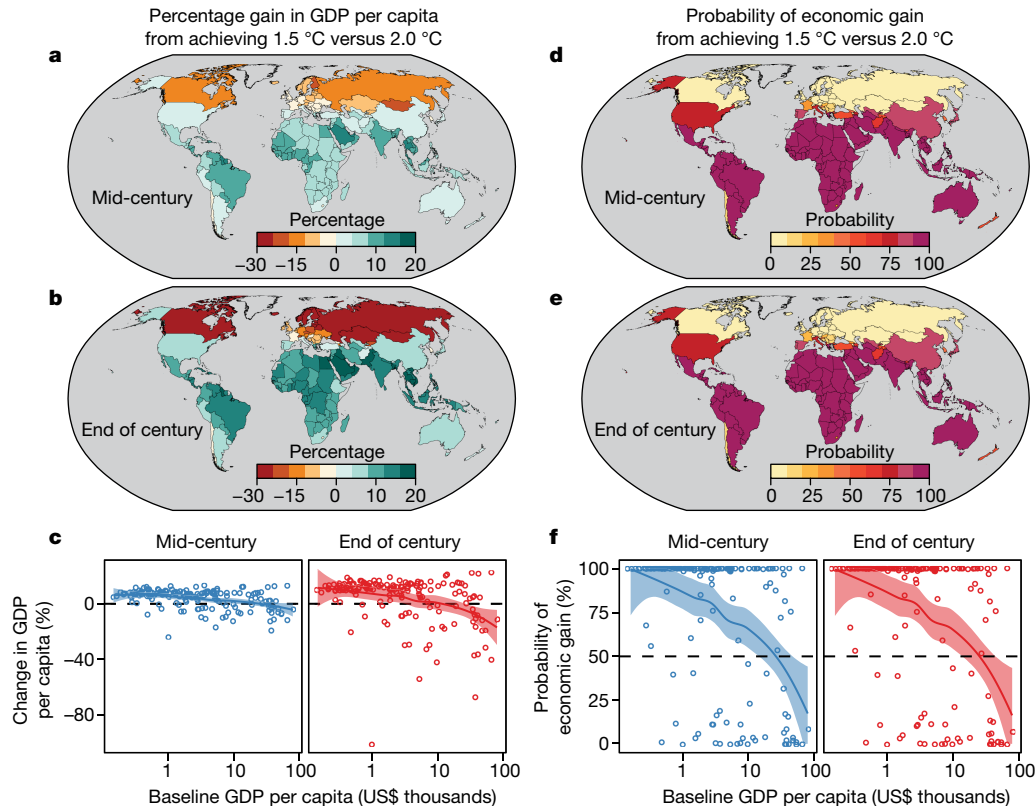


Fig. 3 | Country-level impact of limiting global warming to 1.5°C relative to 2°C. **a**, **b**, Median estimates of impacts on change in GDP per capita under 1.5°C versus 2°C, for mid-century and the end of the century. Positive values indicate reduced damages at 1.5°C of global warming as compared to 2°C. **c**, Median estimated impacts as a function of each country's baseline GDP per capita, with each country weighted equally.

Lines represent local polynomial regression fits to the data with the corresponding 95% confidence intervals shaded in grey. **d–f**, As in **a–c**, but for the probability of per capita GDP gain, calculated as the percentage of bootstrap response functions projecting a net gain in a country's GDP per capita under 1.5°C of global warming as compared to 2°C.

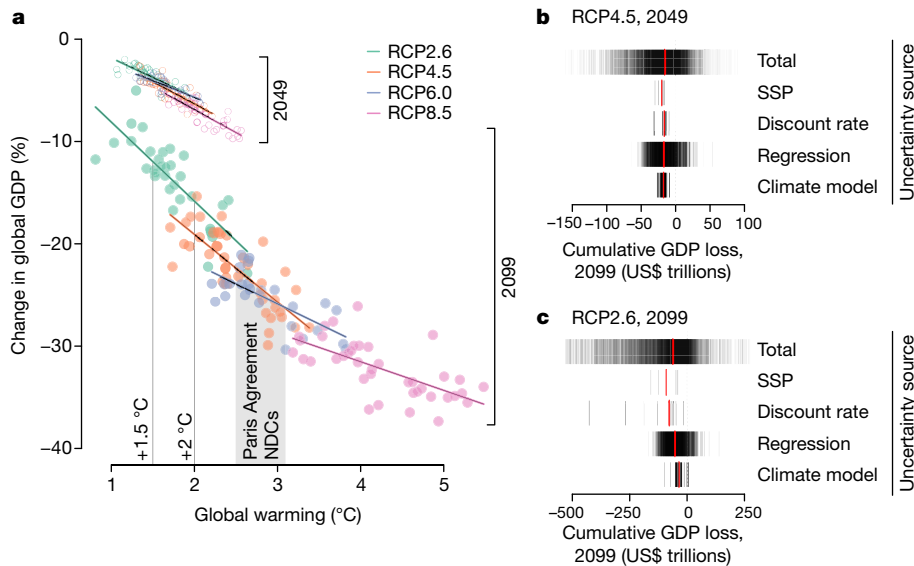


Fig. 4 | The impact of global warming on global GDP per capita, relative to a world without warming, for different forcing levels. a, Projected percentage change in global GDP for different climate models under different RCP forcing scenarios, relative to a no-warming baseline (median bootstrap, SSP1). Colours denote different RCPs. Unfilled points show mid-century projections, filled points show end-of-century projections. Vertical lines show the UN temperature targets as well as the range of estimates of end-of-century warming under current Paris commitments⁷. Warming is relative to pre-industrial levels. **b, c**, Sources of uncertainty in estimates of global warming on cumulative global GDP loss for a given forcing level. Total uncertainty in the impact of warming on global GDP under a given forcing scenario is a combination of uncertainty in how economies respond to warming ('historical

regression uncertainty'), uncertainty across climate models in the amount and pattern of warming for a given level of forcing ('climate model uncertainty'), uncertainty in baseline future growth rates across baseline socioeconomic scenarios ('SSP uncertainty'), and plausible alternatives for how to specify the discount rate ('discount rate uncertainty'). Values show cumulative global GDP losses in trillions of US\$ for mid-century under RCP4.5 (**b**) and the end of the century under RCP2.6 (**c**), either with all factors allowed to vary ('total uncertainty') or with the listed factor allowed to vary and all others fixed at their median (see Methods). Each vertical line is a point estimate; for example, with 32 climate models running RCP2.6 there are 32 estimates shown for 'climate model uncertainty' in **c**. Red lines are the median estimate across each uncertainty distribution.

approach to capturing persistent growth effects¹¹—amplifies the effect of temperature on growth rates and results in larger estimates of benefits under 1.5°C (Extended Data Fig. 4). Other potential sources of uncertainty, such as uncertainty in the secular rate of growth beyond the scenarios prescribed by the SSPs, were not quantified and could increase overall impact uncertainty.

At the country level, both the magnitude and the uncertainty of potential benefits are highly non-uniform. We find that 71% of countries—encompassing about 90% of projected global population—exhibit a >75% chance of experiencing positive economic benefits at 1.5°C relative to 2°C (Fig. 3), and 59% of countries exhibit a >99% chance. These countries include the three largest economies (the USA has a 76% chance of positive benefits; China 85%; Japan 81%) (Fig. 3, maps). They also include a large fraction of the world's poorest countries, with the likelihood of economic gains rising rapidly at lower levels of GDP per capita (Fig. 3c, f). Many of the countries that exhibit a high probability of economic benefits from 1.5°C are concentrated in the tropics and sub-tropics, where both current and future temperatures are warmer than the economic optimum⁴. As a result, even small reductions in future warming in these countries can generate substantial increases in per capita GDP, with many countries in the tropics exhibiting per capita GDP 10%–20% higher at 1.5°C than 2°C by the end of the century (Fig. 3a, b, d, e). The opposite is true for a smaller number of high-latitude countries, where 1.5°C is estimated to slow growth and generate a high probability of negative impacts relative to 2°C. Achieving the 1.5°C target will thus have unequal consequences, with today's poorest countries benefiting the most.

Despite the Paris Agreement's focus on the 1.5°C and 2°C targets, its actual Nationally Determined Contributions (NDCs) are instead consistent with 2.5–3°C of global warming⁷. We estimate that this level of warming could lead to a reduction in global GDP as high as 10% by mid-century and 15%–25% by the end of the century (median estimates across SSPs; Fig. 4 and Extended Data Fig. 6), relative to a world that

did not warm beyond 2000–2010 levels. In addition, failing to meet the NDC commitments is likely to lead to reductions in global GDP that exceed 25% by the end of the century. Uncertainty in these estimates is driven much more by uncertainty in economic parameters—namely, the economic response to warming and the discount rate—than by uncertainty in the pattern and magnitude of temperature change reflected in the climate model ensemble (Fig. 4b and c), highlighting the importance of better constraining these economic parameters²⁰.

Because our future impact estimates are based on observed historical economic responses to temperature variability, our projections will misstate impacts if the relationship between future annual temperatures and climatic extremes differs from what has occurred historically, or if future societies respond differently from societies in the recent past—although there is growing evidence that economic development might not fundamentally alter these economy–environment linkages^{4,15–17}. We also cannot account for historically unprecedented changes, such as large-scale loss of land ice and associated sea level rise, which are more likely to occur^{8,21} at 2°C than 1.5°C and are expected to exacerbate impacts^{22,23}.

To support policy decisions, our estimates of avoided damages need to be compared against the costs of meeting the UN targets. To our knowledge, no comparable estimates of global abatement costs through to the end of the century currently exist. However, a recent estimate²⁴ suggests that achieving emissions levels in 2030 that are consistent with the 1.5°C target will lead to approximately US\$300 billion in additional (non-discounted) abatement costs relative to emissions consistent with 2°C. This estimate of abatement costs is >30 times smaller than our median estimate of (discounted) mid-century avoided damages.

Not accounting for abatement costs, our results suggest that 1.5°C global warming is 'likely'²⁵ to result in substantial economic benefits relative to 2°C, with foregone damages probably in the tens of trillions of dollars and 59% of countries 'virtually certain'²⁵ to benefit. Given that most of these countries feature large populations or high poverty rates

or both, our results suggest that achieving more stringent mitigation targets will probably generate a net global benefit, with particularly large benefits for the poorest populations.

Online content

Any Methods, including any statements of data availability and Nature Research reporting summaries, along with any additional references and Source Data files, are available in the online version of the paper at <https://doi.org/10.1038/s41586-018-0071-9>.

Received: 2 August 2017; Accepted: 28 February 2018;

Published online 23 May 2018.

- UNFCCC Adoption of the Paris Agreement. I: Proposal by the President. Draft Decision CP.21 <https://unfccc.int/resource/docs/2015/cop21/eng/l09r01.pdf> (United Nations Office, Geneva, 2015).
- Nature Editorial Board. The maximum climate ambition needs a firm research backing. *Nature* **537**, 585–586 (2016).
- Hallegatte, S. et al. Mapping the climate change challenge. *Nat. Clim. Chang.* **6**, 663–668 (2016).
- Burke, M., Hsiang, S. M. & Miguel, E. Global non-linear effect of temperature on economic production. *Nature* **527**, 235–239 (2015).
- Collins, M. et al. in *Climate Change 2013: the Physical Science Basis: Working Group I Contribution to the Fifth Assessment Report of the Intergovernmental Panel on Climate Change* (eds Stocker, T. et al.) Ch. 12 (Cambridge Univ. Press, Cambridge, 2014).
- Riahi, K., van Vuuren, D. P. & Kriegler, E. The shared socioeconomic pathways and their energy, land use, and greenhouse gas emissions implications: an overview. *Glob. Environ. Change* **42**, 153–168 (2017).
- Rogelj, J. et al. Paris agreement climate proposals need a boost to keep warming well below 2 °C. *Nature* **534**, 631–639 (2016).
- Schleussner, C.-F. et al. Science and policy characteristics of the Paris Agreement temperature goal. *Nat. Clim. Chang.* **6**, 827–835 (2016).
- Rogelj, J., McCollum, D. L., Reisinger, A., Meinshausen, M. & Riahi, K. Probabilistic cost estimates for climate change mitigation. *Nature* **493**, 79–83 (2013).
- Hallegatte, S., Fay, M., Bangalore, M., Kane, T. & Bonzanigo, L. *Shock Waves: Managing the Impacts of Climate Change on Poverty* (World Bank Publications, Washington, 2015).
- Dell, M., Jones, B. F. & Olken, B. A. Temperature shocks and economic growth: evidence from the last half century. *Am. Econ. J. Macroecon.* **4**, 66–95 (2012).
- Schlenker, W. & Roberts, M. J. Nonlinear temperature effects indicate severe damages to US crop yields under climate change. *Proc. Natl Acad. Sci. USA* **106**, 15594–15598 (2009).
- Hsiang, S. M. Temperatures and cyclones strongly associated with economic production in the Caribbean and central America. *Proc. Natl Acad. Sci. USA* **107**, 15367–15372 (2010).
- Carleton, T. A. & Hsiang, S. M. Social and economic impacts of climate. *Science* **353**, aad9837 (2016).
- Deryugina, T. & Hsiang, S. M. *Does the Environment Still Matter? Daily Temperature and Income in the United States*. NBER working paper 20750 (National Bureau of Economic Research, Cambridge, 2014); <http://www.nber.org/papers/w20750>.
- Colacito, R., Hoffmann, B. & Phan, T. *Temperatures and Growth: A Panel Analysis of the United States*. IDB working paper IDB-WP-676 (Inter-American Development Bank, Washington, 2016); <https://publications.iadb.org/handle/11319/7654>.
- Zhang, P., Deschenes, O., Meng, K. & Zhang, J. Temperature effects on productivity and factor reallocation: evidence from a half million Chinese manufacturing plants. *J. Environ. Econ. Manage.* **88**, 1–17 (2018).
- Taylor, K. E., Stouffer, R. J. & Meehl, G. A. An overview of CMIP5 and the experiment design. *Bull. Am. Meteorol. Soc.* **93**, 485–498 (2012).
- O'Neill, B. C., Kriegler, E. & Ebi, K. L. The roads ahead: narratives for shared socioeconomic pathways describing world futures in the 21st century. *Glob. Environ. Change* **42**, 169–180 (2017).
- Burke, M. et al. Opportunities for advances in climate change economics. *Science* **352**, 292–293 (2016).
- Seneviratne, S. I., Donat, M. G., Pitman, A. J., Knutti, R. & Wilby, R. L. Allowable CO₂ emissions based on regional and impact-related climate targets. *Nature* **529**, 477–483 (2016).
- Cai, Y., Lenton, T. M. & Lontzek, T. S. Risk of multiple interacting tipping points should encourage rapid CO₂ emission reduction. *Nat. Clim. Chang.* **6**, 520–525 (2016).
- Hsiang, S. et al. Estimating economic damage from climate change in the United States. *Science* **356**, 1362–1369 (2017).
- Hof, A. F. et al. Global and regional abatement costs of nationally determined contributions (NDCs) and of enhanced action to levels well below 2 °C and 1.5 °C. *Environ. Sci. Policy* **71**, 30–40 (2017).
- Mastrandrea, M. D. et al. The IPCC AR5 guidance note on consistent treatment of uncertainties: a common approach across the working groups. *Clim. Change* **108**, 675 (2011).

Acknowledgements We thank L. Goulder, S. Hsiang and D. Lobell for comments. We thank the Erol Foundation for funding.

Reviewer information Nature thanks R. Kopp and the other anonymous reviewer(s) for their contribution to the peer review of this work.

Author contributions Author contributions: M.B. and N.S.D. designed the research. M.B., W.M.D. and N.S.D. analysed data, interpreted results and wrote the paper.

Competing interests The authors declare no competing interests.

Additional information

Extended data is available for this paper at <https://doi.org/10.1038/s41586-018-0071-9>.

Reprints and permissions information is available at <http://www.nature.com/reprints>.

Correspondence and requests for materials should be addressed to M.B.

Publisher's note: Springer Nature remains neutral with regard to jurisdictional claims in published maps and institutional affiliations.

METHODS

Deriving the historical response function. To understand the historical relationship between temperature and economic output, we assemble annual data on country-level GDP per capita from the World Bank's World Development Indicators, using data on 165 countries over the period 1960 to 2010. Growth is computed as the first difference of the natural logarithm of the annual purchasing power parity-adjusted per capita GDP series in each country. These data are then merged with temperature and precipitation data from the University of Delaware²⁶. The gridded monthly temperature and precipitation data are aggregated temporally to the annual level and spatially to the country level. We then follow ref.⁴ and estimate a panel fixed effects model:

$$\Delta \log(y_{it}) = \beta_1 T_{it} + \beta_2 T_{it}^2 + \lambda_1 P_{it} + \lambda_2 P_{it}^2 + \mu_i + v_t + \theta_{1i}t + \theta_{2i}t^2 + \varepsilon_{it} \quad (1)$$

where y_{it} is per capita GDP in country i in year t , T and P are the average temperature and precipitation in year t , μ_i are country-fixed effects (dummies) that control for time-invariant differences between countries, v_t are year-fixed effects that account for common global shocks in a given year, and $\theta_{1i}t + \theta_{2i}t^2$ are country-specific linear and quadratic time trends, which allow temperature and growth to evolve flexibly at the country level.

Equation (1) is estimated simultaneously on our global sample of country-years ($N = 6,584$). Point estimates for β_1 and β_2 are statistically significant in this regression ($\beta_1 = 0.0127$, standard error 0.0032, $P < 0.001$; $\beta_2 = -0.0005$, standard error 0.0001, $P < 0.001$).

Equation (1) assumes that there is a single response function (described by β_1 and β_2) that specifies the overall global relationship between income growth and changes in temperature, but that individual countries can respond differently to warming as a function of their average temperature (which can be seen by differentiating equation (1) with respect to temperature). Past work has shown that average temperature—rather than other correlated factors such as average income—is the main source of heterogeneity in how countries' income growth responds to changes in temperature and that estimates of β_1 and β_2 are highly robust to alternative specifications of the fixed effects and time controls⁴.

An additional concern is that countries trade with one another and that unobserved temperature shocks across a trading network might lead to biased coefficient estimates in equation (1). However, if temperature shocks are uncorrelated across trading partners, then estimates of β_1 and β_2 still represent unbiased estimates of own-country temperature shocks on output; if shocks are correlated across trading partners, then β_1 and β_2 represent reduced-form estimates of the net effect in a given country of correlated shocks across that country's trading network. The main concern for our analysis is if the future pattern of temperature change should not correspond to the spatial pattern of historical shocks; however, we are unaware of any relevant research in climate science.

To quantify uncertainty in estimates of β_1 and β_2 , we implement multiple bootstrapping strategies: (1) Sampling by country. From our list of 165 countries, draw (with replacement) a 165-element list of countries—which will omit some countries and contain duplicates of others—and retain all years of data for the selected countries; this is repeated 1,000 times, drawing a new country sample each time, re-estimating equation (1), and retaining estimates of β_1 and β_2 . This approach allows for arbitrary correlation in residuals within countries over time. (2) Sampling by year. This allows for potential cross-sectional correlation in residuals in a given year, and is also repeated 1,000 times. (3) Sampling by five-year block. We divide the data into 10 five-year blocks (that is, 1961–65, 1966–70, and so on through 2010), and sample with replacement from these 10 blocks. This allows for both temporal and cross-sectional dependence in residuals, for example, as caused by global recessions that last multiple years.

Our main results use strategy (1) (sampling by country), but we show that our results are robust, regardless of the strategy used. In what follows, the bootstrapped response functions $h^j(T_{it}) = \hat{\beta}_1^j T_{it} + \hat{\beta}_2^j T_{it}^2$ are indexed with j , where $j \in \{1, 2, \dots, 1,000\}$.

For each $h^j(T_{it})$, we define the 'temperature optimum' as the maximum of the quadratic function, that is, $\frac{-\hat{\beta}_1^j}{2 \times \hat{\beta}_2^j}$ (this is always a maximum because all estimates yield $\hat{\beta}_1^j > 0$ and $\hat{\beta}_2^j < 0$).

To ensure that equation (1) is capturing growth effects and not just level effects, we re-estimate equation (1) with additional lags of temperature (and their squares)^{4,11}. This is important because countries' economic output could 'catch up' in the year following a temperature shock; this catch-up behaviour would not be captured in a model containing only contemporaneous temperature variables, but would be captured in a model that includes lags of temperature and where overall temperature effects are computed by summing contemporaneous and lagged coefficients¹¹. We thus estimate equation (1) with up to five lags l of temperature, that is,

$$h^j(T_{it}) = \sum_{l=0}^5 \{\hat{\beta}_{1,l}^j T_{it-l} + \hat{\beta}_{2,l}^j T_{it-l}^2\} \quad (2)$$

and re-estimate all calculations below with results from these distributed lag models. Our main results with this sensitivity test are shown in Extended Data Fig. 4.

Climate model simulations. To follow the IPCC protocols, we analyse the exact climate model realizations and time periods used by the IPCC in its most recent assessment report⁵. These climate model realizations were generated by the World Climate Research Program under Phase Five of the Climate Model Intercomparison Project (CMIP5)¹⁸. For the historical baseline experiment, the CMIP5 protocol ran each climate model from the mid-1800s to 2005, using the historical climate forcings. For the future scenarios, the CMIP5 protocol used the RCPs, which assume different levels of climate forcing going forward in the 21st century. In total, there are four: RCP2.6, RCP4.5, RCP6.0 and RCP8.5.

Following the IPCC protocols, we use the same historical baseline period (1986–2005) and RCP future periods (2046–2065 and 2081–2100) as did the IPCC. In our bias correction method (see below), there are three RCPs whose global warming ranges are most consistent with the 1.5°C and 2°C targets in these IPCC scenario time periods: RCP4.5 and RCP6.0 during the 2046–2065 period, and RCP2.6 during the 2081–2100 period. (RCP2.6 is the only RCP scenario in which some models project global warming of less than 1.5°C for the end of the century; for mid-century, none of the RCP2.6 model runs project warming above 2°C, and so we do not utilize RCP2.6 for mid-century). We therefore calculate the distribution of GDP outcomes in response to the global warming levels projected during the 2046–2065 period of RCP4.5 and RCP6.0, and during the 2081–2100 period of RCP2.6. In addition, to compare the probability of economic impacts for the UN targets with the probability of those for higher levels of greenhouse gas emissions, we also calculate the distribution of GDP outcomes for the 2046–2065 and 2081–2100 periods of RCP8.5.

Uncertainty in the temperature-driven GDP impacts of a given level of greenhouse gas emissions arises from both uncertainty in the level of global warming associated with that level of emissions and uncertainty in the spatial pattern of temperature at that level of global warming. The IPCC climate analysis protocols span these uncertainty dimensions by analysing one realization of each climate model in each RCP scenario⁵. To follow the IPCC protocols, we analyse the same realizations as the IPCC.

However, it should be noted that the CMIP5 ensemble does not span the full range of each uncertainty dimension in a fully uniform framework. Rather, although the experimental conditions for the ensemble were coordinated between the modelling centres, both the models and the implementation of the simulation conditions vary across the ensemble. For example, the ensemble includes simulations from all national modelling centres that chose to participate, but not every modelling centre archived a simulation in each scenario. As a result, the IPCC selection of one realization of each model in each RCP yields different numbers of realizations—and model combinations—in each RCP (42 realizations in RCP4.5, 32 in RCP2.6, 25 in RCP6.0 and 39 in RCP8.5). Likewise, although each modelling centre conformed to a basic set of coordinated experimental conditions, the exact implementation of those conditions varied between the centres. This combination of coordinated but incomplete experimental uniformity has led the CMIP5 ensemble to be known as 'an ensemble of opportunity'. As in the IPCC, we leverage the CMIP5 ensemble of opportunity to estimate an approximate probability distribution; it should be emphasized that this approach is not identical to sampling across a probabilistic ensemble²⁷.

Because we use GDP data through 2010 and attempt to quantify economic impacts from that year forward, we must also project global and country-level temperature changes forward from the year 2010. To do so, and to control for individual climate model biases in average temperatures, we first calculate the difference between model-projected annual average future temperatures (in 2046–2065 or 2081–2100) and model-simulated annual average temperatures in the baseline 1986–2005 period. We then add those model-projected differences to the actual historical temperature observations.

For each climate model m corresponding to a chosen RCP scenario s at a given time period, we first calculate two quantities: (1) The magnitude of global temperature change ΔT^{sm} , which is the difference in annual average global surface temperature between a 1986–2005 baseline period and a future period (either 2046–2065 or 2081–2100). Gridded temperature projections relative to this baseline period are produced at 2.5° resolution. These are aggregated to a scalar 'global warming' projection by taking an average over all grid cells, with each cell g weighted by the cosine of the latitude of each cell g 's centrepoint L (given the convergence of lines of latitude towards the poles):

$$\Delta T^{sm} = \frac{\sum_g \{\cos(\bar{L}_g) \times (T_{g,\text{end}}^{sm} - T_{g,\text{base}}^{sm})\}}{\sum_g \cos(\bar{L}_g)} \quad (3)$$

(2) The magnitude of each country i 's temperature change ΔT_i^{sm} , analogously computed by taking the average projected temperature change of all cells g but

weighted by their share of country i 's population P_{ig} rather than by their relative surface area. Gridded population distribution data²⁸ is provided at 30-arc-second resolution and is aggregated to 2.5° resolution to match the temperature projection data. Thus, country-level temperature change projections are described by the equation:

$$\Delta T_i^{sm} = \frac{\sum_g \{P_{ig} \times (T_{g,end}^{sm} - T_{g,base}^{sm})\}}{\sum_g P_{ig}} \quad (4)$$

To express the future global-scale temperature values relative to pre-industrial values, as in the UN temperature targets, we add these model-projected differences between the future and the baseline to the global-scale warming that occurred between the pre-industrial period and the end of the period of GDP and temperature observations (which extends to 2010). According to the IPCC, the "globally averaged combined land and ocean surface temperature data as calculated by a linear trend, show a warming of 0.85 [0.65 to 1.06] °C, over the period 1880–2012," and the "total increase between the average of the 1850–1900 period and the 2003–2012 period is 0.78 [0.72 to 0.85] °C"²⁹. We therefore assume that 0.8 °C of warming took place between the pre-industrial period and the end of our observational period. Thus for the global averages ΔT^{sm} , "global warming relative to pre-industrial" is equal to $\Delta T^{sm} + 0.8$ for all s and m .

To generate annual country-specific time series of projected future changes in temperature for input into the simulations below, we assume that temperatures increase linearly between the base period and the end period, and then add the linearized projected change in temperature to the observed average baseline temperature, thus 'bias-correcting' future national temperature time series. Thus for a given climate model–RCP realization, if the observed average historical temperature during the base period is $\bar{T}_{i0} = \frac{\sum_{t=1986}^{2005} T_{it}}{2005 - 1986}$, then the projected temperature in each future year is:

$$\Delta T_{it}^{sm} = \bar{T}_{i0} + \frac{t - t_{base}}{t_{end} - t_{base}} \times \Delta T_i^{sm} \quad (5)$$

where $t_{base} = 2010$ is the initial year of our simulation and t_{end} is either 2049 or 2099. (As before, small t indexes time and capital T refers to temperature). The assumed linear temperature increase appears to be consistent with RCP 4.5 or 6.0 through mid-century; it is perhaps less consistent with RCP2.6 through the end of the century, as RCP2.6 warms through mid-century and then stabilizes through to the end of the century. To understand whether our assumed linear warming path distorts our findings for RCP2.6, we conduct an additional experiment in which we assume all warming under RCP2.6 occurs by 2049, and then temperatures stabilize at this new level between 2050 and 2099 (Extended Data Fig. 5). This scenario has the same projected global warming by the end of the century as our baseline RCP2.6 scenario, but all warming is assumed to happen in the first half of the 21st century. As shown in Extended Data Fig. 5, we find that the scenario with rapid initial warming worsens the overall impacts of climate change and increases the cumulative benefits of limiting warming to 1.5 °C versus 2 °C.

Defining counterfactual growth scenarios. To project growth in GDP absent climate change, we use projections from the SSPs, a framework developed to describe conditions associated with various degrees of climate forcing by the end of the century. In all, there are five SSP narratives, each making different assumptions about mitigation and adaptation challenges, demographic trends, and developments in the energy industry¹⁹. We exploit the time series of projected country-level economic growth and population from 2010 to 2095 associated with the SSP1 narrative, because this appears to be the SSP most consistent with the forcing levels required to achieve 1.5 °C warming in 2049 or 2099⁶ (although, as pointed out by ref. ⁶, with high enough carbon pricing all SSPs could potentially be consistent with 1.5 °C warming by mid-century, and three SSPs could be consistent with 1.5 °C warming by the end of the century). SSP1 is described as an optimistic future with 'low' challenges to adaptation and mitigation. SSP1 is characterized by many developing countries contributing an increasingly large share of global GDP by the end of the century (Extended Data Fig. 1a and b), with a larger share of total global GDP projected to be produced in countries with warmer average temperatures by the end of the century absent climate change (Extended Data Fig. 1c). In addition to using SSP1, we also test the robustness of our results to alternative choices from the other four SSPs (Fig. 4 and Extended Data Fig. 6).

Projecting economic impacts of 1.5 °C versus 2 °C. *Step (1). Assemble input data.* Required input data are the parameters of each response function $h^j(T_{it})$ estimated from each of the j bootstraps of equation (1); projections of country-year average temperature T_{it}^{sm} for each GCM m for a given RCP scenario s through to 2049 or 2099; projections of baseline country-year per capita growth rates λ_{it}^{κ} and populations ω_{it}^{κ} through 2099, for each country i and year t , from a given SSP scenario κ . *Step (2). Calculate country-specific growth trajectories for each bootstrap–RCP–GCM–SSP combination.* Projections are initialized using average temperature

and GDP per capita between 2000–2010 as the baseline for each of the countries in our analysis. For a given historical bootstrap run j and GCM–RCP–SSP projection $sm\kappa$, GDP per capita y in each future year $t + 1$ in country i is projected by the equation:

$$y_{it+1}^{j,sm\kappa} = y_{it}^{j,sm\kappa} \times (1 + \lambda_{it+1}^{\kappa} + \varphi_{it+1}^{\kappa}) \quad (6)$$

where λ_{it+1}^{κ} is the level of economic growth projected by the data corresponding to the particular SSP series and $\varphi_{it+1}^{j,sm\kappa} = h^j(T_{it+1}^{sm}) - h^j(T_{i0})$ is the additional estimated change in the growth rate due to the projected temperature increase above baseline for bootstrap run j and GCM projection ms . We also run a counterfactual no-warming scenario where temperatures are fixed at baseline levels, that is, $T_{it+1} = T_{i0}$ and $\phi_{it} = 0$ for all i and t :

$$y_{it+1}^{0,\kappa} = y_{it}^{0,\kappa} \times (1 + \lambda_{it+1}^{\kappa}) \quad (7)$$

With 165 countries, 1,000 bootstrap estimates of the temperature response function $h(\cdot)$, 100 total temperature time series (corresponding to 42, 25 and 32 climate models for mid-century RCP4.5, mid-century RCP6.0, and end-of-century RCP2.6, respectively, plus the constant-temperature series), five SSPs, and five bootstrap resampling schemes, we analysed more than 400 million distinct country-level economic pathways.

Step (3). Calculate global GDP trajectories for each bootstrap–RCP–GCM–SSP combination. For each GCM–bootstrap–SSP combination in a given period t , global GDP per capita is calculated as the average GDP per capita across countries, weighted by share of world population:

$$y_t^{j,sm\kappa} = \sum_i \frac{\omega_{it}^{\kappa}}{\omega_t^{\kappa}} \times y_{it}^{j,sm\kappa} \quad (8)$$

where $\frac{\omega_{it}^{\kappa}}{\omega_t^{\kappa}}$ is country i 's projected share of global population in year t for a given SSP. We similarly produce a time series of total global GDP by replacing $\frac{\omega_{it}^{\kappa}}{\omega_t^{\kappa}}$ with ω_{it}^{κ} , the country i 's projected population in that year. This is also calculated for the no-warming scenario, yielding counterfactual global GDP time series $y_t^{0,\kappa}$ and $Y_t^{0,\kappa}$, where Y_t denotes GDP.

Step (4). Calculate projected percentage changes in GDP or global GDP relative to the no-warming counterfactual for each bootstrap–RCP–GCM–SSP combination. For each bootstrap–RCP–GCM–SSP combination, we calculate the warming-induced percentage change in GDP relative to the counterfactual no-warming scenario in each country as:

$$\Psi_{it}^{j,sm\kappa} = \frac{y_{it}^{j,sm\kappa}}{y_{it}^{0,\kappa}} - 1 \quad (9)$$

This is calculated for $t = 2049$ for RCP4.5 and RCP6.0, and $t = 2099$ for RCP2.6. The percentage impact on global GDP per capita, $\Psi_t^{j,sm\kappa}$, is calculated similarly for these endpoint years.

Step (5). Calculate projected discounted absolute changes in GDP or global GDP relative to the no-warming counterfactual for each bootstrap–RCP–GCM–SSP combination. The cumulative absolute dollar impact of warming is calculated for each country by taking the annual difference between the unique bootstrap–RCP–GCM–SSP projected GDP time series and the counterfactual no-warming time series, and discounting these differences back to present:

$$\Theta_i^{j,sm\kappa} = \sum_t \frac{Y_{it}^{j,sm\kappa} - Y_{it}^{0,\kappa}}{(1 + r_t)^{t-t_0}} \quad (10)$$

where $Y_{it}^{j,sm\kappa} = y_{it}^{j,sm\kappa} \times \omega_{it}^{\kappa}$ and r_t is the social discount rate that could vary with t . The global absolute impact is calculated by summing country-level impacts: $\Theta^{j,sm\kappa} = \sum_i \Theta_i^{j,sm\kappa}$.

Given the long-running and unresolved debate over how r should be specified, we calculate $\Theta_i^{j,sm\kappa}$ under a range of approaches to specifying r . Specifically, we implement a variety of approaches discussed and implemented by previous authors, including implementations of the Ramsey equation with and without uncertainty and under alternate parameter choices for time preference and the marginal utility of consumption^{30–34}, calibrations to historical market interest rates in the USA^{35,36}, and constant discount rates³⁷ ranging from 2.5%–5%. Choices about the discount rate clearly have large implications for the estimation of damages. For instance, US\$1,000 of damages in 50 years is worth US\$228 today under a 3% annual discount rate, but only US\$87 under a 5% annual rate.

As described by multiple authors^{33,34,38}, choices about r can be approached from the perspective of a social planner wishing to maximize the welfare of society. The central intuitions in this approach are that extra income or consumption is worth more to poor people than it is to rich people, and that with rising incomes a dollar

of additional income is worth less in the future than it is today. Under standard assumptions about the functional form of the 'utility function' that relates changes in consumption to changes in utility, this approach yields the Ramsey formula, which specifies the annual discount rate on consumption as:

$$r = \rho + \eta g \quad (11)$$

where ρ is the pure or social rate of time preference (the rate at which society discounts the utility of future generations), η is the elasticity of marginal utility of consumption (or how fast the utility of consumption declines as consumption increases), and g is the growth rate in consumption. If there is uncertainty about the growth rate in consumption, a third term is added to the Ramsey equation which induces a precautionary savings effect³⁴:

$$r = \rho + \eta g - 0.5\eta^2 \sigma_g^2 \quad (12)$$

where σ_g^2 is the variance in the growth rate. Uncertainty in future consumption growth enters negatively as the social planner, facing the possibility of slow future growth, wishes to transfer more resources to the future.

Using equations (11) and (12) and parameter choices about ρ and η from three benchmark studies^{30–32} (Stern $\rho = 0.1, \eta = 1$; Nordhaus $\rho = 1, \eta = 2$; and Weitzman $\rho = 2, \eta = 2$; see Extended Data Fig. 1), we implement six versions of the Ramsey approach—three without uncertainty in future growth and three with uncertainty. For each bootstrap–RCP–GCM–SSP run, we define the growth rate g_t as the population-weighted average growth rate of GDP per capita:

$$g_t^{jsmk} = \sum_i \frac{\omega_i^{\kappa}}{\omega_i^{\kappa}} (1 + \lambda_{it}^{\kappa} + \varphi_{it}^{jsm}) \quad (13)$$

with parameters defined as in equations (6) and (8) above. Average values across GCMs are shown in Extended Data Fig. 1a. Uncertainty in the growth rate for each future year is calculated as $\sigma_{g_t}^2 = \text{var}(g_t^{jsmk})$, that is, the variance in projected growth rates in a given year across all bootstrap–RCP–GCM–SSP estimates. This probably represents a substantial lower bound on the true uncertainty in the growth rate, as it accounts only for uncertainty induced by additional warming and not for uncertainty in the underlying secular rate of growth (for which the SSPs do not provide uncertainty estimates).

Parameter choices and estimates of future growth rates are then used in either equation (11) or (12) to calculate year-specific discount rates r_t . The resulting estimates of Ramsey-based discount rates are shown in Extended Data Fig. 1b. All versions estimate higher interest rates in earlier periods, which is primarily a result of higher estimated baseline (SSP) growth rates in the earlier half of the century. Discount rates by end of century using the Ramsey approach range from 1.2% (Stern) to 4.2% (Weitzman), with the inclusion of the uncertainty term lowering discount rates only slightly.

Given that future baseline growth rates in developing and developed countries could be different, and given that the marginal effect of warming will probably differ between developing and developed countries given their different baseline temperatures, we also run scenarios where discount rates are allowed to differ between rich and poor countries (defined as being below or above the median level of GDP per capita at baseline). Specifically, using SSP1 data we produce separate population-weighted growth series for poor and rich countries (as shown in Extended Data Fig. 1c), and plug these growth projections into the Ramsey equation for each of the three benchmark choices of ρ and η to produce the six time series of discount rates that appear in Extended Data Fig. 1d. These income-specific discount rates, which are higher for poor countries than for rich countries given differences in baseline growth rates, are then applied to the relevant country groupings in the calculations below. As shown in Extended Data Fig. 3, allowing for income-specific discount rates results in higher median estimates of the global benefit of restricting warming to 1.5°C. This is because global benefits are driven largely by impacts in the largest economies, including the USA and China, and allowing for income-specific discount rates lowers the rates for rich countries relative to the pooled scheme (for example, compare Extended Data Fig. 1b against Extended Data Fig. 1d), which translates to larger cumulative benefits in large economies projected to be harmed by warming (which again includes both the USA and China).

Beyond the Ramsey framework, another approach to specifying the discount rate uses the observed evolution of market interest rates over long periods combined with models of interest rate behaviour to project interest rates. We extract estimates from two of these exercises^{35,36}, both of which assume an initial interest rate of 4% and then project interest rates to fall by almost half by end of century (Groom and Newell-Pizer; Extended Data Fig. 1b). Unlike for the Ramsey discount rates, we assume these market discount rates are the same across bootstrap–RCP–GCM–SSP combinations, and just vary over time as shown in the plot.

For each bootstrap–RCP–GCM–SSP combination, each of these fourteen discount rates (six Ramsey with global average income, three Ramsey with rich/poor differences, two market-based, and fixed rates of 2.5%, 3% and 5%) are calculated for each and used in equation (10) to calculate the present value (in 2010) of the damages from warming.

Step (6). Calculate percentage or absolute damages at 1.5°C versus 2°C. To calculate relative damages at 1.5°C versus 2°C for a given bootstrap–RCP–SSP combination, we take estimates of percentage impacts Ψ_i^{jsmk} or discounted absolute impacts Θ_i^{jsmk} across GCMs and fit a linear least-squares regression that relates estimated damages to the amount of global warming projected by the climate model by the end of the projection period (ΔT^{sm}). So for absolute damages in a given country, this regression is:

$$\Theta_i^{jsmk} = \beta_i^{jsc} \Delta T^{sm} + \varepsilon_i \quad (14)$$

This relation is shown to be well approximated at the global level by a linear model (Fig. 1e–g). The slope of the linear fit β_i^{jsc} is that bootstrap's estimate of the per-degree-Celsius impact of global temperature change on GDP per capita in country i . Halving this value thus gives us the impact of a half-degree change in global temperature for a given bootstrap, which, given linearity, is the estimated impact of limiting global warming to 1.5°C relative to 2.0°C in that country. Equation (14) is then re-estimated for each country and for each bootstrap, generating 1,000 estimates of impacts in each country for each RCP and SSP combination. We also estimate equation (14) at the global level to generate comparable results on percentage and absolute damages to global GDP. Global results are shown in Figs. 1 and 2, and country-level results are shown in Fig. 3a and b.

Step (7). Calculate probability of economic benefits of limiting warming to 1.5°C versus 2°C. Finally, we calculate the probability of economic gain under the 1.5°C versus 2°C scenarios—that is, the probability that damages from 1.5°C of global warming will be smaller than damages from 2°C of global warming—as the fraction of estimates of β_i^{jsc} across 1,000 bootstrap runs that are negative. This is calculated for the world as a whole, as well as separately for each country (Fig. 3c and d).

Quantifying impacts of global warming beyond 2°C. Recent estimates suggest that countries' current mitigation commitments (NDCs) are unlikely to limit global warming to 2°C and are instead more likely to be consistent with warming in a 2.5–3°C range⁷. To evaluate the impact of warming under these alternative warming outcomes, as well as for warming that exceeds 3°C, we recalculate estimates of Ψ_i^{jsmk} and Θ_i^{jsmk} across all RCPs s and for all SSPs κ . This provides estimates of the global impact of various warming scenarios relative to a no-warming counterfactual.

As shown in Fig. 4 and Extended Data Fig. 6, impacts are larger at higher levels of warming, with estimates suggesting that if current NDCs are achieved, global GDP could be 15%–25% lower by the end of the century as compared to a world that did not warm. Impacts for warming beyond 3°C are even larger, but decline less steeply at the highest levels of warming (consistent with ref. 4). This is because for hot countries that are substantially harmed by high levels of warming, GDP levels are bounded below by zero, whereas for cold countries that are substantially benefited by future warming, GDP levels can grow unbounded.

Quantifying sources of uncertainty in overall impacts of global warming. Our impact estimates (for example, on discounted global world product Θ^{jsmk} from equation (10) above) are derived by combining historical regression results, future climate change projections from climate models, assumptions on baseline future growth rates from SSPs, and discount rates. Each of these has associated uncertainty, which we propagate throughout the analysis. In particular, total uncertainty in the impact of warming on global GDP under a given forcing scenario is a combination of uncertainty in how economies respond to warming (what we term 'historical regression uncertainty'), uncertainty across climate models in the amount and pattern of warming for a given level of forcing ('climate model uncertainty'), uncertainty in baseline future growth rates across SSPs ('SSP uncertainty'), and plausible alternatives for how to specify the discount rate ('discount rate uncertainty'). To quantify the relative contribution of each to overall impact uncertainty under a given level of forcing (RCP), we hold three out of four variables fixed and allow the fourth to vary. Variables are fixed as follows: historical regression uncertainty is fixed at the regression point estimate, discount rates are fixed at 3%, the SSP is fixed at the SSP providing the median impact estimate (typically SSP3), and the climate model projection is fixed at the model giving the median global warming projection for either mid-century or the end of the century.

Results for discounted cumulative global GDP loss due to warming are shown in Fig. 4b–d. For both 2049 (RCP4.5) and 2099 (RCP2.6), historical regression uncertainty—that is, uncertainty in how economies have responded to warming in the recent past—is the dominant source of uncertainty in overall impact projections for a given forcing level, followed by uncertainty due to alternative possible specifications of the discount rate. For instance, holding all other sources of uncertainty fixed for the end of the century, historical regression uncertainty alone leads to a 95% confidence interval of impact estimates of –US\$122 trillion to

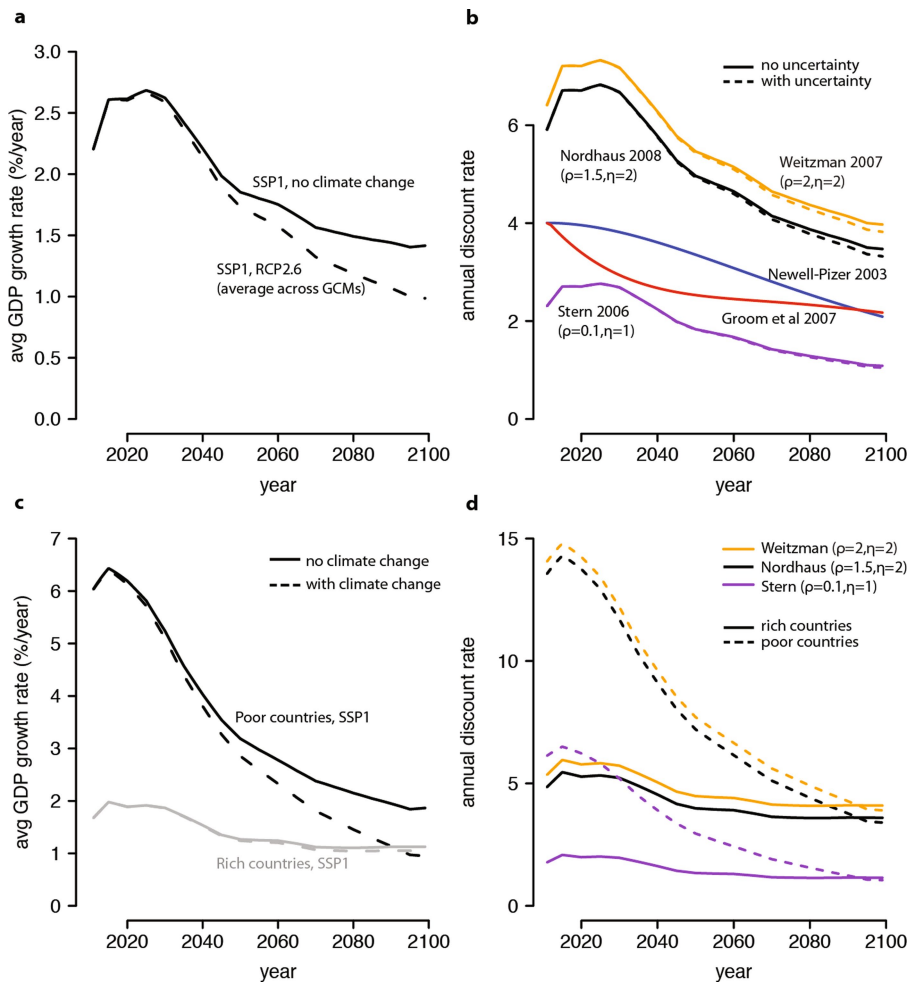
US\$32 trillion, discount rate uncertainty to a 95% confidence interval of –US\$375 trillion to –US\$25 trillion, and climate model uncertainty to a 95% confidence interval of –US\$78 trillion to US\$4 trillion. Thus the overall uncertainty in impacts induced by uncertainty in economic parameters is around 2–4 times higher than that resulting from climate model uncertainty.

There are multiple caveats to this analysis, including that historical uncertainty would be larger if regression models with additional lags were also included, and that discount rate uncertainty could be understated if our 14 alternative discounting approaches do not span the range of ‘plausible’ discount rates.

While further constraining the range of plausible discount rates is perhaps challenging, not least owing to ethical considerations central to the choice of social-welfare-based discount rates³³, reducing uncertainty around how economies will respond to warming could be more tractable. Promising avenues could include detailed empirically based bottom-up assessments of climate impacts at the country level²³, leveraging existing sub-national or firm (company)-level data to estimate impacts^{15,17}, or using new fine-scale remote-sensing-based estimates of economic output to greatly increase the temporal and spatial specificity of outcome measurements^{39,40}.

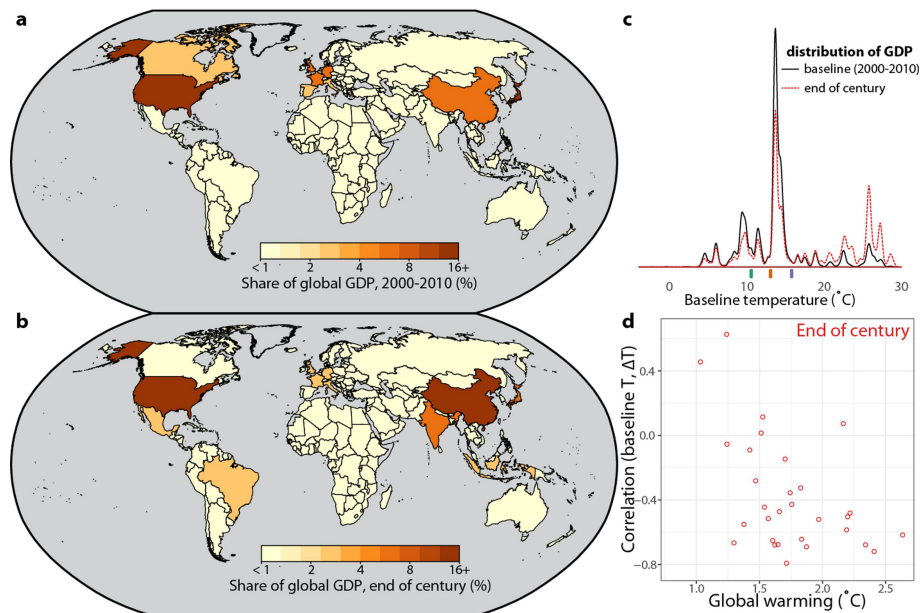
Data availability. All data and code that support the findings of this study are available at <https://purl.stanford.edu/vn535jm8926>.

26. Matsuura, K. & Willmott, C. J. *Terrestrial Air Temperature: 1900–2010 Gridded Monthly Time Series* (version 3.01) (Center for Climatic Research, Univ. Delaware, Newark, 2012); <http://climate.geog.udel.edu/~climate/>.
27. Tebaldi, C. & Knutti, R. The use of the multi-model ensemble in probabilistic climate projections. *Phil. Trans. R. Soc. Lond. A* **365**, 2053–2075 (2007).
28. Balk, D. et al. Determining global population distribution: methods, applications and data. *Adv. Parasitol.* **62**, 119–156 (2006).
29. Hartmann, D. L. et al. Observations: atmosphere and surface. In *Climate Change 2013: the Physical Science Basis: Working Group I Contribution to the Fifth Assessment Report of the Intergovernmental Panel on Climate Change* (eds Stocker, T. et al.) (Cambridge Univ. Press, Cambridge, 2013).
30. Stern, N. *The Economics of Climate Change: The Stern Review*. (Cambridge Univ. Press, Cambridge, 2006).
31. Weitzman, M. A review of the Stern review on the economics of climate change. *J. Econ. Lit.* **45**, 703–724 (2007).
32. Nordhaus, W. D. *A Question of Balance: Weighing the Options on Global Warming Policies*. (Yale Univ. Press, Yale, 2008).
33. Goulder, L. H. & Williams, R. C. III The choice of discount rate for climate change policy evaluation. *Clim. Change Econ.* **3**, 1250024 (2012).
34. Arrow, K. J. et al. Should governments use a declining discount rate in project analysis? *Rev. Environ. Econ. Policy* **8**, 145–163 (2014).
35. Newell, R. G. & Pizer, W. A. Discounting the distant future: how much do uncertain rates increase valuations? *J. Environ. Econ. Manage.* **46**, 52–71 (2003).
36. Groom, B., Koundouri, P., Panopoulou, E. & Pantelidis, T. Discounting the distant future: how much does model selection affect the certainty equivalent rate? *J. Appl. Econ.* **22**, 641–656 (2007).
37. Greenstone, M., Kopits, E. & Wolverton, A. Developing a social cost of carbon for us regulatory analysis: a methodology and interpretation. *Rev. Environ. Econ. Policy* **7**, 23–46 (2013).
38. Quiggin, J. Stern and his critics on discounting and climate change: an editorial essay. *Clim. Change* **89**, 195–205 (2008).
39. Henderson, J. V., Storeygard, A. & Weil, D. N. Measuring economic growth from outer space. *Am. Econ. Rev.* **102**, 994–1028 (2012).
40. Jean, N. et al. Combining satellite imagery and machine learning to predict poverty. *Science* **353**, 790–794 (2016).



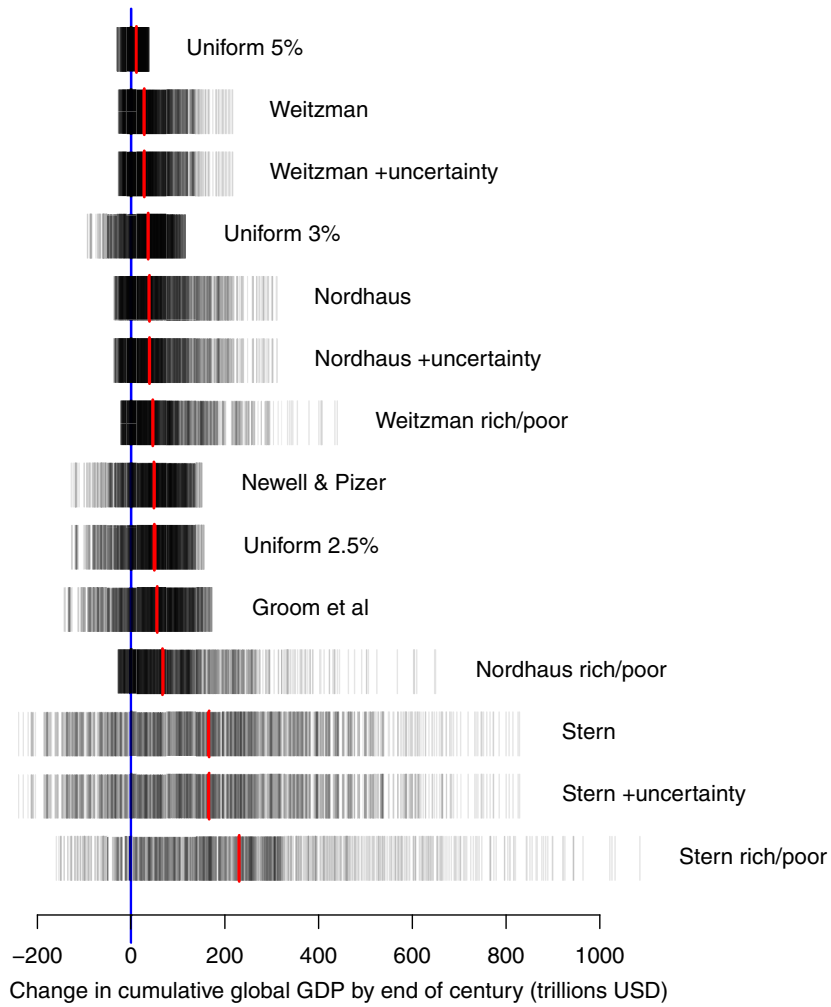
Extended Data Fig. 1 | Discount rate scenarios used in calculation of cumulative discounted impacts of future warming. **a**, Projected global average annual growth rates under SSP1 with and without climate change; estimates are averaged across bootstraps and climate models. Projected growth rates with climate change are used to define future consumption growth in Ramsey-based discount rates. **b**, Evolution of discount rates under different schemes through 2099. Ramsey-based schemes are Stern³⁰, Weitzman³¹ and Nordhaus³², with corresponding assumptions

about the pure rate of time discount ρ and the elasticity of marginal utility of consumption η shown in parentheses. Dashed lines are versions of these Ramsey-based discounting schemes that account for growth-rate uncertainty. Non-Ramsey schemes are Newell and Pizer³⁵ and Groom³⁶. **c**, Projected average annual growth rates separately for rich and poor countries under SSP1, with and without climate change. **d**, Corresponding Ramsey-based discount rates calculated separately for rich and poor countries, using income-specific growth rates from **c**.



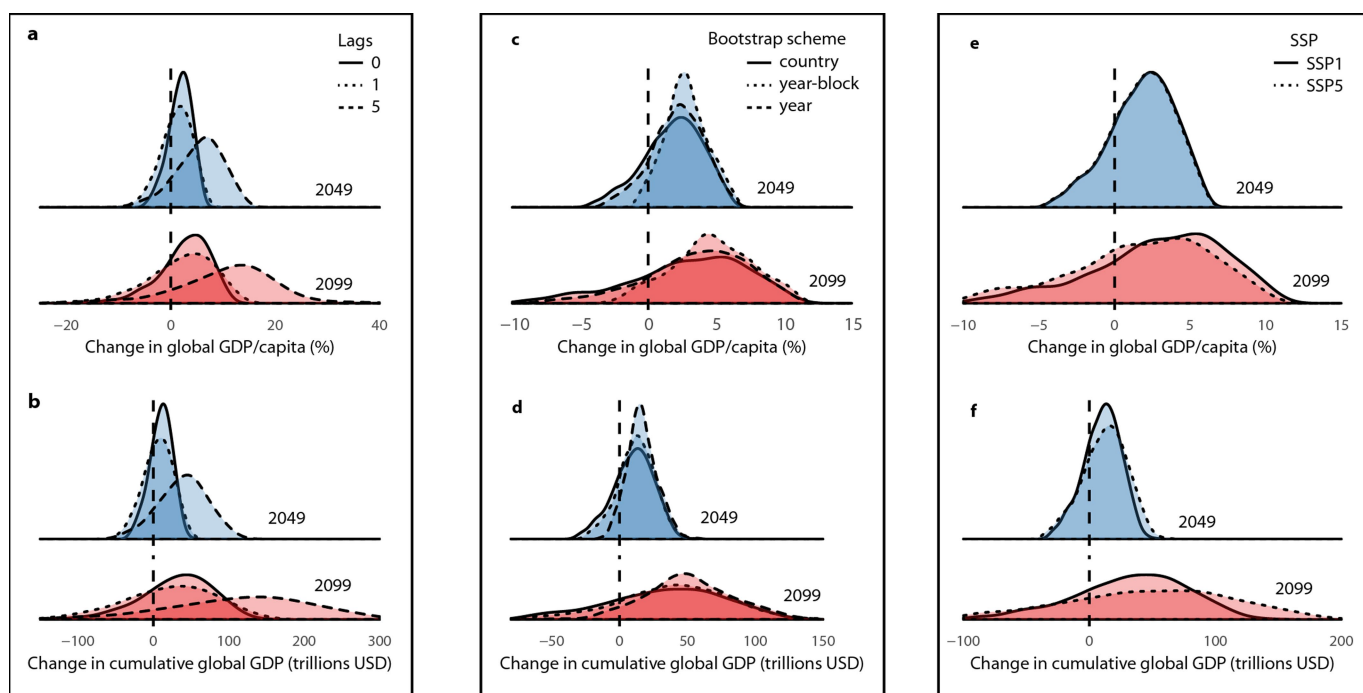
Extended Data Fig. 2 | Global GDP impacts can be negative at +1 $^{\circ}\text{C}$ but positive at +2 $^{\circ}\text{C}$ for some high-temperature-optimum bootstrap runs. a, b, Country share of global GDP at baseline (a) and by the end of the century (b) under SSP1, assuming no climate change. **c,** Distribution of global GDP by temperature, under baseline (black) and the end of the century SSP1 without climate change (red dashed); absent climate change, a substantial portion of global GDP is projected to be produced in countries with hotter average temperatures. **d,** Climate-model-predicted average global warming under RCP2.6 by the end of the century (x axis) versus the correlation between country-level baseline average temperature and country-level predicted warming in each model. In models that warm less at the global scale, countries that are currently warm tend to exhibit relatively larger warming, while in models that warm more at the global scale, countries that are currently cool tend to exhibit relatively larger warming. Future impacts on global GDP are a sum of country-specific impacts, which are a function of where each country is on the temperature

response function (Fig. 1a) and the projected amount of future warming in that country; a given percentage impact in a country with a large GDP has a larger effect on global GDP than the same percentage impact in a country with small GDP. For high-temperature-optimum response functions (for example, Fig. 1g), impacts can be negative at +1 $^{\circ}\text{C}$ but positive at +2 $^{\circ}\text{C}$ because (i) absent climate change, a much larger proportion of total global GDP is projected by SSP1 to be produced in countries that are currently warmer than the optimum, and (ii) climate models with lower overall global warming projections under RCP2.6 tend to have higher relative warming in countries that are currently warm. This generates negative impacts at about 1 $^{\circ}\text{C}$, where impacts are dominated by negative effects in warm countries (largely in the developing world), but positive impacts at about 2 $^{\circ}\text{C}$, where high-latitude countries instead warm disproportionately and experience benefits that outweigh the damages in tropical countries.



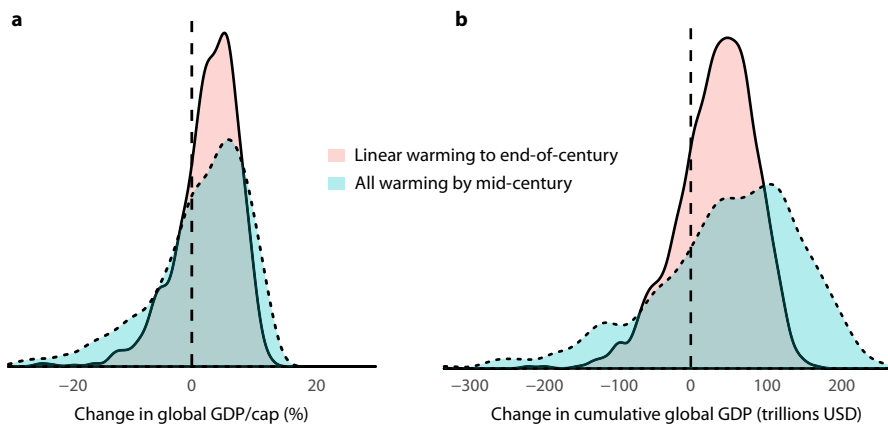
Extended Data Fig. 3 | Change in cumulative global GDP under 1.5°C versus 2°C global warming by the end of the century under different discounting schemes. Positive values indicate benefits (reduced losses) at 1.5°C versus 2°C. Each vertical line corresponds to a bootstrap

estimate of benefits under each discounting scheme^{30–32,35,36}. Red lines indicate median across bootstraps for each discounting scheme. Uniform schemes correspond to those in Extended Data Table 1; other schemes are described in Methods.



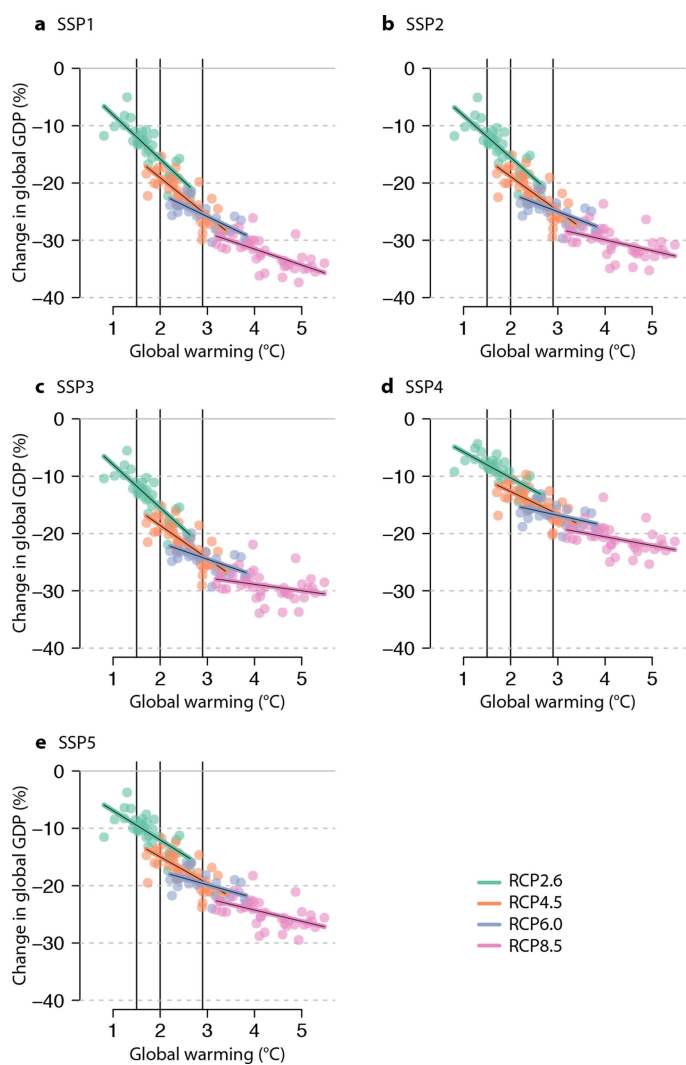
Extended Data Fig. 4 | Robustness of results to alternative specifications. Change in global GDP per capita in 2049 and 2099 based on regression models that include 0, 1 or 5 lags (**a** and **b**); bootstrap schemes that sample by country, five-year block or single year (**c** and **d**); or

alternative SSPs (**e** and **f**). Top panels show percentage changes in global GDP per capita under 1.5°C versus 2°C; the bottom panels show change in cumulative global GDP in US\$ trillions under a 3% discount rate.



Extended Data Fig. 5 | Robustness under alternative warming paths. Benefit—in terms of per capita GDP (**a**) and cumulative GDP (**b**)—of 1.5°C versus 2°C by end of century under the baseline assumption that overall projected warming occurs linearly between the baseline year and 2099 (pink), versus projected benefit assuming that all projected warming occurs by 2049 and temperatures remain constant thereafter (blue). Both

scenarios have the same projected global warming by the end of the century. For the same level of overall warming by the end of the century, scenarios with rapid initial warming worsen the overall impacts of climate change and increase the cumulative benefits of limiting warming to 1.5°C versus 2°C.



Extended Data Fig. 6 | Projected change in global GDP (%) under global warming by the end of the century, for each SSP. Panels a–e show the change in GDP for different climate models under different RCP forcing scenarios, relative to a no-warming baseline (median bootstrap) for SSPs 1–5, respectively. Results are as in Fig. 4a, but for each SSP. Each dot represents an RCP-climate model projected change in global GDP under a given SSP; colours represent the four RCPs. Lines are least-squares fits to the points corresponding to the different RCPs with matching colour scheme. The three vertical black lines denote the 1.5°C target, the 2°C target and the median-estimated warming expected under current Paris commitments (2.9°C)⁷. Warming is relative to pre-industrial levels.

Extended Data Table 1 | Change in cumulative global GDP (in US\$ trillions) under 1.5°C versus 2°C global warming by the end of the century under different discounting schemes

discount scheme	1%	5%	10%	25%	50%	75%	90%	95%	99%
Uniform 5%	-31	-18	-11	0	11	21	29	33	40
Weitzman	-29	-17	-12	4	28	65	112	144	217
Weitzman +uncertainty	-29	-17	-12	4	28	65	112	144	217
Uniform 3%	-95	-54	-32	3	36	65	88	101	119
Nordhaus	-39	-23	-16	5	39	91	160	206	312
Nordhaus +uncertainty	-39	-23	-16	5	39	91	160	206	313
Weitzman rich/poor	-22	-14	-6	11	46	96	176	244	442
Newell & Pizer	-130	-72	-43	5	49	86	115	132	156
Uniform 2.5%	-129	-73	-43	5	50	87	118	136	161
Groom et al	-145	-81	-48	5	56	98	132	151	179
Nordhaus rich/poor	-28	-17	-7	17	67	140	257	360	657
Stern	-240	-136	-88	24	166	336	515	618	840
Stern +uncertainty	-240	-136	-88	24	166	336	515	619	841
Stern rich/poor	-171	-99	-38	71	231	414	623	740	1091

Values show estimated impacts at different quantiles of the estimated impact distribution for each discounting scheme (uniform schemes³⁷, Weitzman³¹, Nordhaus³², Newell and Pizer³⁵, Groom³⁶ and Stern³⁰), and correspond to estimates shown in Extended Data Fig. 3. Positive values indicate benefits (reduced losses) at 1.5°C versus 2°C.

Extended Data Table 2 | Probability that limiting global warming to 1.5°C will generate benefits relative to 2°C warming

% Δ global GDP/capita by mid-century			Cumulative Δ global GDP by mid-century						
benefit threshold	RCP4.5	RCP6.0	benefit threshold	RCP4.5			RCP6.0		
				2.5%	3.0%	5.0%	2.5%	3.0%	5.0%
0%	0.80	0.73	0	0.76	0.76	0.75	0.69	0.68	0.68
1.25%	0.63	0.53	\$10 trillion	0.56	0.53	0.32	0.47	0.43	0.23
2.50%	0.42	0.31	\$20 trillion	0.33	0.27	0.03	0.24	0.18	0.01
3.75%	0.21	0.13	\$30 trillion	0.14	0.08	0.00	0.08	0.04	0.00
5.00%	0.07	0.03	\$40 trillion	0.04	0.01	0.00	0.01	0.00	0.00

% Δ global GDP/capita by end-of-century		Cumulative Δ global GDP by end-of-century			
benefit threshold	RCP2.6	benefit threshold	RCP2.6		
			2.5%	3.0%	5.0%
0%	0.76	0	0.78	0.78	0.76
2%	0.62	\$10 trillion	0.72	0.71	0.53
4%	0.45	\$20 trillion	0.68	0.63	0.28
6%	0.27	\$50 trillion	0.50	0.38	0.00
8%	0.12	\$100 trillion	0.18	0.05	0.00
10%	0.03	\$150 trillion	0.02	0.00	0.00

Left panels show benefits in terms of percentage change in global GDP per capita by mid-century and the end of the century. For instance, by mid-century under RCP4.5 there is a 42% probability of benefits exceeding 2.5% of global GDP per cap. Right panels show benefits in terms of cumulative change in global GDP by mid-century and the end of the century, under three different discount rates for each relevant RCP. For instance, by the end of the century, there is a 50% probability of benefits exceeding US\$50 trillion using a discount rate of 2.5%.

Extended Data Table 3 | Probability that limiting global warming to 1.5°C will generate different levels of benefits relative to 2.0°C warming, under different discounting schemes

discount scheme	0	\$10 trillion	\$20 trillion	\$40 trillion	\$100 trillion	\$200 trillion	\$350 trillion
Uniform 5%	0.76	0.53	0.28	0.01	0.00	0.00	0.00
Weitzman	0.79	0.67	0.57	0.40	0.13	0.02	0.00
Weitzman +uncertainty	0.79	0.67	0.57	0.40	0.13	0.02	0.00
Uniform 3%	0.78	0.71	0.63	0.47	0.05	0.00	0.00
Nordhaus	0.80	0.70	0.63	0.50	0.22	0.06	0.01
Nordhaus +uncertainty	0.80	0.70	0.63	0.50	0.22	0.06	0.01
Weitzman rich/poor	0.86	0.76	0.68	0.54	0.24	0.08	0.02
Newell & Pizer	0.78	0.72	0.68	0.55	0.17	0.00	0.00
Uniform 2.5%	0.78	0.72	0.68	0.56	0.18	0.00	0.00
Groom et al	0.78	0.73	0.69	0.59	0.24	0.00	0.00
Nordhaus rich/poor	0.87	0.80	0.73	0.63	0.38	0.17	0.05
Stern	0.80	0.78	0.76	0.72	0.62	0.44	0.23
Stern +uncertainty	0.80	0.78	0.76	0.72	0.62	0.44	0.23
Stern rich/poor	0.86	0.85	0.83	0.80	0.70	0.54	0.32

Benefits are in terms of cumulative change in global GDP by the end of the century (RCP2.6). Discounting schemes are: uniform schemes³⁷, Weitzman³¹, Nordhaus³², Newell and Pizer³⁵, Groom³⁶ and Stern³⁰).

The COVID-19 lockdowns: a window into the Earth System

Noah S. Diffenbaugh¹, Christopher B. Field², Eric A. Appel³, Ines L. Azevedo, Dennis D. Baldocchi, Marshall Burke⁴, Jennifer A. Burney⁵, Philippe Ciais⁶, Steven J. Davis⁷, Arlene M. Fiore⁸, Sarah M. Fletcher, Thomas W. Hertel, Daniel E. Horton, Solomon M. Hsiang⁹, Robert B. Jackson¹⁰, Xiaomeng Jin¹¹, Margaret Levi, David B. Lobell¹², Galen A. McKinley¹³, Frances C. Moore, Anastasia Montgomery, Kari C. Nadeau¹⁴, Diane E. Pataki, James T. Randerson¹⁵, Markus Reichstein, Jordan L. Schnell¹⁶, Sonia I. Seneviratne¹⁷, Deepti Singh, Allison L. Steiner and Gabrielle Wong-Parodi¹⁸

Abstract | Restrictions to reduce human interaction have helped to avoid greater suffering and death from the COVID-19 pandemic, but have also created socio-economic hardship. This disruption is unprecedented in the modern era of global observing networks, pervasive sensing and large-scale tracking of human mobility and behaviour, creating a unique test bed for understanding the Earth System. In this Perspective, we hypothesize the immediate and long-term Earth System responses to COVID-19 along two multidisciplinary cascades: energy, emissions, climate and air quality; and poverty, globalization, food and biodiversity. While short-term impacts are dominated by direct effects arising from reduced human activity, longer-lasting impacts are likely to result from cascading effects of the economic recession on global poverty, green investment and human behaviour. These impacts offer the opportunity for novel insight, particularly with the careful deployment of targeted data collection, coordinated model experiments and solution-oriented randomized controlled trials, during and after the pandemic.

COVID-19 is disrupting lives and livelihoods around the world. The most important consequences are the public health crisis and associated economic and humanitarian disasters, which are having historic impacts on human well-being. In addition, after more than four months of widespread sheltering and other restrictions, it is clear that the scale and persistence of socioeconomic disruption represent an unprecedented modification of human interactions with the Earth System, the impacts of which will be long-lasting, widespread and varying across space and time (FIG. 1).

Some obvious and immediate effects are reflected in the worldwide reports of reduced traffic congestion, clearer skies, cleaner waterways and the emergence of wildlife into human settlements. In addition to anecdotal reports, effects

are being detected in a variety of long-term physical observations (from improved air quality to reduced seismic noise) and socioeconomic indicators (such as reduced mobility and declining economic growth and greenhouse-gas emissions). While some of these impacts might be considered beneficial to the environment, negative consequences are also emerging, including cascading effects for poverty, food security, mental health, disaster preparedness and biodiversity.

As with previous calamities, such as volcanic eruptions^{1–3}, electrical blackouts⁴ and the short-term reductions in human mobility following the 11 September attacks⁵, the current COVID-19 crisis will inevitably present a new test bed for understanding how the Earth System works, including the critical role of humans⁶. This test bed could provide answers to long-standing

questions, such as the processes linking heterogeneous local pollutant emissions and regional atmospheric chemistry and air quality, or the relationship between global economic integration and poverty-driven environmental degradation. The uniquely pervasive disruption also has the potential to reveal novel questions about the Earth System that have not previously been asked, and many diverse efforts are already underway to learn from this inadvertent Earth System modulation.

In this Perspective, we examine the impacts of COVID-19-related social disruption on two multidisciplinary pathways: energy, emissions, climate and air quality; and poverty, globalization, food and biodiversity. We first consider hypotheses about how the COVID-19 disruption could influence the Earth System along these pathways and then explore the potential for rapid advances in understanding if we are able to carefully observe, test and characterize Earth System processes during and after the COVID-19 event.

COVID-19 disrupts the Earth System

Under usual daily life, the human footprint on the Earth System is vast. As a result, a very large perturbation is required to cause an observable difference from this ‘business-as-usual’ baseline: COVID-19 is providing that perturbation. As of July 2020, as much as half the world’s population has been under some version of sheltering orders⁷ (FIG. 2a). These orders have substantially reduced human mobility and economic activity (FIG. 2b), with ~70% of the global workforce living in countries that have required closures for all non-essential workplaces and ~90% living in countries with at least some required workplace closures⁸.

The scale of this socioeconomic disruption is likely to be detected in the Earth System at local to global scales (FIG. 1). Some responses are direct, while others will result from interactions between humans, ecosystems and climate. The impacts of the socioeconomic disruption are, thus, also likely to vary across timescales: although the direct impacts of the reduction in human mobility will be strongest during the sheltering period, many of the most lasting impacts could result from cascading effects

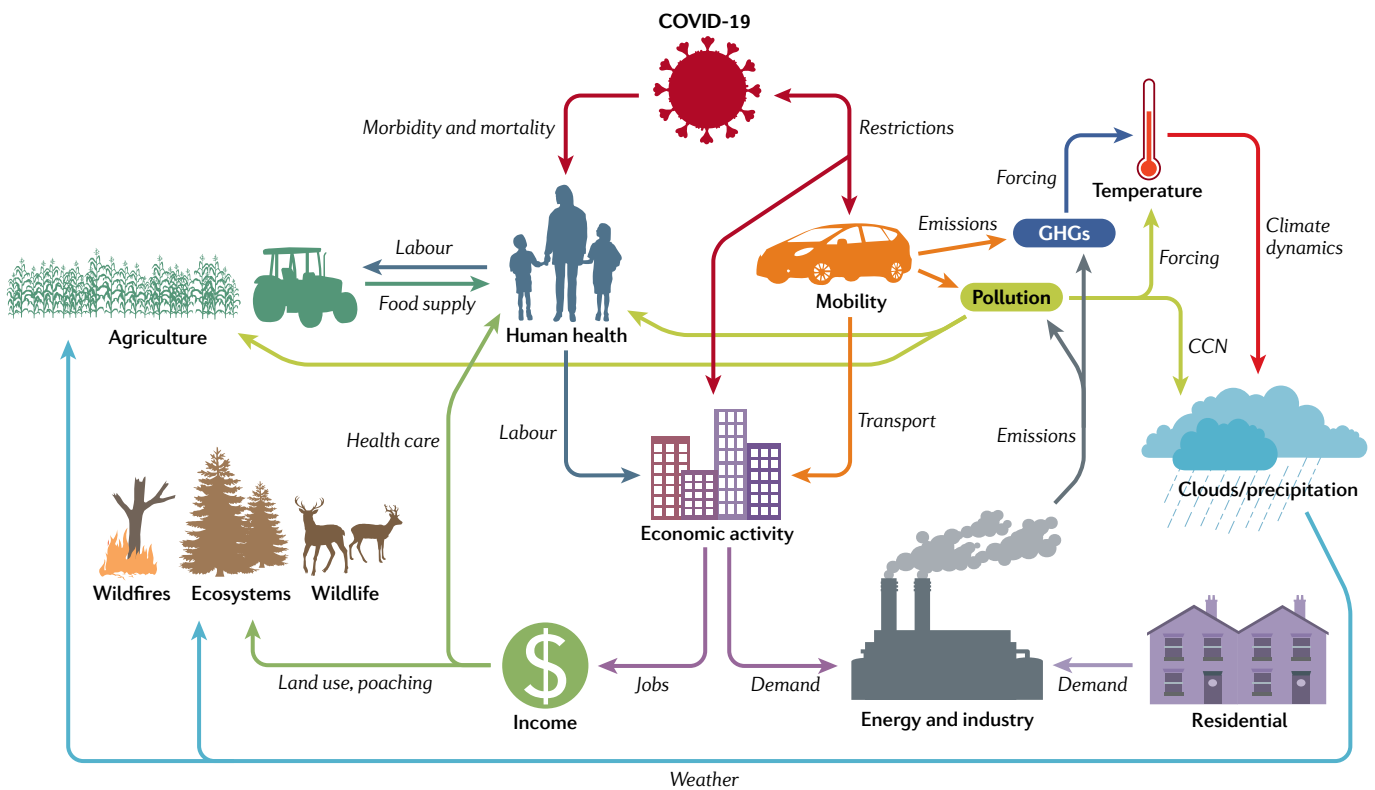


Fig. 1 | Earth System interactions linked to the COVID-19 socioeconomic disruption. Two pathways highlight the potential for multi-dimensional Earth System responses: energy, emissions, climate and air quality; and poverty, globalization, food and biodiversity. Interactions will manifest differently in different regions and on different timescales, with the sign of the interaction potentially changing across different phases of the event. Note that these interactions are indicative of primary hypotheses, but not all possible interactions are shown. CCN, cloud condensation nuclei; GHGs, greenhouse gases.

initiated by the economic recession, some of which (such as those induced by changes in public policy, the structure of the economy and/or human behaviour) could persist for decades following the initial economic recovery.

The reduction of human activities, and the efforts to manage their revival, have varied around the world (FIG. 2). Given the variations in the timing, strength and approach to sheltering⁷, it may be possible to track effects through the components of the Earth System. Likewise, because the large-scale reduction in human activity will necessarily be temporary, it will be possible to observe whether or how Earth System processes return to their previous states after activity returns to something approaching pre-pandemic levels. The event, therefore, provides a unique test bed for probing hypotheses about Earth System sensitivities, feedbacks, boundaries and cascades^{6,9–11}, presuming that the observing systems are in place to capture these responses (BOX 1).

Path I: Energy, emissions, climate and air quality. Impacts on energy consumption, and associated emissions of greenhouse gases and air pollutants, are likely to cascade across timescales (FIG. 1). In the near-term,

reductions in mobility and economic activity have reduced energy use in the commercial, industrial and transportation sectors, and might have increased energy use in the residential sector^{12,13}. These direct impacts will interact with secondary influences from energy markets, such as the severe short-term drop in oil prices in March and April 2020 (REF.¹⁴). Further, as with past economic recessions^{15,16}, energy demands — and the mix of energy sources — are likely to evolve over the course of the economic recovery in response to market forces, public preferences and policy interventions^{17,18}. This evolution could have long-term effects on the trajectory of decarbonization if, for example, the economic disruption delays the implementation of ambitious climate policy or results in decreased investments in low-carbon energy systems¹⁶. Alternatively, large government stimulus spending could target green investments that overhaul outdated infrastructure and accelerate decarbonization¹⁸.

Misunderstandings have arisen with regards to declines in carbon dioxide emissions caused by COVID-19-related disruption, with some interpreting short-term reductions to suggest that austerity of energy consumption could

be sufficient to curb the pace of global warming. A reduction in fossil CO₂ emissions proportional to the economic decline¹⁵ would be dramatic relative to previous declines. For example, the decline in daily CO₂ emissions peaked at >20% in the largest economies during the period of sheltering¹³ (FIG. 2c) and the cumulative reduction in global emissions was ~7% from January through April 2020 (REF.¹²) (FIG. 2d). However, these daily-scale declines are temporary¹³ and the rebound in emissions that is already evident^{13,19} (FIG. 2c) supports the likelihood of a reduction in annual emissions that is smaller than 7%.

Nevertheless, a 5% drop in annual fossil CO₂ emissions from 37 billion metric tonnes per year²⁰ would exceed any decline since the end of World War II (REF.¹³). There is a strong basis that such a reduced atmospheric CO₂ growth rate would lead to a reduced ocean carbon sink²¹ and, thus, also a temporary reduction in the rate of ocean acidification. On the other hand, a 5% decrease would still leave annual 2020 emissions at ~35 billion metric tonnes, comparable to emissions in 2013 (REF.²⁰). Such a decline — and associated changes in the ocean and land carbon sinks — might not be statistically detectable above the year-to-year variations

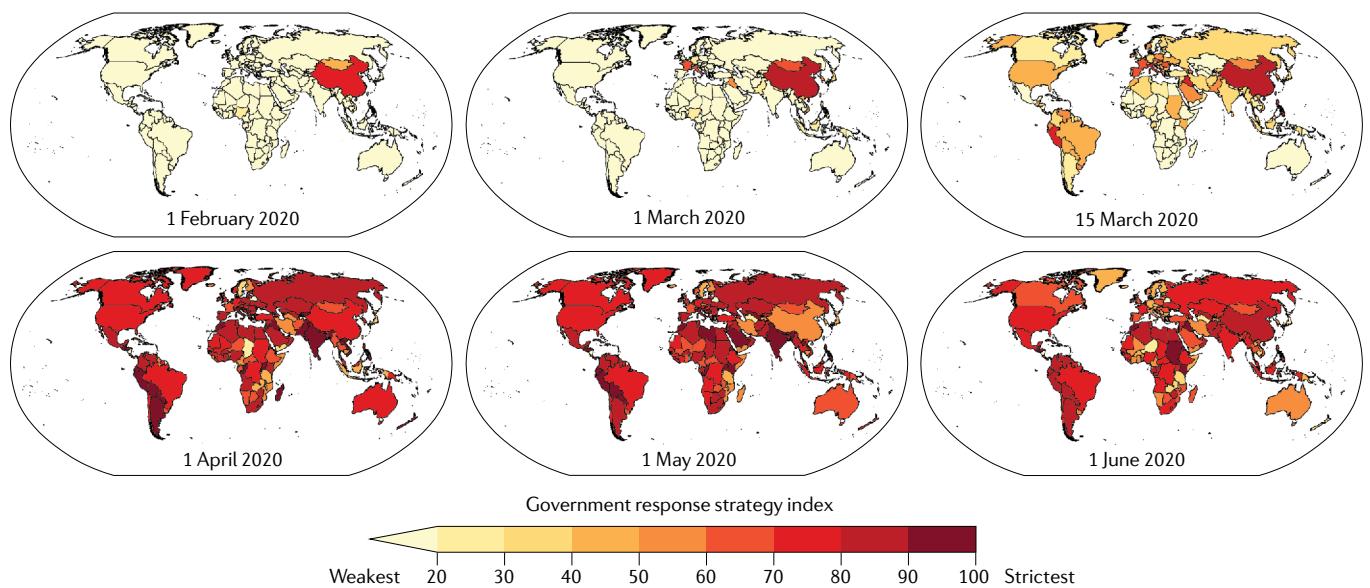
in the natural carbon cycle and, regardless, global atmospheric CO₂ concentrations will inevitably rise in 2020, continuing a long-term trend. Progress in understanding the carbon-cycle responses to COVID-19 will, therefore, be challenging and, at a minimum, will require new methods for tracking the unprecedented short-term perturbation in emissions through the Earth System.

Based on past events and fundamental understanding, there are a number of hypotheses of how sheltering-induced changes in atmospheric emissions could influence the climate system more broadly

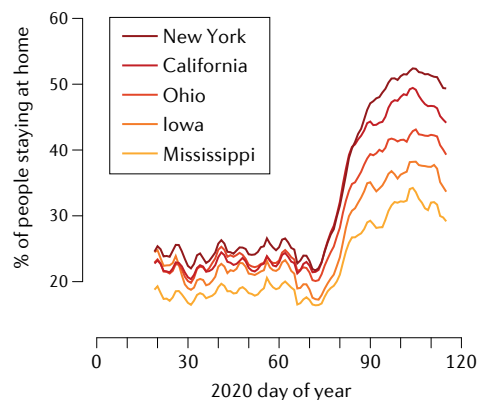
(FIG. 1). On short timescales, reduced air travel decreases the abundance of contrails, which can be detected in the radiation budget (as occurred during the brief cessation of air travel following the 11 September attacks⁵). The response of atmospheric aerosols to sheltering is likely to vary regionally, with changes in emissions, meteorology and atmospheric chemistry influencing the outcome (BOX 2). While reductions in aerosols have occurred in many locations (FIG. 3), they have also been observed to increase in others²², highlighting the important role of secondary chemistry in these assessments. Changes in atmospheric

aerosols could further influence cloud and precipitation processes^{23,24}, and might be detectable in the local surface energy budget²⁵. A reduction in scattering aerosols will also cause warmer surface temperatures over emitting regions²⁶ (FIG. 4), potentially manifesting as more frequent and/or intense heatwaves^{27,28}. If aerosol reductions persist across the Northern Hemisphere, this could have short-term impacts on the onset, intensity and/or intraseasonal variability of monsoon rainfall^{29–31}, particularly given that both local and remote aerosol emissions can influence variability within the monsoon season³¹.

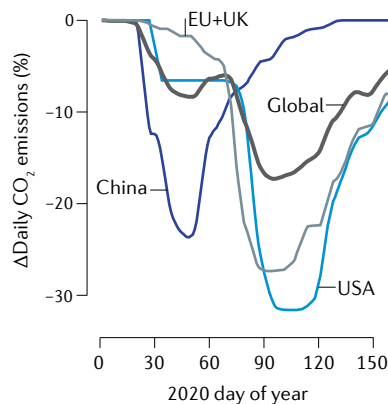
a Timing of sheltering intensity



b Sheltering intensity



c Daily CO₂ emissions



d Cumulative CO₂ emissions

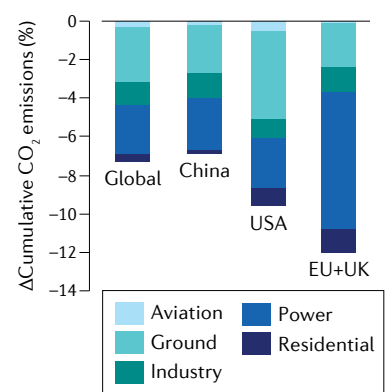


Fig. 2 | Sheltering orders and changes in mobility and CO₂ emissions.

a | The Oxford Government Response Stringency Index⁷ on six different dates between 1 February and 1 June. **b** | Percentage of people staying at home, as estimated by mobility data from cell phones³¹, for five US states. **c** | Percentage change in carbon dioxide emissions^{12,93} for the World, China, the USA and Europe. Each day's value is the percentage departure in 2020 from the respective day-of-year emissions in 2019, accounting for seasonality. **d** | Percentage change in cumulative carbon dioxide

emissions^{12,93} for January through April 2020 compared with January through April 2019 for the World, China, the USA and Europe. The differences in timing of sheltering and mobility in different areas of the world are a source of information that can be used in understanding causality in the Earth System response. In the case of carbon dioxide emissions, the early onset and subsequent relaxation of sheltering in China is clearly reflected in the timing of reduction and subsequent recovery of emissions in China relative to the USA and Europe.

Box 1 | Datasets for understanding the Earth System impacts of COVID-19 disruption

A wide range of data could be leveraged to understand Earth System changes during the COVID-19 pandemic. These include long-term, operationally deployed Earth observations from satellite remote-sensing platforms and atmospheric, oceanic and surface measurement networks. Although long-term socioeconomic data are also operationally available, a 1–2-year processing lag can inhibit real-time analysis. Access to long-term private-sector data could remove some of these barriers. A range of shorter-term and/or intermittent observations are also available. These include stationary and mobile measurements of the atmosphere, ocean and near-surface environment, as well as energy, trade, transportation and other socioeconomic data available at either fine resolution for short periods or coarse resolution for longer periods.

One of the most potent opportunities will be to safely deploy observations in geographic areas or economic sectors where there is already a rich pre-existing data baseline; where Earth System models have generated specific, testable hypotheses; or where initial observations suggest that a strong or unexpected response is already emerging. This strategy could include deployment of stationary and/or mobile sensors, short-term online or phone surveys, and ‘citizen-science’ opportunities via crowd-sourcing platforms such as the USA National Phenology Network, iNaturalist, PurpleAir and Smoke Sense. There are also abundant opportunities to leverage newer, emerging datasets — such as from cell-phone GPS, social media, e-commerce and the private satellite industry — that, if handled with care to preserve privacy, could help to bridge the gaps in long-term, operational data.

Despite the prevalence of extensive datasets, the current COVID-19 crisis is revealing limitations in the ability to measure critical variables in real time. For example, the event has made clear that the world is ill-equipped to make real-time measurements of economic activity and its immediate consequences. It is also revealing deficiencies in real-time-measurement capacity for emissions of some air pollutants and greenhouse gases, as well as highlighting longer-known issues like a relative inability to assess the vertical structure of pollution in the atmosphere. The crisis is demonstrating the urgent need for improved data, models and analysis to understand and correct those deficiencies.

Many sectors would benefit from a public repository containing the heterogeneous data that are critical to fully understand this unique planetary-scale disruption. Some data sources are public, some are proprietary and some do not yet exist. As has been proven repeatedly in recent years, an open, public repository providing all of these heterogeneous data in a uniform, coordinated format would enable novel, unpredictable insights across multiple research disciplines, long after the event has passed.

On longer timescales, changes in the energy intensity of the economy, the carbon intensity of energy or the pace of deforestation could affect the long-term trajectory of global climate (through the trajectory of greenhouse gas emissions and associated land and ocean carbon-cycle feedbacks). These effects could go in either direction: for example, in the US electricity sector, coal plants will likely shut down at an accelerated pace as a result of the economic slowdown, continuing a long-term decline³². However, in the transportation sector, policy intervention to stimulate the economy might loosen emissions standards³³, increasing emissions relative to the pre-pandemic trajectory.

The short-term reductions in pollutant emissions have already resulted in noticeable changes in air quality in some regions (BOX 2). If sustained, improved air quality could yield multiple benefits. These include improved crop health³⁴, as air pollution can reduce regional harvests by as much as 30% (REF.³⁵). In addition, ambient air pollution is a significant cause of premature death and disease worldwide³⁶, even from short-term exposure^{37,38}. Several well-documented historical examples illustrate how decreased

ambient air pollution can improve human health³⁹. These include effects from short-term reductions in traffic, travel and/or industrial activities associated with events such as the 1996 Atlanta Olympic Games⁴⁰ and 2008 Beijing Olympics^{41–45}. While associations between air quality and health outcomes are hypothesized in studies of the current pandemic^{46,47}, understanding the role of air quality as an indicator for the epidemic trajectory is an emerging challenge. Further, any health improvements resulting from improved air quality during the pandemic should not be viewed as a ‘benefit’ of the pandemic but, rather, as an accidental side effect of the sheltering that was imposed to protect public health from the virus.

Some of the most lasting impacts of the COVID-19 crisis on climate and air quality could occur via insights into the calculation of critical policy parameters. Two of the most important, and controversial, are the value of mortality risk reduction (sometimes termed the value of a statistical life, or VSL) and the pure rate of time preference (or PRTP), which is one component of the social discount rate and measures willingness to trade off well-being over

time. The VSL is important to the analysis of all environmental regulation in the United States and can determine whether environmental regulations as mundane as a labelling requirement for toxic chemicals will pass a cost–benefit test. The PRTP is important in evaluating long-term societal trade-offs — most notably, climate-change regulation — and can be important in calculating an economic value of avoiding climate damages^{48,49}. With a higher PRTP, aggressive mitigation of greenhouse gases becomes less attractive, while a low rate, which places relatively higher value on the well-being of future generations, suggests that far more aggressive regulation of today’s emissions is warranted.

Both the VSL and the PRTP can be difficult to quantify. However, the COVID-19 crisis is making these trade-offs more explicit, as governments, communities and individuals make historic decisions that reflect underlying preferences for current and future consumption and the trade-off between different types of economic activity and individual and collective risk. The diverse responses to the unusual conditions during the pandemic could reveal far more about how different societies manage these trade-offs than has been revealed in the last half-century. As those insights are incorporated into the formal policy-making apparatus, they will have lasting effects on the regulations that impact the long-term trajectory of climate and air quality.

Path II: Poverty, globalization, food and biodiversity. By amplifying underlying inequities in the distribution of resources, the socioeconomic disruption caused by the response to COVID-19 will almost certainly have negative long-term impacts on human health and well-being. In particular, the economic shock is likely to increase the extent and severity of global poverty⁵⁰, both from direct impacts on health, employment and incomes and through disruptions of supply chains and global trade⁵¹. The severe impacts on poverty rates and food security that are already emerging⁵⁰ are indicative of these disruptions and are a sign of how tightly many of the world’s poorest households are now interwoven into the global economy. The unwinding of these relationships in the wake of restrictions on human mobility and associated economic shocks will provide insight into the role of economic integration in supporting livelihoods around the world. A severe and prolonged deepening of global poverty is also likely to reduce available resources for climate mitigation and adaptation,

increasing climate risks and exacerbating climate-related inequities.

The global agriculture sector is a key sentinel for the response of poverty to the pandemic. Primary near-term questions centre around how food security and agriculture-dependent incomes might be affected by unprecedented shocks to local labour supply and global supply chains. A first-order impact has been the income shock associated with widespread sheltering⁸. Loss of wages in both low-income and high-income countries with limited social safety-nets will drive food insecurity and poverty⁵⁰.

It is possible that agricultural production in rural areas will proceed largely unaffected, particularly for larger producers of field crops that tend to be heavily mechanized. However, in many locations and for many specialty crops, agriculture still relies heavily on field labour; sufficient labour supply during the key planting and harvest periods is crucial, and there are frequently labour shortages at these critical times. How these pre-existing labour-supply challenges are affected by the scale and scope of sheltering remains to be seen. In the USA, meat-packing plants have become hotbeds of COVID-19, raising the question of whether excessive concentration of this industry might have led to a loss of resilience⁵². Sheltering-induced return migration from urban to rural areas, as has been widely reported in India, could alleviate agricultural labour shortages in some developing countries. However, mandated sheltering could cause reductions in plantings, which, in combination with the prospect of sheltering during the harvest season, could reduce subsequent harvests.

Such supply-side shocks could combine with general disruption of global trade⁵³ to trigger a cascading series of export bans like those that occurred in 2007–2008 (REF.⁵⁴), which caused a spike in grain prices and contributed to unrest around the world⁵⁵. Initial export restrictions are already emerging⁵⁶. Given that agriculture prices are important for both consumers and producers, such bans tend to hurt rural producers in favour of protecting urban consumers in the exporting countries⁵⁷. They can also lead to food shortages in import-dependent countries and rapid increases in international commodity prices⁵⁸, as well as acting to amplify the impacts of climate variability on poverty⁵⁹. However, global grain stocks are much larger today than they were in 2007, which should help buffer some sheltering-related production shortfalls, should they arise.

Deepening of global poverty is likely to have lasting negative environmental impacts (including deforestation, land degradation, poaching, overfishing and loosening of existing environmental policies), as a larger share of the global population is pushed towards subsistence. For example, after decades of efforts to replace environmental degradation with earnings from ecotourism, the collapse of tourism in the wake of COVID-19 is coinciding with a rapid increase in illegal poaching in southern African parks⁶⁰. The rapid response is a potential indicator of the importance of the large African tourism industry for the preservation of endangered species. However, further analysis is needed to distinguish the contributions of income and governance/enforcement. Likewise, deforestation in the Brazilian Amazon surged to >2,000 km² in the first five months of 2020, an increase of ~35% compared to the same period in 2019 (REF.⁶¹).

Governance appears to be playing a key role in this initial short-term resurgence during the COVID-19 sheltering. Over the longer term, historical drivers^{62,63} suggest that a prolonged poverty shock is likely to increase deforestation and biodiversity loss. These cascading impacts on ecosystems and biodiversity offer a sobering contrast to the reports of wildlife ‘rebounds’ occurring in response to local sheltering⁶⁴.

Changes in human behaviour and decision-making induced by the pandemic are also likely to cascade through the globalized Earth System over the long term. For example, although sheltering orders are reducing personal vehicle use, the long-term impacts are less clear and will be determined, in part, by how human behaviours respond to the pandemic. If, for instance, the pandemic causes people to feel more dependent on cars as ‘safe places’, that dependence could act to further reinforce the prominence of the automobile at the

Box 2 | Interpreting energy, emissions, climate and air quality responses

Changes in atmospheric pollutants have co-occurred with COVID-19 sheltering restrictions^{22,78,79}, including broadly publicized reductions in satellite-derived tropospheric NO₂ columns⁹⁵ (FIG. 3a). The sheltering period can shed light on processes controlling atmospheric constituents on local to global scales. However, accurate attribution requires careful consideration of emissions, meteorology and atmospheric chemistry.

Anthropogenic forcing

The large regional variations in pollutant emissions will create spatial heterogeneity in the response of air quality to sheltering. While some regions show decreases in aerosols (FIG. 3b), post-shutdown increases have been observed in urban regions in China due to secondary chemistry⁷². Sheltering measures were implemented during spring/autumn transitions (FIG. 2), when energy demand, usage and fuel mix fluctuate sharply. Further, observed changes in atmospheric constituents might also be influenced by longer-term emission reductions. These factors must be carefully considered when attributing changes to COVID-19 restrictions. The COVID-19 disruption provides impetus to combine existing energy-consumption data with robust ground-based and space-based atmospheric-chemical measurements to characterize local pollutant emissions and the resulting atmospheric chemistry that drives air quality.

Distinguishing signal from noise

Natural climate variability must be accounted for to quantify the human influence on short-term Earth System changes^{96–98}. In the case of quantifying the response of regional air pollution to sheltering, several limitations must be overcome. Irregular sampling frequencies over limited observing periods are a primary barrier. For example, space-based retrievals of air pollutants such as NO₂ are sensitive to physical (such as daily boundary-layer variations) and chemical (such as seasonal lifetime variability) processes. In the Northern Hemisphere, peak sheltering has coincided with the period when NO₂ lifetimes are transitioning from winter maximum to summer minimum, affecting estimation of emissions differences from satellite column density retrievals (FIG. 3a). Further, as NO₂ columns cannot be retrieved under clouds, concentration differences calculated within the period of sheltering, or between 2020 and previous years, could arise due to variable meteorology.

Opportunities for the future

COVID-19 sheltering could help elucidate Earth System processes along the energy–emissions–climate–air quality pathway. For example, observations during this period could yield insights into road-traffic contributions to local air quality, as passenger-car emissions decline but trucking emissions persist. Connections between emissions and climate may be revealed from observations in regions with large aerosol forcing signals, offering much-needed tests for local-to-global responses simulated by Earth System models (FIG. 4). For example, asymmetric hemispheric warming is a robust model response to regional reductions in aerosol emissions²⁶; can this signal be distinguished from long-term aerosol trends when accounting for internal variability? These queries sample the rich opportunities to advance understanding of processes governing linkages between energy use, emissions, climate and air quality.

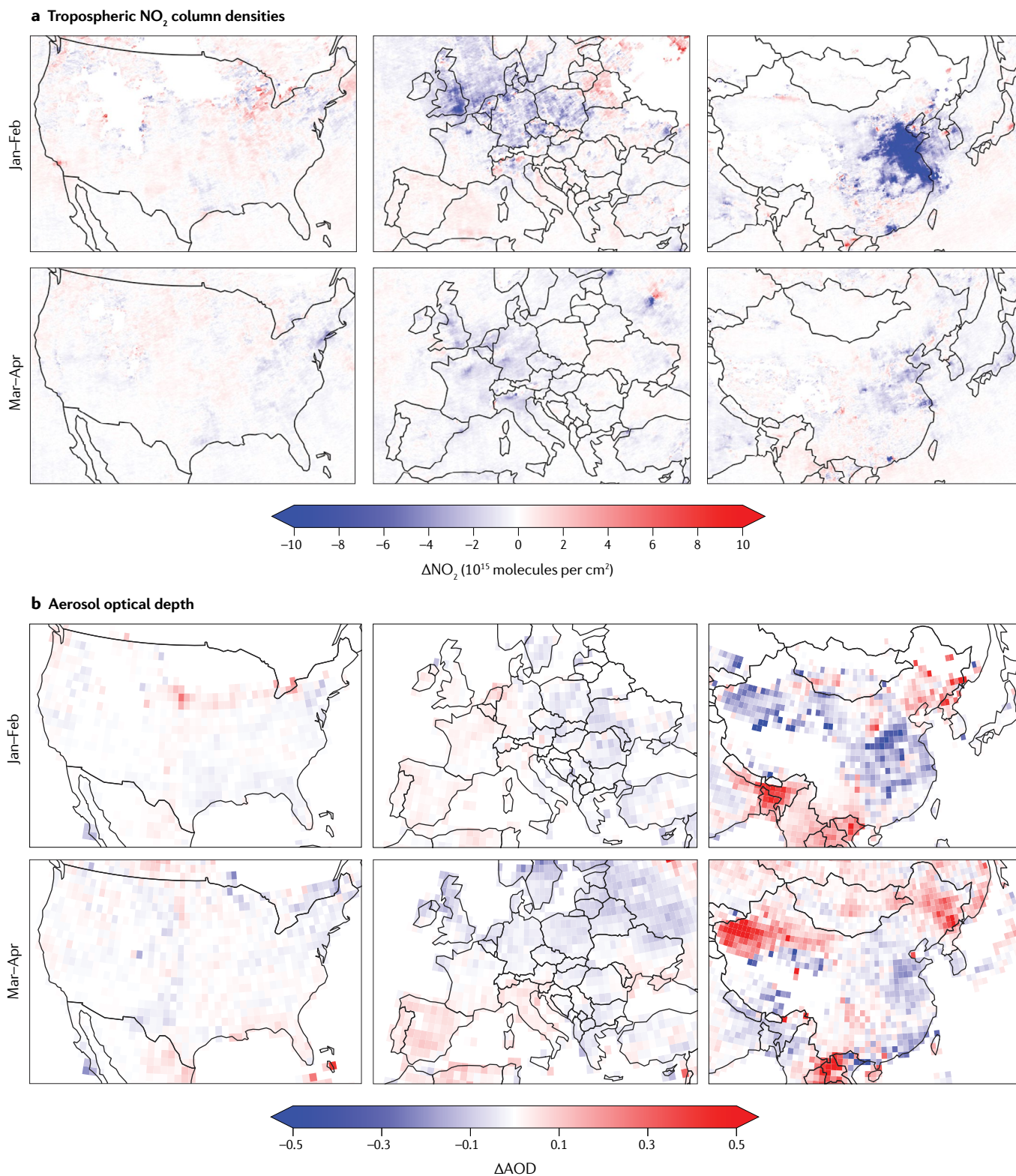


Fig. 3 | Variability in air-quality indicators during the 2020 winter-spring transition. Difference in tropospheric NO₂ column density (panel a) and aerosol optical depth (panel b) for select months between 2020 and 2019. Aerosol optical depth (AOD) data are from the NASA Visible Infrared Imaging Radiometer Suite; NO₂ data are from the NASA Ozone Monitoring Instrument, processed as in REF.⁹⁴. Year-to-year changes in air quality reflect a complex array of processes in addition to COVID-19 restrictions.

For example, strong NO₂ decreases over Northeast China coincide with the Wuhan lockdown⁹⁵, while those over the UK in January–February predate COVID-19 restrictions. Relative to NO₂, AOD data show less regional coherency. Confident attribution to COVID-19 restrictions highlights a new challenge to explain these observed spatio-temporal differences and to place them in the context of the longer-term satellite and ground-based observations (BOX 2).

expense of public transit. On the other hand, some cities might seek to maintain reductions in traffic by permanently closing some streets and encouraging residents to rely more on walking and bicycles. Another potentially consequential outcome could be a change in the kind of housing and work environments people will prefer in the future. The pandemic favours access to outdoor space and disfavours use of tall buildings with elevators. If these human preferences are sustained for years after the pandemic passes, over the long term, the combination could lead to more sprawling suburbs and fewer residential and office towers, with corresponding consequences for the Earth System.

More broadly, priorities and incentives embedded in government aid and economic stimulus will influence financial investment. For example, rollbacks of environmental restrictions by governments seeking to accelerate economic recovery³³ (including fuel standards, mercury, clean water, and oil and gas production on federal lands) could have consequences that outlast the pandemic. Alternatively, efforts to support economic recovery could be directed towards electrification of transportation, along with green jobs that rebuild public transit, housing and critical infrastructure in an environmentally sensitive way¹⁸. In the private sector, pandemic-induced changes in perceptions of economic security and human needs could increase investment in technologies or platforms that lower the risk of future pandemics, such as reducing human interactions by introducing more robotics into workplaces. Although the precise trajectory is unknown, the long-term impacts of the pandemic on resource demand and efficiency will be heavily influenced by the response of human behaviour and decision-making, which is likely to vary among and within countries, as has occurred with health practices and policies during the pandemic.

Investigative frameworks

The COVID-19 sheltering has, thus far, been relatively brief, but its impacts are already emerging in the Earth System. Some of these responses, such as those directly connected to mobility and emissions of atmospheric pollutants, might pass when the sheltering passes (FIG. 2c, BOX 2), while others will persist long past the economic recovery (FIG. 1). Given the complexity of Earth System interactions, understanding these short-term, medium-term and long-term responses will require careful deployment of a diverse portfolio of investigative frameworks.

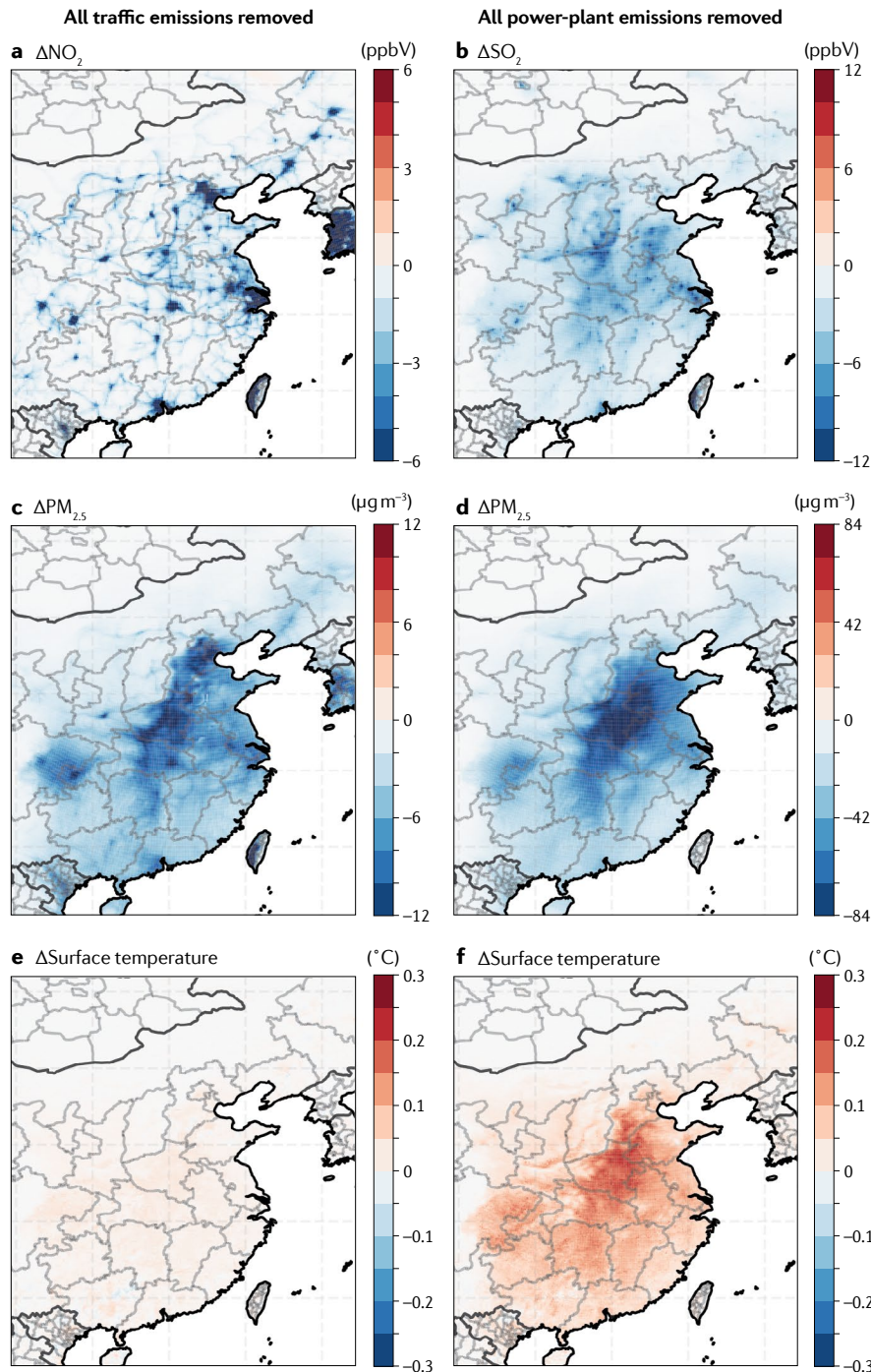


Fig. 4 | Idealized sensitivity to removal of emissions from traffic and power generation. NO₂ (panel a), SO₂ (panel b), PM_{2.5} (panels c and d) and surface-temperature (panels e and f) changes for the month of January simulated by the Community Multiscale Air Quality/Weather Research and Forecasting (CMAQ-WRF) model in response to domain-wide removal of traffic (left panels) or power-plant (right panels) emissions. Experiments simulate one month using January 2010 emission factors and January 2013 meteorological fields. They are, thus, idealized illustrations of the potential for Earth System models to pose hypotheses, illuminate and constrain key processes, and identify data-gathering priorities; as these simulations predate the COVID-19 pandemic, they should not be considered an attempt to recreate COVID-19 conditions.

A major challenge will be to test causality when so many important, interacting influences are changing simultaneously. These include potentially confounding

effects from large reductions in human activity, government interventions to stem the economic collapse, simultaneous market responses to both the economic

shock and government stimulus, and underlying variations such as climate variability and pre-COVID-19 economic conditions. In addition, observational continuity is being affected by sheltering, including atmospheric, oceanic and land surface observations that contribute to the global observing system⁶⁵. Given these challenges, insight must be generated from a combination of ongoing and newly deployed observations, dedicated modelling experiments, solutions-oriented randomized controlled trials (RCTs) and sophisticated quantitative analysis. To maximize effectiveness, these approaches will need to place as much focus on Path II (poverty, globalization, food and biodiversity) as on Path I (energy, emissions, climate and air quality). A key imperative will be to quickly develop and deploy techniques that can bring multiple lines of evidence together to distinguish causality.

A new view to spatial and temporal dynamics of Earth System processes. Because the timing of different government actions is known⁷, the spatio-temporal phasing of the socioeconomic disruption can be used to understand regional variations in the Earth System response. In essence, although interventions are occurring around the globe, we are not really experiencing a global shutdown but, rather, a complex patchwork of slowdowns in activity that vary widely in timing, duration, magnitude and baseline starting conditions (FIG. 2a). This variation is increasing as the event moves from the initial global disruption to heterogeneous resumption of activity (FIG. 2a) and extends across the seasonal transition from Northern Hemisphere winter to summer (and potentially beyond). Further, the scale of economic impacts suggest the possibility of sustained recession — or even depression — following the cessation of large-scale sheltering^{51,66}. An extended period of substantially reduced economic activity would produce a trajectory of Earth System forcing that remains different from the pre-COVID-19 forcing, well after the COVID-19 restrictions are removed.

These spatial and temporal gradients in human activity are a source of information that becomes even more valuable in the context of observations that are repeated through time⁶⁷ or that take advantage of the fact that variations in human interventions are at least partly independent of other co-varying, confounding factors⁶⁸. The magnitude of the socioeconomic disruption is also large enough that it presents the opportunity to design data-gathering

campaigns to systematically test hypotheses about both Path I and Path II that would not be observable without the disruption.

For example, the unprecedented reduction in daily fossil CO₂ emissions (FIG. 2c) could lend insight into the processes governing land and ocean carbon sinks, provided that careful testing demonstrates that a signal can be detected amid the noise of natural variability, and that observations can be safely maintained during the event. Rapid declines in emissions can also help to narrow existing uncertainties around anthropogenic sources and their imprint on atmospheric trace gas and aerosol concentrations (BOX 2). Methane emissions from oil and gas fields offer one immediate example: so far during the event, oil and gas companies in the USA still maintained ~11 million barrels of daily crude oil production throughout the spring of 2020, despite a 44% reduction in gasoline sales for the USA in April¹⁴. Not surprisingly, US inventories continue to climb, reaching their highest levels of the past four decades in June. If oil production slumps this summer, monitoring from satellites, aircraft, towers and on-the-ground sensors will provide an unprecedented opportunity to quantify any change in methane and ethane emissions, including decreases caused by lower production or increases caused by reduced oversight from workers or inspectors. But that will only be possible if the scientific community organizes and there is sufficient operational flexibility to allow for the collection of critical data.

A similar opportunity exists to study the effectiveness of wildfire suppression on air quality. In the USA, federal, state and local fire agencies are adjusting strategies in order to limit use of ground crews and their exposure to COVID-19 (REF.⁶⁹). These strategies could influence aerosol loads from wildfires (which would have potential health consequences⁷⁰). It will, thus, be possible to systematically evaluate the effectiveness of this aggressive fire-suppression approach using existing satellite and ground-based observations.

Earth System models that predict responses and guide observations. Computational models are frequently used to test the response of the Earth System to changes in external forcing, including for quantifying a counterfactual history without human emissions and for generating climate scenarios under future forcing from greenhouse gases or solar geoengineering. In recent decades, Earth System models have become increasingly sophisticated and

complex, and have been shown to accurately reproduce⁷¹, and predict^{72,73}, many aspects of the Earth System⁶. However, limitations to validating the response to large changes in forcing have remained a persistent source of uncertainty, and the models still contain only rudimentary representations of the Path II impacts. The magnitude of the current socioeconomic disruption thus presents a unique setting for systematic Earth System model evaluation and development.

Earth System models could be deployed for a number of benefits. Because the magnitude of COVID-19 socioeconomic disruption is historically unprecedented, it will not be possible to identify all possible Earth System responses based on theory or historical experience alone. Earth System models could be used to create hypotheses that cannot be otherwise foreseen. Generating simulations early in the event — and leveraging pre-existing idealized experiments (FIG. 4) — could inform data collection and preservation, including any new observations that might be needed in order to validate unexpected modelling results (such as predictions of Path I and Path II impacts generated using existing empirical relationships^{74,75}). After the event, when the temporal and spatial evolution of specific Earth System forcings is known, coordinated experiments⁷⁶ would allow multiple Earth System models to be compared in a unified framework. The fact that the socioeconomic disruption is deliberately temporary will increase the ability to use data collected during and after the event to verify modelling results.

The event could also be used to evaluate the potential efficacy of specific policy interventions for both Path I and Path II impacts. For example, because atmospheric chemistry and pollutant accumulation in the near-surface environment are subject to variable meteorological conditions and highly nonlinear chemical interactions, consideration of policy interventions to improve air quality (such as incentives for electric-vehicle adoption) have relied heavily on theoretical arguments and model simulations. The scale of emissions reductions induced by the socioeconomic disruption opens an opportunity to use observations of primary and secondary pollutants to evaluate the performance of chemical-transport models in simulating a number of complex features of the event (FIG. 4).

For example, comparison of observations over northern China during the 2020 winter lockdown versus the same calendar

period in 2019 shows higher ground-level ozone (as expected from theory and modelling, as NO_x emissions decline in a high-NO_x emission region⁷⁷), which enhances atmospheric oxidizing capacity and subsequent formation of secondary aerosols, such as occurs in extreme-haze events^{22,78,79}. In addition, sheltering policies have affected the emission-producing transportation, manufacturing and power-generation sectors¹², though the degree and scope of shutdown in these individual sectors vary considerably¹³. Further, much of this change occurred against the backdrop of the transition from winter to spring, a period when insolation, water vapour and meteorology are changing rapidly. This transition was made even more complex this year by a large-scale dynamical pattern that resulted in a relatively cold spring over much of the central and eastern USA. Together, these challenges present a unique opportunity to evaluate Earth System model simulations of the air-quality response to emissions reductions in specific sectors (BOX 2).

In addition to implications for air quality, the representation of aerosol effects has been one of the key sources of uncertainties in Earth System models^{71,80,81}. Should changes in regional aerosol concentrations occur as a result of the COVID-19 sheltering, the event could be used to verify simulated climatic consequences of policies to improve air quality, such as meteorological impacts like short-term increases in heat and precipitation extremes due to ‘unmasking’ of the effect of greenhouse gases⁸². A key concern is that these short-term, local signals (FIG. 4) need to be evaluated in the longer-term context of both internal climate variability and regulation-induced trends in aerosol emissions (BOX 2). However, the pervasiveness and persistence of the socioeconomic disruption may provide sufficient statistical power to test predictions generated by Earth System models.

Solution-oriented interventions that create randomized research trials. Many of the long-term impacts hypothesized in this Perspective will be determined by the response of human behaviour and decision-making. Systematically testing these human responses can be challenging. However, the scale of government response to the COVID-19 pandemic creates the opportunity to leverage solution-oriented interventions to create randomized research trials that can simultaneously provide assistance and insight about both Path I and Path II impacts.

Similar to the RCTs that are used to test the efficacy of vaccines and therapeutics, RCTs have been deployed to study a variety of other human outcomes, the effectiveness of which was recognized with this year’s Nobel Prize in Economics. Although RCTs have been less frequently aimed at environmental outcomes, RCT feasibility has been demonstrated in a number of relevant contexts, including agricultural microcredit⁸³ and payment for ecosystem services^{84–86}. In addition, basic benchmarking studies have been conducted in single locations⁸⁷. Together, these past studies provide the foundational research infrastructure that would be necessary to deploy RCT-based interventions in the COVID-19 context.

RCTs could be used to study vulnerability, resilience and disaster response in the face of extreme events that occur during sheltering⁸⁸. Another prime candidate would be policy interventions designed to prevent the kind of long-term socio-environmental damage that becomes increasingly likely as the disruption becomes more severe and sustained⁵¹. For example, the emerging poverty shock⁵⁰ can be expected to lead to substantial deforestation, land degradation and nutrient loss, even over the next few growing seasons, as smallholder farmers struggle to produce food with fewer inputs and households revert to harvested biomass for cooking. Similar socio-environmental cascades might occur in marine ecosystems. Solution-oriented RCTs would use random assignment (when the trial is of limited scale) or randomized phasing of participation (for comprehensive programmes) to test whether direct payments or other conditional mechanisms, such as payments for protection of ecosystem services, are effective in staving off environmental damages. Studies could compare the efficacy of a given treatment across different locations or domains, and could also benchmark generalized interventions (such as unconditional cash transfers) against more targeted solutions. In addition to helping vulnerable individuals and communities weather the COVID-19-driven poverty shock, such RCTs would provide a much deeper understanding of how and where poverty and environmental degradation are most tightly linked, and what types of interventions are doubly-protective of people and the environment.

A similar opportunity could exist in conjunction with COVID-19 relief and recovery funding. For example, if infrastructure spending is specifically included in recovery measures, that

spending would provide an opportunity to systematically study the long-term effectiveness of green investments¹⁸ (including infrastructure and government programmes like jobs and conservation corps) in achieving Path I outcomes such as reduced greenhouse gas emissions and Path II outcomes such as increased resilience to climate extremes^{18,89}. Even if federal or state stimulus measures do not explicitly include funding or requirements for these investments, the existing efforts of various states and localities to consider climate and other environmental outcomes in infrastructure investments⁸⁹ would create an opening for well-designed, opportunistic research trials built around variations in how government stimulus funding is applied in the context of varying state and local jurisdictional constraints.

Voluntary, solution-oriented actions could create similar opportunities for both Path I and Path II impacts. For example, large fractions of residential developments in the western USA are at the wildland–urban interface. The lack of ‘defensible space’ around homes substantially increases wildfire risk. It has been proposed that residents who are able to shelter in place could allocate more effort to reducing their fire risk by increasing the defensible space around their homes⁹⁰. With some foresight and investment, this effort could be used to study the effectiveness of defensible space. Other solution-oriented efforts that can be voluntarily undertaken while safely sheltering, such as local food production and preparation, could also be leveraged to study the effectiveness of adaptation and resilience interventions, as well as the effects of changes in consumption patterns on household carbon and environmental footprints.

Summary and future perspectives

The socioeconomic disruption associated with COVID-19 represents a highly unusual alteration of the human interaction with the Earth System. This alteration is likely to generate a series of responses, illuminating the processes connecting energy, emissions, air quality and climate, as well as globalization, food security, poverty and biodiversity (FIG. 1). In many cases, these long-term, indirect Earth System responses could be larger — and of opposite sign — than the short-term environmental effects that have been immediately visible around the world. The potential for long-term impacts via Earth System cascades and feedbacks highlights the opportunity to use this period as an unintended experiment,

and to use the knowledge gained to better predict, model and monitor Earth System processes during and after the event.

Given the uncertainty about the length of sheltering orders — and the nature of any interventions that may follow — it is impossible to know how long this inadvertent experiment will last. This uncertainty provides motivation for documenting hypotheses during this initial stage of the global crisis, so that data can be gathered and evaluated within the framework of a priori predictions, rather than post hoc analyses. Some hypotheses are only testable or conclusively verifiable by maintaining and/or deploying data collection during this early stage. Unless prohibited by safety concerns, it is important that these data continue to be collected so that the Earth System response to COVID-19 can be understood. By generating specific hypotheses based on initial observations, existing empirical relationships and process-based models, and then testing those hypotheses with existing and novel data sources, the COVID-19 socioeconomic disruption can provide novel insights into the processes that govern Earth System function and change.

Our primary motivation is to search for insight about the basic functioning of the Earth System that could be helpful in managing and recovering from the event, and in avoiding future impacts. Predicting the impacts of the sheltering on different components of the Earth System can help to aid in environment-related disaster preparedness in different regions. For example, analysis of the Earth System response can enable early detection of hotspots of environmental risk or degradation emerging during the event. Similarly, predicting, monitoring and understanding Earth System processes can help to support a sustainable economic, social and environmental recovery from the event. Although there is uncertainty about the length of the pandemic, the economic effects seem very likely to last for years. The individual, societal and government responses to these economic effects will influence the long-term trajectory of the human footprint on the Earth System.

The current socioeconomic disruption is a singular perturbation of that human footprint. Advancing understanding of this forcing, and the processes by which different components of the Earth System respond, can help to enhance robustness and resilience now and in the future.

Noah S. Diffenbaugh^{1,2,3}, Christopher B. Field^{1,2}, Eric A. Appel^{1,2,3}, Ines L. Azevedo^{2,4}, Dennis D. Baldocchi⁵, Marshall Burke^{1,2,6}, Jennifer A. Burney^{1,7}, Philippe Ciais⁸, Steven J. Davis⁹, Arlene M. Fiore^{10,11}, Sarah M. Fletcher^{2,12}, Thomas W. Hertel¹³, Daniel E. Horton^{14,15}, Solomon M. Hsiang¹⁶, Robert B. Jackson^{1,2}, Xiaomeng Jin¹⁰, Margaret Levij^{17,18}, David B. Lobell^{1,2,6}, Galen A. McKinley^{10,11}, Frances C. Moore¹⁹, Anastasia Montgomery¹⁴, Kari C. Nadeau^{2,20}, Diane E. Pataki²¹, James T. Randerson¹⁰, Markus Reichstein²², Jordan L. Schnell^{15,23}, Sonia I. Seneviratne^{10,24}, Deepti Singh²⁵, Allison L. Steiner²⁶ and Gabrielle Wong-Parodi^{1,2}

¹Department of Earth System Science, Stanford University, Stanford, CA, USA.

²Stanford Woods Institute for the Environment, Stanford University, Stanford, CA, USA.

³Department of Materials Science and Engineering, Stanford University, Stanford, CA, USA.

⁴Department of Energy Resources Engineering, Stanford University, Stanford, CA, USA.

⁵Department of Environmental Science, Policy, and Management, University of California, Berkeley, Berkeley, CA, USA.

⁶Center on Food Security and the Environment, Stanford University, Stanford, CA, USA.

⁷School of Global Policy & Strategy, University of California, San Diego, La Jolla, CA, USA.

⁸Laboratoire des Sciences du Climat et de l'Environnement, Gif sur Yvette, France.

⁹Department of Earth System Science, University of California, Irvine, Irvine, CA, USA.

¹⁰Department of Earth & Environmental Sciences, Columbia University, Palisades, New York, NY, USA.

¹¹Lamont-Doherty Earth Observatory, Columbia University, Palisades, New York, NY, USA.

¹²Department of Civil and Environmental Engineering, Stanford University, Stanford, CA, USA.

¹³Department of Agricultural Economics, Purdue University, West Lafayette, IN, USA.

¹⁴Department of Earth and Planetary Sciences, Northwestern University, Evanston, IL, USA.

¹⁵Institute for Sustainability and Energy at Northwestern, Northwestern University, Evanston, IL, USA.

¹⁶Goldman School of Public Policy, University of California, Berkeley, Berkeley, CA, USA.

¹⁷Department of Political Science, Stanford University, Stanford, CA, USA.

¹⁸Center for Advanced Study in the Behavioral Sciences, Stanford University, Stanford, CA, USA.

¹⁹Department of Environmental Science and Policy, University of California, Davis, Davis, CA, USA.

²⁰Division of Allergy, Immunology, & Rheumatology, Stanford University, Stanford, CA, USA.

²¹School of Biological Sciences, University of Utah, Salt Lake City, UT, USA.

²²Department of Biogeochemical Integration, Max Planck Institute for Biogeochemistry, Jena, Germany.

²³Cooperative Institute for Research in Environmental Sciences, University of Colorado Boulder, Boulder, CO, USA.

²⁴Institute for Atmospheric and Climate Science, ETH Zurich, Zürich, Switzerland.

²⁵School of the Environment, Washington State University Vancouver, Vancouver, WA, USA.

²⁶Department of Climate and Space Sciences and Engineering, University of Michigan, Ann Arbor, MI, USA.

✉e-mail: diffenbaugh@stanford.edu

<https://doi.org/10.1038/s43017-020-0079-1>

Published online 29 July 2020

- Soden, B. J., Wetherald, R. T., Stenchikov, G. L. & Robock, A. Global cooling after the eruption of Mount Pinatubo: a test of climate feedback by water vapor. *Science* **296**, 727–730 (2002).
- Farquhar, G. D. & Roderick, M. L. Pinatubo, diffuse light, and the carbon cycle. *Science* **299**, 1997–1998 (2003).
- Gu, L. H. et al. Response of a deciduous forest to the Mount Pinatubo eruption: enhanced photosynthesis. *Science* **299**, 2035–2038 (2003).
- Marufu, L. T. et al. The 2003 North American electrical blackout: an accidental experiment in atmospheric chemistry. *Geophys. Res. Lett.* **31**, L13106 (2004).
- Travis, D. J., Carleton, A. M. & Lauritsen, R. G. Contrails reduce daily temperature range. *Nature* **418**, 601 (2002).
- Steffen, W. et al. The emergence and evolution of Earth System Science. *Nat. Rev. Earth Environ.* **1**, 54–63 (2020).
- Hale, T., Webster, S., Petherick, A., Phillips, T. & Kira, B. *Oxford COVID-19 Government Response Tracker* <https://covidtracker.bsg.ox.ac.uk> (2020).
- ILO. ILO Monitor: COVID-19 and the world of work. Fifth edition, 30 June 2020. International Labour Organization https://www.ilo.org/wcmsp5/groups/public/@dgreports/@dcomm/documents/briefingnote/wcms_749399.pdf (2020).
- Lenton, T. M. et al. Tipping elements in the Earth's climate system. *Proc. Natl Acad. Sci. USA* **105**, 1786–1793 (2008).
- Steffen, W. et al. Trajectories of the Earth System in the Anthropocene. *Proc. Natl Acad. Sci. USA* **115**, 8252–8259 (2018).
- Rockström, J. et al. Planetary boundaries: exploring the safe operating space for humanity. *Ecol. Soc.* **14**, 32 (2009).
- Liu, Z. et al. COVID-19 causes record decline in global CO₂ emissions. Preprint at *arXiv* <https://arxiv.org/abs/2004.13614v3> (2020).
- Le Quéré, C. et al. Temporary reduction in daily global CO₂ emissions during the COVID-19 forced confinement. *Nat. Clim. Change* **10**, 647–653 (2020).
- EIA. Short-Term Energy Outlook (STEO). July 2020. U.S. Energy Information Administration https://www.eia.gov/outlooks/steo/pdf/steo_full.pdf (2020).
- Jackson, R. B. et al. Global energy growth is outpacing decarbonization. *Environ. Res. Lett.* **13**, 120401 (2018).
- Peters, G. P. et al. Rapid growth in CO₂ emissions after the 2008–2009 global financial crisis. *Nat. Clim. Change* **2**, 2–4 (2012).
- Feng, K., Davis, S. J., Sun, L. & Hubacek, K. Drivers of the US CO₂ emissions 1997–2013. *Nat. Commun.* **6**, 7714 (2015).
- Hanna, R., Xu, Y. & Victor, D. G. After COVID-19, green investment must deliver jobs to get political traction. *Nature* **582**, 178–180 (2020).
- Zheng, B. et al. Satellite-based estimates of decline and rebound in China's CO₂ emissions during COVID-19 pandemic. Preprint at *arXiv* <https://arxiv.org/abs/2006.08196v1> (2020).
- Friedlingstein, P. et al. Global carbon budget 2019. *Earth Syst. Sci. Data* **11**, 1783–1838 (2019).
- McKinley, G. A., Fay, A. R., Eddebar, Y. A., Gloege, L. & Lovenduski, N. S. External forcing explains recent decadal variability of the ocean carbon sink. *AGU Adv.* <https://doi.org/10.1029/2019AV000149> (2020).
- Le, T. et al. Unexpected air pollution with marked emission reductions during the COVID-19 outbreak in China. *Science* <https://doi.org/10.1126/science.abb7431> (2020).
- Ramanathan, V., Crutzen, P. J., Kiehl, J. T. & Rosenfeld, D. Aerosols, climate, and the hydrological cycle. *Science* **294**, 2119–2124 (2001).
- Rosenfeld, D. et al. Flood or drought: how do aerosols affect precipitation? *Science* **321**, 1309–1313 (2008).
- Wild, M. Global dimming and brightening: a review. *J. Geophys. Res. Atmos.* **114**, D00D16 (2009).
- Westervelt, D. M. et al. Local and remote mean and extreme temperature response to regional aerosol emissions reductions. *Atmos. Chem. Phys.* **20**, 3009–3027 (2020).

27. Mickley, L. J., Leibensperger, E. M., Jacob, D. J. & Rind, D. Regional warming from aerosol removal over the United States: results from a transient 2010–2050 climate simulation. *Atmos. Environ.* **46**, 545–553 (2012).
28. Mascioli, N. R., Fiore, A. M., Previdi, M. & Correa, G. Temperature and precipitation extremes in the United States: quantifying the responses to anthropogenic aerosols and greenhouse gases. *J. Clim.* **29**, 2689–2701 (2016).
29. Bollasina, M. A., Ming, Y. & Ramaswamy, V. Anthropogenic aerosols and the weakening of the South Asian summer monsoon. *Science* **334**, 502–505 (2011).
30. Lin, L., Wang, Z., Xu, Y., Fu, Q. & Dong, W. Larger sensitivity of precipitation extremes to aerosol than greenhouse gas forcing in CMIP5 models. *J. Geophys. Res.* **123**, 8062–8073 (2018).
31. Singh, D., Bollasina, M., Ting, M. & Diffenbaugh, N. S. Disentangling the influence of local and remote anthropogenic aerosols on South Asian monsoon daily rainfall characteristics. *Clim. Dyn.* **52**, 6301–6320 (2019).
32. EIA. Annual Energy Outlook 2020. U.S. Energy Information Administration https://www.eia.gov/outlooks/aeo/pdf/AEO2020_Full_Report.pdf (2020).
33. Bodine, S. P. COVID-19 Implications for EPA's Enforcement and Compliance Assurance Program. United States Environmental Protection Agency <https://www.epa.gov/sites/production/files/2020-03/documents/ocameemooncovid19implications.pdf> (2020).
34. Burney, J. & Ramanathan, V. Recent climate and air pollution impacts on Indian agriculture. *Proc. Natl Acad. Sci. USA* **111**, 16319–16324 (2014).
35. Avner, S., Mauzerall, D. L., Liu, J. & Horowitz, L. W. Global crop yield reductions due to surface ozone exposure: 2. Year 2030 potential crop production losses and economic damage under two scenarios of O₃ pollution. *Atmos. Environ.* **45**, 2297–2309 (2011).
36. Cohen, A. J. et al. Estimates and 25-year trends of the global burden of disease attributable to ambient air pollution: an analysis of data from the Global Burden of Diseases Study 2015. *Lancet* **389**, 1907–1918 (2017).
37. Liu, C. et al. Ambient particulate air pollution and daily mortality in 652 cities. *N. Engl. J. Med.* **381**, 705–715 (2019).
38. WHO. Ambient air pollution: A global assessment of exposure and burden of disease. World Health Organization <https://apps.who.int/iris/bitstream/handle/10665/250141/9789241511353-eng.pdf> (2016).
39. Schraufnagel, D. E. et al. Health benefits of air pollution reduction. *Ann. Am. Thorac. Soc.* **16**, 1478–1487 (2019).
40. Friedman, M. S., Powell, K. E., Hutwagner, L., Graham, L. M. & Teague, W. G. Impact of changes in transportation and commuting behaviors during the 1996 Summer Olympic Games in Atlanta on air quality and childhood asthma. *JAMA* **285**, 897–905 (2001).
41. Li, Y., Wang, W., Kan, H., Xu, X. & Chen, B. Air quality and outpatient visits for asthma in adults during the 2008 Summer Olympic Games in Beijing. *Sci. Total Environ.* **408**, 1226–1227 (2010).
42. Wang, S. et al. Quantifying the air pollutants emission reduction during the 2008 Olympic Games in Beijing. *Environ. Sci. Technol.* **44**, 2490–2496 (2010).
43. Su, C. et al. Assessing responses of cardiovascular mortality to particulate matter air pollution for pre-, during- and post-2008 Olympics periods. *Environ. Res.* **142**, 112–122 (2015).
44. He, G., Fan, M. & Zhou, M. The effect of air pollution on mortality in China: Evidence from the 2008 Beijing Olympic Games. *J. Environ. Econ. Manage.* **79**, 18–39 (2016).
45. Rich, D. Q. et al. Association between changes in air pollution levels during the Beijing Olympics and biomarkers of inflammation and thrombosis in healthy young adults. *JAMA* **307**, 2068–2078 (2012).
46. Wu, X., Nethery, R. C., Sabath, B. M., Braun, D. & Dominici, F. Exposure to air pollution and COVID-19 mortality in the United States: a nationwide cross-sectional study. Preprint at *medRxiv* <https://www.medrxiv.org/content/10.1101/2020.04.05.20054502v2> (2020).
47. Liang, D. et al. Urban air pollution may enhance COVID-19 case-fatality and mortality rates in the United States. Preprint at *medRxiv* <https://www.medrxiv.org/content/10.1101/2020.05.04.20090746v1> (2020).
48. Burke, M., Davis, W. M. & Diffenbaugh, N. S. Large potential reduction in economic damages under UN mitigation targets. *Nature* **557**, 549–553 (2018).
49. Moore, F. C. & Diaz, D. B. Temperature impacts on economic growth warrant stringent mitigation policy. *Nat. Clim. Change* **5**, 127–131 (2015).
50. UNDESA. World Economic Situation and Prospects as of mid-2020. *United Nations* https://www.un.org/development/desa/dpad/wp-content/uploads/sites/45/publication/WESP2020_MYU_Report.pdf (2020).
51. Guan, D. et al. Global economic footprint of the COVID-19 pandemic. *Nat. Hum. Behav.* **4**, 577–587 (2020).
52. Lusk, J. Ruminations on solutions to the COVID-related food disruptions. *Jayson Lusk* <http://jaysonlusk.com/blog/2020/5/12/ruminations-on-solutions-to-the-covid-related-food-disruptions> (2020).
53. WTO. Methodology for the WTO trade forecast of April 8 2020. World Trade Organization https://www.wto.org/english/news_e/pres20_e/methodpr855_e.pdf (2020).
54. Martin, W. & Anderson, K. Export restrictions and price insulation during commodity price booms. Policy Research Working Paper no. WPS 5645. World Bank Group <http://documents.worldbank.org/curated/en/583201468337175309/Export-restrictions-and-price-insulation-during-commodity-price-booms> (2011).
55. Battisti, D. S. & Naylor, R. L. Historical warnings of future food insecurity with unprecedented seasonal heat. *Science* **323**, 240–244 (2009).
56. Laborde, D., Mamun, A. & Parent, M. COVID-19 Food Trade Policy Tracker. International Food Policy Research Institute <https://www.ifpri.org/project/covid-19-food-trade-policy-tracker> (2020).
57. Diao, X. & Kennedy, A. Economywide impact of maize export bans on agricultural growth and household welfare in Tanzania: a dynamic computable general equilibrium model analysis. *Dev. Policy Rev.* **34**, 101–134 (2016).
58. Anderson, K. & Nelgen, S. Agricultural trade distortions during the global financial crisis. *Oxf. Rev. Econ. Policy* **28**, 235–260 (2012).
59. Ahmed, S. A., Diffenbaugh, N. S., Hertel, T. W. & Martin, W. J. Agriculture and trade opportunities for Tanzania: past volatility and future climate change. *Rev. Dev. Econ.* **16**, 429–447 (2012).
60. Roth, A. Poachers kill more rhinos as coronavirus halts tourism to Africa. *New York Times* (8 Apr 2020) <https://www.nytimes.com/2020/04/08/science/coronavirus-poaching-rhinos.html> (2020).
61. INPE. Earth observation general coordination. Monitoring program of the Amazon and other biomes. Deforestation – legal Amazon. National Institute for Space Research <http://terrabrasilis.dpi.inpe.br/app/dashboard/alerts/legal/amazon/aggregated/> (2020).
62. Barrett, C. B., Travis, A. J. & Dasgupta, P. On biodiversity conservation and poverty traps. *Proc. Natl Acad. Sci. USA* **108**, 13907–13912 (2011).
63. Oldekop, J. A., Sims, K. R. E., Karna, B. K., Whittingham, M. J. & Agrawal, A. Reductions in deforestation and poverty from decentralized forest management in Nepal. *Nat. Sustain.* **2**, 421–428 (2019).
64. Rutz, C. et al. COVID-19 lockdown allows researchers to quantify the effects of human activity on wildlife. *Nat. Ecol. Evol* <https://doi.org/10.1038/s41559-020-1257-z> (2020).
65. WMO. COVID-19 impacts observing system. World Meteorological Organization <https://public.wmo.int/en/media/press-release/covid-19-impacts-observing-system> (2020).
66. Baker, S. R., Bloom, N., Davis, S. J. & Terry, S. J. COVID-induced economic uncertainty. NBER Working Paper No. 26983. National Bureau of Economic Research <http://www.nber.org/papers/w26983.pdf> (2020).
67. Runge, J. et al. Inferring causation from time series in Earth system sciences. *Nat. Commun.* **10**, 2553 (2019).
68. Peters, J., Janzing, D. & Schölkopf, B. *Elements of Causal Inference: Foundations and Learning Algorithms* 288 pp (MIT Press, 2017).
69. Murkowski, L. April 2, 2020. Letter to Secretary Barnhardt and Secretary Perdue. U.S. Senate Committee on Energy & Natural Resources https://www.energy.senate.gov/public/index.cfm?files=serve&file_id=988D2496-CB4C-4D63-8213-EE5F0DD30CA0 (2020).
70. Prunicki, M. et al. The impact of prescribed fire versus wildfire on the immune and cardiovascular systems of children. *Allergy* **74**, 1989–1991 (2019).
71. Flato, G. et al. in *Climate Change 2013: The Physical Science Basis. Contribution of Working Group I to the Fifth Assessment Report of the Intergovernmental Panel on Climate Change* (eds Stocker, T. F. et al.) 741–866 (Cambridge Univ. Press, 2013).
72. Hausfather, Z., Drake, H. F., Abbott, T. & Schmidt, G. A. Evaluating the performance of past climate model projections. *Geophys. Res. Lett.* **47**, e2019GL085378 (2020).
73. Diffenbaugh, N. S. Verification of extreme event attribution: using out-of-sample observations to assess changes in probabilities of unprecedented events. *Sci. Adv.* **6**, eaay2368 (2020).
74. Heft-Neal, S., Lobell, D. B. & Burke, M. Using remotely sensed temperature to estimate climate response functions. *Environ. Res. Lett.* **12**, 14013 (2017).
75. Carleton, T. A. & Hsiang, S. M. Social and economic impacts of climate. *Science* **353**, aad9837 (2016).
76. Eyring, V. et al. Overview of the Coupled Model Intercomparison Project Phase 6 (CMIP6) experimental design and organization. *Geosci. Model. Dev.* **9**, 1937–1958 (2016).
77. Sillman, S., Logan, J. A. & Wofsy, S. C. The sensitivity of ozone to nitrogen oxides and hydrocarbons in regional ozone episodes. *J. Geophys. Res. Atmos.* **95**, 1837–1851 (1990).
78. Huang, X. et al. Enhanced secondary pollution offset reduction of primary emissions during COVID-19 lockdown in China. *Natl. Sci. Rev.* <https://doi.org/10.1093/nsr/nwaa137> (2020).
79. Shi, X. & Brasseur, G. P. The response in air quality to the reduction of Chinese economic activities during the COVID-19 outbreak. *Geophys. Res. Lett.* **47**, e2020GL088070 (2020).
80. Storelvmo, T. et al. Lethargic response to aerosol emissions in current climate models. *Geophys. Res. Lett.* **45**, 9814–9823 (2018).
81. Bellouin, N. et al. Bounding global aerosol radiative forcing of climate change. *Rev. Geophys.* **58**, e2019RG000660 (2020).
82. Samsat, B. H. et al. Climate impacts from a removal of anthropogenic aerosol emissions. *Geophys. Res. Lett.* **45**, 1020–1029 (2018).
83. Burke, M., Bergquist, L. F. & Miguel, E. Sell low and buy high: arbitrage and local price effects in Kenyan markets. *Q. J. Econ.* **134**, 785–842 (2018).
84. Alix-García, J. M. et al. Payments for environmental services supported social capital while increasing land management. *Proc. Natl Acad. Sci. USA* **115**, 7016–7021 (2018).
85. Alix-García, J. M., Sims, K. R. E. & Yañez-Pagans, P. Only one tree from each seed? Environmental effectiveness and poverty alleviation in Mexico's Payments for Ecosystem Services Program. *Am. Econ. J. Econ. Policy* **7**, 1–40 (2015).
86. Jayachandran, S. et al. Cash for carbon: a randomized trial of payments for ecosystem services to reduce deforestation. *Science* **357**, 267–273 (2017).
87. GiveDirectly. Research at GiveDirectly. <https://www.givedirectly.org/research-at-give-directly/> (2020).
88. Phillips, C. A. et al. Compound climate risks in the COVID-19 pandemic. *Nat. Clim. Change* **10**, 586–588 (2020).
89. Climate-Safe Infrastructure Working Group (CSIWG). Paying it Forward: The Path Toward Climate-Safe Infrastructure in California. *State of California* <https://www.adaptationclearinghouse.org/resources/paying-it-forward-the-path-toward-climate-safe-infrastructure-in-california.html> (2018).
90. Field, C. B. & Appel, E. A. Will the pandemic make the West more vulnerable to wildfires? *New York Times* (15 May 2020) <https://www.nytimes.com/2020/05/14/opinion/wildfires-coronavirus.html> (2020).
91. SafeGraph. U.S. Geographic Responses to Shelter in Place Orders: Percent Staying Home. *SafeGraph* <https://www.safegraph.com/dashboard/covid19-shelter-in-place> (2020).
92. Le Quéré, C. et al. Supplementary data to: Le Quéré et al. (2020). Temporary reduction in daily global CO₂ emissions during the COVID-19 forced confinement (Version 1.0). Global Carbon Project. *Integrated Carbon Observation System* <https://www.icos-cp.eu/gcp-covid19> (2020).
93. Liu, Z. et al. Carbon Monitor: a near-real-time daily dataset of global CO₂ emission from fossil fuel and cement production. Preprint at *arXiv* <https://arxiv.org/abs/2006.07690v1> (2020).
94. Jin, X., Fiore, A., Boersma, K. F., De Smedt, I. & Vallin, L. Inferring changes in summertime surface ozone–NO_x–VOC chemistry over U.S. urban areas from two decades of satellite and ground-based observations. *Environ. Sci. Technol.* **54**, 6518–6529 (2020).

95. Bauwens, M. et al. Impact of coronavirus outbreak on NO₂ pollution assessed using TROPOMI and OMI observations. *Geophys. Res. Lett.* **47**, e2020GL087978 (2020).
96. Hawkins, E. & Sutton, R. The potential to narrow uncertainty in regional climate predictions. *Bull. Am. Meteorol. Soc.* **90**, 1095–1107 (2009).
97. Deser, C., Knutti, R., Solomon, S. & Phillips, A. S. Communication of the role of natural variability in future North American climate. *Nat. Clim. Change* **2**, 775–779 (2012).
98. Horton, D. E. et al. Contribution of changes in atmospheric circulation patterns to extreme temperature trends. *Nature* **522**, 465–469 (2015).

Acknowledgements

This article grew from discussions initiated in the Uncommon Dialogue programme of the Stanford Woods Institute for

the Environment. The authors acknowledge support from Stanford University. K.C.N. acknowledges financial support from NIEHS R01 and Sean N. Parker Center at Stanford. G.A.M. acknowledges support from NSF OCE-1948624. T.W.H. acknowledges support from USDA-NIFA 2019-67023-29679 and Hatch 1003642. D.E.H., A.M. and J.L.S. acknowledge support from the Ubben Program for Climate and Carbon Science at the Institute for Sustainability and Energy at Northwestern. P.C. acknowledges support from the European Research Council Synergy grant SyG-2013-610028 IMBALANCE-P and the ANR CLAND Convergence Institute.

Author contributions

All authors made substantial contributions to discussion of content and review/editing of the manuscript. N.S.D., C.B.F., J.A.B., A.M.F., T.W.H., D.E.H., F.C.M., K.C.N., M.R. and A.L.S. contributed the initial writing. N.S.D., C.B.F., D.D.B., M.B.,

P.C., S.J.D., A.M.F., D.E.H., R.B.J., X.J., A.M. and J.L.S. researched data for the article. N.S.D. and C.B.F. convened the group and coordinated the drafting and revisions of the figures and manuscript. N.S.D. assembled the initial draft.

Competing interests

The authors declare no competing interests.

Peer review information

Nature Reviews Earth & Environment thanks the anonymous reviewer(s) for their contribution to the peer review of this work.

Publisher's note

Springer Nature remains neutral with regard to jurisdictional claims in published maps and institutional affiliations.

© Springer Nature Limited 2020